DYNAMIC MODELLING OF THE EMULSION COPOLYMERIZATION OF SBR

DYNAMIC MODELLING
OF THE
EMULSION COPOLYMERIZATION
OF
STYRENE/BUTADIENE

By

TARAS OSCAR BROADHEAD, B.ENG.

A Thesis

Submitted to the School of Graduate Studies

in Partial Fulfilment of the Requirements

for the Degree

Master of Engineering

McMaster University

1984

MASTER OF ENGINEERING (1984) McMASTER UNIVERSITY
(Chemical Engineering) Hamilton, Ontario

TITLE: Dynamic Modelling of the Emulsion Copolymerization of Styrene/Butadiene

AUTHOR: Taras Oscar Broadhead, B.Eng. (McMaster University)

SUPERVISORS: Dr. A. E. Hamielec
Dr. J.F. MacGregor

NUMBER OF PAGES: (xxv), 267

ABSTRACT

A computer model is developed to simulate the emulsion copolymerization of styrene/butadiene in perfectly stirred batch, semi-batch or continuous flow reactors. The model considers free radical initiation by a redox mechanism, micellar particle nucleation, radical concentration as a function of particle size, radical entry rate and termination rate and diffusion controlled termination and propagation reactions. It predicts conversion, copolymer composition, particle number, number and mass average molecular masses and tri- and tetra-functional branch frequencies. A simple method of estimating the particle size distribution is included in the model. Heat balances over the reactor and cooling jacket are considered and proportional-integral control of the reactor temperature is simulated.

The model is used to simulate SBR copolymerization and styrene homopolymerization experimental data from the literature. These simulations tested only certain parts of the model and it is concluded that a more complete verification of the model can only be achieved by running a series of designed experiments. Qualitatively, the molecular mass, particle size distribution and reactor temperature predictions appear to be reasonable. The lack of appropriate temperature dependent rate constants currently limits the molecular mass predictions to isothermal conditions.

A comparison of semi-batch operating policies designed to control copolymer composition is presented to illustrate the potential application of the model.

ACKNOWLEDGEMENTS

I gratefully acknowledge the contributions to this work by:

Drs. A. E. Hamielec and J. F. MacGregor, supervisors of this project, for their excellent advice, patience and encouragement;

Dr. L. Garcia-Rubio for his interest and help in getting started;

Dr. P. A. Taylor for his constructive and most appreciated advice;

Dr. J. Warkentin for his interest;

the faculty and staff of McMaster's Chemical Engineering Department for their technical and administrative assistance;

fellow students Frank Wong, Yannis Kanetakis and Eric Hoffman for their advice and cooperation;

Glenn Lord for the use of his Library of Previous Knowledge;

my parents for their support and encouragement;

and the Natural Sciences and Engineering Research Council and the Department of Chemical Engineering at McMaster for their most appreciated financial support.

TABLE OF CONTENTS

LIST OF TABLES

LIST OF FIGURES

NOMENCLATURE

Greek Symbols

α	Ratio of monomers required for a desired copolymer composition.
α_i	The difference between the volume expansion coefficients of species "i" in the solid and liquid states where i = S,B,P (see subscripts section)(1/K)
γ	Interfacial tension N/m
γ_i	Solubility of species "i" in water, where i = S,B
ε	Ratio of particle to micelle capture rates - capture efficiency
θ	Mean residence time in the reactor (min.)
μ	Volume growth rate of a particle
π	3.141592653
ρ_A	Total rate of radical entry } $(\frac{\text{mol}}{\text{min.dm}^3\text{H}_2\text{O}})$
ρ_{cp}	Radical capture rate by particles }
ρ_{cm}	Radical capture rate of micelles $(\frac{\text{mol}}{\text{min.dm}^3\text{H}_2\text{O}})$
ρ_i	Density of species "i", where i = B,s,w,p,m (g/dm^3)
τ	Nucleation time of a particle generation (min.)
$\Delta\tau$	Generation period (min.)
τ_I	Controller integral time (min.)
τ_J	Thermal time constant for the cooling jacket (min.)
τ_R	Thermal time constant for the reactor (min.)
ϕ_i	Volume fraction of species "i" in the particles where i = s,B,m,p

ϕ_i^{SAT}	Volume fraction of species "i" in a saturated polymer particle, where i = m,p
Φ_i	Fraction of "i" ended radicals, i = s,B
χ	Monomer-polymer interaction parameter
ω_{ip}	$(v_m K_{imw} K_{iwp} + v_w K_{iwp} + v_p)$
Ω_{ip}	$(V_m K_{imw} K_{iwp} + V_w K_{iwp} + V_p)$ where i = s,B

Roman Symbols

A_m	Total area of the micelles (dm^2)
A_p	Total area of the polymer particles (dm^2)
A_s	Emulsifier surface area covering potential (dm^2/mol)
A_J	Area of heat transfer through the cooling jacket (dm^2)
ACCM	Accumulated mass fraction of styrene in the polymer
ACNiP	Accumulated moles of species "i" in the copolymer, i = s,B
$[i]_j$	Concentration of species "i" in the phase "j" i = s,B,m,I,Fe,Fe^{2+},Fe^{3+},RA(SFS),E,X,MI,$R^{\cdot}$ j = m,w,p (mol/dm^3)
$[E]_{cmc}$	Critical micelle concentration or saturation concentration of emulsifier in the water phase (mol/dm^3)
C_{pi}	Molar heat capacity of species "i", where i = s,B,w,d (J/mol.K)
$\tilde{C}_{pi}$	Heat capacity of species "i" on a mass basis, where i = s,B,w,p (J/mol.K)
C_k	Ratio of propagation to polymer rate to the propagation with monomer rate
C_m	Ratio of the transfer to monomer rate to the propagation rate

C_p	Ratio of the transfer to polymer rate to the propagation rate
C_x	Ratio of the transfer to chain transfer agent rate to the propagation rate
D_w	Diffusion coefficient for radicals through water
ℓ	Error - the difference between the actual and desired (T^{set}) reactor temperatures (K)
$\bar{E}_a$	The average of the styrene and butadiene propagation rate activation energies. (cal/mol)
f	Initiator decomposition efficiency factor
F_i	Molar flow of species "i" out of the reactor, where i = S,B,I,Fe,RA,E,X
$\tilde{F}_i$	Mass flow of species "i" out of the reactor, where i = S,B,I,Fe,RA,E,X
F(r)	Number density of particles of radius r
FeY^{-2},FeY^{-1}	Iron/EDTA ligands
g_1	Reactor thermal process gain
g_2,g_3	Cooling jacket thermal process gain
ΔH,H	Enthalpy (J)
ΔH_p	Heat of polymerization (J)
$I^{\cdot}$	Initiator radical
I_2	Initiator molecule (potassium persulphate)
I_m	Modified Bessel function
ICC	Instantaneous copolymer composition
k_1	Redox initiation (iron oxidation) rate constant (dm^3/mol.min.)
k_2	Rodox initiation (iron reduction) rate constant (dm^3/mol.min.)
k_{cm}	Radical capture by micelle rate constant (dm/min.)

k_{cp}	Radical capture by particle rate constant (dm/min.)
k_d	Initiator thermal decomposition rate (1/min.)
k_{de}	Radical desorption rate constant (1/min.)
k_{fij}	Transfer to monomer rate constant. Reaction of an "i" ended radical with a "j" monomer unit, where i = S,B and j = S,B (subsequent rate constant subscripts are defined similarly)
k_{fix}	Transfer to chain transfer agent rate constant. Reaction of an "i" ended radical with a transfer molecule "x". (dm^3/mol.min.)
k_{fpij}	Transfer to polymer rate constant. Reaction of an "i" ended radical with an incorporated or "bound" "j" monomer unit. (dm^3/mol.min.)
k_{MI}	Radical reaction with monomer soluble impurity rate constant. (dm^3/mol.min.)
k_p	Overall propagation rate constant (dm^3/mol.min.)
k_{pc}	Propagation of an initiator frament radical rate constant. (dm^3/mol.min.)
k_{pij}	Propagation rate constant. Reaction of an "i" ended radical with a "j" monomer unit, where
k^*_{pin}	Propagation with polymer rate constant. Reaction with an "i" radical with an incorporated double bond in the "n^{th}" conformation, where n = 1(trans), 2(cis) and 3(1,2 or vinyl)
k^{sat}_{tp}	Termination rate constant (potentially diffusion controlled) in the saturated latex particle (dm^3/mol.min.)
K_c	Controller gain
K_{imw}	Partition coefficient for species "i" between monomer and water, where i = S,B,I,X
K_{iwp}	Partition coefficient for species "i" between water and polymer phase, i = S,B,I,X

KPS	Potassium persulphate
M_i	Mass of species "i" in the reactor, where i = S,B,I,Fe,RA,E,X (g)
$\tilde{M}_i$	Molecular mass of species "i" where i = S,B,I,Fe,RA,E,X,W (g/mol)
$\tilde{M}_{eff}$	Effective molecular mass of a repeat unit in the copolymer chain (g/mol)
$\bar{M}_N$	Number average molecular mass (g/mol)
$\bar{M}_W$	Mass (weight) average molecular mass (g/mol)
$\bar{n}$	Average number of radicals per particle
$\bar{n}(t,\tau)$	Average number of radicals per particle at time "t" for the generation nucleated at time "τ"
N_A	Avogadro's number
N_p	Number of polymer particles in the reaction
N_{pp}	Number of polymer particles per dm^3 of water
N_i	Moles of species "i" where i = S,B,I,Fe,RA,E,X (mol)
N_i (V)	Number of particle of volume "V" with i radicals per particle
N_m	Number of micelles
Q_o	Zero polymer moment $Q_o = \sum_r [P_r]$
Q_1	First polymer moment $Q_1 = \sum_r r [P_r]$
Q_2	Second polymer moment $Q_2 = \sum_r r^2 [P_r]$
$Q_{J\ LOSS}$	Heat loss from the cooling jacket (J/min.)
$Q_{R\ LOSS}$	Heat loss from the reactor (J/min.)
r_m	Radius of a micelle (dm)
r	Radius of a particle (dm)
r_s	Reactivity ratio defined as k_{pss}/k_{psB}
r_b	Reactivity ratio defined as k_{pbb}/k_{psb}

R	Gas constant
Radius	Radius of the cylindrical reactor
RO·	Peroxide initiator radical
ROOH	Hydroperoxide molecule
R_I	Rate of initiation (mol/min dm^3H_2O)
R_{fx}	Rate of consumption of chain transfer agent
R_{pi}	Rate of polymerization of species "i" where i = S,B. (mol/min.)
SFS	Sodium formaldehyde sulphoxylate
shrink	Volume contraction rate of the organic phase (mol/min.)
t	Time (min.)
T	Reactor temperature (K)
T_c	Cooling water "bias" or steady state temperature (K)
T_{in}	Input flow temperature (K)
$T_J, \Delta T_J$	Cooling jacket temperature and temperature increment (K)
T_{gi}	Glass transition temperature for species "i", where i = S,B,P
T_{ref}	Reference temperature (K)
T_s	Linearization point for reactor transfer function (K)
T^{set}	Set point temperature (K)
U	Overall heat transfer coefficient ($J/min.dm^2K$)
v_i	Volume flow of phase "i" where i = o,p,t,w (dm^3/min.)
V_i	Volume of species "i" where i = S,B (dm^3)
V_i	Volume of phase "i" where i = m,o,w,p (dm^3)
V_{pp}	Volume of pure polymer (dm^3)

$\hat{V}_p$	Volume of a single particle (dm^3)
$\hat{V}_p(t,\tau)$	Volume of a single particle at time t , nucleated at time τ(dm^3)
V_p^{Sat}	Volume of the saturated polymer phase (dm^3)
V_F	Fractional free volume
V_F^{sat}	Fractional free volume of a saturated particle
V_{FCRi}	Critical free volume at which propagation of monomer "i" becomes diffusion controlled
V_{FTMIN}	Critical free volume at which termination reactions occur by propagation
$\overline{V}_M$	Molar volume of monomer (m^2/mol)
V_R	Volume of the reactor (dm^3)
V_T	Total volume of reactor contents (dm^3)
W(r)	Fraction of polymer molecules of chain length r
W_p	Mass of polymer (kg)
X	Fractional conversion on a mass basis
X^+	Unknown oxidation product of SFS
X_c	Fractional conversion at which monomer droplets disappear
X_{mp}	Apparent conversion within the polymer particles
Y_o	Radical concentrations (mol/dm^3)

Subscripts

B	Butadiene
E	Emulsifier
Fe	Iron
Fe^{2+}	Ferrous iron ion
Fe^{3+}	Ferric iron ion
I	Initiator (KPS or ROOH)

M	Monomer
MI	Monomer soluble impurities
O	Organic (phase)
P	Polymer
$R^{\cdot}$	Radical
RA	Reducing agent (SFS)
S	Styrene
t	total
w	Water
x	Chain transfer agent (CTA)

... thank-you Kathleen

CHAPTER 1

INTRODUCTION

1.1 Styrene/Butadiene Copolymer

Copolymers of styrene/butadiene, commonly known as SBR, GR-S or BUNA-S, are the most important and widely used of all synthetic rubbers. The most significant application of styrene/butadiene copolymer is in the manufacture of automotive tires. It is also used in a large number of other, diverse applications including adhesives, hosing and tubing, belting, footwear, foamed products, sponge, wire and cable coatings, mechanical goods and water-proofed goods. The wide range of physical qualities required in these applications are achieved through the manipulation of copolymer structure at the polymerization stage or by altering the physical properties of the copolymer by post polymerization processing.

After the copolymer is formed, carbon black is often added to improve tensile strength and abrasion resistance. Oils may be compounded with the copolymer to decrease the viscosity of, or plasticize, a high molecular mass product and give it the more desirable qualities of a low molecular mass product at a lower cost. The copolymer may also be vulcanized. This entails the reaction of the copolymer with elemental sulphur to form intermolecular crosslinks which

increase the copolymer tensile strength and abrasion resistance. Other additives, such as anti-oxidants or pigments are also added after polymerization is complete.

Copolymer molecular structure is characterized by variables which Brydson [1981] grouped into two categories: macro-structural variables and micro-structural variables. The macro-structural variables include: copolymer composition, molecular mass distribution, molecular mass averages, degree of chain linearity and the extent of gel. Many physical properties such as glass transition temperature, tensile strength and hardness vary in a near linear relationship with the proportion of monomers incorporated in the polymer. For example, a copolymer with high styrene content is glassy, whereas a copolymer with high butadiene content is rubbery. Average molecular masses have been correlated with viscosity. It is generally accepted that a higher molecular mass polymer will have superior physical qualities, however lower molecular polymers are easier to process. A number of physical properties are attributed to molecular mass distribution. Narrow molecular mass distribution SBR is generally harder to process. Carbon black is more easily incorporated into broad distribution SBR. The degree of die swell during extrusion is also a function of molecular mass distribution. The degree of linearity, or conversly, the degree of branching as well as the extent of formation of micro-gel (cross-links resulting from reactions involving double bonds bound

in the copolymer) are also correlated with polymer physical properties. It is generally desired to minimize the extent of both of these phenomena.

The variables of copolymer chain micro-structure are the extent of cis, trans or vinyl (1, 2 addition) conformations of incorporated butadiene units and the distribution of monomers in the chain. While the ratio of cis:trans butadiene double bond conformation does not seem to have a strong effect on polymer quality, the amount of vinyl butadiene units is strongly related to the glass transition temperature of the polymer. The distribution of monomers in a chain has a significant effect on the polymer physical properties. In free radical processes, copolymers with randomly distributed monomer units are produced which have the properties desired in tire manufacture. Ideal block SBR copolymers made by the anionically initiated solution process have properties of both thermoplastic and elastomeric materials.

1.2 Process Description

Styrene-butadiene copolymer is presently manufactured commercially by solution and emulsion polymerization processes. The more recently developed solution process, employing anionic initiators, affords a greater degree of control over copolymer properties such as molecular mass, molecular mass

distribution, branching frequency and chain micro-structure. Under clean conditions, long linear polymer chains can be produced. Narrow molecular mass distributions (Mw/Mn = 1.5 to 2.0) are produced and it is possible to create ideal block copolymers. Multi-functional coupling agents may be used to produce T, X or even star-shaped branched molecules. A major disadvantage of the solution process is the higher cost associated with solvent recovery. Despite these known advantages and a significant technical potential, the production of solution SBR still represents a relatively small fraction of the total SBR production (about 15% as reported by Brydson [1981]).

The more established emulsion polymerization process was developed during the years spanning the second and Korean wars, when supplies of natural rubber were threatened. Two polymerization processes, the "hot" and "cold" processes, evolved over this time.

Early in the development of the emulsion SBR process, polymerizations were carried out at 50°C or higher. This was necessary to attain sufficiently high radical production rates. It was from this relatively high reaction temperature that the "hot" process took its name. Water soluble initiators such as potassium persulphate ($K_2S_2O_8$), benzoyl peroxide, cumene hydroperoxide and azobisisobutyronitrile (AIBN) were used. The mechanism of initiation with persulphates, which are the most common initiators, is unknown. Initiation

proceeds at a rate much lower than that expected from the thermal decomposition of the initiator. However, acceptable initiation rates are achieved when dodecyl mercaptans are added to the recipe. Mercaptans are primarily added as molecular mass modifiers, but they also promote radical production. The emulsifiers used in the "hot" SBR process are typically fatty acid or disproportionated rosin acid soaps or a mixture of these. Although the primary role of emulsifiers is to stabilize the emulsion, they can influence the physical properties of the final product, such as tack. At 50°C, the polymerization proceeds at approximately 5 or 6% conversion per hour and is terminated at a point in the range of 65 to 72% conversion. A typical "hot" (alternately, "mutual", "standard" or "GR-S" recipe is as follows:

Table 1.1

Representative "Hot" SBR Recipe

Butadiene	75	(phm)
Styrene	25	
n-Dodecyl Mercaptan	0.5	
$K_2S_2O_8$	0.3	
Soap Flakes	5.0	
Water	180	

A mass fraction of 23.5% styrene in the final products has been recognized (Brydson [1981]) as having the best overall properties for most purposes.

The polymer produced by the "hot" process is characteristically a highly branched polymer with a broad molecular mass

distribution (Mw/Mn = 4 to 6) and an undesirably large fraction of microgel. Efforts to improve the molecular mass properties of SBR led to the development of the "cold" SBR process.

In the early 1950's, the development of initiator systems which could produce large initiation rates at temperatures as low as -40°C made low temperature polymerization of SBR possible. SBR produced at 5°C has a much narrower molecular mass distribution, fewer branches per molecule, less gel and a desirably lower proportion of vinyl (1,2) butadiene units.

The initiating system which has ultimately become the most successful in cold SBR use is the sodium formaldehyde sulphoxylate/iron/p-menthane hydroperoxide redox couple. A typical recipe for cold SBR as given by Morton [1973], is:

Table 1.2

Representative "Cold" SBR Recipe

Butadiene	71	(phm)
Styrene	29	
t-dodecyl Mercaptan	0.18	
p-menthane hydroperoxide	0.08	
Ferrous Sulphate ($FeSO_4 \cdot 7H_2O$)	0.03	
Trisodium phosphate ($Na_3PO_4 \cdot 10 H_2O$)	0.50	
EDTA	0.035	
SFS	0.08	
Resin Acid Soap	4.5	
Water	200	

Ferrous sulphate provides iron ions which activate the initiators, p-menthane hydroperoxide. The mercaptan serves

strictly as a chain transfer agent in this recipe. Trisodium phosphate is used as a buffer. An alkali such as potassium hydroxide may be used to control pH (typically, pH = 10). Ethylenediaminetetraacetic acid, EDTA, is needed to complex iron ions to control their concentration. Additional ingredients such as surface active agents, like naphthalene sulphonate, used to supplement the emulsifier system, or small quantities of potassium chloride, used to reduce the viscosity of the emulsion, may be used. The polymerization is typically terminated at 60 to 65% conversion. At 5^{o}C in a batch, 60% conversion is achieved in approximately 12 hours.

Although some SBR is produced in batch and semi-batch reactors, by far the largest amount of emulsion SBR is produced in "cold" stirred tank ractor trains.

Historically, SBR was first produced in a batch reactor using the "hot" recipe. Isothermal batch reactors are still used in applications which do not require large production rates and can tolerate drift in composition and high levels of branching. For example, adhesives and coating latexes are produced in hot batches. To accommodate larger demands for tire rubber, continuous trains were employed. When redox initiation technology made low temperature polymerization possible, continuous trains were used to produce "cold" SBR. Presently, SBR trains may consist of 6 to 12, large well stirred compartmented reactors.

Semi-batch (or semi-continuous) processes are also

very important in SBR production. In such processes ingredients are added continuously over time without withdrawing any product. The feed streams may consist of monomers, emulsifiers or surfactants, water or modifiers in any combination. Initiators (or a solution of initiator) are usually added separately. Feed streams may also be pre-emulsified before addition. Through prudent choice of emulsifier feed rate particle size distributions may be controlled successfully. More importantly, semi-batch operation allows effective control of copolymer compositions. Also, depending upon the monomers and their feed rate policies, composition gradients may be obtained which give the particles a core-shell morphology.

1.3 Project Scope

Due to poor market prospects, production of SBR has reached a static level over the past decade. One of the keys to revitalizing the mature SBR industry will be an indepth understanding of the physical and chemical principles involved in the emulsion polymerization process. This understanding should provide insights that will remove present limitations and improve the product.

This thesis represents an initial step in a research program whose goal is to re-examine the production of emulsion SBR. The objective of this thesis is to develop a dynamic

computer model to simulate the production of SBR in batch, semi-batch and continuous flow reactors. It is desired that the model be general so that with minor modification and appropriate rate constants it could be used to simulate most Case 2 emulsion systems. Having developed the model, the objective is to test the model both qualitatively and quantitatively with available data from the literature. Inadequacies observed at this point will serve as a basis for re-evaluation of assumed mechanisms and perhaps lead to designed experiments to elucidate mechanisms or inadequately determined model parameters. A series of experiments which will rigorously test the present model is envisioned as the next step. These experiments will lead to a second and more sophisticated level of modelling. It is hoped that eventually a model will be developed which will represent a concise and relatively complete summary of fundamental and technical knowledge and will serve as a tool to suggest new directions for meaningful experimental work.

Chapter 2 of this thesis presents a review of relevant literature. The focus of the review is on the modelling of the fundamental mechanisms of emulsion polymerization and copolymerization. Pertinent SBR experimental work is also presented. A brief survey of emulsion copolymer models is given.

The development of the stirred tank emulsion copolymerization model is presented in Chapter 3. The defining

assumptions are presented and discussed as each equation is developed. The results of a parameter sensitivity study to discern the most important model parameters are given.

In Chapter 3 a number of qualitative and quantitative model checks, which verify certain model algorithms, are presented. Three sources of SBR data and two sources of styrene homopolymerization data are simulated.

In Chapter 5 a series of batch, continuous and semi-batch (semi-continuous) simulations are presented. Model predictions previously unverified are discussed qualitatively. The predictions are presented in the form of a case study to illustrate the model's predictive potential.

Chapter 6 restates the important conclusions of the thesis and recommends directions for future work.

CHAPTER 2

LITERATURE REVIEW

2.1 Introduction

The purpose of this chapter is to cite theories, mechanisms and experimental work which were instrumental in the development of the dynamic computer model. Furthermore, relevant work which will serve as a basis for discussion or for future improvements to the model will be presented. The emphasis of the following presentation is on the mathematical modelling of the phenomena involved in emulsion polymerization. The success or otherwise of the methods presented in the literature will be discussed.

The method of presentation is as follows. A cursory presentation of the most ideal case of emulsion polymerization will be given. Following this, subsequent subsections will examine certain aspects of emulsion polymerization, qualify or correct stated assumptions, present mathematical expressions and cite their use in the literature.

2.2 Fundamentals

2.2.1 General

The purpose of this subsection is to introduce the technical terms used in this thesis. The ideal case of the emulsion polymerization of a single water insoluble monomer

in a batch reactor is presented. Details important in the model development will be examined in subsequent subsections.

In an emulsion polymerization, an organic discontinuous phase is dispersed in water. Initially, monomer is dispersed as fine droplets by severe mixing in the water. Emulsifiers are added to stabilize the monomer droplet emulsion. An excess of emulsifier is added such that the water becomes saturated and small emulsifier aggregates, called micelles, are formed. The monomer is sparingly soluble in water such that its diffusion through the aqueous phase is not limited. An equilibrium distribution of monomer between droplets and micelles is achieved. An initiation system is added to the reacting mixture which forms radicals in the aqueous phase. These radicals react with a few of the aqueous phase monomer molecules to form oligomeric radicals. Eventually these radicals penetrate the organic/aqueous interface. Due to the large number of micelles typically formed, radicals only penetrate micelles and not monomer droplets. When a radical innoculates or "stings" a micelle, polymerization is initiated and conceptually a polymer particle is created or "nucleated".

In a batch reactor, the course of an emulsion polymerization is subdivided into three stages or intervals. Stage 1 is the period of particle nucleation. Stage 1 ends when all micelles disappear. Micelles disappear because: 1) they are transformed into polymer particles, or

2) they dissolve, diffuse to and stabilize growing polymer particles. The rate of increase of conversion of monomer to polymer increases during stage 1 as the number of particles increases. Stage 2 represents a period of constant volumetric growth of polymer particles. Stage 2 ends when monomer droplets disappear. While monomer droplets are present, it is assumed that the monomer concentration in the polymer particles is constant and at an equilibrium or "saturation" value. The radical concentration, in the absence of reactions with impurities and desorption of radicals from particles and assuming instantaneous mutual termination of two resident radicals, is ideally 1/2 radical per particle.

The third stage is characterized by a gradual decrease and eventual cessation of polymerization as the monomer in the particles is depleted by reaction. The three stages in emulsion polymerization are illustrated in Figure 2.1 taken from Rudin [1982].

The introductory review of Rudin [1982] or the more comprehensive reviews of Gardon [1970], Ugelstad, et al. [1976] or Friis, et al. [1982] are recommended for the interested reader.

2.2.2 Monomer, Water, Polymer Equilibria

An emulsion polymerization reaction mixture is dispersed in a maximum of four distinct liquid phases. These are: the aqueous, continuous phase, the polymer particle phase,

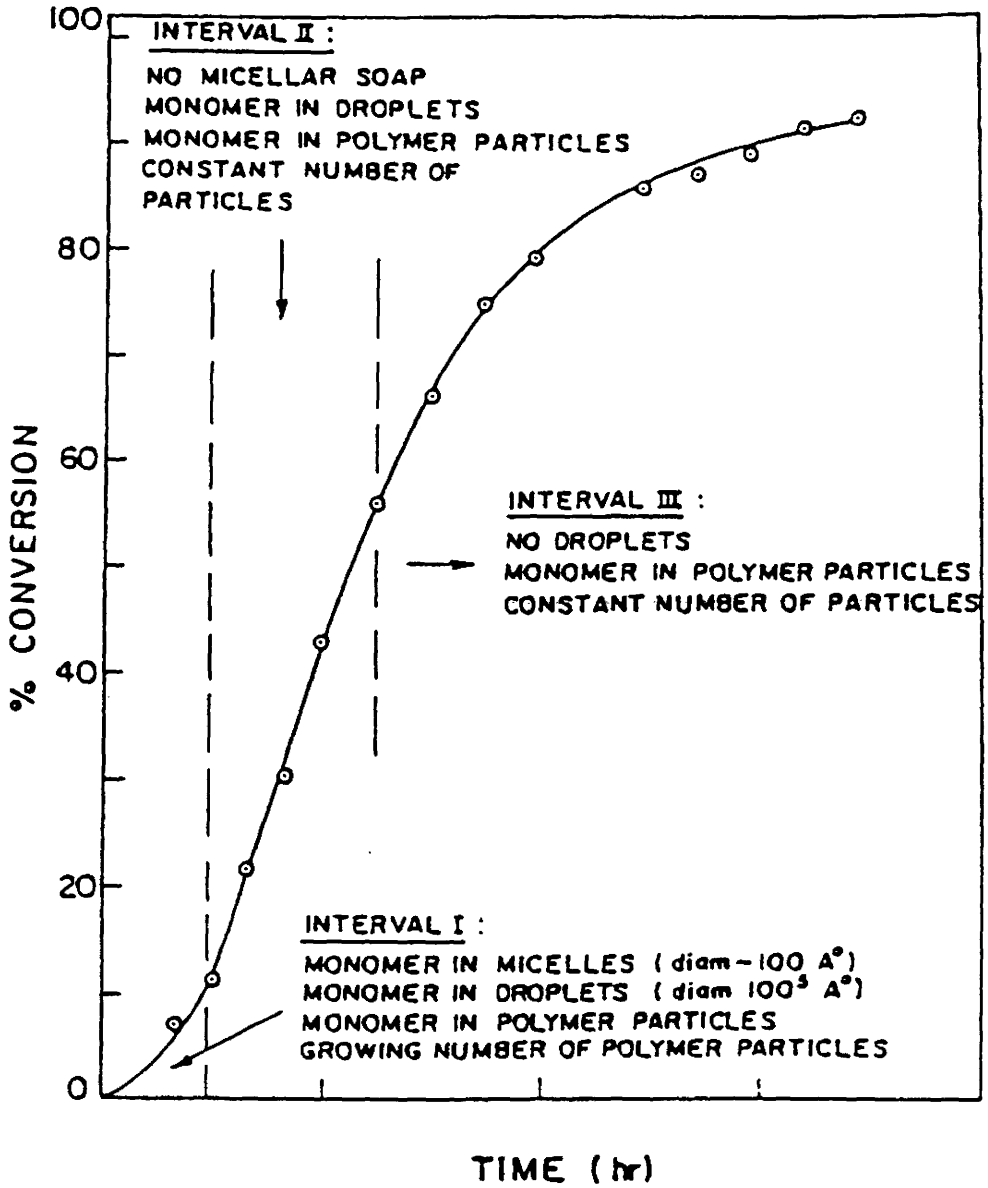

FIGURE 2.1 Course of an emulsion polymerization.

the monomer droplet phase and the micelle phase. The latter three mentioned phases collectively constitute the "organic" or "oil" phase. The nature and relative proportions of the four phases change over the period of polymerization. Micelles and monomer droplets disappear at the ends of stages 1 and 2 respectively and the polymer particles grow and then shrink after reaching a maximum volume at the end of stage 2.

Monomers are distributed among these phases. Knowledge of the concentrations of monomers in each phase is important in the modelling of an emulsion polymerization.

It is generally assumed that an equilibrium distribution of monomers exists between all phases. This assumption depends on the diffusion of monomers through the water phase not being limited by the low monomer solubility and the fact that a large surface area for diffusion exists between the organic and aqueous phases.

The concentrations of monomers in the water phase are typically disregarded in the ideal case. They may be estimated from the monomer solubilities in water but are, in fact, functions of the concentrations of other water phase organic species such as emulsifiers, mercaptans or other monomers. It is observed that during stage 3, the monomer concentration in the water phase remains close to its saturation value. The concentration of water in the organic phases is disregarded.

The polymerization of significantly water soluble monomers deviates from classical emulsion polymerization kinetics. Water phase polymerization and the concentration of water in the organic phases are important in such cases.

Styrene and butadiene both have very low solubility in water and generally conform to the ideal case.

The concentration of monomer in the micelles is dependent on the emulsifier type, emulsifier concentration, monomer type and aqueous phase electrolyte concentration. Generally, it is assumed that this concentration is equal to the monomer concentration in the particles.

The concentration of monomer in the polymer particles is commonly expressed as the volume fraction of monomer in the particles, ϕ_m, or conversly as the polymer volume fraction in the particles, ϕ_p ($\phi_p = 1 - \phi_m$). The proportion of monomers in the particles may be determined from a balance of the free energy of mixing of the monomer in the polymer and the interfacial free energy between the particle and the aqueous phase. On this basis, Morton, et al. [1954] developed the following expression for ϕ_p for a homopolymer system.

$$\frac{2\bar{V}_m\gamma}{rRT} = - [\ell n(1-\phi_p) + \phi_p + \chi \phi_p^2] \qquad (2.1)$$

All parameters used in equation (2.1) are defined in the Nomenclature section. Gardon [1968] has found that the value of the monomer-polymer interaction parameter, χ, lies in the

range 0.2 to 0.6 for most monomers. The interfacial tension, γ is a function of soap concentration, distribution of polar chain ends at the surface of the particles and electrolyte, mercaptan and monomer concentrations in the water phase. Gardon [1968] has extended Morton's equation to describe the partial swelling of polymer particles during stage 3 as well as the effect of intermolecular crosslinks. Crosslinks store elastic energy upon swelling and therefore must be considered in the energy balance.

A second level of complexity is introduced to the monomer concentration considerations when two monomers are involved. The monomers may not be equally soluble in the copolymer. Furthermore, one monomer may enhance or diminish the solubility of the other. Krigbaum, et al. [1954] developed a fundamental expression describing the equilibrium of a ternary phase of a polymer and two monomers with a binary phase of two monomers. Their expression can be applied to emulsion copolymerization if the activity of the monomers in the water phase is ignored. It should be pointed out that the expression of Krigbaum, et al. [1954] only specifies the ratio of monomers and not ϕ_p. Gardon [1968] outlines the use of the aforementioned equation.

There is a paucity of literature dealing with the distribution of monomers in the particles for the SBR system. The results of the few studies surveyed are summarized below.

Meehan [1949] performed emulsion polymerization

experiments with butadiene and styrene/butadiene in a 25:75 mass ratio at 30 and 50°C. Potassium persulphate was used as the initiator. The conclusions of these experiments were: 1) The mixture of monomers in the monomer droplets was essentially ideal. 2) For the butadiene homopolymerization experiments, the equilibrium of monomer between droplets and particles was tested and proven. 3) The conversion at which the styrene/butadiene monomer droplets disappeared, X_c, was approximately 52%. This value was independent of temperature over the range 30 - 50°C and independent of particle size and number. 4) Monomers appeared in both droplets and particles in essentially the same proportion. Meehan [1949] determined that slightly more styrene in proportion resided in the particles than in the droplets on closer examination.

Burnett, et al. [1970a] determined monomer to polymer mass ratios in the particles for styrene/butadiene in a mass ratio of 29:71 at 5, 15 and 25°C. They used a redox initiation system. They observed: 1) a pronounced decrease in the mass ratio of monomers to polymer during stage 2 of polymerizatin which they attributed to crosslinking; 2) that the conversion at the end of stage 2, X_c, decreased with increasing temperature and the observed range of X_c was 55 to 65%; 3) the particles were enriched in butadiene. The enrichment in butadiene of the particles increased in prominence with conversion. Burnett, et al. [1970a] suggested

that equilibrium may not have been attained during their experiments, accentuating their observed decline in the polymer phase monomer concentrations.

Gardon [1968] cites the data of Bovey, et al. who observed an occasional minimum in styrene composition in SBR polymerizations. Bovey, et al. suggested that this minimum may be due to a diffusion controlled supply of monometers to the particles. As an alternative, Gardon [1968] proposed that the observed minimum could be due to a change in polymer particle monomer composition with conversion. This proposition is not consistent however with the results of Burnett, et al. [1970a] who observed no minimum in composition along with a pronounced variation in particle monomer composition.

Gardon [1968] observed that the range of variation of ϕ_m during stages 1 and 2 is very narrow for many monomers. He concluded that using a constant value of ϕ_m should not lead to a significant error in predicting polymerization kinetics, particle size or molecular mass. Many emulsion polymerization models in the literature assume a constant ϕ_m. Over the course of polymerization, ϕ_m is given by:

$$\phi_m = \phi_m^{SAT} \quad , \text{ for } X < X_c \qquad (2.2)$$

and

$$\phi_m = \frac{(1-X)}{(1-X(1-\frac{\rho_m}{\rho_p}))} \quad , \text{ for } X > X_c$$

The parameter ϕ_m^{SAT} is the experimentally determined monomer volume fraction in the saturated particles.

Hansen, et al. [1979] and subsequently Hoffman [1982] have used equation (2.1) of Morton, et al. [1954] along with an empirical relationship for surface tension as a function of emulsifier concentration to estimate ϕ_m. Min, et al. (1974) altered the equation of Morton, et al. [1954] to consider the water solubility of monomer.

In copolymer systems, individual comonomer concentrations must be estimated. Friis, et al. [1982] outlined a procedure based on the approximation that the monomer composition in the particles equals the composition of total unreacted monomers in the reactor. Their method requires an estimate of ϕ_m. Hoffman [1982] applied the method of Friis, et al. [1982] along with a ϕ_m calculated using the equation of Morton, et al. [1954).

The alternative to estimating comonomer concentrations is to develop appropriate correlations from experimental data. Nomura, et al. [1982] have taken this approach for styrene/methymethacrylate polymerization.

2.2.3 Mechanisms of Radical Production

Redox Initiation

The initiating system of choice in cold SBR manufacture employs p-menthane hydroperoxide (PMH)/iron/sodium formaldehyde sulphoxylate (SFS). In an emulsion, PMH partitions between

the aqueous and organic phases, favouring the organic phase. Radicals are generated in the water phase by the reaction of PMH with a complex of Fe^{2+} - ethylenediaminetetraacetic acid (EDTA) which is strictly water soluble. The fact that PMH partitions between phases provides a constant source of peroxide in the water phase and consequently a relatively constant rate of radical generation. Complexing iron with EDTA limits the concentration of Fe^{2+} ion and also prevents undesirable side reactions such as the formation of $Fe(OH)_3$ or iron-fatty acid salts. EDTA is typically added in excess of its theoretical 1:1 ratio with iron because it aids in stabilizing the latex by complexing polyvalent ions.

The initiating mechanism is a redox reaction. The PMH is reduced to a radical and a negatively charged hydroxide species while the iron (2+) is oxidized to the iron (3+) state. The function of SFS is to reduce iron (3+) back to iron (2+). Uraneck [1968] has summarized this mechanism as follows:

$$ROOH + FeY^{-2} \xrightarrow{k_1} RO^{\cdot} + FeY^{-1} + OH^{-1} \qquad (2.3)$$

$$FeY^{-1} + SFS \underset{\leftarrow}{\overset{k_2}{\rightarrow}} FeY^{-2} + X^{+} \qquad (2.4)$$

$$RO^{\cdot} + M \xrightarrow{k_{pc}} ROM^{\cdot} \qquad (2.5)$$

where ROOH represents PMH, FeY^{-2} represents the Fe^{2+}. EDTA complex, FeY^{-1} represents the Fe^{3+}. EDTA complex, X^{+} represents the unknown oxidation product of SFS, $RO^{\cdot}$ represents

the peroxide radical and M represents a monomer unit.

Uraneck [1968] reports that equation (2.3) is representative of the redox reaction of a number of hydroperoxides. Also, the reaction rate appears to be independent of pH in the range 3.7 to 10.3.

The stoichiometry of reaction (2.4) is uncertain. Andersen, et al. [1965] have found that slightly less than one mole of Fe^{3+} is reduced per mole of SFS. Furthermore, both equilibrium and second order rate constants have been fit by Andersen, et al. [1965] to equation (2.4) equally well. There is no evidence that this reaction is reversible.

Andersen, et al. [1965] observed that radicals are produced in reaction (2.4). On this evidence, they proposed the following, more specific, reaction mechanism identifying the unknown reaction product of SFS.

$$Fe^{3+} + HOCH_2SO_2^- + OH^- \xrightarrow{k_2} Fe^{2+} + HCHOSO_2^-\cdot + H_2O \qquad (2.6)$$

Uraneck [1968] reports experimental evidence that equation (2.5) is correct for SBR polymerization.

Hoffman [1982] included the potassium persulphate (KPS)/iron/SFS redox couple in an emulsion copolymerization model. The kinetic basis of the redox couple was equivalent to equations (2.3), (2.4) and (2.5) with the exception that KPS rather than ROOH was considered. To simplify the

mathematical analysis, Hoffman [1982] assumed a "pseudo" steady state for ions. This may be expressed mathematically as:

$$\frac{d[Fe^{2+}]}{dt} << k_1 [Fe^{2+}][KPS] \approx k_2 [Fe^{3+}][SFS] \quad (2.7)$$

Since the total iron concentration in the water phase is constant, that is

$$[Fe]t,w = [Fe^{2+}]_w + [Fe^{3+}]_w \quad (2.8)$$

then expressions for $[Fe^{2+}]$ and $[Fe^{3+}]$ can be derived. For example,

$$[Fe^{2+}]_w = \frac{k_2[Fe]t,w\ [SFS]_w}{k_1\ [KPS]_w + k_2\ [SFS]_w} \quad (2.9)$$

The rate of initiation is calculated assuming equation (2.3) is the only reaction producing radicals; or

$$R_I = k_1\ [Fe^{2+}]_w\ [KPS]_w \quad (2.10)$$

Some error should be expected as a result of assuming a pseudo steady state hypothesis for ions. Penlidis [1982] modelled the KPS/iron/SFS redox system and showed that a steady state was achieved after 30 minutes of reaction. Considering that a typical reaction may last 700 minutes or more and that the nucleation period may be 100 minutes, it is possible that the error incurred because of the steady state hypothesis for ions is small.

Persulphate Initiation

Persulphates are widely used as initiators in commercial hot SBR recipes. In the emulsion polymerization of styrene the mechanism of initiation has been confirmed (Uraneck [1968]) to be the thermal decomposition of persulphate. It may be illustrated:

$$S_2O_8 \xrightarrow{k_d} 2\ SO_4^-\cdot \qquad (2.11)$$

$$SO_4^-\cdot + M \xrightarrow{k_{pc}} -SO_4\ M\cdot \qquad (2.12)$$

The rate of initiation is first order in persulphate concentration. Mercaptans, added as chain transfer agents, play no part in the initiation mechanism as evidenced by Kolthoff, et al. [1955]. They observed that the amount of persulphate incorporated in the polymer was independent of the amount of mercaptan present.

When butadiene is copolymerized with styrene, the rate of conversion of monomer to polymer is extremely small. Kolthoff, et al. [1947] found that at 50°C, a 75:25 (mass basis) mixture of butadiene and styrene reached a conversion of less than 2% after 12 hours. This low conversion rate has been observed in styrene/butadiene copolymerization for all ratios of styrene to butadiene except when styrene is in great excess. Similar observations have been made for other diene systems (Blackley [1975]). When a small amount of high molecular mass aliphatic mercaptan is added to the reacting

mixture, the conversion rate is increased dramatically. In a parallel experiment to that mentioned above, Kolthoff, et al. [1947] observed 70% conversion in 24 hours when 0.0005 parts per hundred monomer (pphm) of n-dodecyl mercaptan was added to the reacting mixture. When 0.005 pphm of the mercaptan was added, 70% conversion was obtained in 12 hours. The rate of conversion becomes practically independent of mercaptan concentration once a small amount of mercaptan has been added. Surprisingly the conversion rate is also independent of persulphate concentration over wide limits.

The promoting effect of mercaptans was studied by Kolthoff, et al. [1947]. They found that the promoting effect was at a maximum for aliphatic mercaptans of chain length 12. Also, normal mercaptans were found to be slightly better promoters than secondary or tertiary mercaptans. Using n-dodecyl mercaptan as a basis for comparison, Kolthoff, et al. [1947] categorized other mercaptans into two groups. The first group consisted of those mercaptans which are poor promoters of reaction. The second group consisted of mercaptans which interfere with reaction. Mercaptans of chain length greater than 12, generally fall into the first group. Shorter chain mercaptans fall into the second group. Kolthoff, et al. [1947] rationalized that the interfering ability of short chain mercaptans is due to their increased water solubility and radical forming ability enhancing the rate of

water phase termination.

Kolthoff, et al. [1947] detected that persulphate does activate some monomer molecules in styrene/butadiene mixtures, but they believed that these activated molecules are poor initiators of chain propagation.

Kolthoff, et al. [1951d] studied the reactions of persulphates and mercaptans in soap solutions. Mercaptans are oxidized by persulphates to disulphides. Kolthoff, et al. [1951d] observed that the oxidation rate was first order in persulphate concentration and independent of both the concentration and molecular mass of the mercaptan. The decomposition rate of persulphate was independent of mercaptan level. Kolthoff, et al. [1951d] developed a mechanism to explain their findings which considered the reaction of persulphate with fatty acid soap to form carboxylate radicals which subsequently reacted with mercaptans. Only at high pH (pH>13) were mercaptans suspected of reacting directly with persulphate.

The interaction between persulphate and mercaptan is often assumed to be a redox reaction. Uraneck [1968] states that many monomers are initiated with redox couples involving persulphates. However, he points out that reducing agents other than mercaptans do not significantly promote persulphate initiation in the styrene/butadiene system. The observations of Starkweather, et al. [1947] complement this fact. They found that a styrene/butadiene system initiated with

persulphate and activated with potassium ferricyanide was still markedly promoted by the addition of mercaptans.

Blackley [1975] presents the following tentative mechanism explaining the promoting ability of mercaptans,

$$S_2O_8 \xrightarrow{k_d} SO_4^-\cdot \qquad (2.13)$$

$$SO_4^-\cdot + HSR \xrightarrow{k_s} HSO_4^- + SR\cdot \qquad (2.14)$$

$$M + RS\cdot \xrightarrow{k_p} RSM\cdot, \text{ etc.} \qquad (2.15)$$

He points out that the uncharged radicals produced in equation (2.14) would be more easily captured by negatively charged micelles and particles than charged persulphate-ended radicals. Furthermore, Blackley [1975] proposes that equation (2.14) conforms with the overall stoichiometry of the mechanism of Kolthoff, et al. [1951d].

The following criticisms are offered on Blackley's mechanism. If the negative charge of the persulphate ended radicals hinders polymerization by preventing micellar capture of radicals, similarly slow rates of polymerization should be observed for styrene and indeed other systems. Furthermore, in claiming that equation (2.14) is consistent with the persulphate mercaptan oxidation reaction of Kolthoff, et al. [1951d], Blackley [1975] disregards the observed (Kolthoff, et al. [1947]) independence of persulphate initiated styrene/butadiene systems of the concentration of persulphate.

Most importantly, Blackley's mechanism does not link the presence of dienes and the reduced reaction rate.

A tentative mechanism for the initiation of dienes by persulphate with mercaptans is offered in Appendix A1.

2.2.4 Particle Nucleation

The ideal picture of particle nucleation presented is subsection 2.2.1 assumed particles were formed only when a radical entered a micelle. In fact, the events leading to the nucleation of a particle are complex and not well understood. It is conceived that in addition to entering a micelle, a radical may react with monomers in the water until it exceeds its solubility and precipitates. Alternately, growing water phase oligomers may flocculate to form an insoluble mass. It is assumed that emulsifier associates and stabilizes the newly formed polymer particles. These mechanisms are known as homogeneous nucleation mechanisms. The extent to which either micellar or homogeneous mechanisms contribute to the total number of particles varies from system to system. It is likely however that all mechanisms have some importance under varying conditions. Monomer and polymer solubility in water, monomer solubility in polymer, the nature and concentration of initiator and the nature and concentration of emulsifier are all important factors in governing the mechanisms of nucleation.

Homogeneous nucleation is commonly disregarded for

water insoluble monomers like styrene or butadiene. The rate of water phase polymerization is low for such monomers. It is assumed that radicals enter micelles before they grow to an insoluble length. Experimental evidence of Kolthoff, et al. [1951a] indicates that homogeneous nucleation does occur in the styrene/butadiene system to a small extent (approximately 0.8% conversion in 3 hrs. for the GR-S recipe of Table 1). Kolthoff, et al. [1951a] concluded, however, that micellar nucleation was the dominant mechanism of particle production for the SBR system. For this reason, the theory and modelling of homogeneous nucleation is not presented.

One approach to quantifying the micellar nucleation mechanism is to assume that radical absorption by micelles and particles is proportional to their respective surface areas. This is known as the collision theory. The rate at which radicals are captured by micelles, ρ_{cm}, for example, would be calculated:

$$\rho_{cm} = k_{cm} [R\cdot]_w \tag{2.16}$$

where the capture constant, k_{cm}, is given by:

$$k_{cm} = 4\pi C \sum_i r_{m,i}^2 N_{m,i} \tag{2.17}$$

where C is a proportionality constant, independent of particle size and $N_{m,i}$ is the number of micelles of radius $r_{m,i}$. Recent experimental evidence of Kao, et al. [1983] supports the collision theory for radical capture during stages 2 and 3.

Based on the collision theory and case 2 kinetics, Smith and Ewart (Friis, et al. [1982] or Ugelstad, et al. [1976]) developed expressions for the number of particles nucleated as a function of initiation rate and emulsifier level for the two extreme cases where: a) only micelles capture radicals, and b) micelles and particles compete for radicals in proportion to their surface areas. These two hypotheses gave the following relationship:

$$N_p = \alpha\left(\frac{R_I N A}{\mu}\right)^{2/5} (A_s[E])^{3/5} \qquad (2.18)$$

where $\alpha = 0.53$ for case a) and $\alpha = 0.37$ for case b).

The symbol μ represents the volume growth rate for particles of all sizes. These relationships differ only by their proportionality constants implying that if the true case is somewhat between these extremes, only a small error is incurred. Friis, et al. [1982] report that the dependencies shown in equation (2.18) have been observed in the styrene polymerization experiments of Gerrens but are not valid in general for systems in which the desorption of radicals is important.

It is of interest to note that Roe (Ugelstad, et al. [1976]) found the same dependencies of N_p on initiation rate and emulsifier level for case II systems as did Smith and Ewart. However, he assumed that particles were formed by the precipitation of polymeric radicals. This indicates that for monomers of low water solubility, nucleation may be modelled

adequately using either interpretation of physical events.

A more intuitive concept of radical absorption is based on diffusion theory. The absorption constant used in equation (2.16) is given in this case by:

$$k_{cm} = 4\pi D_w \sum_i r_{m,i} N_{m,i} \qquad (2.19)$$

where D_w is the diffusion coefficient of radicals in water. Ugelstad, et al. [1976] cite the experimental results of Fitch and Shih and Gatta and co-workers which support a first order dependence of absorption rate on particle radius.

The diffusion mechanism predicts that micelles and small particles should have larger capture rates per unit area than large particles. In conflict with this theoretical prediction, experimental evidence suggests that micelles are significantly less efficient in capturing radicals. Harada, et al. [1972] suggest that this observation may be due to: a) an energy barrier between radicals and micelles or b) significant radical desorption from micelles. From their experiments, Harada, et al. [1972] suggested that the ratio of radical capture by particles to capture by micelles, on an area basis, was 1.28×10^5. Ugelstad, et al. [1976] report a range of values for this ratio of 10^2 to 10^7 depending on the monomer type.

Ugelstad et al. [1976] have proposed a nucleation mechanism which considers diffusion with reaction. Because radicals are consumed in particles with a resident radical,

the concentration of radicals at the surface of such particles is low, enhancing the diffusion of radicals to these particles. This may explain the apparent radical capture efficiency.

Some of the emulsion polymerization models surveyed considered only stages 2 and 3. These models assumed a fixed number of particles of a predetermined, typically monodispersed, particle size distribution such as mgiht arise from a seeded latex. Of the models which did consider particle nucleation, the choice of mechanism generally reflects the monomer systems simulated. The following authors published models which only considered micellar nucleation: Nomura, et al. [1971] and Sundberg [1979] for styrene polymerization; Min, et al. [1979] for vinyl chloride; Nomura, et al. [1982] for styrene/methylmethacrylate; and Lin, et al. [1981] for styrene/acrylonitrile. Models for monomers with higher water solubility typically consider both homogeneous and micellar nucleation. For example: Kiparissides, et al. [1979] for vinyl acetate and the related models of Cauley, et al. [1982] for methyl methacrylate, and Pollock [1983] and Penlidis [1982] for vinyl acetate; Min, et al. [1974][1978] and the related models of Kirrilov, et al. [1978] and Schork [1981] for methylmethacrylate and Pramojaney [1982] for vinyl acetate; Hoffman [1982] for styrene/butadiene and acrylonitrile/butadiene; and Hoffman, E. J. [1984] for styrene/acrylonitrile.

2.2.5 Average Number of Radicals per Particle

A technical advantage of emulsion over solution polymerization stems from the high rates of polymerization which are obtained at low radical generation rates while simultaneously obtaining high molecular mass copolymer. This is attributed to the diminished frequency of radical termination resulting from the segregation of radicals in particles.

During stage 1 of polymerization, it is commonly believed that the average number of radicals per particle $\bar{n}$, is in the range of 0.667 to 1. This stems from the conception of radicals effectively entering only micelles because of the large number of micelles. Radicals may reside in a newly formed particle for a long time before a second radical enters to terminate the first. Ugelstad, et al. [1976] point out that since $\bar{n}$ typically has a lower value during stage 2 (1/2 or less) a maximum in polymerization rate should be observed near the end of stage 1. This maximum has not been observed experimentally. Instead, Ugelstad, et al. [1976] suggest that radicals enter particles with a radical more frequently than micelles (this is discussed in section 2.2.4) and as a result, $\bar{n}$ during stage 1 is probably at its stage 2 value.

The ideal case of emulsion polymerization, commonly referred to as Case II, assumes that a radical resides in a particle until a second radical enters and instantaneously terminates the first. The average number of radicals per

particle is consequently 1/2 during stages 2 and 3. Deviation from Case II behaviour is due to desorption of radicals from particles (constituting Case I behaviour), reaction with monomer and water soluble impurities, water phase termination, coalescence of particles and the possibility of more than one radical existing in a single particle (Case III behaviour).

Dynamic population balances can be written on the basis of the aforementioned phenomena for the numbers of particles with zero, one, two and more radicals per particle. The resulting differential equations are functions of particle numbers, particle volume and the rate constants for the appropriate chemical and physical phenomena. The solution of these equations may be greatly simplified with the application of a "quasi" or "pseudo" steady state hypothesis for radicals. The steady state hypothesis is applied in two ways. First, it is assumed that the rate of change of the number of radicals per particle with time is much faster than the same rate with volume. Second, the rate of production of radicals in the water phase and desorption of radicals from particles (i.e. the rate of radical appearance in the water phase) is not significantly different from the rate of radical entry into particles and water phase termination (i.e. the rate of radical disappearance from the water). Ugelstad, et al. [1976] give an excellent discussion of the applicability of the steady state hypotheses. Applying the steady state hypotheses

to the particle balances gives a series of simultaneous algebraic equations for particles with zero, one, two or more radicals. Assuming a monodisperse particle size distribution (PSD), Stockmayer [1957] and later, O'Toole [1965] solved the series of algebraic equations to give an expression for the average number of radicals per particle ($\bar{n}$). Their solution was:

$$\bar{n} = \left(\frac{a}{4}\right) \frac{I_m(a)}{I_{m-1}(a)} \tag{2.20}$$

where I_m and I_{m-1} are modified Bessel functions of the first kind and

$$a = (8\alpha)^{1/2} = \left(8 \rho_A \hat{V}_p / N_{pp} k_{tp} \right) \tag{2.21}$$

and

$$m = k_{de} \hat{V}_p / k_{tp} \tag{2.22}$$

All parameters are defined in the Nomenclature section. Stockmayer [1957], O'Toole [1965] and Ugelstad, et al. [1976] have proposed simpler solutions for $\bar{n}$ for special cases. Ugelstad, et al. [1967] have presented a very useful continued fraction approximation to the Bessel function solution of the form

$$\bar{n} = \left(\frac{1}{2}\right) \cdot \cfrac{2\alpha}{m + \cfrac{2\alpha}{1+m+\cfrac{2\alpha}{2+m+\cfrac{2\alpha}{3+m+\cfrac{2\alpha}{4+m+\ldots}}}}} \qquad (2.23)$$

This solution converges for all $\alpha \geq 0$, $m \geq 0$. Ugelstad, et al. [1967] also analyzed the effects of reabsorption of radicals and water phase termination on $\bar{n}$. They concluded that water phase termination did not have a significant effect on $\bar{n}$. Friis, et al. [1982] and Nomura, et al. [1983a] have reported experimental agreement with this conclusion. Nomura, et al. [1983a] have summarized the results of a number of experimental investigations from the literature, compared them to the predictions of the Bessel function solution and have concluded that this solution is largely valid.

Nomura, et al. [1983a] have considered the particle population balances for copolymers in which particles are differentiated by the number of resident radicals as well as by the identity of the radical's terminal unit. By defining homopolymer equivalent composite rate constants which are functions of monomer and polymer composition, Nomura, et al. [1983a] applied the Stockmayer-O'Toole Bessel function solution to copolymers. Their solution was used to successfully predict the emulsion copolymeriztion of styrene/methylmethacrylate. Friis, et al. [1982] pointed out that the

Stockmayer-O'Toole solution could be applied for copolymers directly if radical desorption were not important and if termination were diffusion controlled or a geometric mean of the homo and cross termination rate constants were used.

Gardon (Ugelstad, et al. [1976]) solved the unsteady state particle balances for a monodisperse latex of a homopolymer for which radical desorption was not important. His solutions were not significantly different from the Stockmayer-O'Toole solutions for the same problems. Ugelstad, et al. [1976] suggest that this is further evidence of the validity of the steady state hypothesis. Brooks [1980] has solved the unsteady state particle balances for monodisperse populations for the case in which radical desorption is significant. His conclusions were: that considering more than two radicals per particle is generally unnecessary and that the steady state hypothesis is valid at lower radical generation rates.

Min, et al. [1974][1978] developed partial differential equations representing the numbers of particles with zero, one, two or more radicals as functions of both time and volume. Their analysis was very thorough including: radical entry into and radical generation within the particles, radical desorption from and termination in the particles, particle coalescence, particle formation by micellar and homogeneous nucleation and inflow and outflow of radicals. Rather than solving the partial differential equations,

however, Min, et al. [1978] applied the steady state hypothesis and obtained a solution giving radical density per particle as a function of volume. Sundberg [1979], Lichti, et al. [1977] [1983] and Kiparissides, et al. [1981] have solved the partial differential particle balances to give distributions of particles with zero and one and, in the case of Kiparissides, et al. [1981], zero, one and two radicals per particle. To predict $\bar{n}$ they must sum elements of all particle size distributions. These methods are discussed in more detail in section 2.2.7.

A wide number of approaches have been taken to calcualte $\bar{n}$ in the literature models. Nomura, et al. [1971] simply used $\bar{n}=\frac{1}{2}$ in simulating styrene polymerization. Kiparissides, et al. [1979] used an approximate solution of the steady-state population balance equations presented by Ugelstad, et al. [1976]. Hoffman [1982] used the continued fraction method of Ugelstad, et al. [1967]. Kirrilov, et al. used the Stockmayer-O'Toole solution. Nomura, et al. [1982] and Lin, et al. [1981] solved the steady-state balances for particles with only zero or one radicals. Their solution was in the form of a quadratic formula.

2.2.6 Molecular Mass Distribution

As explained in Chapter 1, molecular mass properties are closely associated with the physical properties of

polymers. The elementary reactions which govern molecular mass development are: 1) propagation with monomer and polymer molecules; 2) transfer to monomer, polymer, and chain transfer agent (CTA); and 3) radical termination. These reactions are illustrated in section 3.1.

Polymers are large molecules by virtue of the fact that the rate of monomer unit addition (i.e. propagation) is much larger than the rate of dead polymer chain production (by transfer or termination reaction). For this reason, the propagation reaction is implicitly important in the molecular mass development without actually producing polymer chains. To control molecular mass, one must effect the relative rates of polymer forming reactions to propagation such as by adding a chain transfer agent or by varying the reaction temperature.

Termination reactions are often not considered important (Sundberg, et al. [1982], Friis, et al. [1974]) in the molecular mass development of emulsion polymers. Termination reactions occur less frequently due to the segregation of radicals in the particles. Transfer reactions are generally assumed to control the molecular mass development.

The molecular mass development (MMD) of commercially produced SBR is governed by transfer to chain transfer agent (Uraneck [1976]). Chain transfer agents (CTA s) are species which readily react with polymeric radicals. They liberate a hydrogen atom to the polymer radical and terminate the

radical's growth. In this process, the CTA becomes a radical and starts propagating a new chain. Uraneck [1976] presents a detailed discussion of the use of CTA s in SBR polymerization. The important observation and conclusions of his work are summarized as follows. Mercaptans, the CTA s typically used in SBR production are only slightly soluble in water. Their solubilities and rates of diffusion relative to the reaction rate and the diffusion rate of monomers may greatly influence their ability to control molecular mass. Since their concentration in the polymer particles may be diffusion controlled, stirring or changes in recipe or technique affecting CTA solubility may have a direct effect on the rate of the transfer reaction. For example, some emulsifiers have been observed to make CTA s more efficient. Uraneck [1976] proposes that CTA s diffuse through the water phase in association with emulsifiers and that apparently, some emulsifiers (specifically resin acid soaps) associate better with mercaptans. The techniques of pre-agitation and pre-emulsification have also been used to enhance CTA activity. Chain transfer reactivity is also affected by temperature, however diffusion limitations are more dominant. The pH of the aqueous phase may affect the transfer rate. Initiator molecules, notably p-menthane hydroperoxide, may react as CTA's. Their contribution is typically insignificant compared to the mercaptan transfer rates. The reader is

referred to Uraneck [1976] for further discussion.

In the transfer to polymer reaction, an oligomeric radical abstracts a hydrogen atom from a polymer molecule, terminating itself and creating a radical site midway along the polymer backbone. This new radical site propagates a long so-called tri-functional branch. Because the rate of transfer to polymer is dependent on polymer concentration, the rate of branch formation is constant during stages 1 and 2 of emulsion polymerization and increases drastically during stage 3 of polymerization as the concentration of polymer in the particle increases. Furthermore, since the concentration of polymer at the reaction site is higher in emulsion compared to bulk systems, it is expected that emulsion polymers should be more branched. The results of Friis et al. [1974] confirm this expectation. Poly (styrene) does not participate in transfer to polymer reactions due to a lack of labile hydrogen atoms. It is suspected, therefore, that tri-functional branches arise from the incorporated butadiene units in the SBR molecule.

Chain transfer agents are used commercially to decrease the degree of branching in SBR. It is conceived that the frequency of branch forming reactions is not changed, but rather that the CTA causes more molecules (of a shorter length) to be produced. Therefore, the number of branches per molecule is decreased.

Another form of branching observed in SBR as well as all other diene polymerizations is known as tetrafunctional branching or crosslinking. The mechanism proposed by Flory (Uraneck [1968]) for such branching involves the raction of a polymeric radical with an incorporated double bond of a dead polymer chain. This reaction results in a tri-functionally branched radical with the active site one bond length from the branch. This active site propoagates a second branch. Burnett, et al. [1973] proposed that crosslinking occurs by the coupling of tri-functionally branched molecules. They base their hypothesis on the observation that internal double bonds are effectively 1,2 - disubstituted ethylenes and consequently should have a low reactivity.

Tetrafunctional branching (or crosslinking) leads to the formation of huge molecules which appear in the polymer as an isoluble gel. Without CTA, the insoluble gel forms at very low conversions in SBR or other diene polymerizations. Chain transfer agents delay the formation of gel significantly. It is suspected that it does so in the same manner as it reduces tri-functional branching.

Because the rate of tetra-functional branching is dependent on polymer concentration, in an emulsion polymerization, it is expected that this rate is constant during stages 1 and 2 and increases during stage 3. Uraneck [1968] reports experimental observation of constant levels of crosslinking during stages 1 and 2. Burnett, et al [1973] report the onset

of predominant crosslinking in the conversion range 52-57% which corresponds to approximately the end of stage 2. It should be noted that the sharp increase in tetra-functional branch frequency may be accentuated by increased diffusional resistance for CTA in the water once the monomer droplets have disappeared.

Mitchell, et al. [1948] noted that the formation of gel was delayed and the degree of linearity increased as the proportion of styrene in the copolymer was increased. This reflects the decreased proportion of both labile hydrogens and incorporated double bonds associated with bound butadiene, affecting tri- and tetra-functional branching respectively.

On the basis that transfer to CTA controls the molecular mass development of SBR (Uraneck [1976]), Hoffman [1982] modelled the SBR molecular mass distribution (MMD) using the equations for linear polymers:

$$w(r) = r\,\tau^2 \exp(-r\tau)$$

$$\tau = \frac{R_{fx}}{R_{fx}+R_p} \qquad (2.24)$$

where r is the number of repeat units per molecule, R_{fx} is the rate of CTA disappearance and R_p is the rate of polymerization. Hoffman [1982] estimated intrinsic viscosity using the Mark-Houwink equation and an estimate of the viscosity average degree of polymerization based on equation (2.24). He also

considered the effects of diffusion controlled transport on chain transfer reaction rate using an empirical correlation.

This approach may be adequate for cold SBR, however when considering polymerizations to high conversion or at higher temperatures, branching reactions must be considered.

The mathematical analysis of the MMD of branched polymers is complicated. Full distributions have not, as yet, been solved for analytically. Instead, molecular mass averages are predicted from the analysis of the moments of the molecular mass distribution. Moment analyses have been published by Min, et al. [1974][1978], Friis, et al. [1974] and Hamielec [1981][1982a]. Hamielec [1981] also refers to the work of Graessley, et al.. Molecular mass moment equations have been used in the emulsion polymerization models of Pollock [1983], Penlidis [1982] and Pramojaney [1982]. By defining "pseudo" or composite rate constants which are functions of monomer and polymer compositions and the kinetic constants of homo and cross polymerization, Hamielec [1982b][1983] has extended the homopolymer moment equations to copolymerization. This approach is taken in the present model. The required equations are summarized in Section 3.2.8.

2.2.7 Particle Size Distribution

Polymer particles in an emulsion polymerization generally have a distribution of sizes. This distribution is

due to two factors. Firstly, particles nucleated over a prolonged period of time will be of different sizes as a result of their different durations of growth. Secondly, particles of the same size will have a statistical distribution of periods of radical residence and growth. Furthermore, larger particles will have a broader distribution of radical residence periods.

Experimentally determined particle size distributions (PSD s) can serve as "fingerprints", providing clues for the identification of basic mechanisms. Theoretical predictions are useful in analyzing experimental PDS s as illustrated by the work of Lichti, et al. [1983] who postulated a nucleation mechanism based on fitting theoretical PSD s to experimental ones. Particle size distribution plays an important role in controlling latex properties such as bulk viscosity. It is important, therefore, to be able to manipulate PSD s for polymers used as paints, adhesives and spray coatings.

The coalescence of particles, which has not been widely studied, may play an important and, indeed, controlling role in the development of PSD s. In most of the modelling approaches surveyed, it is assumed that enough emulsifier is present to completely stabilize the particles. The accuracy of this assumption is vitally important to the success and validity of PSD models.

The simplest approach to modelling the PSD is to assume all particles are of the same size (monodisperse).

The volume of a single particle is calculated with the knowledge of the total volume or mass of polymer and an estimate of the number of particles. Particles are generally assumed spherical so that particle radii and surface areas are calculated easily from particle volume.

The assumption of a monodisperse PSD is widely applied in the literature. It is typically justified on the basis of particle nucleation times being very short compared to particle growth times or by restricting the model's use to stages 2 and 3 of polymerization and assuming a monodisperse seed latex.

Nomura, et al. [1971], Nomura, et al. [1982] and Lin, et al. [1981] have presented monodisperse PSD models which adequately predicted their respective experimental results. The models of Ballard, et al. [1981] and Hoffman [1982] also assumed monodisperse PSD's.

To consider a full PSD, a population balance on particles must be employed. The general form of such a population balance as presented by Kiparissides, et al. [1981] is:

$$\frac{\partial n(\underline{z},t)}{\partial t} + \nabla\cdot\dot{\underline{z}}n(\underline{z},t) = f(\underline{z},t) \qquad (2.5)$$

where $N(\underline{z},t)$ is a number density function, $\underline{z}$ is a vector of particle properties or states, $\dot{\underline{z}}$ represents the rate of change of a particle of state $\underline{z}$ and $f(z,t)$ represents the net generation rate of particles.

Dickinson (Kiparissides, et al. [1979]) and more recently Kiparissides, et al. [1979], Pollock [1983] and Penlidis [1982] have used balances which classify populations of particles by their birth or nucleation time, τ (i.e. $z = \tau$). Each class of particles has properties such as volume, monomer concentration, or average number of radicals per particle, $\bar{n}$, which correspond to their age and conditions in the reactor during their residence. Equations of the form (2.25) were solved for total particle number, volume, surface area and diameter as well as for conversion and molecular mass moments. Particle size distributions are derived from the knowledge of particle number and volume for every age class of particles. The works of Kiparissides, et al. [1979] and Pollock [1983] give detailed developments.

Another approach to applying population balances is to differentiate particles of a population according to their size (i.e. $z=v$). This method is outlined in detail by Min, et al. [1974]. Their development is notable in that it considers particle coalescence. Rather than apply and solve the complete population balance, Min et al. [1978] wrote equivalent expressions for the leading integer moments of the PSD. These are ordinary differential equations and are easily solved. To obtain a PSD, Min, et al. [1978] recommended using estimates of the mean size and distribution dispersion from the moment analysis with a predetermined distribution form.

The size oriented population balance has also been applied to distributions of particles of specific radical density (i.e., $\underline{z} = (N_i, V)^T$). Equations are written for numbers of particles, N_i, with i = 0, 1 and sometimes 2 radicals per particle. Solution of these partial differential equations yields distributions for particles of a given size (V) and radical density. The overall distribution is obtained by summing the individual distributions. An estimate of $\bar{n}$ can be obtained using:

$$\bar{n} = \frac{\sum_{i=0}^{\infty} i\, N_i(V)}{\sum_{i=0}^{\infty} N_i(V)} \qquad (2.26)$$

This approach has been applied successfully by Sundberg [1979], Lichti, et al. [1983] who included radical desorption and Hoffman, E. J. [1984] for particles with either 0 or 1 radical per particle and by Kiparissides, et al. [1981] for particles with 0, 1 or 2 radicals per particle. Sundberg [1979] outlines this particular method in detail.

2.2.8 Diffusion Controlled Kinetics

The translation of macro-radicals through a monomer/polymer solution becomes diffusion controlled as the concentration of polymer increases. Initially, only termination reactions between macro-radicals are retarded. Radical concentrations increase as a result, causing an increase in the

rate of conversion. In an emulsion polymerization, termination reactions may be diffusion controlled from inception since the particles, the sites of reaction, consist of monomer saturated polymer in proportions corresponding to conversions of 20 to 70%. However, since the particles remain saturated throughout stages 1 and 2, a constant termination rate is maintained whether termination is diffusion controlled or not.

As the polymer concentration increases further, polymer molecules may become so severely entangled that they become effectively "frozen". Active radical chain ends are restricted to move only by propagation. The rate of the termination which falls progressively during the initial stages of diffusion control, reaches a plateau at this point. The rate of conversion subsequently decreases along with the decrease in monomer concentration.

As the polymer concentration increases even further, the diffusion of small molecules becomes controlled and the conversion rate decreases dramatically. If the reaction temperature is below the glass transition temperature, Tg, of the polymer, a point may be reached where the monomer/polymer mixture forms a glass and polymerization effectively ceases at conversions below 100%. Soh, et al. [1982a] and Marten, et al. [1979] give good accounts of the phenomena of diffusion controlled termination and propagation.

The degree to which diffusion controlled kinetics

affect the conversion history and molecular mass development varies from system to system. Furthermore, all of the previously outlined phases of diffusion controlled kinetics may not manifest themselves in every case. Since most SBR is produced in CSTR trains with a terminal conversion between 60 to 70%, the copolymer has a very low glass transition temperature and the latex particles are typically very small, diffusion controlled kinetics are not important in SBR manifacture. However, for "hot" SBR recipes reacted to high conversions, particularly recipes requiring a high proportion of styrene, diffusion controlled kinetics may be important.

Assuming that termination reactions become diffusion controlled after a critical conversion and a critical molecular mass associated with the onset of chain entanglement, Marten, et al. [1979] applied the free volume theory of Bueche [1962] for the diffusion coefficient of a polymer to derive an expression for the termination constant. For emulsion polymers, their analysis is simplified by ignoring the molecular mass dependence of the termination constant. This is rationalized by the observation (Harris, et al. [1982], Sundberg, et al. [1982]) that molecular masses are typically controlled by transfer reactions at lower conversions in emulsion polymerization and that molecular masses are relatively constant over much of the conversion history. Soh, et al. [1982a] have expressed concern over the nature and extent of chain length (molecular mass) dependence of the

diffusion controlled termination constant in bulk polymerization. They belive that the inadequacy of many published models to predict mass average molecular mass stems from the neglect of this chain length dependence. They also point out, however, that chain length dependence is hard to prove experimentally. The final expression for the diffusion controlled termination constant for emulsion polymerization, as given by Harris, et al. [1982], is a function of the value of the termination constant and free volume of the saturated particle and an adjustable parameter. Soh, et al. [1983a] present an alternative analysis for diffusion controlled termination.

Lord [1984] has extended the free volume analysis of Marten et al. [1979] for copolymerization. For diffusion controlled termination, Lord [1984] and Friis, et al. [1982] argue that only a single termination constant need be estimated since termination is diffusion controlled from inception. The equation of Harris, et al. [1982] is, consequently, appropriate for copolymers.

The effects of diffusion controlled termination influence the calculation of the average number of radicals per particle, $\bar{n}$. Friis, et al. [1973], Harris, et al. [1982] and Sundberg, et al. [1982] used the diffusion controlled termination constant value in the Stockmayer-O'Toole equation (equation (2.21)) to calculate $\bar{n}$. It should be noted that the steady state hypothesis for radicals was applied in

deriving this equation. Chiu, et al. [1982] object to this practice. Their argument is that if termination is diffusion controlled, the steady state hypothesis cannot be correct. They further object to the assumption that termination and propagation become diffusion controlled only after a critical free volume (or conversion). They proposed a model in which diffusion was considered throughout the reaction and in which the steady state hypothesis (SSH) was not applied. Though their model predictions of radical concentration and number and mass average molecular masses differed at high conversions from an equivalent model with the SSH, the conversion predictions of the two models were identical.

Sundberg, et al. [1982] modelled the period of "diffusion by propagation" by simply limiting the fall of the termination constant to a minimum value. Stickler [1983] applied the Smoluchowski equation for diffusion to derive an expression for the termination constant proportional to the product of the propagation rate constant and the monomer concentration, $k_p [M]_p$. Soh, et al. [1982b] have derived a similar equation in a slightly different manner.

Marten, et al. [1979] developed an expression for diffusion controlled propagation based on diffusion theory. Lord [1984] has extended their analysis for copolymerization. Four propagation constants must be considered of which all may become diffusion controlled at different times. Lord [1984] has shown that only two critical points of diffusion

controlled propagation need be determined. These are the points at which the fastest propagation reaction with each monomer type becomes diffusion controlled. Lord [1984] has successfully tested his algorithm with styrene/acrylonitrile experimental data.

Diffusion controlled kinetics have not been considered in most of the emulsion polymerization models published. Min, et al. [1978], Kirrilov, et al. [1978] and Friis, et al. [1973] have accounted for diffusion controlled termination using empirical correlations. Hoffman, E. J. [1984] has applied the analysis of Lord [1984] to the emulsion copolymerization of styrene/acrylonitrile.

2.3 Emulsion Copolymer Model Survey

In the previous sections of this chapter, approaches to modelling the physical and chemical phenomena of emulsion polymerization have been outlined. Both homopolymer and copolymer cases have been considered. In this section, a short survey of emulsion copolymer models will be presented.

Hoffman [1982] has presented perhaps the most complete emulsion copolymerization model. He considered the isothermal batch, semi-batch (semi-continuous) and continuous (CSTR) production of styrene/butadiene and acrylonitrile/butadiene copolymers. A redox initiation mechanism was assumed. Particle nucleation was assumed to occur by both heterogeneous (micellar) and homogeneous mechanisms. The homogeneous

nucleation algorithm of Hansen, et al. [1979] was employed. Water phase propagation, termination and reaction with impurity were considered. In estimating the average number of radicals per particle, $\bar{n}$, radical desorption from particles was disregarded, but reactions with a monomer soluble impurity were included.

Particles were assumed to all be of the same size (monodisperse). The volume fraction of monomer in the particles was calculated using the equation Morton, et al. [1954]. The concentration of each monomer in the particles was estimated from the ratio of unreacted monomers in the reactor after Friis, et al. [1982].

Transfer to chain transfer agent was assumed to control the molecular mass development thereby allowing the adoption of a development for linear polymer. Provision was made to empirically account for the diffusion limited concentration of CTA. The model predicted conversion, copolymer composition and intrinsic viscosity (as a measure of molecular mass).

Nomura, et al. [1982] developed an isothermal batch reactor model which they applied to the emulsion copolymerization of styrene/methylmethacrylate. Their model did not consider water phase reactions. Particle nucleation was also disregarded; monodisperse seed latexes were assumed. To estimate $\bar{n}$, Nomura, et al. [1982] wrote population balances for each monomer-ended radical type, applied the steady-state

hypothesis for radicals and, assuming instantaneous termination, solved the resulting recursion relations for particles with 0 or 1 radicals. In the aforementioned particle balances, they assumed only monomer radicals could desorb and that there was no difference between radicals with or without an incorporated initiator fragment.

Monomer concentrations were calculated with empirical correlations. In developing these correlations, Nomura, et al. [1982] found that concentration was a very weak function of particle size, composition, ionic strength and interfacial tension.

As presented, the model was to be used to estimate radical desorption constants.

In a more recent publication, Nomura, et al. [1983b] expanded their model by including a micellar nucleation mechanism. Their model predicted particle number, conversion and copolymer composition. In general they found their conversion and particle number predictions adequate, however, they noted that the lack of accounting for diffusion controlled termination limited the model's predictions to lower conversions.

Ballard, et al. [1981] have presented an isothermal batch copolymer model for stages 2 and 3 of emulsion polymerization. Their model has been used to simulate styrene/methylmethacrylate and styrene/butadiene copolymerizations. Their model solves the dynamic population balance equations,

assuming a monodisperse seed latex, for particles with 0 or 1 "A" or "B" ended radicals (where "A" and "B" are the two comonomer species). The mechanisms of entry, desorption, propagation, transfer and termination are all included in the aforementioned particle balances. They also outline a procedure for averaging the rate constants of the previously mentioned mechanisms for use with a homopolymer particle balance.

Ballard, et al. [1981] solve differential equations for copolymer composition and copolymer sequence distributions (CSD s). The CSD s are defined as the relative number of contiguous sequences of one of the comonomers in the copolymer.

The model of Lin, et al. [1981] is based on the previously presented model of Nomura, et al. [1982]. Lin, et al. simulated the isothermal batch copolymerization of styrene acrylonitrile at the azeotropic composition. They ignored water phase reactions in spite of the high water solubility of acrylonitrile. They also assumed diffusion processes do not control polymerization and only monomer radicals desorb. The calculation of $\bar{n}$ is identical to that of Nomura, et al. [1982]. Particles are assumed monodisperse. The nucleation period was modelled empirically using a linear relationship. Monomer concentrations are assumed constant up to the end of stage 2 are depleted. The viscosity average degree of polyization is estimated for the copolymer.

Lin, et al. [1981] report that their model predictions

are adequate at low conversions until the effect of diffusion controlled termination becomes important.

The model of Hoffman, E. J. [1984] was developed to simulate the isothermal batch and semi-batch copolymerization of styrene/acrylonitrile. This model accounts for both micellar and homogeneous nucleation mechanisms. The homogeneous nucleation mechanism of Hansen, et al. [1979] is applied. Water phase reactions are also accounted for.

The concentrations of monomers in the particles are estimated from a correlation obtained from previously collected thermodynamic data. The model is not restricted to simulating azeotropic copolymerization and accounts for diffusion controlled ractions after Lord [1984].

Kalfus, et al. [1978] have presented a copolymer composition equation which forms the basis of an isothermal batch or semi-batch model for SBR polymerization. This equation is based on the reaction scheme attributed to Alfrey which considers the effects of the penultimate monomer unit on the reactivity of polymeric radicals. In their scheme, Kalfus, et al. [1978] assume the chain structure effects the reactivity of the radical rather than the penultimate monomer unit. They catagorize chain structures into two groups, "straight" and "entangled". After a critical polymer concentration, polymeric radicals become "entangled" and react more slowly than "straight" radicals. Kalfus, et al. [1978] attribute this change in reactivity mainly to diffusion

controlled termination, but stress that other factors are also lumped into this change. The constants used in their model are fit empirically and have no physical significance. They assume constant monomer concentrations in stage 2 and estimate the relative amounts of each monomer in the particles based on the overall ratio of unreacted monomers.

An interesting aspect of their work is that Kalfus, et al. [1978] investigated the effects of "dosing" or adding some of the faster reacting monomer during polymerization to maintain a constant composition. This topic will be discussed in Chapter 5 of this work.

The following chapter presents the development and discussion of an emulsion copolymerization model for SBR which has been developed largely on the material presented in this chapter.

CHAPTER 3

MODEL DEVELOPMENT

3.1 Introduction

This chapter develops all of the equations used in the dynamic stirred tank emulsion copolymerization reactor model. The assumptions used are stated as each equation is developed. The required symbols are defined in the Nomenclature section. Values or expressions for the fundamental constants used in the model are given in Appendix B1. Listings of the computer model and appropriate documentation are provided in McMaster Institute for Polymer Production Technology Technical Report # M1PPT-B-001.

The model is based on the following elementary chemical reaction scheme.

1. Redox Initiation

$$ROOH + Fe^{2+} \xrightarrow{k_1} RO\cdot + Fe^{3+} + OH^- \qquad (3.1)$$

$$Fe^{3+} + SFS \xrightarrow{k_2} Fe^{2+} + X^+ \qquad (3.2)$$

Initiation reactions take place in the water phase. Redox initiators are used to initiate polymerizations at low temperatures ($5^{\circ}C$). The symbol ROOH represents a hydroperoxide. P-menthane hydroperoxide, shown below, is commonly used in SBR recipes.

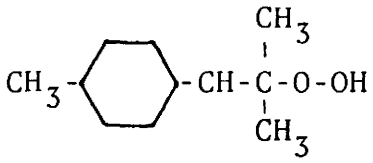

p-menthane hydroperoxide

The product X^+ represents the unknown oxidation product of the reducing agent, sodium formaldehyde sulfoxylate, SFS. Iron ions are provided by ferrous sulphate septahydrate ($FeSO_4 \cdot 7H_2O$). The complexing agent, EDTA (see section 2.2.3) is ignored in this case.

2. Thermal Initiation

$$I_2 \xrightarrow[\Delta]{k_d} 2I\cdot \qquad (3.3)$$

The sybol I_2 represents a water soluble initiator, typically potassium persulphate ($K_2S_2O_8$). The thermal initiation rate of SBR is not represented by equation (3.3). A tentative initiation mechanism for SBR is presented in Appendix A1. Equation (3.3) is appropriate for styrene homopolymerization.

The following reactions all take place within the polymer particles.

3. Propagation:

i) with monomer

$$\sim S\cdot + S \xrightarrow{k_{pss}} \sim SS\cdot \qquad (3.4)$$

$$\sim B\cdot + S \xrightarrow{k_{pBs}} \sim BS\cdot \qquad (3.5)$$

$$\sim S\cdot + B \xrightarrow{k_{psB}} \sim SB\cdot \qquad (3.6)$$

$$\sim B^{\cdot} + B \xrightarrow{k_{pBB}} \sim BB^{\cdot} \qquad (3.7)$$

The symbol $\sim$ represents a macro molecule. It is assumed that the reactivity of a macro-radical depends only on the identity of its terminal monomer unit. Effectively all of the monomer is consumed by propagation reactions. Therefore, the overall reaction rate is determined by the sum of the rates of the above propagation reactions.

ii) with polymer

$$\sim B^{\cdot} + \sim\!=\!\sim \xrightarrow{k^{*}_{pB}} \sim_{B}{}^{\cdot}\!\sim \qquad (3.8)$$

$$\sim S^{\cdot} + \sim\!=\!\sim \xrightarrow{k^{*}_{ps}} \sim_{S}{}^{\cdot}\!\sim \qquad (3.9)$$

The above expressions ((3.8) and (3.9)) represent the reactions of a polymer radical with an internal double bond of a dead polymer chain. The branched polymer radicals formed in these reactions propagate further to form tetra-functionally branched polymer molecules. The rate of tetra-functional branching, commonly referred to as crosslinking, depends on the rates of expressions (3.8) and (3.9). It should be noted that the internal double bonds may exist in three different conformations (cis, trans and 1,2) and therefore there may be three different rate constants for each of (3.8) and (3.9).

4. Chain Transfer

In emulsion polymerization, polymer molecules are made predominantly by transfer reactions.

i) to monomer

$$\sim S^{\cdot} + S \xrightarrow{k_{fss}} \sim S + S^{\cdot} \qquad (3.10)$$

$$\sim S^{\cdot} + B \xrightarrow{k_{fsB}} \sim S + B^{\cdot} \qquad (3.11)$$

$$\sim B^{\cdot} + S \xrightarrow{k_{fBs}} \sim B + S^{\cdot} \qquad (3.12)$$

$$\sim B^{\cdot} + B \xrightarrow{k_{fBB}} \sim B + B^{\cdot} \qquad (3.13)$$

In the temperature range of SBR processes, transfer to styrene radicals (equations (3.10) and (3.12)) is negligible.

ii) to polymer

$$\sim S^{\cdot} + \overset{H}{\sim S\sim} \xrightarrow{k_{fpss}} \sim SH + \overset{\cdot}{\sim S\sim} \qquad (3.14)$$

$$\sim S^{\cdot} + \overset{H}{\sim B\sim} \xrightarrow{k_{fpsB}} \sim SH + \overset{\cdot}{\sim B\sim} \qquad (3.15)$$

$$\sim B^{\cdot} + \overset{H}{\sim S\sim} \xrightarrow{k_{fpBs}} \sim BH + \overset{\cdot}{\sim S\sim} \qquad (3.16)$$

$$\sim B^{\cdot} + \overset{H}{\sim B\sim} \xrightarrow{k_{fpBB}} \sim BH + \overset{\cdot}{\sim B\sim} \qquad (3.17)$$

The radicals formed in equations (3.14) through (3.17) by the abstraction of hydrogen atoms from a dead polymer chain by a macro radical propagate a trifunctional branch. The rate of trifunctional branch production is governed by the rates of the transfer to polymer reaction.

The rate of reactions involving the abstraction of a hydrogen atom from an incorporated styrene unit is negligibly small in the temperature range of interest.

iii) to chain transfer agent (X)

$$\sim S^{\cdot} + X \xrightarrow{k_{fsx}} \sim S + X^{\cdot} \qquad (3.18)$$

$$\sim B^{\cdot} + X \xrightarrow{k_{fBx}} \sim B + X^{\cdot} \qquad (3.19)$$

Chain transfer agents are molecules which readily give up a hydrogen atom to terminate a macro radical and form a transfer radical. These reactions provide a mechanism for controlling molecular mass development.

5. Termination

Termination reactions are not assumed important in the molecular mass development of emulsion polymers. They are important, however, in determining $\bar{n}$. Since it is not crucial to know the exact mechanism of termination for this purpose, none was specified in this model.

3.2.1 Distribution of Species between Phases

The reacting species in an emulsion polymerization are partitioned between the monomer, polymer and aqueous phases. Initiation reactions take place in the water phase. Polymerization reactions take place in the polymer phase. The concentrations of each species in the phase of interest

are required before reaction rates can be estimated.

It was assumed that all organic soluble materials are distributed in equilibrium amounts in all three phases. This is supported by the assumption of a perfectly stirred reactor. It is recognized, however, that the diffusion of chain transfer agent through the aqueous phase may be limited and that the following analysis may not appropriately account for the distribution of CTA.

It is also assumed that the monomer concentrations in the particles are independent of particle size.

Partition coefficients of the following form are used in the model.

$$K_{imw} = \frac{[i]_m}{[i]_w} \quad ; \quad K_{iwp} = \frac{[i]_w}{[i]_p} \tag{3.20}$$

K_{imw} and K_{iwp} are the partition coefficients between monomer and water and water and polymer phases respectively; $[i]_j$ is the concentration of species "i" (i = S,B,X and I) in phase "j" (j = m,w or p). Expressions for concentrations or molar flows of interest are obtained as follows.
A mass balance for the total moles of initiator in the reactor gives:

$$N_I = [I]_m V_m + [I]_w W_w + [I]_p V_p \tag{3.21}$$

If the concentration of initiator in the water phase, $[I]_w$,

were of interest, one could substitute for $[I]_m$ and $[I]_w$ in terms of $[I]_w$ using equations of the form (3.20). Solving for $[I]_w$ gives:

$$[I]_w = \frac{N_I}{K_{Imw} V_m + V_w + V_p / K_{Iwp}} \tag{3.22}$$

Any concentration of interest may be calculated in the same manner, for example:

$$[S]_p = \frac{N_s}{K_{smw} K_{swp} V_m + K_{swp} V_w + V_p} \tag{3.23}$$

Concentrations can also be calculated using the same procedure, from molar and volume flow rates. For example,

$$[S]_p = \frac{F_s}{K_{smw} K_{swp} v_m + k_{swp} v_w + v_p} \tag{3.24}$$

Equating (3.23) and (3.24) provides a convenient expression for molar flow rates of the form:

$$F_s = N_s \cdot \frac{K_{smw} K_{swp} v_m + K_{swp} v_w + v_p}{K_{smw} K_{swp} V_m + K_{swp} V_m + V_p} \tag{3.25}$$

The constant partition coefficients used in this model were estimated by Wong [1984] from limited steady state SBR plant data. In estimating the partition coefficients it was assumed that the ratio of monomers in the monomer droplets equalled the ratio of monomers in the polymer particles. Mathematically:

$$\frac{[S]_p}{[S]_p} = \frac{[S]_m}{[B]_m} \equiv \text{constant} \qquad (3.26)$$

Contrary evidence to this assumption has been presented in section 2.2.2 though the sources were contradictory as to which monomer had the greatest affinity for the polymer. With better data or perhaps an appropriate thermodynamic property estimation routine (i.e. UNIFAC/UNIQUACK), proper partition coefficients could be estimated.

It is envisioned that while all phases are present, the constant partition coefficients used here are valid. However, when phases are not saturated or are not in equilibrium, some error should be anticipated. For example, if a continuous reactor were started up full of water, the initial monomer fed would saturate the water before forming droplets. A rough estimate based on typical monomer feed rates and water solubilities has indicated the time required to saturate the water in an industrial sized reactor would only be a fraction of a minute.

3.2.2 Polymer Phase Radical Concentration

To calculate the reaction rate, an estimate of the concentration of radicals in the polymer phase, Y_o, is required. In emulsion polymerization Y_o is proportional to the average number of radicals per particle, $\bar{n}$. The continued fraction approximation to the Stockmayer-O'Toole Bessel function solution (section 2.2.5) for $\bar{n}$ of Ugelstad, et al. [1967] is

used in this model. Rather than use equation (2.24) directly, the continued fraction was written to 10 terms and reduced algebraically to give:

$$\bar{n} = \frac{1}{2} \cdot \left[\frac{113400+204120\alpha+70560\alpha^2+7350\alpha^3+223\alpha^4+\alpha^5}{113400+90720\alpha+17640\alpha^2+1050\alpha^3+13\alpha^4}\right] \qquad (3.27)$$

where

$$\alpha = \frac{\rho_A \hat{V}_p}{N_{pp} k_{tp}} \qquad (3.28)$$

for the condition of no radical desorption (i.e., $m = (k_{de} \hat{V}_p / k_{tp}) = 0$). Implied in the use of this solution are the assumptions of: 1) a "pseudo" steady state for radical concentrations, 2) no water phase termination, 3) no polymer phase reaction with impurity, and 4) a monodisperse particle population. It was intended that a mean termination constant for styrene and butadiene based on their relative proportions would be used in equation (3.28) as suggested by Friis, et al. [1982] and Nomura, et al. [1983a]. However, only a styrene termination constant was found in the literature. Since diffusion controlled kinetics or Case III kinetics are not important in styrene/butadiene copolymerization, this should not represent a serious limitation to the model.

Polymer phase reactions with impurities could be accounted for by the adjustment to the solution of Ugelstad, et al. [1967] proposed by Hoffman [1982]:

$$m = \left(\frac{k_{de}}{k_{tp}} + \frac{k_{MI}[MI]}{k_{tp}}\right) \hat{V}_p \qquad (3.29)$$

where k_{MI} is the rate constant for the reaction of radicals with monomer soluble impurities, MI. If this correction were to be used, the continued fraction equation (2.24) would have to be employed.

In the polydisperse particle version of this model $\bar{n}$ is calculated for each particle size. A weighted average of the $\bar{n}$'s is required in order to calculate the overall rate of reaction. This is explained further in section 3.2.9. With an estimate of $\bar{n}$, the radical concentration in the polymer particles, Y_o is calculated using:

$$Y_o = \frac{\bar{n}N_p}{V_p N_A} \qquad (3.30)$$

3.2.3 Balances on Initiating Species

Redox Initiation

The assumed reaction scheme for the p-menthane hydroperoxide/iron/sodium formaldehyde sulphoxylate redox couple is illustrated in equations (3.1) and (3.2). Since interferring reactions involving Fe^{2+} and Fe^{3+} are not modelled, the EDTA ligand, shown in equations (2.3) and (2.4) is ignored. The pH dependency of the initiation rate is also ignored. The method of modelling used is that of Hoffman [1982]. A "pseudo" steady state is assumed for iron ions. The validity of this assumption was discussed in

section 2.2.3.

The development of equations is based on the observation that the total iron concentration is not affected by reaction.

$$[Fe]_{t,w} = [Fe^{2+}]_w + [Fe^{3+}]_w \tag{3.31}$$

The application of the pseudo steady state hypothesis, outlined in section 2.2.3, results in:

$$[Fe^{2+}]_w = \frac{k_2[Fe]_{t,w}[RA]_w}{k_1[I]_w + k_2[RA]_w} \tag{3.32}$$

and

$$[Fe^{3+}]_w = \frac{k_1[I]_w[Fe]_{t,w}}{k_1[I]_w + k_2[RA]_w} \tag{3.33}$$

Reducing agent, RA, and total iron concentrations are calculated:

$$[RA]_w = N_{RA}/V_w \tag{3.34}$$

and

$$[Fe]_{t,w} = N_{Fe}/V_w \tag{3.35}$$

since both are only soluble in water. The calculation of the initiator concentration was shown in section 3.2.1.

Assuming radicals are formed only in equation (3.1), the rate of redox initiation is:

$$R_I = k_1 [Fe^{2+}]_w [I]_w \tag{3.36}$$

To account for the moles of iron and reducing agent, the following equations may be written.

$$\frac{dN_{Fe}}{dt} = F_{Fe,in} - N_{Fe} \frac{v_w}{V_w} \tag{3.37}$$

and

$$\frac{dN_{RA}}{dt} = F_{RA,in} - N_{RA} \frac{v_w}{V_w} - k_2 [Fe^{3+}]_w [RA]_w \tag{3.38}$$

Thermal Initiation

Unfortunately, the mechanism of persulphate initiation of styrene/butadiene monomer mixtures is unknown. An hypothetical reaction scheme from which a model may be developed is presented in Appendix A1 but was not applied in this work. For the purposes of modelling a hot SBR process, a constant rate of initiation, R_I was used.

To model styrene homopolymerization, the thermal initiation rate, based on equation (3.3) is:

$$R_I = 2 f k_d [I]_w \tag{3.39}$$

A balance on the moles of initiator, considering both initiating mechanisms is:

$$\frac{dN_I}{dt} = F_{I,in} - F_I - k_1 [Fe^{2+}]_w [I]_w V_w - k_d [I]_w V_w \tag{3.40}$$

It should be noted that when the conditions for either initiating mechanism is met, the other mechanism will be inactive.

3.2.4 Particle Balance

Polymer particles are assumed to be created by the collision of a radical with a micelle. Homogeneous nucleation, the effects of water phase propagation and termination and the desorption of radicals from particles are neglected on the basis that the monomers are not water soluble.

Disregarding desorption and water phase termination implies that all radicals generated enter micelles or particles, that is:

$$\rho_A = R_I \tag{3.41}$$

Furthermore, ignoring all water phase reactions and desorption allows one to specify the ratio of radicals entering micelles and creating new particles as the ratio of radical capture over the total capture rate. In accordance with the collision theory, capture rates are proportional to particle or micelle surface areas. Mathematically, the number of radicals forming new particles may be expressed:

$$\frac{k_{cm}A_m[R^\cdot]_w}{k_{cm}A_m[R^\cdot]_w + k_{cp}A_p[R^\cdot]_w} \cdot R_I \tag{3.42}$$

Simplifying the above expression and dividing through by k_{cm} gives:

$$\frac{A_m}{A_m + \epsilon A_p} \tag{3.43}$$

where ϵ is defined as (k_{cp}/k_{cm}) and represents the relative capture efficiency of particles to micelles. The use of a

capture efficiency has been discussed in section 2.2.4. For the present, $\epsilon = 1$.

In the simplest form of the model, the particles are assumed monodisperse. The particle area is given by:

$$A_p = (6\pi^{\frac{1}{2}} N_p^{\frac{1}{2}} V_p)^{\frac{2}{3}} \tag{3.44}$$

assuming particles are spherical. The symbol N_p represents the total number of particles. If the full particle size distribution is considered, the area of all particles of each size must be summed.

The area of micelles is estimated from the total surface covering potential, A_s, of the emulsifier in the reactor.

$$TSA = A_s \, (N_E - [E]_{cmc} \cdot V_w) \tag{3.45}$$

and

$$A_m = TSA - A_p \tag{3.46}$$

Nucleation stops when the condition ($A_m \leq 0$) is true.

The differential equation for the number of particles in the reactor is:

$$\frac{dN_p}{dt} = \left(\frac{v_w N_p}{V_w}\right)_{in} - \left(\frac{v_w N_p}{V_w}\right) + \frac{A_m}{A_m + \epsilon A_p} R_I \, V_w \, N_A \tag{3.47}$$

Assuming emulsifier is not consumed in any reaction and a perfectly stirred reactor:

$$\frac{dN_E}{dt} = F_{E,in} - N_E \cdot \frac{v_T}{V_T} \tag{3.48}$$

Finally, it is of interest to note the effect of ϵ on particle nucleation. If $\epsilon = 1$, micelles capture radicals equally efficiently as particles leading to PSD's which are skewed to large particle sizes since a large proportion of the particles are created instantaneously. Increasing ϵ causes the nucleation period to be less dramatic initially. Particle size distributions should be less skewed toward large particle sizes.

3.2.5 Monomer and Polymer Balances

Polymer particles are assumed to be "mini-bulk" reactors. This implies that bulk kinetics and rate constants apply. The conventional expression of the rate of incorporation of styrene monomer into the polymer (or the rate of depletion of monomer) is:

$$R_{ps} = \frac{k_{pss}k_{pBB}(r_s[S]_p^2 + [S]_p[B]_p)\ Y_o}{k_{pBB}r_s[S]_p + k_{pss}r_B[B]_p} \tag{3.49}$$

and for butadiene:

$$R_{pB} = \frac{k_{pss}k_{pBB}(r_B[B]_p^2 + [S]_p[B]_p)Y_o}{k_{pBB}r_s[S]_p + k_{pss}r_B[B]_p} \tag{3.50}$$

The calculation of the average concentration of radicals Y_o, was outlined in section 3.2.2.

The equations for the total moles of monomers in the reactor are:

$$\frac{dN_s}{dt} = F_{s,in} - N_s \frac{\omega_{sp}}{\bar{\Omega}_{sp}} - R_{ps}\ V_p \tag{3.51}$$

and

$$\frac{d_{NB}}{dt} = F_{B,in} - N_B \frac{\omega_{Bp}}{\Omega_{Bp}} - R_{pB}V_p \qquad (3.52)$$

Where the terms $N \frac{\omega}{\Omega}$ represent molar outflows as calculated in section 3.2.1. A convenient method of accounting for the mass of polymer produced is to sum the moles of "bound" monomers in the copolymer. A comparison of the amounts of each "bound" monomer provides an estimate of the accummulated copolymer composition.

The equations for the moles of bound monomer are:

$$\frac{d(ACNSP)}{dt} = \frac{\tilde{F}_{p,in} \cdot ACCM_{,in}}{\tilde{M}_s} - ACNSP. \frac{v_p}{V_p} + R_{ps}V_p \qquad (3.53)$$

and

$$\frac{d(ACNBP)}{dt} = \frac{\tilde{F}_{p,in}(1-ACCM_{,in})}{\tilde{M}_B} - ACNBP \cdot \frac{v_p}{V_p} + R_{pB}V_p \qquad (3.54)$$

Conversion is defined as the ratio of the mass of polymer to the total mass of monomers and polymer in the reactor.

$$X = \frac{\tilde{M}_s \cdot ACNSP + \tilde{M}_B \cdot ACNBP}{\tilde{M}_s(N_s + ACNSP) + \tilde{M}_B(N_B + ACNBP)} \qquad (3.55)$$

The consequences of conversion defined in this manner should be examined. For a batch reactor or a continuous reactor at steady state the present definition is consistent with the conventional definition. For semi-batch reactors or filling (transient) continuous reactors the conversion is not equivalent to the conventional overall conversion. This stems from

the fact that not all of the monomers to be fed to a semi-batch reactor are considered in the present conversion definition.

Typical aberrations of the conversion prediction include a non-zero initial condition when a seed latex is employed or constant conversions over long periods when semi-batch policies in which monomer concentrations are kept constant are used. In the latter case, an estimate of the mass of polymer formed is a better indication of the conversion. This is calculated simply as:

$$WP = \tilde{M}_s \cdot ACNSP + \tilde{M}_B \cdot ACNBP \tag{3.56}$$

It may be of interest to estimate the apparent conversion within the particles. Defining the volume fractions of each component of the polymer phase as:

$$\phi_s = \frac{\tilde{M}_s \cdot [S]_p}{\rho_s} \tag{3.57}$$

$$\phi_B = \frac{\tilde{M}_B \cdot [B]_p}{\rho_B} \tag{3.58}$$

$$\phi_p = 1 - \phi_s - \phi_B \tag{3.59}$$

From these quantities, the apparent conversion in the particles, X_{mp}, is:

$$X_{mp} = \frac{\rho_p \phi_p}{(\rho_p \phi_p + \rho_s \phi_s + \rho_B \phi_B)} \tag{3.60}$$

The accummulated copolymer composition is simply:

$$ACCN = \frac{ACNSP}{ACNSP+ACNBP} \tag{3.61}$$

based on the mole fraction of styrene in the polymer, or on a mass basis:

$$ACCM = \frac{\tilde{M}_S \cdot ACNSP}{\tilde{M}_S \cdot ACNSP+\tilde{M}_B \cdot ACNBP} \tag{3.62}$$

Instantaneous copolymer composition, defined as the mole fraction of styrene added to the polymer instantaneously, is calculated:

$$ICC = \frac{R_{ps}}{R_{ps}+R_{pB}} \tag{3.63}$$

3.2.6 Liquid Phase Balances

Because the volumes of the three phases in the reactor vary as conversion progresses and because material is exchanged between phases, the volumes of each phase must be accounted for.

The total volume flow out of the reactor differs from the inflow by the amount the organic phase contracts because of polymerization. Hoffman [1982] expressed the rate of contraction of the organic phase by:

$$shrink = V_p \left(\tilde{M}_S \, R_{ps}\left(\frac{1}{\rho_s}-\frac{1}{\rho_p}\right) + \tilde{M}_B \, R_{pB}\left(\frac{1}{\rho_B}-\frac{1}{\rho_p}\right)\right) \tag{3.64}$$

The total volume outflow is then expressed:

$$v_T = v_{T,in} - \text{shrink} \tag{3.65}$$

Component outflows may be calculated assuming a perfectly stirred reactor.

$$v_w = \frac{V_w}{V_o+V_p} v_T \; ; \quad v_o = \frac{V_o}{V_w+V_o} v_T \tag{3.66}$$

Since the reactor is assumed perfectly stirred and no water is produced or consumed in any reaction, the following equation may be written.

$$\frac{dV_w}{dt} = v_{w,in} - v_w \tag{3.67}$$

A differential equation for the shrinking organic phase may be written as:

$$\frac{dV_o}{dt} = v_{o,in} - v_o - \text{shrink} \tag{3.68}$$

This equation is not necessary. An estimate of the organic phase volume may be obtained by algebraic manipulation of N_S, N_B, ACNSP and ACNBP. The organic phase volume is required to estimate the monomer phase volume once the polymer phase volume is calculated.

The polymer phase volume is the most difficult to estimate. The distribution of monomers in the polymer particles was assumed independent of particle size and copolymer

composition. Also, the volumes of the components of the polymer particles are assumed additive. The differential equation developed for the polymer phase was:

$$\frac{dV_p}{dt} = v_{p,in} - \frac{V_p}{V_T} v_T + \frac{(\tilde{M}_s R_{ps} + \tilde{M}_B R_{pB}) V_p}{\phi_p \rho_p} \qquad (3.69)$$

This equation is only valid in stages 1 and 2. Therefore, ϕ_p used in equation (3.69) represents the volume fraction of polymer in the saturated particles. It must be stressed that particles entering and exiting the reactor must also be saturated for equation (3.69) to be correct. During stage 3, after the monomer droplets disappear, the organic and polymer volumes are equal. Therefore, equation (3.69) may be disregarded when $V_m \leq 0$ and V_p can be set equal to V_o. If this model were to be extended for a CSTR train, careful attention should be paid to the calculation of organic and polymer volumes.

If the simulated reaction is expected to proceed from 0 to 100% conversion directly, the monomer phase volume may be estimated as:

$$V_m = V_o - V_p \qquad (3.70)$$

during stages 1 and 2. If, however, an unsaturated latex seed is simulated which may possibly become saturated during the course of the simulation, an independent estimate of the saturated polymer volume is needed.

The volume fraction of polymer in the monomer may be

expressed in terms of monomer concentrations in the monomer droplets by combining equations (3.57), (3.58), (3.59) and (3.20). The resulting equation is:

$$\phi_p = 1 - \frac{\tilde{M}_S}{\rho_S} \cdot \frac{[S]_m}{K_{smw}K_{swp}} - \frac{\tilde{M}_B}{\rho_B} \cdot \frac{[B]_m}{K_{Bmw}K_{Bwp}} \qquad (3.71)$$

If monomer droplets exist, assuming the monomers mix ideally, the concentration of monomers should only depend on monomer droplet composition and monomer density. An estimate of the monomer concentration may be obtained from the total unreacted monomers in the reactor if it is assumed that monomers partition equally well in both monomer and polymer phases (equation (3.26)). The resulting expressions are:

$$[S]_m = \frac{(N_S - \gamma_S V_w)}{\frac{\tilde{M}_S(N_S - \gamma_S V_w)}{\rho_S} + \frac{\tilde{M}_B(N_B - \gamma_B V_w)}{\rho}} \qquad (3.72)$$

and

$$[B]_m = \frac{N_B - \gamma_B V_w}{\frac{\tilde{M}_S(N_S - \gamma_S V_w}{\rho_S} + \frac{\tilde{M}_B(N_B - \gamma_B V_w)}{\rho_B}} \qquad (3.73)$$

Substituting the above expressions into equation (3.71) will give an estimate of the value of ϕ_p if a monomer phase were present, ϕ_p^{SAT}. The volume of the saturated polymer phase is:

$$V_p^{SAT} = V_{pp}/\phi_p^{SAT} \qquad (3.74)$$

where V_{pp} is the volume of pure polymer. The volume of monomer

phase is:

$$V_m = V_o - V_p^{SAT} \tag{3.75}$$

if $V_m \geq 0$.

3.2.7 Energy Balances

The reactor and cooling jacket design assumed in this model is shown in figure 3.1. The reactor was assumed cylindrical with a height to diameter ratio of approximately 1:1. Because it was assumed perfectly stirred, no temperature or concentration gradients are expected in the reactor. Cooling was assumed through the walls of the reactor only. On this assumption the following expression was derived to estimate the area for heat transfer through the walls of the reactor as a function of reactor (cylinder) radius and volume of latex.

$$A_J = (2\ V_T/\text{Radius}) \tag{3.76}$$

The cooling jacket was also assumed perfectly stirred to preclude any temperature variation within the jacket. The variables used in the following balances are shown in figure 3.1.

Reactor Balance

The following assumptions were made in deriving an energy balance for the reactor contents: 1) Only water, monomers and polymer are in sufficient quantities to have

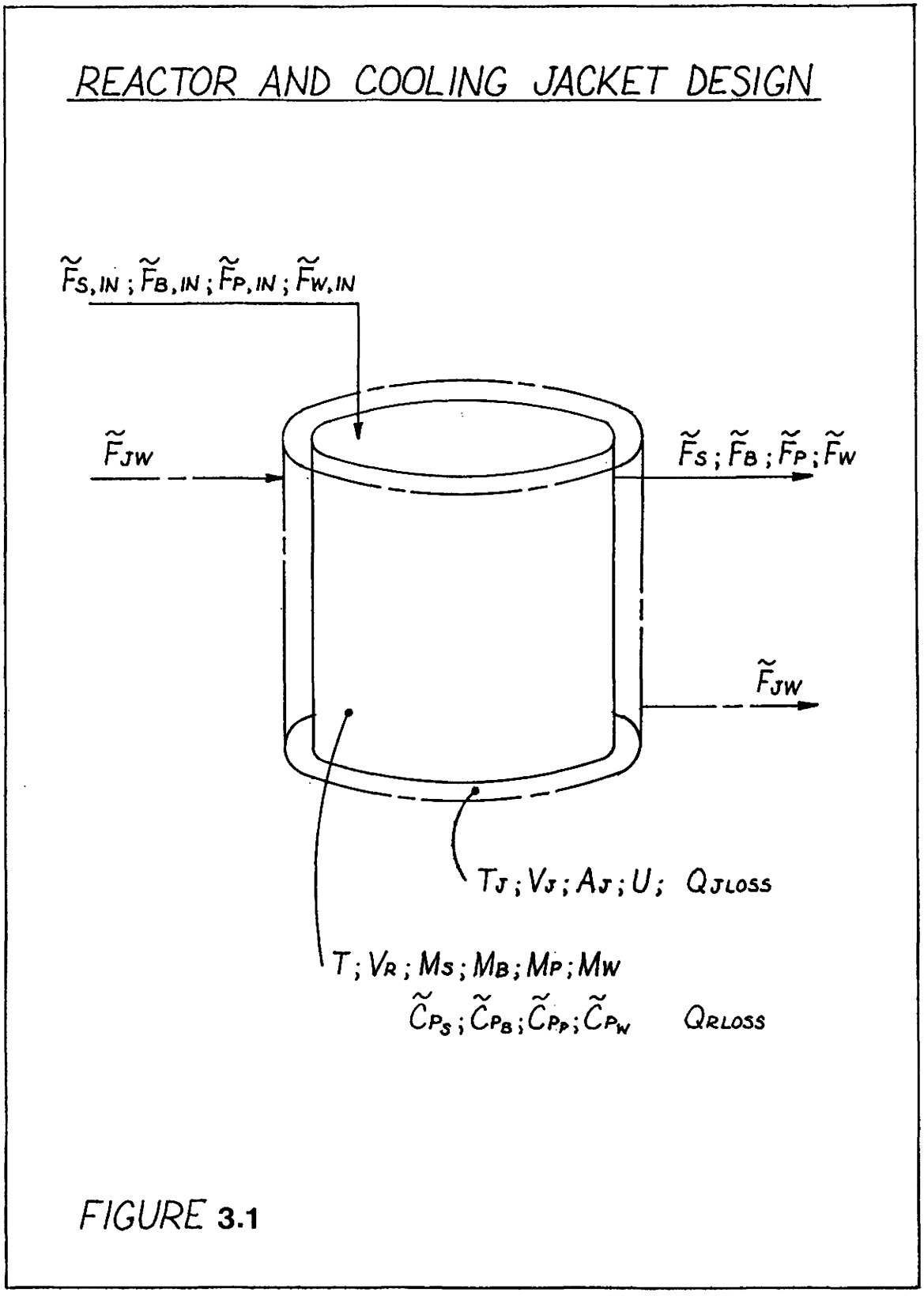
REACTOR AND COOLING JACKET DESIGN
$\tilde{F}_{S,IN}$; $\tilde{F}_{B,IN}$; $\tilde{F}_{P,IN}$; $\tilde{F}_{W,IN}$
$\tilde{F}_{JW}$
$\tilde{F}_S$; $\tilde{F}_B$; $\tilde{F}_P$; $\tilde{F}_W$
$\tilde{F}_{JW}$
T_J ; V_J ; A_J ; U ; Q_{JLOSS}
T ; V_R ; M_S ; M_B ; M_P ; M_W
$\tilde{C}_{P_S}$; $\tilde{C}_{P_B}$; $\tilde{C}_{P_P}$; $\tilde{C}_{P_W}$ Q_{RLOSS}

FIGURE **3.1**

any sensible heat effect. 2) Only the heat of the propagation reactions is considered. 3) The heat of vapourization of butadiene is ignored. 4) The heat capacity of the reactor walls are ignored. Because some confusion may arise due to the presence of a reference temperature in the final expression, a complete derivation is given.

An energy balance around the reactor contents can be written as:

$$\frac{dH_{tot}}{dt} = \dot{H}_{in} - \dot{H}_{out} + \dot{H}_{generation} - \dot{H}_{loss} \qquad (3.77)$$

Applying the definition of enthalpy, the energy balance can be expressed as:

$$\frac{d(\Sigma_i M_i \tilde{C}_{pi}(T-T_{ref}))}{dt} = \Sigma_i \tilde{F}_{i,in} \tilde{C}_{pi} (T_{in}-T_{ref})$$

$$- \Sigma_i \tilde{F}_{i,out} \tilde{C}_{pi}(T-T_{ref}) + R_p V_p \Delta H_p$$

$$- UA_J (T-T_J)$$

$$- Q_{R\ LOSS} \qquad (3.78)$$

where the summations are taken over the four components of interest (water, styrene, butadiene and copolymer). The accumulation term can be expanded as follows:

$$\frac{d(\sum_i M_i \tilde{C}_{pi}(T-T_{ref}))}{dt} = \sum_i M_i \frac{d\tilde{C}_{pi}(T-T_{ref})}{dt}$$

$$+ \sum_i \tilde{C}_{pi}(T-T_{ref}) \frac{dM_i}{dt} \qquad (3.79)$$

The second term on the right hand side of this equation can be simplified using a mass balance:

$$\sum_i \frac{dM_i}{dt} = \sum_i \tilde{F}_{i,in} - \sum_i \tilde{F}_{i,out} \qquad (3.80)$$

Combining (3.78), (3.79) and (3.80) and cancelling terms gives the energy balance as:

$$\sum_i M_i \tilde{C}_{pi} \frac{dT}{dt} = \sum_i \tilde{F}_{i,in} \tilde{C}_{pi} (T_{in}-T) + R_p \Delta H_p V_p$$

$$- UA_J (T-T_J) - Q_{R\ LOSS} \qquad (3.81)$$

If the heat of reaction is defined at a specific reference temperature, it may be corrected for the reaction temperature as follows:

$$\Delta H_p(T) = \Delta H_{reactants} (T-T_{ref}) + \Delta H_p (T_{ref})$$

$$+ \Delta H_{products} (T_{ref}-T) \qquad (3.82)$$

Applying the definition of enthalpy and multiplying by the appropriate reaction rate gives:

$$\Delta H_p(T) R_p V_p = \Delta H_p(T_{ref}) R_p V_p + R_{ps} V_p C_{ps} (T - T_{ref})$$

$$+ R_{pB} V_p C_{pB} (T - T_{ref})$$

$$+ (\tilde{M}_s R_{ps} + \tilde{M}_B R_{pB}) V_p \tilde{C}_{pp} (T_{ref} - T) \qquad (3.83)$$

The final balance is obtained by substituting (3.83) into (3.81).

$$\sum_i M_i \tilde{C}_{pi} \frac{dT}{dt} = \sum_i \tilde{F}_{i,in} \tilde{C}_{pi} (T_{in} - T)$$

$$+ \Delta H_p(T_{ref}) R_p V_p + R_{ps} V_p C_{ps} (T - T_{ref})$$

$$+ R_{pB} V_p C_{pB} (T - T_{ref})$$

$$+ (\tilde{M}_s R_{ps} + \tilde{M}_B R_{pB}) V_p \tilde{C}_{pp} (T_{ref} - T)$$

$$- U A_J (T - T_J) - Q_{R\ LOSS} \qquad (3.84)$$

Cooling Jacket Balance

For the cooling jacket balance, a constant overall heat transfer coefficient is used and the jacket was assumed full and perfectly mixed. The final form of the cooling jacket balance was:

$$\frac{dT_J}{dt} = (\tilde{F}_{Jw} \tilde{C}_{pw} (T_{J,in} - T_J) + U A_J (T - T_J)$$

$$- Q_{J\ LOSS}) / (\rho_w V_J \tilde{C}_{pw}) \qquad (3.85)$$

Controller Differential Equation

For the purposes of this model, reactor temperature was controlled by manipulating the temperature of the cooling jacket feed. The temperature adjustment of the cooling jacket feed was assumed to be instantaneous. Schematic and block diagrams of the control system are given in figures 3.2 and 3.3.

A proportional-integral controller of the following form was simulated.

$$\Delta T_{J,in} = K_c \, \ell + \frac{K_c}{\tau_I} \int_0^t \ell \, dt \qquad (3.86)$$

where the error, ℓ is the difference between the desired and actual reactor temperatures.

$$\ell = T - T^{set} \qquad (3.87)$$

The integral term of the controller was simulated with the following differential equation.

$$\frac{d[\int \ell dt]}{dt} = T - T^{set} \qquad (3.88)$$

The control action is implemented through the following equation.

$$T_{J,in} = T_c + \Delta T_{J,in} \qquad (3.89)$$

where $\Delta T_{J,in}$ represents the control action and T_c represents a steady-state or bias term. The controller gain, K_c, and integral time, τ_I, were tuned using a linearized process

CONTROL SCHEMATIC

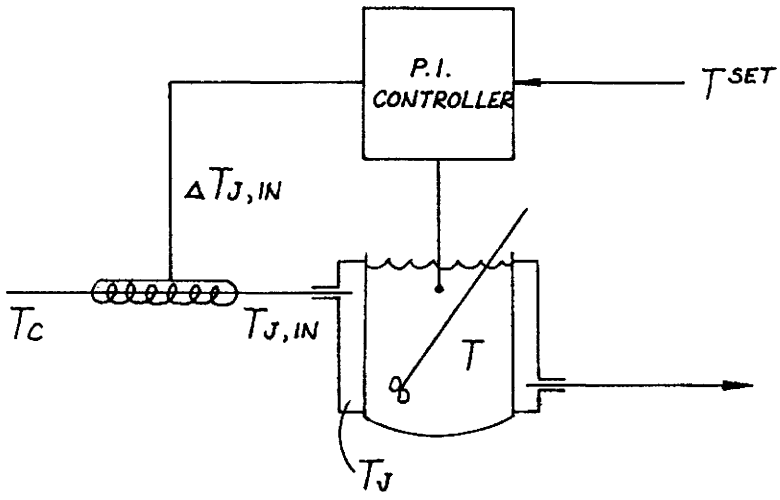

FIGURE 3.2

BLOCK DIAGRAM

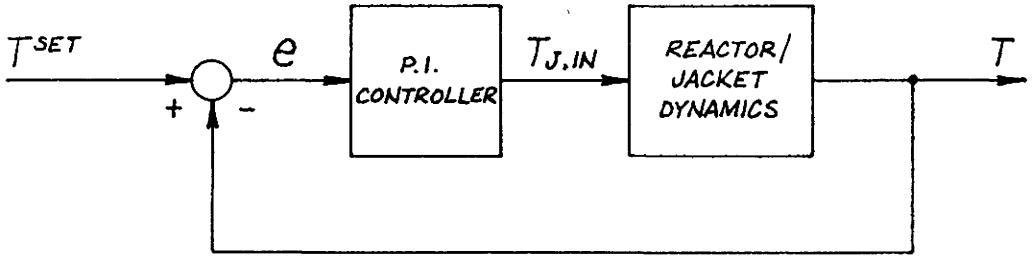

FIGURE 3.3

model and a stability analysis. The tuning method is presented in Appendix A2. An unconstrained manipulated variable was assumed in most of the simulations, however, constraining the manipulated variable did not pose a problem.

3.2.8 Molecular Mass Distribution

The elementary chemical reactions governing the development of the molecular mass of styrene/butadiene copolymer are the propagation reactions with monomer and polymer and the transfer reactions with monomer, polymer and chain transfer agent. These reactions are illustrated and discussed briefly in section 3.1 and are discussed in more detail in section 2.2.6. The following facts and assumptions, summarized from these previous sections, form the basis of the molecular mass development analysis. Transfer and not termination reactions are important in the formation of polymer molecules. The transfer to chain transfer agent (CTA) reaction is dominant. A subsequent test of these assumptions revealed that under normal conditions, the rate of transfer to CTA was a factor of 10^2 larger than the termination rate. Tri-functional branches result from the transfer to polymer reaction. Tetra-functional branches, or crosslinks, are formed by the propagation to polymer reaction. The importance of all of the aforementioned rates depends on their relative magnitude compared to the propagation rate.

Differential equations for the zero, first and second

moments of a copolymer molecular mass distribution have been presented by Hamielec [1982b]. In his development, a steady state was assumed for radical concentrations. Furthermore, copolymer composition was assumed constant between chains. This assumption is expected to break down if composition drifts substantially and will have its greatest adverse effect in the case where branching is important.

The equations needed to solve the molecular mass distribution are as follows.

1) The fractions of styrene and butadiene ended radicals.

$$\Phi_s = k_{pBs}\,[S]_p/(k_{pBs}[S]_p + k_{psB}\,[B]_p) \tag{3.90}$$

$$\Phi_B = 1 - \Phi_s \tag{3.91}$$

These equations are based on the assumption that for large molecules, the rates of cross propagation can be equated.

2) The combined propagation constant and ratios of combined transfer to propagation.

$$k_p = \Phi_s(k_{pss}[S]_p + k_{psB}[B]_p) + \Phi_B(k_{pBs}[S]_p + k_{pBB}[B]_p) \tag{3.92}$$

$$C_m = [\Phi_s(k_{fss}[S]_p + k_{fsB}[B]_p) + \Phi_B(k_{fBs}[S]_p + k_{fBB}[B]_p)]/k_p \tag{3.93}$$

$$C_x = [\Phi_s k_{fsx} + \Phi_B\, k_{fBx}]/[k_p/[M]_p] \tag{3.94}$$

$$C_p = [\Phi_s(k_{fpss}\ ACCN + k_{fpsB}\ (1\text{-}ACCN)) + \Phi_B(k_{fpBs}\ ACCN + k_{fpBB}\ (1\text{-}ACCN))]/[k_p/[M]_p] \quad (3.95)$$

$$C_k = [\Phi_s(k^*_{ps1} + k^*_{ps2} + k^*_{ps3}) + \Phi_B\ (k^*_{pB1} + k^*_{pB2} + k^*_{pB3})]\ \frac{(1\text{-}ACCN)}{[k_p/[M]_p]} \quad (3.96)$$

Constants k^*_{ps1}, k^*_{ps2} and k^*_{ps3} represent the reaction rate constants of a styrene-ended radical with an internal double bond of a copolymer in the cis, trans and (1,2) conformations respectively. Constants k^*_{pB1}, k^*_{pB2} and k^*_{pB3} are defined similarly.

3) Differential moment balances.

$$\frac{d(V_pQ_o)}{dt} = (v_pQ_o)_{in} - (v_pQ_o) + (C_m + C_x\frac{[X]_p}{[M]_p} - C_k\ \frac{Q_1}{[M]_p})k_p[M]_pY_oV_p \quad (3.97)$$

$$\frac{d(V_pQ_1)}{dt} = (v_pQ_1)_{in} - (v_pQ_1) + k_p\ [M]_p\ Y_o\ V_p \quad (3.98)$$

$$\frac{d(V_pQ_2)}{dt} = (v_pQ_2)_{in} - (v_pQ_2) + \frac{2(1+C_k\frac{Q_2}{[M]_p})(1+C_x\frac{[X]_p}{[M]_p}+(C_k+C_p)\cdot\frac{Q_2}{[M]_p})\ k_p[M]_pY_oV_p}{(C_m + C_x\ \frac{[X]_p}{[M]_p} + C_p\ \frac{Q_1}{[M]_p})} \quad (3.99)$$

$$\frac{d(V_p Q_o \bar{B}_{N3})}{dt} = (v_p Q_o \bar{B}_{N3})_{in} - (v_p Q_o \bar{B}_{N3}) + C_p Q_1 k_p Y_o V_p \quad (3.100)$$

$$\frac{d(V_p Q_o \bar{B}_{N4})}{dt} = (v_p Q_o \bar{B}_{N4})_{in} - (v_p Q_o \bar{B}_{N4}) + C_k Q_1 k_p Y_o V_p \quad (3.101)$$

4) Molecular mass averages

$$\tilde{M}_{eff} = ACCN \cdot \tilde{M}_s + (1\text{-}ACCN)\ \tilde{M}_B \quad (3.102)$$

$$\bar{M}_N = \tilde{M}_{eff} \cdot Q_1/Q_o \quad (3.103)$$

$$\bar{M}_w = \tilde{M}_{eff}\ Q_2/Q_1 \quad (3.104)$$

Estimates of the required kinetic constants were obtained by Wong [1984]. He found absolute values for each constant by fitting some plant data and then incorporated an Arrhenius temperature dependence using activation energies from the literature. Independent estimates of the required rate constants are desired.

3.2.9 Particle Size Distribution

The approaches to modelling the particle size distribution (PSD) presented in this section assume that the concentrations of monomers in the particles are independent of

particle size and that particles do not coalesce or agglomerate.

In the simplest form of the model, all particles are assumed to be of the same size. Furthermore, the average number of radicals per particle ($\bar{n}$) is implicitly assumed equal in all particles. The volume of a single particle, $\hat{V}_p$, is:

$$\hat{V}_p = V_p/N_p \tag{3.105}$$

Particle area is calculated as outlined in section 3.2.4 (equation (3.44)).

The conceptual approach to modelling the full PSD was to discretize the particle population according to age. Each subdivision is referred to as a "generation". The volumes of all subsequent particle generations are inferred from the volume of particles of the first generation (those particles nucleated at time zero) and the nucleation time of the generation of interest. In this way, only the volume growth of a single particle of the first generation is integrated. The appropriate differential equation is:

$$\frac{d\hat{V}_p}{dt} = \frac{k_{pss}k_{pBB}[r_s[S]_p^2+2[S]_p[B]_p+r_B[B]_p^2]\frac{\bar{n}}{N_A}}{k_{pBB}r_s[S]_p+k_{pss}r_B[B]_p} \tag{3.106}$$

It should be noted that this single particle is assumed to remain in the reactor all the time; it does not wash out.

The first, simpler approach to modelling the PSD assumes $\bar{n} = \frac{1}{2}$ for all particles. This is a very good

assumption for cold SBR. Since $\bar{n}$ and the concentration of monomers are equal in all particles, the volume growth rate of particles is equal. The volume of a particle in a particular generation at any time will be equal to the difference in the first generation particle volumes at the time of interest and at the time of nucleation of the generation of interest. If $\hat{V}_p(t,\tau)$ represents the volume of a particle at time, t, which was nucleated at time, τ, then the aforementioned relationship may be expressed by:

$$\hat{V}_p(t,\tau) = \hat{V}_p(t,0) - \hat{V}_p(\tau,0) \qquad (3.107)$$

This equation is illustrated in figure 3.4. The curve enclosed by the unbroken axis represents the arbitrary volume-time history of a particle nucleated at time zero. The curve enclosed by the broken axis represents the volume-time history of a particle nucleated at time τ. The two volume-time histories are different from inception of each generation, however, if appropriately shifted they can be superimposed. Equation (3.107) represents the process of shifting the broken axis relative to the unknown axis.

The PSD is constructed by storing the number of particles and the volume of a single particle of each generation. The number of particles generated in any time interval $(\tau+\Delta\tau,\tau)$ is given by:

$$N_p(\tau+\Delta\tau,\tau) = \frac{A_m}{A_m+\epsilon_{Ap}} R_I V_w N_A \Delta\tau \qquad (3.108)$$

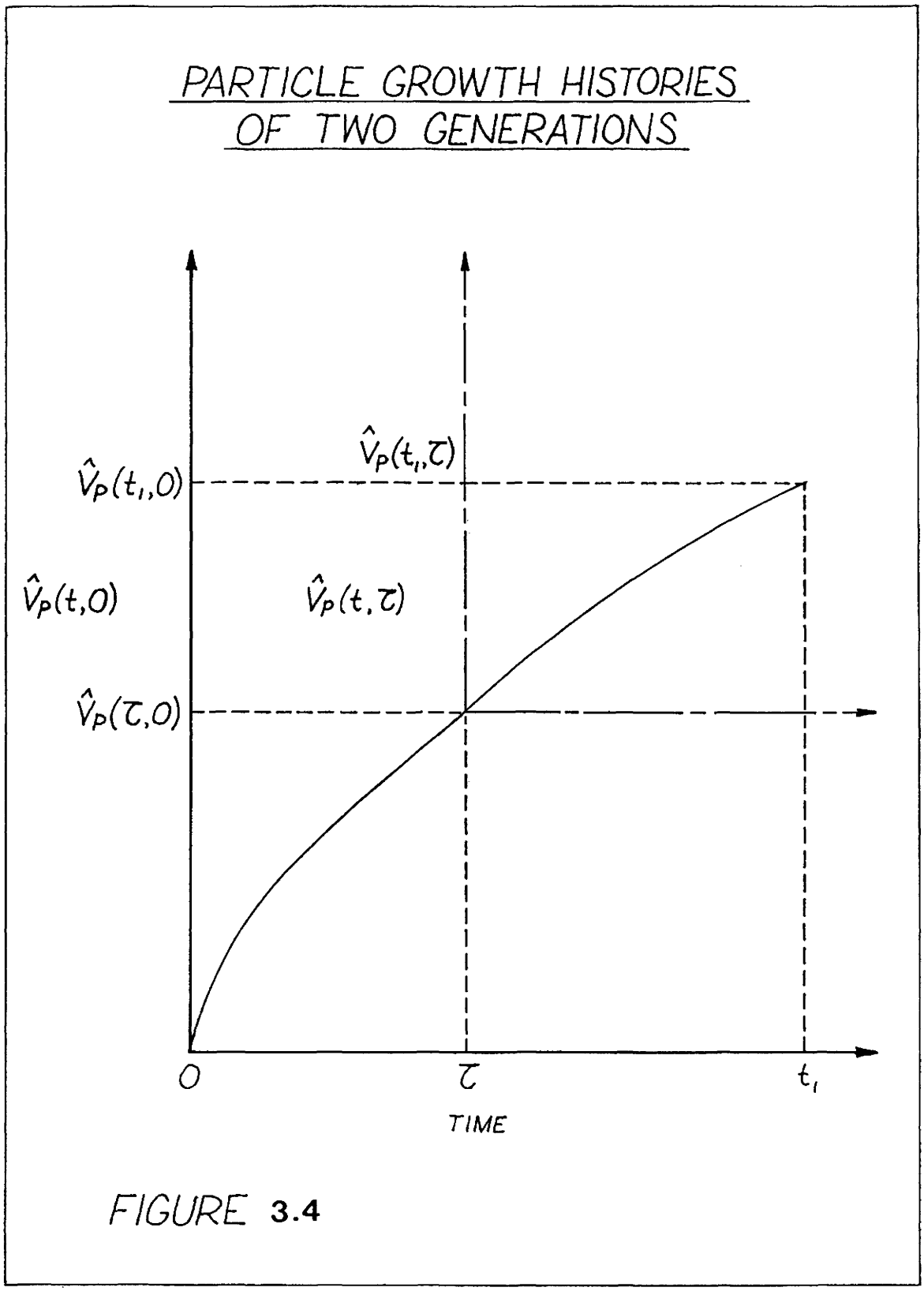
PARTICLE GROWTH HISTORIES
OF TWO GENERATIONS
$\hat{V}_p(t_1,\tau)$
$\hat{V}_p(t_1,0)$
$\hat{V}_p(t,0)$
$\hat{V}_p(t,\tau)$
$\hat{V}_p(\tau,0)$
0
τ
t_1
TIME

FIGURE **3.4**

It is assumed that no particles are fed to the reactor. Therefore, the number of particles of a specific generation is constant after the end of its nucleation period unless the reactor is overflowing. When the reactor is overflowing, the number of particles of a specific generation is given by:

$$N_p(t,\tau) = N_p(\tau+\Delta\tau,\tau)\exp\left(-\frac{(t-(\tau+\Delta\tau))}{\theta}\right) \qquad (3.109)$$

where θ is the mean residence time of the reactor. This assumes that the reactor is a perfect CSTR. Particle area is calculated by summing the area of each monodisperse generation.

The second approach to modelling the PSD does not assume $\bar{n} = \frac{1}{2}$ for all particles. Instead, $\bar{n}$ is calculated for all generations using equation (3.27) at the beginning of each generation time and is assumed constant over the generation period. It has been observed that this is a fairly good assumption, generally, but is expected to break down if the termination reaction is severly diffusion controlled and $\bar{n}$ increases dramatically. The volume of the initial generation is used to calculate a volume increment over the generation time. This volume increment is adjusted for subsequent generations, τ, as follows:

$$\Delta\hat{V}_p(t,\tau) = \Delta\hat{V}_p(t,0)\cdot\frac{\bar{n}(t,\tau)}{\bar{n}(t,0)} \qquad (3.110)$$

where $\Delta\hat{V}_p(t,\tau)$ is the increment in particle volume and $\bar{n}(t,\tau)$ is the average number or radicals per particle at time t, nucleated at time τ.

The PSD is presented as a plot of the normalized number frequency of particles versus particle radius. The number frequency may be calculated:

$$F(r) = \frac{N_p(t,\tau)}{N_p(t)\cdot\Delta r} \tag{3.111}$$

where Δr represents the difference in particle radii between consecutive generations. In this model it was found convenient to calculate Δr using:

$$\Delta r = r(t,\tau) - r(t,\tau-\Delta\tau) \tag{3.112}$$

The radius is calculated assuming a spherical particle.

The advantage of the PSD calculation methods outlined in this section is that only one differential equation need be integrated. The methods outlined in section 2.2.7 required systems of integro-differential, partial differential or difference differential equations to be solved.

In the present approach along with the other population balance approaches of section 2.2.7, the statistical variation of the distribution arising from the variation of the numbers of radicals per particle in a size class is missing. The distributions calculated indicate the average volume growth of each particle. The tails of the distribution

are missing. This error is small for broad PSD's. For narrow PSD's, the error is relatively more important, however, narrow distributions are adequately modelled as being monodisperse. Discussion and examples of distributions calculated for both batch and CSTR reactors are given in sections 5.2 and 5.3 respectively.

It is of interest to evaluate the benefit of considering the full PSD. This was done by comparing predictions of monodisperse and polydisperse models for a case in which particle nucleation is prolonged throughout the course of reaction. A semi-batch reaction was simulated in which emulsifier was post fed in excess throughout the simulation. The predicted PSD is given in figure 3.5. The predictions of particle density and conversion are shown in figures 3.6 and 3.7 respectively. Surprisingly, only a small deviation (less than 5%) is observed in the particle density prediction. Practically no difference in conversion is observed. Given two particle populations of equal total volume and number, it can be shown that the monodisperse population will have a smaller total surface area than a polydisperse population. However, because other modelling assumptions, such as the form of the nucleation mechanism adopted, affect the particle size distribution prediction, it is impossible to anticipate how the full and monodisperse PSD s should differ. Therefore, no definitive statement on the importance of the PSD on model predictions can be made. It may be concluded, however, that

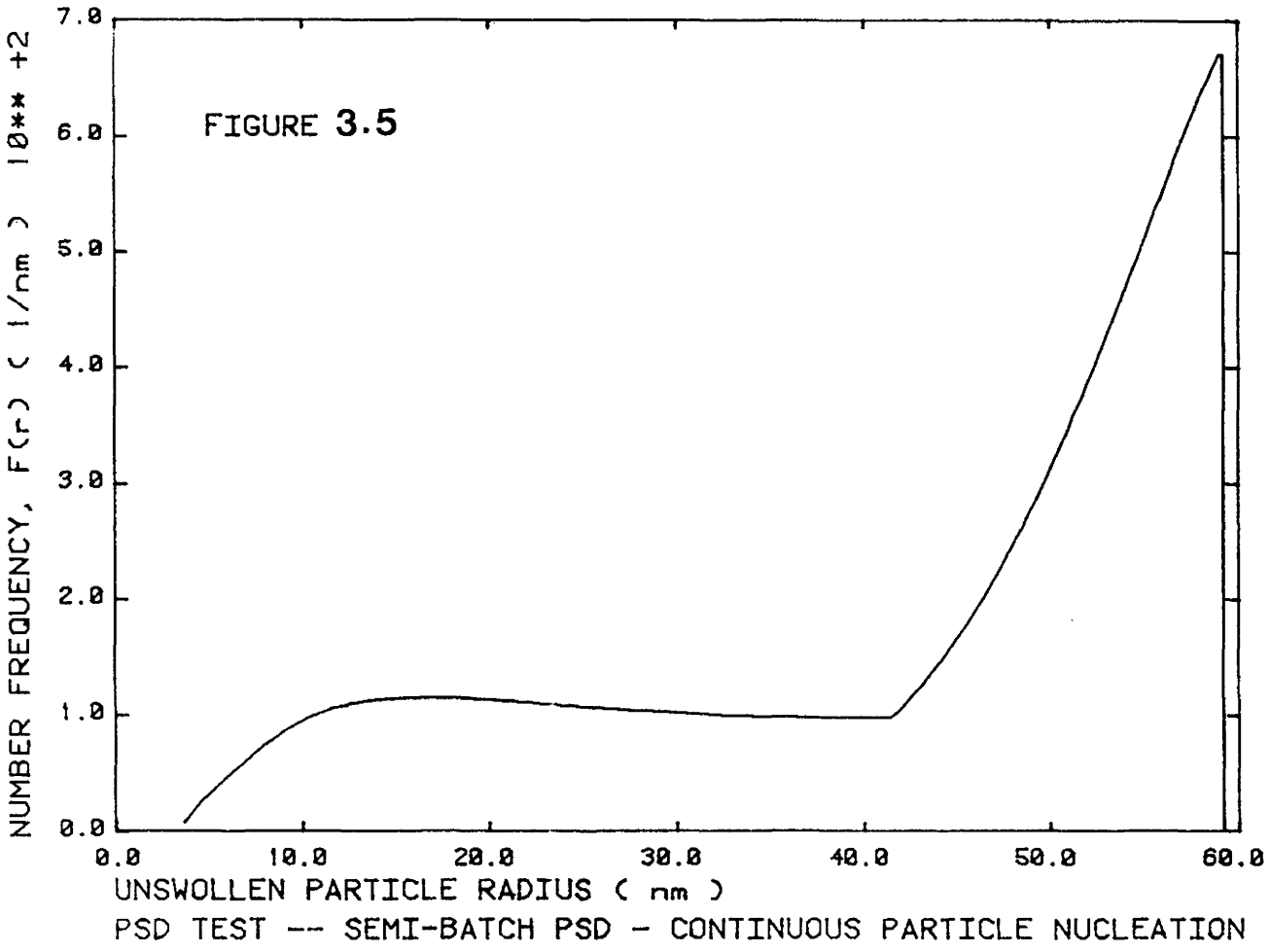
FIGURE 3.5
NUMBER FREQUENCY, F(r) (1/nm) 10** +2
7.0
6.0
5.0
4.0
3.0
2.0
1.0
0.0
0.0
10.0
20.0
30.0
40.0
50.0
60.0
UNSWOLLEN PARTICLE RADIUS (nm)
PSD TEST -- SEMI-BATCH PSD - CONTINUOUS PARTICLE NUCLEATION

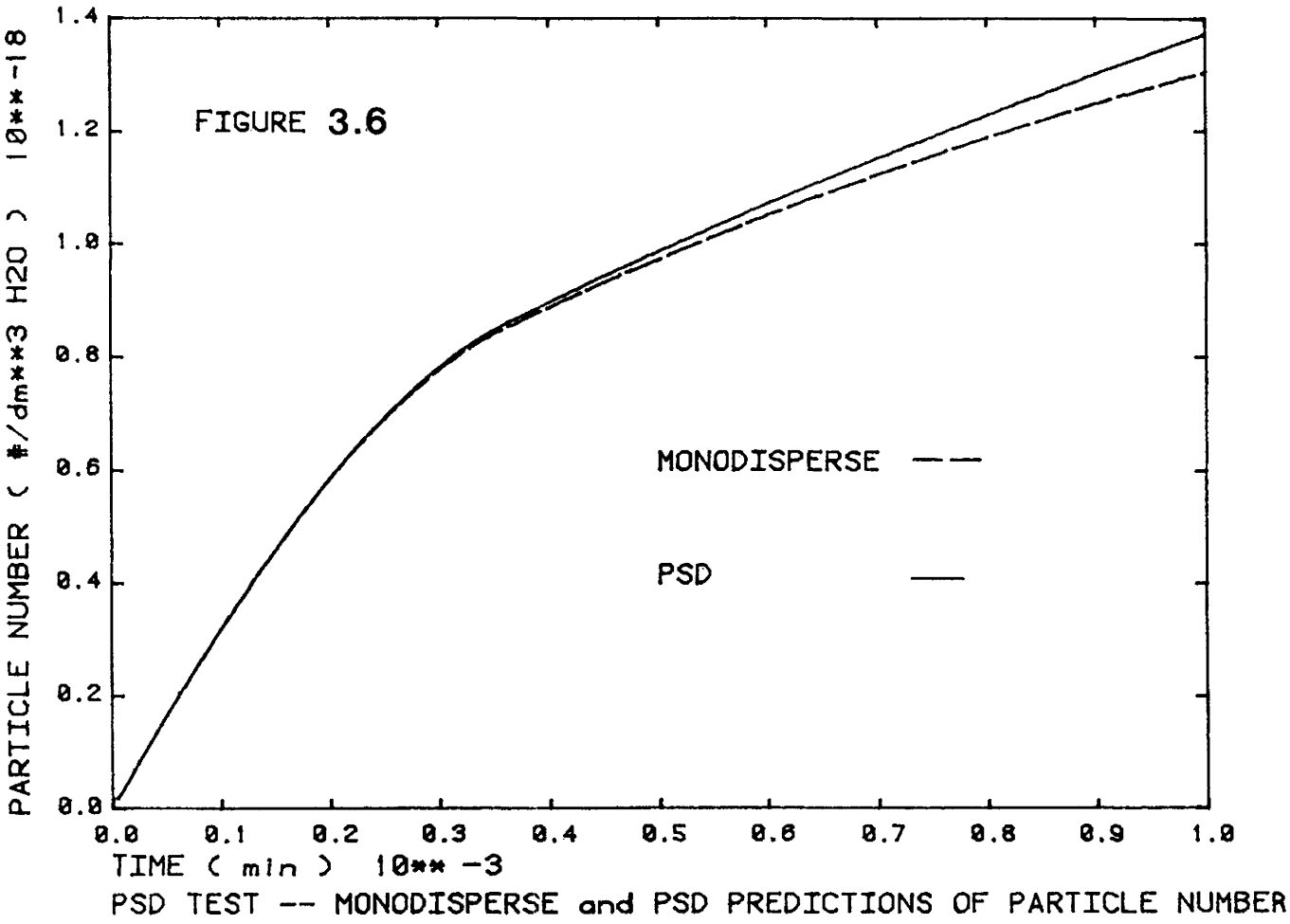

PSD TEST -- MONODISPERSE and PSD PREDICTIONS OF PARTICLE NUMBER

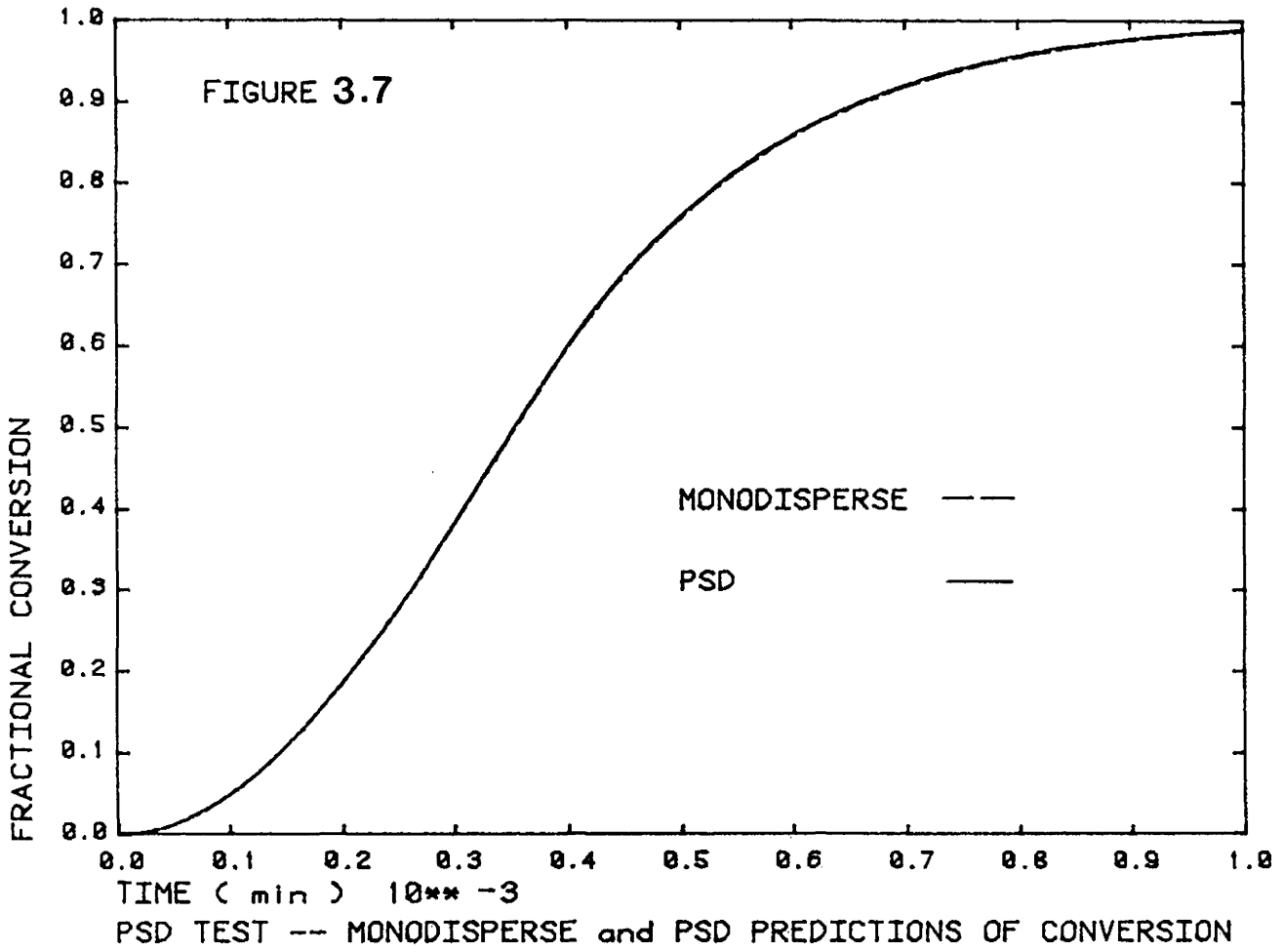
FIGURE 3.7
FRACTIONAL CONVERSION
1.0
0.9
0.8
0.7
0.6
0.5
0.4
0.3
0.2
0.1
0.0
MONODISPERSE
PSD
0.0 0.1 0.2 0.3 0.4 0.5 0.6 0.7 0.8 0.9 1.0
TIME (min) 10** -3
PSD TEST -- MONODISPERSE and PSD PREDICTIONS OF CONVERSION

in this model, no improvement in model predictions was observed when the full PSD was considered. The PSD was of interest, however, in studying the nature of the nucleation period and for obtaining an estimate of the latex properties which are associated with PSD.

3.2.10 Diffusion Controlled Kinetics

Diffusion controlled kinetics are not important in cold SBR manufacture. They may be important in hot SBR production where terminal conversions are higher, latex particles are larger and the proportion of styrene in the copolymer may be higher. However, in other systems diffusion controlled termination and propagation may cause autoaccelerating reaction rates, multiple steady states and limiting conversions which complicate reactor operation and control. Though not important for SBR copolymerization, diffusion controlled kinetics were incorporated into the present model in anticipation of future applications of the model.

The free volume approach of Marten, et al. [1979] as adapted by Harris, et al. [1982] for emulsion polymers and by Lord [1984] for copolymers is applied in this model. A brief overview of the equation development is given in section 2.2.7. It is stressed that the molecular mass dependence of the diffusion controlled termination constant is ignored in this development as suggested by Harris, et al. [1982] and Sundberg, et al. [1982].

The diffusion controlled termination constant is calculated using

$$k_{tp} = k_{tp}^{sat} \left(\exp\left(-A\left(\frac{1}{V_F} - \frac{1}{V_F^{sat}}\right)\right)\right) \qquad (3.113)$$

where k_{tp}^{sat} is the diffusion controlled termination constant corresponding to V_F^{sat}, the fractional free volume of the saturated polymer particle. The fractional free volume, V_F, is given by:

$$\begin{aligned} V_F = {} & (0.025 + \alpha_s(T-T_{gs}))\ \phi_s \\ & + (0.025 + \alpha_B(T-T_{gB}))\ \phi_B \\ & + (0.025 + \alpha_p(T-T_{gp}))\ \phi_p \end{aligned} \qquad (3.114)$$

where ϕ_s, ϕ_B and ϕ_p are the volume fractions of styrene, butadiene and copolymer respectively in the particles and are defined by equations (3.57), (3.58) and (3.59).

The parameter V_F^{sat} was calculated assuming stage 2 ended at 57% conversion (i.e. $X_c = 0.57$). To estimate k_t^{sat}, the correlation for the diffusion controlled styrene termination constant of Hui and Hamielec (Friis, et al. [1973]) was used with X = 0.57. The region of "termination by propagation" was modelled simply by limiting the fall of the termination constant.

Unless very high proportions of styrene are incorporated into the polymer, SBR polymerization occurs above its glass

transition temperature. In this region, diffusion controlled propagation is not encountered. However, for completeness, a calculation of diffusion controlled propagation is included.

The approach of Lord [1984] was applied in a slightly modified form. Rather than considering each of the four propagation reactions to become diffusion controlled individually, reactions of radicals with the same monomer unit were grouped together. Styrene propagation was assumed to become diffusion controlled first. If the free volume drops below a certain critical value, V_{Fcrs}, then:

$$\text{if } V_F < V_{Fcrs}$$

$$k_{pss} = k_{pss0} \exp\left(-B\left(\frac{1}{V_F} - \frac{1}{V_{Fcrs}}\right)\right) \qquad (3.115)$$

$$k_{pBs} = k_{pss}$$

This approximate approach will cause the less reactive propagation constant to assume a higher value (i.e. the value of the more reactive constant) temporarily. This should not pose a problem for copolymer systems with reactivity ratios approximately equal to 1.

Eventually, the butadiene monomer propagation may also become diffusion controlled. Then;

$$\text{if } V_F < V_{Vcrb}$$

$$k_{pBB} = k_{pBB0} \exp\left(-B\left(\frac{1}{V_F} - \frac{1}{V_{Fcrb}}\right)\right) \qquad (3.116)$$

$$k_{psB} = k_{pBB}$$

The constants k_{pss0} and k_{pBB0} represent the chemically controlled propagation constants. When the propagation constants become diffusion controlled, the reactivity ratios must be re-evaluated.

$$r_s = k_{pss}/k_{psB} \quad ; \quad r_B = k_{pBB}/k_{pBs} \qquad (3.117)$$

When the fractional free volume drops to 0.025, the reacting mixture becomes a glass and the propagation constants should become effectively zero (solid state propagation).

3.3 Parameter Sensitivity Study

3.3.1 Object

To justly criticize the model adequacy, the accuracy with which the model parameters are known must be determined. Parameters obtained through model fitting or estimated from experience or intuition may be in considerable error. Even parameters obtained from the literature may be evaluated at inappropriate conditions. A sensitivity study was undertaken

for the present model to determine which parameters affect the model predictions most and consequently need to be known most accurately.

3.3.2 Method

All chemical and most physical constants were studied. Output variables which are affected by each studied parameter were identified. The parameters were purturbed one at a time, positively and negatively by 10% of their value. The magnitude and direction of the corresponding steady-state deviations in the output variables were noted.

Such an approach does not illucidate the interactions between parameters. A factorially designed study would be ideal for this purpose, however, for the number of parameters of the present model, such an effort would be monumental.

It should be noted that some parameters may become more or less important at different operating conditions. For example, some parameters are functions of copolymer composition or reaction temperature. For this study, the conditions and ingredients for cold SBR production in a CSTR were simulated. These conditions were consistent with the conditions under which some of the parameters were fit from data.

3.3.3 Results and Discussion

The results of the parameter sensitivity study are presented in Tables 3.1 through 3.4. In some cases, only one of a similar group of parameters was presented to minimize redundancy.

The rate constant for the iron oxidation reaction, k_1, has a moderate effect on conversion, X, and particle number N_p. Surprisingly, the parameter k_2, which governs the rate of Fe^{2+} regeneration has a negligible effect on X or N_p. This stems from the fact that the reducing agent is typically in excess such that most of the iron present is in the Fe^{2+} state.

After considering the effect of the composition of monomers in the particles, it is clear that the propagation constants, k_{pss} and k_{pBB}, have a significant effect on X and N_p as well as the molecular mass variables ($\bar{M}_n$, $\bar{M}_w$, $\bar{B}_{N3}$, $\bar{B}_{N4}$). Propagation constants are available in the literature, however, their reported values may differ widely as shown by Kao, et al. [1983] for the styrene propagation constant. Clearly, in choosing constants from the literature one must take great care to ensure the conditions of the experiments performed were appropriate. The reactivity ratios, r_s and r_B, appear to have a significant effect on composition and only a small effect on conversion.

The parameters affecting the molecular mass variables have no effect on any of the primary variables such as X or

Table 3.1

Parameter Sensitivity Study Results: Chemical Constants (Average of Absolute Response to (+/-) 10% change in the parameters)

Parameter Studied	Percent Output Deviation in Response to a 10% Change in the Parameters					
	X	N_p	ACCN	$\overline{M}_N$	$\overline{B}_{N3}$	$\overline{B}_{N4}$
Base Case	9.73 (%)	4.10×10^{18} #/dm^3 H_2O	0.1157	105900 9/mol	0.052 #/molecule	0.121 #/molecule
k_1	2.9	2.8				
k_2	0	0				
k_{pss}	0.1	0.1		0.1		
k_{pBB}	4.6	4.0		8.2		
r_s	0	0	0.7			
r_b	-1.4*1	0	-7.3*1			
k_{fss}	0	0		0	0	0
k_{fBs}	0	0		-0.7*1	-0.7*1	-0.7*1
k_{fpsB}	0	0		0	0.1	0
k_{fpBB}	0	0		0	1.1	0
k_{fBx}	0	0		-6.0	-6.0	-6.0
k_{fsx}	0	0		-0.1	-0.1	0
$k^*_{ps_1}$	0	0		0.4	3.6	0.4

*1 A negative response was observed to a positive purturbation. This is denoted by a (-)ve sign.

Table 3.2

Parameter Sensitivity Study Results: Physical Constants (Average of Absolute Response to (+/-) 10% Change in the Parameters)

Parameter Studied	Percent Output Deviation in Response to a Change in Parameters			
	X	N_p	$\bar{D}_N$	$A_m/(A_m + A_p)$
Base case	10.15 %	4.327×10^{18} #/dm^3 H_2O	36.8 nm	0.3024
p	5.1	4.7	-3.2*1	
M_E	0	0	0	0
A_s	7.3	7.2		6.9
$[E]_{CMC}$	-1.5*1	-1.4*1		-1.4
	X	T_J		
Base case		268.8 K		
C_{pB}	0	-0.1*1		
C_{pp}	0	0.1		
ΔH_p	0	-1.8*1		
U	0	1.7		

*1 A negative response to a positive purturbation. This is noted by a (-)ve sign.

Table 3.3

Parameter Sensitivity Study Results: Diffusion Controlled Kinetics Parameters (Average of Absolute Response to (+/-) 10% Change in the Parameters)

Parameter	Percent Output Deviation in Response to a Change in Parameters	
	X	$\bar{n}$
Base case	9.73 %	0.5009
α_s	0	-0.4
α_B	-0.1	-0.7
α_p	-0.1	-2.8
T_{gs}	0	0.3
T_{gp}	0.3	13.4
V_F^{SAT}	0.2	3.5
$V_{F_{crs}}$	0	0
A	0.1	2.1
B	0	0
$k_{t_{p0}}$	0	-0.8

A negative response to a positive purturbation is denoted by a (-)ve sign.

Table 3.4

Parameter Sensitivity Study Results: Partition Coefficients (Average of Absolute Response to (+/-) 10% Change in the Parameters)

Parameter	Percent Output Deviation in Response to a Change in Parameters			
	X	N_p	$[S]_p$	$[B]_p$
Base case	9.72 %	4.102×10^{18} #/dm^3 H_2O	0.853 mol/dm^3	4.562 mol/dm^3
K_{SMW}	3.9	7.1	-1.2	-9.7
K_{SWP}	3.9	7.1	-1.2	-9.7
K_{BMW}	-4.4	2.3	-8.8	-0.3
K_{BWP}	-4.4	2.3	-8.9	-0.3
Base case			R_I 2.605×10^{-7} (mol/$dm^3 H_2O$ min)	1.824×10^{-6} $\frac{mol}{min}$
K_{IMW}	-2.3	-2.3	-8.0	-8.0
K_{IWP}	0.4	0.4	1.3	1.3
		$\overline{M}_N$	$\overline{B}_{N3}$	$\overline{B}_{N4}$
Base case		105900	0.0519	0.1206
K_{XMW}	0	4.5	4.5	4.5
K_{XWP}	0	5.3	5.3	5.3

A negative response to a positive purturbation is denoted by a negative sign.

N_p. The transfer to chain transfer agent (CTA) constant has the most prominent effect of all molecular mass parameters. This is significant since the transfer to CTA reaction may be diffusion controlled and consequently not known accurately. The transfer to monomer parameters affect all molecular mass variables. The transfer to polymer parameter only affects tri-functional branch point frequencies. Interestingly, the propagation with polymer constant affects all molecular mass variables and the tri-functional branch frequency more than the tetra-functional branch frequency.

Diffusion controlled termination and propagation are not important in cold SBR polymerization. Consequently, the associated parameters have little effect on the model predictions. Luckily, the diffusion controlled kinetic parameter which affects the model predictions slightly is the glass transition temperature of the polymer T_{gp}. It is fairly well known.

Of the physical constants examined, the copolymer density, ρ_p, and the soap covering potential, A_s, have the greatest effect on X and N_p. The density of cold SBR is known, however, the densities of copolymers of different compositions are needed for hot SBR simulations. It would be useful to correlate copolymer density with composition.

Since the reactor temperature is controlled, purturbations in the heat balance parameters have no effect on the primary output variables (X and N_p). Their effects were

observed in the jacket and jacket feed temperatures T_J and $T_{J,in}$. Only the heat of polymerization, ΔH_p, and the overall heat transfer coefficient, U, have significant effects on T_J. In the present model, ΔH_p is only roughly estimated and should be re-evaluated in light of its significance. The importance of the overall heat transfer coefficient indicates that it is a useful design parameter.

The partition coefficients for the monomers have a significant effect on both conversion and particle number. It is noted that in fact the product of the partition coefficients is important rather than their absolute values. If both coefficients of a particular monomer are adjusted by reciprocal amounts, X and N_p are not affected significantly. It is also noted that a perturbation of a partition coefficient of one monomer has a significant effect on the concentration of the other monomer. The initiator partition coefficients have a significant effect on X and N_p. The CTA coefficients have a significant effect on the molecular mass variables. Both initiator and CTA partition coefficients were roughly estimated for this model and should be re-evaluated. It is also suspected that the initiator and CTA partition coefficient values may be confounded with the parameters k_1 and k_{fsx}, k_{fBx} respectively.

3.3.4 Summary and Conclusions

The parameters which were found to have the most

important effect on the model predictions were: A_s, k_{pss}, k_{pBB}, k_1, r_s, r_B, k_{fsx}, k_{fBx}, ρ_p and the partition coefficients. The partition coefficients were considered to be the least well known of the parameters and it is recommended that they be determined experimentally for each specific reaction condition and comonomer composition if the model is to be applied quantitatively. Parameters k_1 and k_{fsx}, k_{fBx} were also considered poorly known and it was suggested that the parameters may be confounded with their respective partition coefficients. In general, the molecular mass parameters had no effect on conversion.

Values for the parameters A_s, k_{pss}, k_{pBB}, r_s, r_B and ρ_p are available in the literature. However, where reaction conditions or copolymer compositions vary from the conditions under which the reported parameters were determined, the above parameters should be re-evaluated.

CHAPTER 4

MODEL TESTING

4.1 Introduction

Ideally, the model should be tested and verified with an appropriately designed experimental program. All facets of the model could be tested and all semi-empirical constants, such as the initiator decomposition efficiency, could be estimated. Unfortunately, an experimental program was beyond the scope of this project. Instead, the model is tested using a number of data sets published in the literature. Not having been designed for this purpose, the literature data sets do not provide enough information to test all of the model algorithms. Furthermore, indications of experimental error are not given which makes the quality of the model fit difficult to judge. In some cases, the data were interpolated from graphs which further increases their uncertainty.

In section 4.3 the model is tested with three sets of SBR data from the literature. Along with indicating the model adequacy, these tests should help evaluate the constants used in the model. Section 4.4 presents simulations of styrene homopolymerization data. These simulations check the predictions of the model as a dynamic CSTR and test the diffusion controlled termination and propagation algorithms. The

next section (4.2) presents qualitative checks of the nucleation mechanism and the steady-state CSTR predictions.

4.2 General Trends of Model Predictions

4.2.1 Test of Model Dependence on Initiator and Emulsifier Concentrations

Smith and Ewart found the following dependence for particle number in a batch reactor following case II kinetics:

$$N_p \propto R_I^{0.4} [E]^{0.6} \qquad (4.1)$$

This was discussed in section 2.2.4. The particle nucleation mechanism of the present model is fundamentally similar to that of Smith and Ewart in that radicals are assumed to be captured by micelles in proportion to the fraction of micellar to total organic phase surface area in the reactor. To check the behaviour of the model, simulations were performed with varying initiator and emulsifier levels.

The results obtained from the monodispersed particle model clearly indicated that the Smith-Ewart dependencies hold. The observed initiator dependence was to the 0.41 power. The observed emulsifier dependence was to the 0.61 power. The close agreement follows from the fact, shown in section 3.2.9, that the difference in particle number and particle area predictions of the monodisperse and polydisperse models was small.

4.2.2 Comparison with the Steady-State Model of Wong [1984]

The steady-state CSTR model for SBR developed by Wong [1984] uses the same fundamental assumptions as the present model. Furthermore, the redox initiation kinetic parameters, k_1 and k_2, the partition coefficients and the kinetic parameters affecting molecular mass used in the present model were estimated by Wong [1984] from some limited plant data. Other constants used in the two models differ only slightly.

As a qualitative check of the present dynamic model, it was proposed that the steady-state predictions after all transients have decayed should match those of Wong [1984]. This should verify that the model predictions are physically reasonable for the steady-state operation of a CSTR.

The simulated recipe is given in Appendix B2. The results of the simulation are given in Table 4.1.

The values in the table show that the two models agree very well, with the exception, perhaps, of the mass average molecular mass. The small differences observed in conversion, number average molecular mass and branch frequencies are attributed to the slight differences of some of the constants used.

The mass average molecular mass ($\overline{M}_w$) predicted by the dynamic model is significantly larger than that predicted by the steady-state model. The dynamic prediction is a physically

Table 4.1

Comparison of Steady State and Dynamic Model Predictions

Variable	Steady-State Model Predictions	Dynamic Model Predictions
X	0.103	0.100
ACCN	0.114	0.114
ACCM	0.198	0.199
$N_p(\#/\ell_{H_2})$	$4.54 * 10^8$	$4.42 * 10^8$
Production rate (kg/min)	5.64	5.48
$\overline{M}_n$ (g/mol)	80000	88000
$\overline{M}_w$ (g/mol)	257000	306000
$\overline{B}_{N3}$ (#/molecule)	0.245	0.273
$\overline{B}_{N4}$ (#/molecule)	0.0275	0.0306
$\overline{D}_N$ (nm)	25.9	26.3
$\overline{D}_W$ (nm)	34.6	34.5
$\overline{D}_w/\overline{D}_N$	1.33	1.31

acceptable value, however upon examining its time history it was apparent that the $\overline{M}_w$ prediction was not at steady-state and was, in fact, increasing slightly. This increase was observed to occur over a very long time period.

Though the final value was not greatly different from that quoted, the fact that the time to steady-state was very long is suspicious. This is discussed in more detail in Chapter 5 and in Appendix A3.

In conclusion, the steady-state predictions of the dynamic model are consistent with those of Wong [1984].

4.3 Simulation of SBR Literature Data

4.3.1 Data of Mitchell and Williams [1948]

Mitchell and Williams [1948] examined the batch emulsion copolymerization of styrene/budadiene at 50°C when styrene was in excess relative to butadiene. Only conversion versus time data were reported. Potassium persulphate was used as the initiator. As mentioned earlier, the mechanism of initiation of dienes by persulphate is unknown though it is recognized that mercaptans play a role in initiation. Mitchell and Williams [1948] noted that the rate of initiation and the length of the induction periods before polymerization increased with the proportion of styrene in the charge. The durations of the induction periods were not published.

To simulate the Mitchell and Williams [1948] data, their recipe had to be modified as shown in Appendix B2. The

physical properties of the emulsifier used by Mitchell and Williams were difficult to specify because the emulsifier was a mixture of fatty acid soaps enhanced by a commercial stabilizing agent. Instead, the properties of an equal mass of sodium dodecyl sulphate were assumed. To fit the model predictions to the data, only one parameter, the rate of initiation, R_I, was adjusted. This was rationalized on the basis that the lack of understanding of the initiation mechanism, the presence of impurities as indicated by the induction periods and the assumption regarding the emulsifier properties could all be lumped into one constant which would affect the nucleation mechanism. The same estimate of R_I was used for every run at the same temperature but at different styrene: butadiene charge ratios. The possibility of diffusion controlled reactions was disregarded. The goal of this simulation was not to fit the data accurately but to predict the general trends of the conversion histories.

The results of the simulations are presented in figures 4.1 through 4.5. A table of the constants used in this simulation is given in Appendix B2. The value or R_I used is $5 \times 10^{-9} mol/min.dm^3 H_2O$. The fit of the data is probably reasonable given the experimental error. The trend of increasing reaction rate with increasing styrene composition is clearly shown.

With the quality of predictions observed, it is difficult to make a statement on the adequacy of the partition

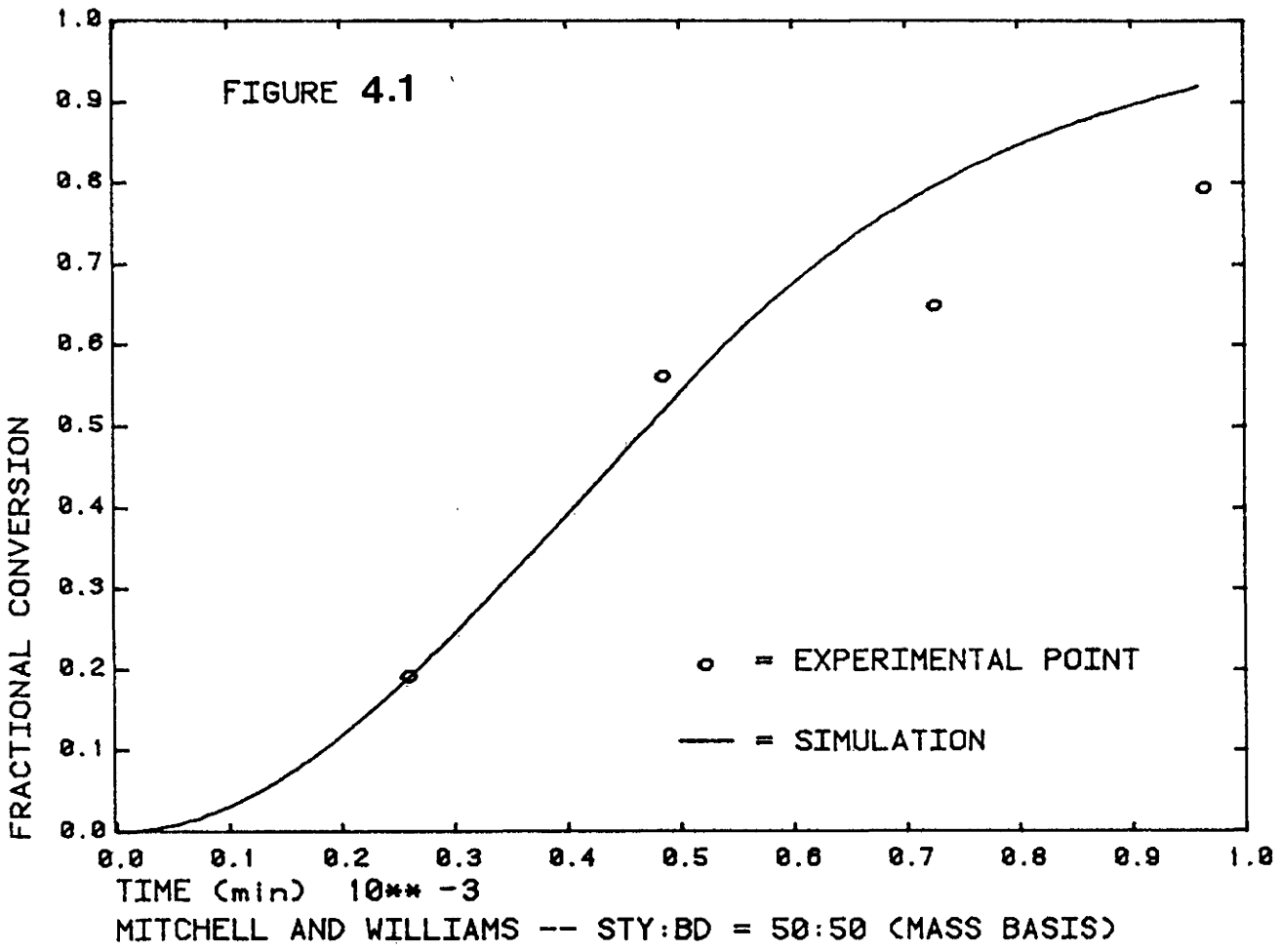
FIGURE 4.1
FRACTIONAL CONVERSION
1.0
0.9
0.8
0.7
0.6
0.5
0.4
0.3
0.2
0.1
0.0
0.0 0.1 0.2 0.3 0.4 0.5 0.6 0.7 0.8 0.9 1.0
o = EXPERIMENTAL POINT
—— = SIMULATION
TIME (min) 10** -3
MITCHELL AND WILLIAMS -- STY:BD = 50:50 (MASS BASIS)

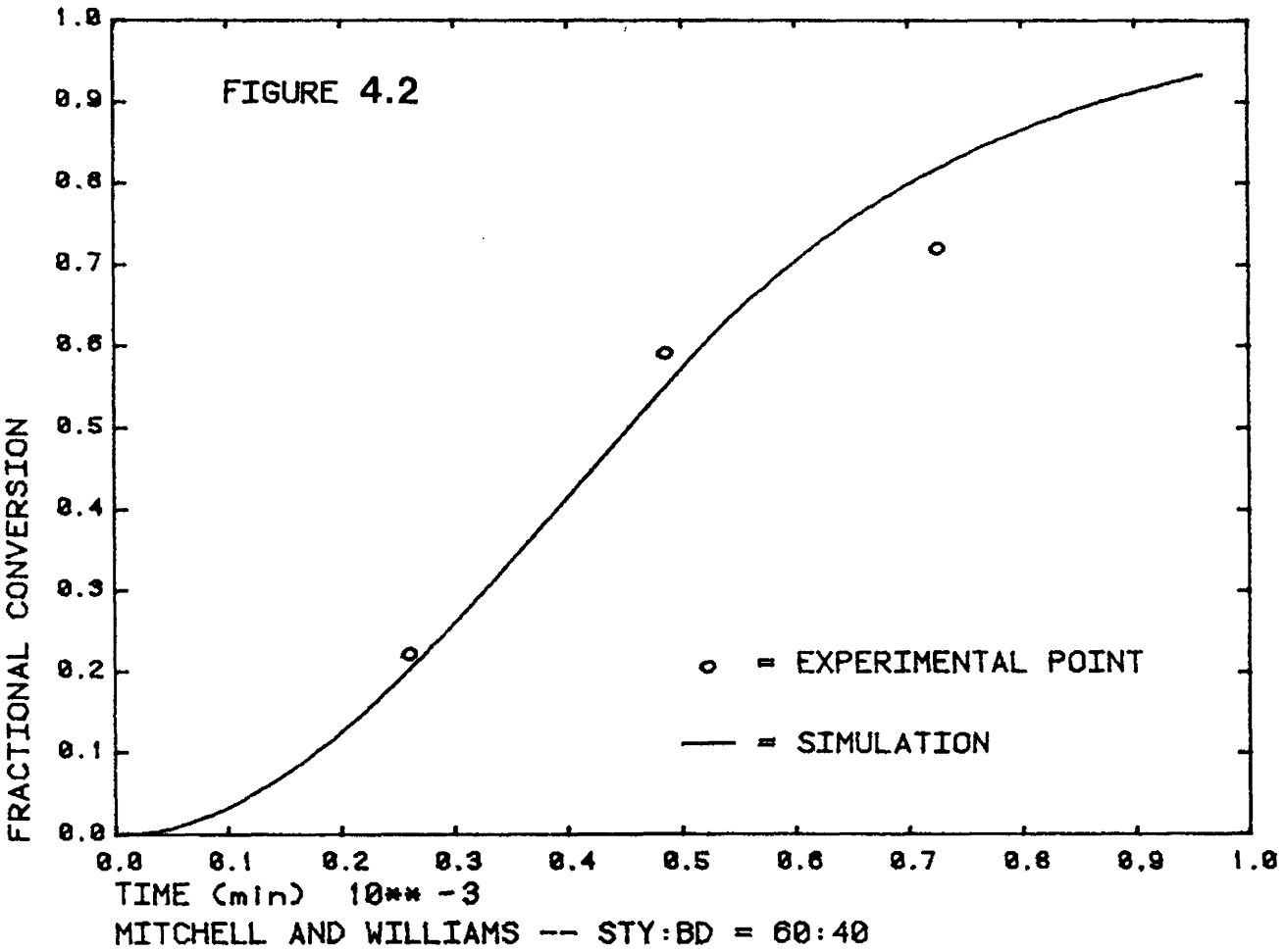
FIGURE 4.2
FRACTIONAL CONVERSION
1.0
0.9
0.8
0.7
0.6
0.5
0.4
0.3
0.2
0.1
0.0
0.0 0.1 0.2 0.3 0.4 0.5 0.6 0.7 0.8 0.9 1.0
o = EXPERIMENTAL POINT
— = SIMULATION
TIME (min) 10** -3
MITCHELL AND WILLIAMS -- STY:BD = 60:40

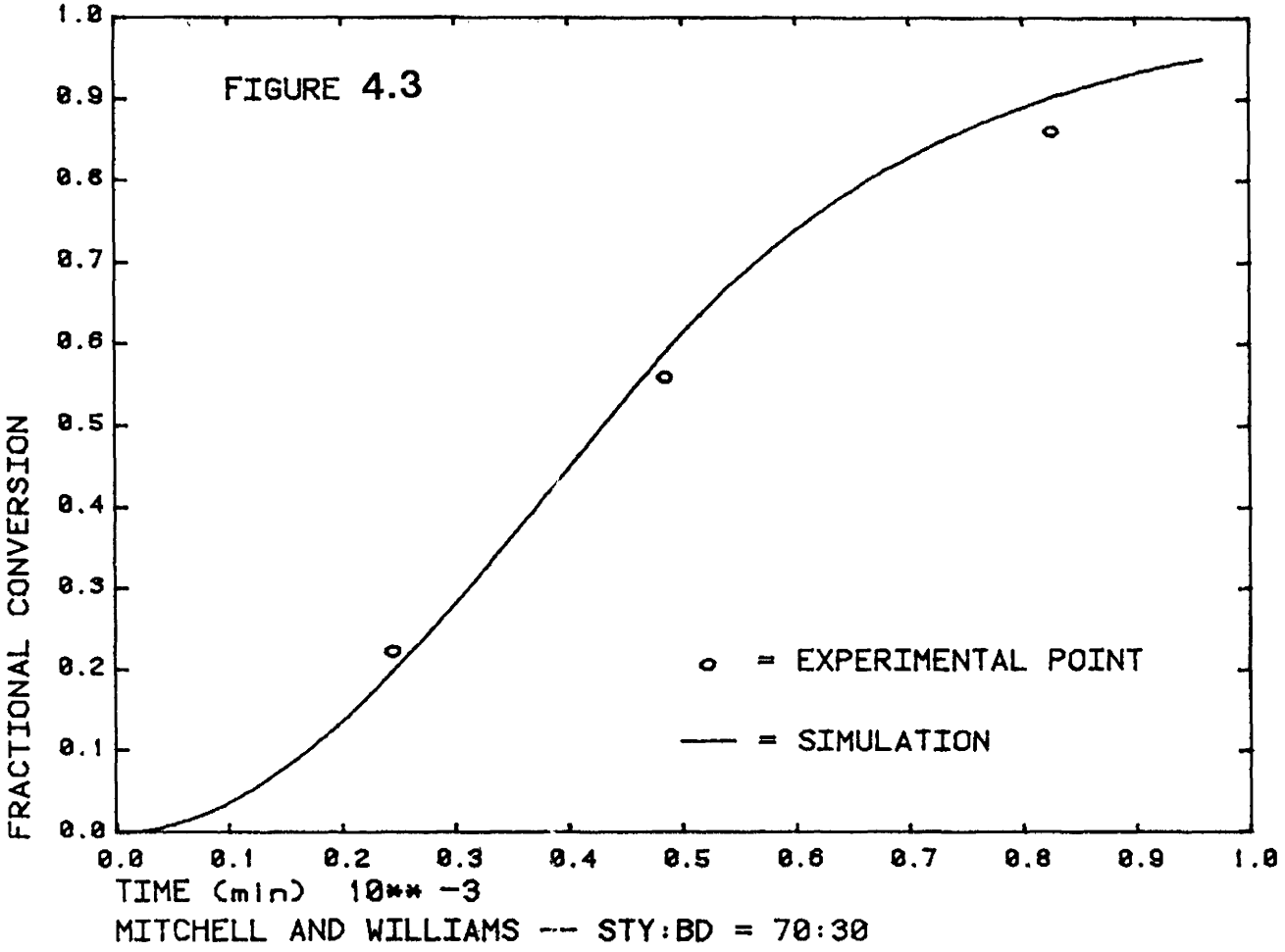
FIGURE 4.3
FRACTIONAL CONVERSION
1.0
0.9
0.8
0.7
0.6
0.5
0.4
0.3
0.2
0.1
0.0
0.0 0.1 0.2 0.3 0.4 0.5 0.6 0.7 0.8 0.9 1.0
o = EXPERIMENTAL POINT
—— = SIMULATION
TIME (min) 10** -3
MITCHELL AND WILLIAMS -- STY:BD = 70:30

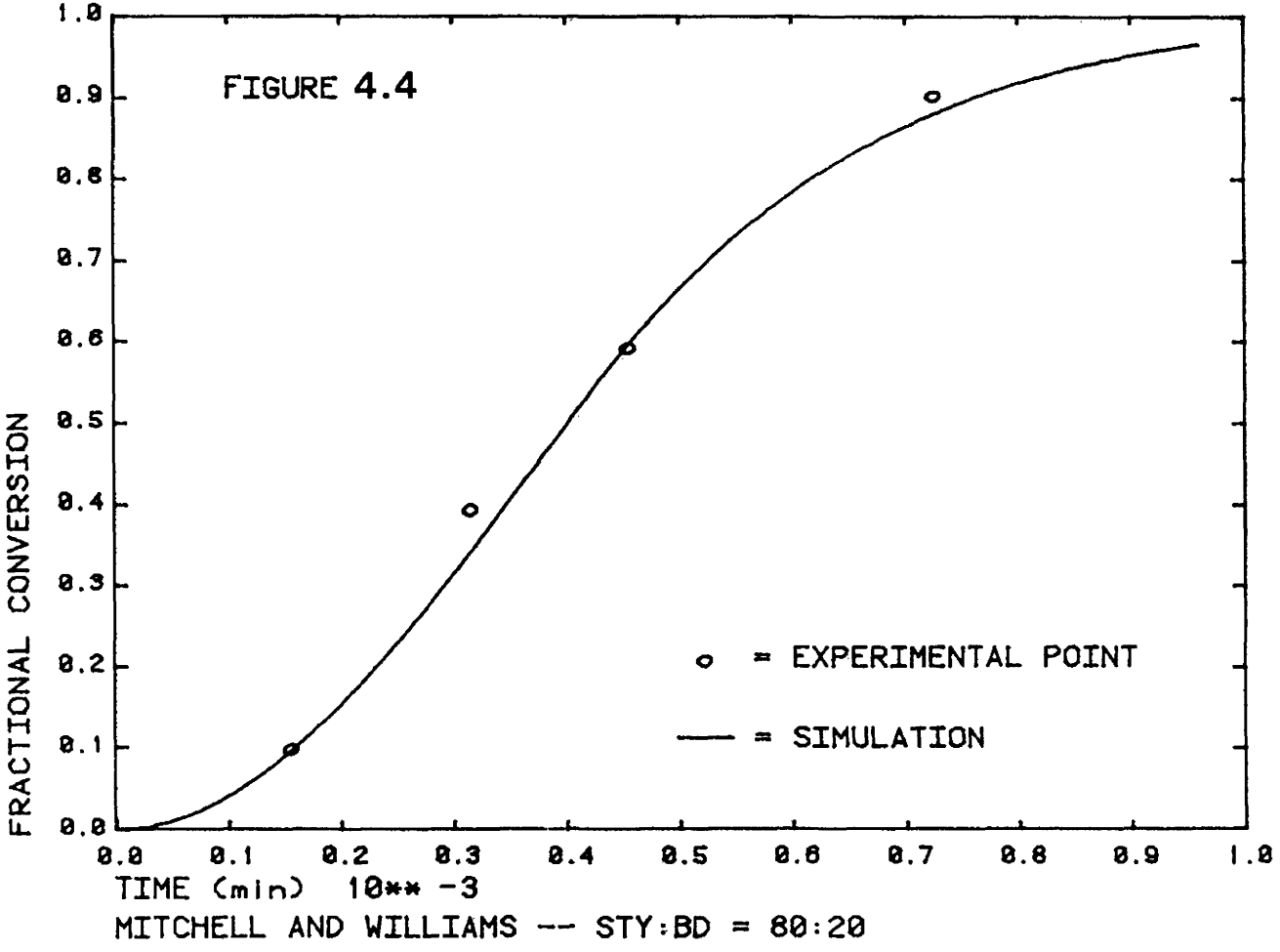
FIGURE 4.4
FRACTIONAL CONVERSION
1.0
0.9
0.8
0.7
0.6
0.5
0.4
0.3
0.2
0.1
0.0
0.0 0.1 0.2 0.3 0.4 0.5 0.6 0.7 0.8 0.9 1.0
o = EXPERIMENTAL POINT
— = SIMULATION
TIME (min) 10** -3
MITCHELL AND WILLIAMS -- STY:BD = 80:20

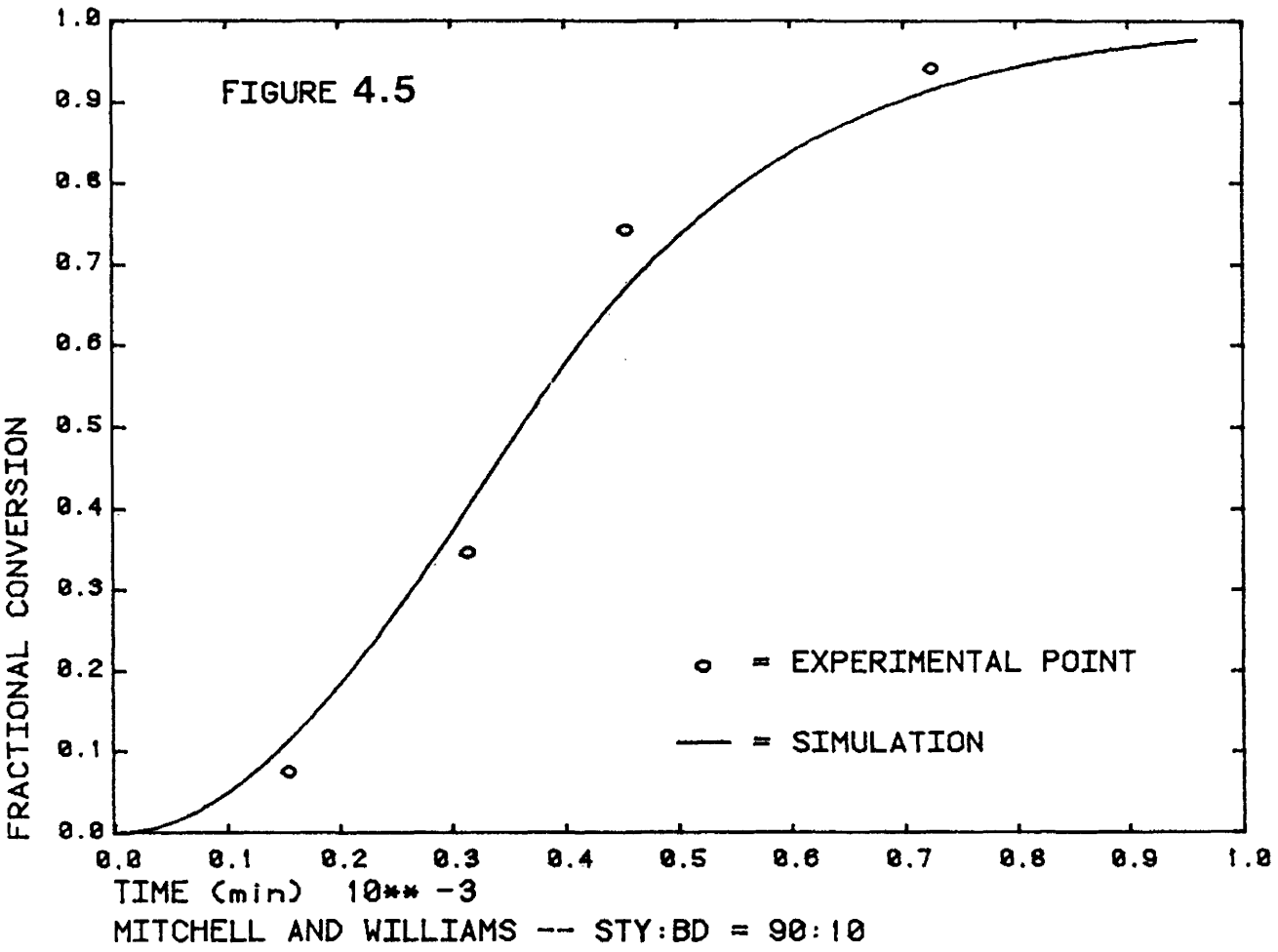
FIGURE 4.5
FRACTIONAL CONVERSION
1.0
0.9
0.8
0.7
0.6
0.5
0.4
0.3
0.2
0.1
0.0
0.0 0.1 0.2 0.3 0.4 0.5 0.6 0.7 0.8 0.9 1.0
o = EXPERIMENTAL POINT
—— = SIMULATION
TIME (min) 10** -3
MITCHELL AND WILLIAMS -- STY:BD = 90:10

coefficients. It is recognized that the partition coefficients used were fit originally from data collected under significantly different reaction conditions and for different monomer ratios. The value of the rate of initiation, R_I, finally chosen is reasonable considering the effect of dienes on initiation. However, it should be remembered that the effects of impurities and of the approximation of emulifier physical constants are included in the value of R_I.

In conclusion, the model was able to simulate the trends in the conversion data of Mitchell and Williams [1948]. However, since they reported no information on the numbers or diameters of the particles, the initiation mechanism, the length of inhibition period or the molecular masses, the model could not be thoroughly evaluated with this data.

4.3.2 Data of Carr, et al. [1950]

Carr, et al. [1950] and Kolthoff, et al. [1951a] [1951b] studied the effect of emulsifier amount and type on the emulsion polymerization of SBR. They used the standard hot recipe shown in Table 1.1. The data set simulated in this work is from Carr, et al. [1950], and consists of a series of experiments using equal masses of different chain length fatty acid soaps. The soaps studied were lauric (C-12), myristic (C-14), palmitic (C-16) and stearic (C-18) acids. Plots of the experimental data show the conversion profiles

generally have the same slope over their stage 2 period indicating that approximately the same numbers of particles were being nucleated in each case. The curves differ mainly in the length of their respective nucleation periods. No inhibition periods are apparent in the plots.

In simulating these experiments, emulsifier parameters for the different fatty acid soaps were taken from the literature (Brandrup and Immergut [1975]). Otherwise the parameters and constants presented in Appendix B1 were used. Once again, the problem of specifying the persulphate/diene initiation rate was encountered. The rate of initiation found in the previous section (section 4.3.1) was used as a first estimate. This value (R_I = 5 x 10^{-9} mol/min dm^3) was found to be a good first estimate. However, it was noted the change in emulsifier parameters (A_s and $[E]_{cmc}$) alone was insufficient to fit all of the data sets adequately. This suggested that the identity of the emulsifier had other, more dramatic effects on the polymerization. The following potential explanations for the effect of emulsifiers on the polymerization were proposed: 1) Different chain length emulsifiers form different sized micelles. 2) The efficiency of capture of a micelle may be a function of emulsifier molecular mass. 3) The different emulsifiers have different levels of impurity. The impurity may retard nucleation. 4) Since the same mass of emulsifier was used in each case, the number of emulsifier molecules added would be different.

Therefore, if the emulsifier were taking part in the radical forming reactions, different rates of initiation could be explained on emulsifier availability. 5) Since no buffering agent is mentioned in the recipe, perhaps the different moles of soaps added altered the pH of the solution to different extents. The pH may have an effect on the persulphate initiation reaction.

Kolthoff, et al. [1951b] and Kolthoff, et al. [1951d] have observed that the initiation rate of persulphates is affected by the amount and type of emulsifier. Kolthoff, et al. [1951d] proposed that emulsifiers and sulphate radicals react to form carboxylate radicals. Kolthoff, O'Connor and Hansen [1955] proposed instead that emulsifiers enhance the solubility of monomers, aiding water phase polymerization and consequently decreasing the frequency of water phase termination with the net effect of making the initiator more efficient. Hamielec [1984a] proposed that the fatty acid soaps may participate in the initiation mechanism in a manner similar to the reaction of acrylic acid with persulphate in aqueous solutions as described by Manickam, et al. [1979].

The first two proposed explanations for the effect of different emulsifiers on nucleation prompted the fitting of a micellar capture efficiency factor, ε, of the form described in section 3.2.4. It was found that varying ε not only altered the nucleation period but also the number of particles dramatically. Satisfactory fits were not obtained.

The latter three proposed explanations rationalized the fitting of the rate of generation of radicals, R_I, for each emulsifier type. The results of this exercise are shown in figures 4.6 through 4.9. The variation of R_I with emulsifier type is shown in Table 4.2 along with the numbers of particles predicted in each case.

The model fit to the experimental data was satisfactory. The fitted rates of initiation were consistent in magnitude with the value found in section 4.3.1. It should be recognized that the fitted rates of initiation could include the effects of other phenomena, such as reactions with impurities or increased initiation efficiency as described by Kolthoff, O'Connor and Hansen [1955].

Though the variation and magnitude of the rates of initiation have been rationalized, the lack of particle number or particle diameter data precludes the verification of the nucleation mechanism. The adequacy of the model fit suggests that the kinetic expressions, the chemical constants and the partition coefficients used are reasonable. It may even be said that the collision theory adopted in the model appears adequate, however, given that R_I was fit empirically, the diffusion or alternate theories cannot be discounted.

4.3.3 SBR 1500 Recipe

Experimental conversion - time and composition - conversion data for cold SBR (1500 grade) were published as

Table 4.2

Radical Generation Rate, Polymer Particle Concentration Predictions and Emulsifier Parameters for Various Emulsifiers

Emulsifier	A_s $(\frac{dm^2}{molecule})x10^{-7}$	$[E]_{CMC}$ $(\frac{mol}{dm^3})x10^{2}$	R_I (fit) $(\frac{mol}{min\ dm^3\ H_2O})x10^{9}$	N_P (predicted) $(\#/dm^3 H_2O)x10^{-17}$
C-12	2.49	2.5	2.5	5.3
C-14	2.05	0.65	5	6.4
C-16	1.51	0.17	9	6.4
C-18	1.41	0.049	10	6.0

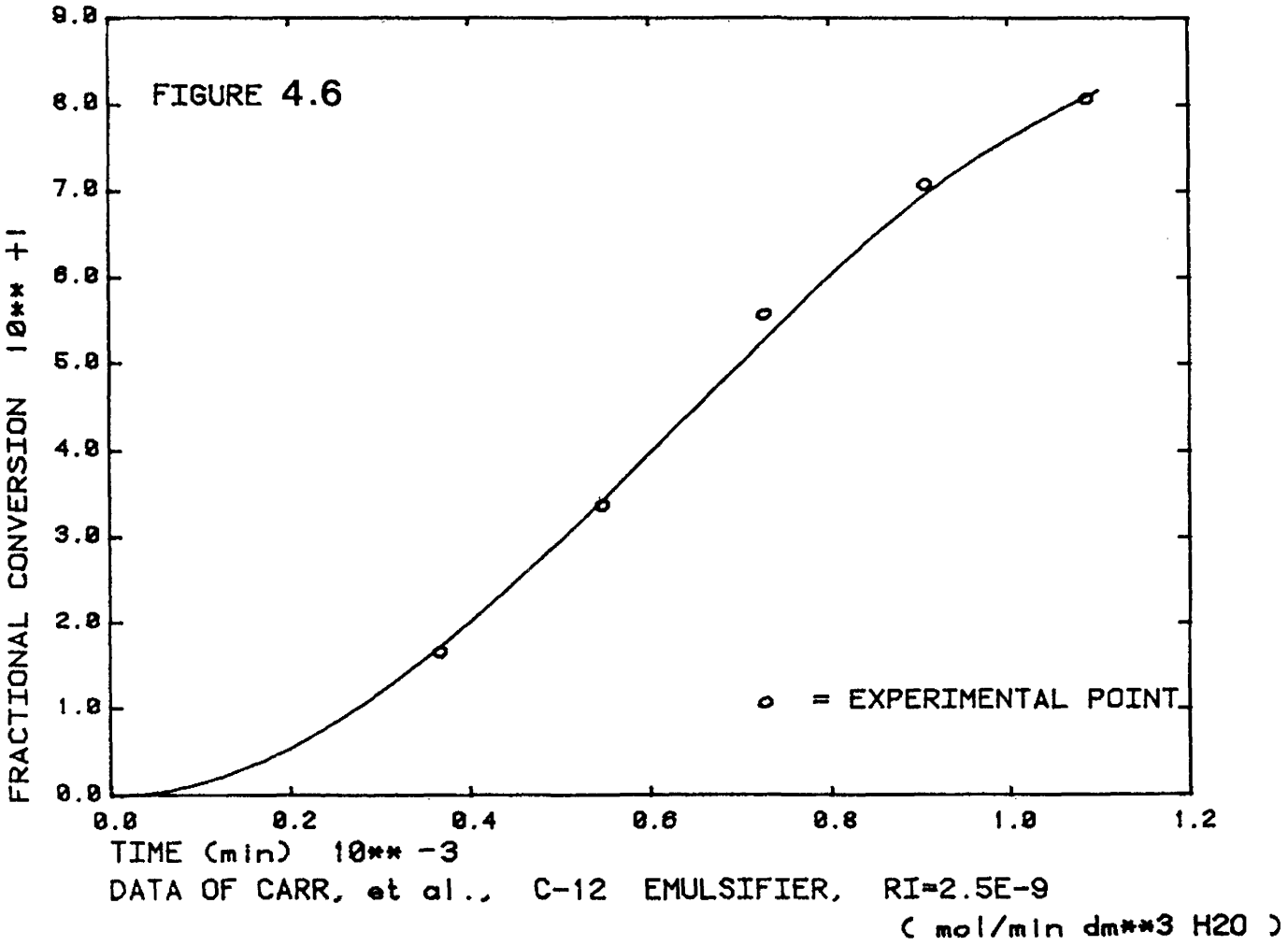
FIGURE 4.6
FRACTIONAL CONVERSION 10** +1
9.0
8.0
7.0
6.0
5.0
4.0
3.0
2.0
1.0
0.0
0.0
0.2
0.4
0.6
0.8
1.0
1.2
o = EXPERIMENTAL POINT
TIME (min) 10** -3
DATA OF CARR, et al., C-12 EMULSIFIER, RI=2.5E-9
(mol/min dm**3 H2O)

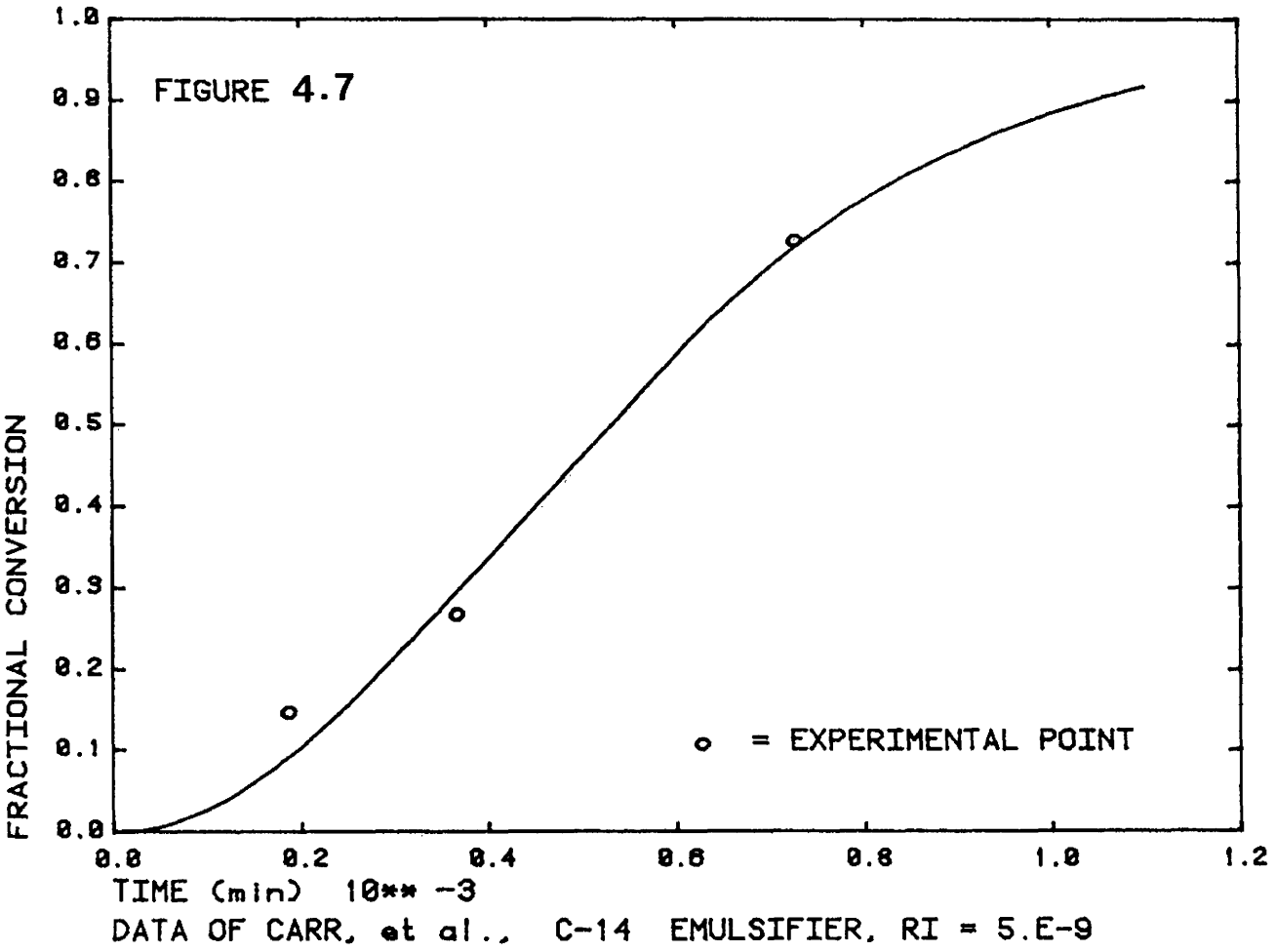
FIGURE 4.7
FRACTIONAL CONVERSION
1.0
0.9
0.8
0.7
0.6
0.5
0.4
0.3
0.2
0.1
0.0
0.0
0.2
0.4
0.6
0.8
1.0
1.2
o = EXPERIMENTAL POINT
TIME (min) 10** -3
DATA OF CARR, et al., C-14 EMULSIFIER, RI = 5.E-9

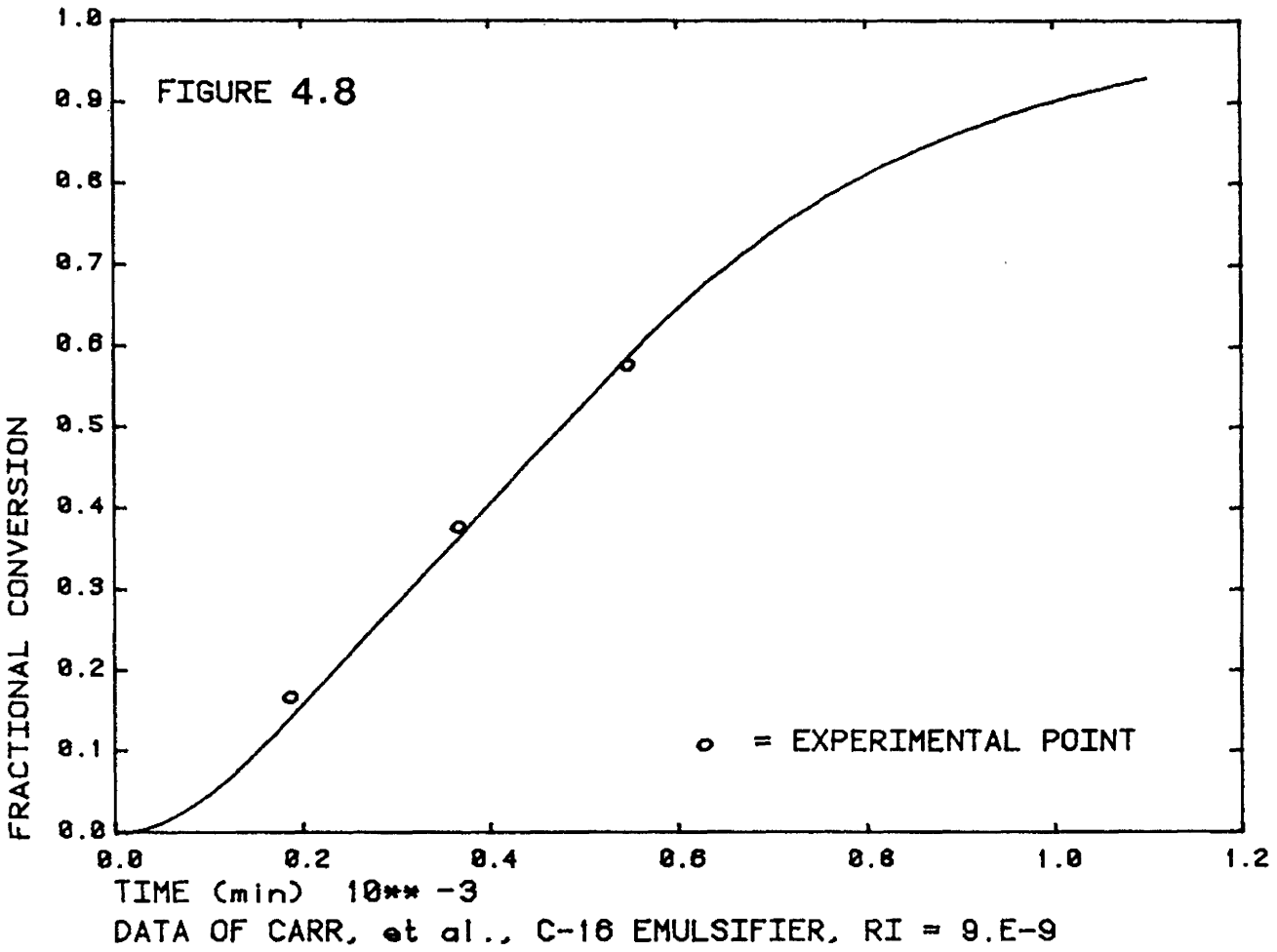
FIGURE 4.8
FRACTIONAL CONVERSION
1.0
0.9
0.8
0.7
0.6
0.5
0.4
0.3
0.2
0.1
0.0
0.0
0.2
0.4
0.6
0.8
1.0
1.2
o = EXPERIMENTAL POINT
TIME (min) 10** -3
DATA OF CARR, et al., C-16 EMULSIFIER, RI = 9.E-9

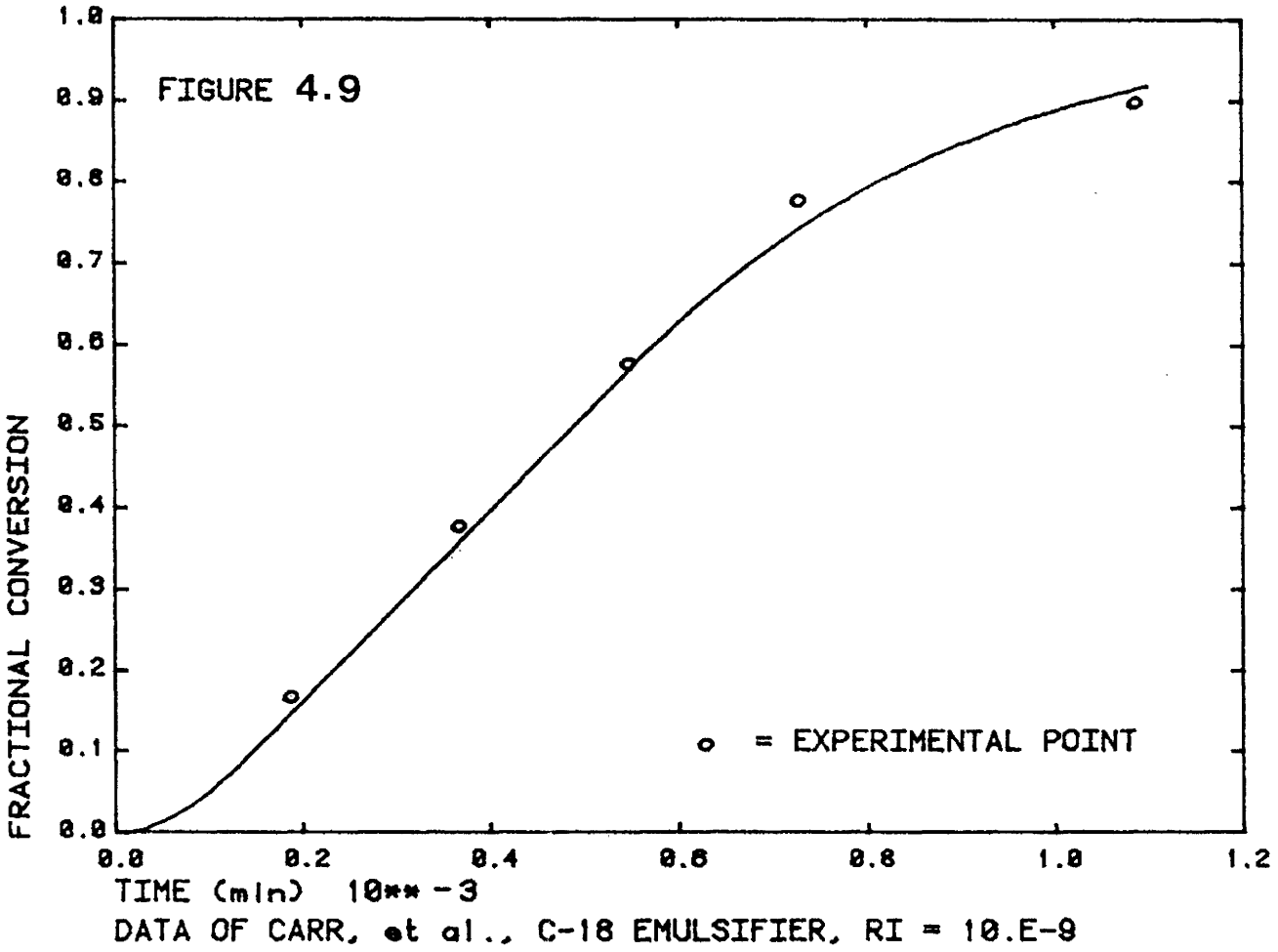
FIGURE 4.9
FRACTIONAL CONVERSION
1.0
0.9
0.8
0.7
0.6
0.5
0.4
0.3
0.2
0.1
0.0
0.0
0.2
0.4
0.6
0.8
1.0
1.2
o = EXPERIMENTAL POINT
TIME (min) 10** -3
DATA OF CARR, et al., C-18 EMULSIFIER, RI = 10.E-9

part of an overview of SBR production in the Encyclopedia of Polymer Science and Technology [1966]. These data were presented in graph form. Examination of the data indicated that an induction period of approximately 2 hours preceded polymerization. An inconsistency in the composition-conversion data was noted. The SBR 1500 recipe indicated an initial charge of 29 parts by mass of styrene. The composition of the copolymer formed at 100% conversion, however, is 28 parts by mass styrene. The data also showed that diffusion controlled termination and propagation are not important.

The SBR 1500 recipe, listed in Table B2, requires approximately twice the amount of initiating species (p-menthane hydroperoxide, iron and sodium formaldehyde sulphoxylate) prescribed by the cold SBR recipe used by Wong [1984] (given in Table B2.1). Understandably, simulation of the SBR 1500 recipe without modification, with the initiator constants of Wong [1984], led to a significant overestimation of conversion. The cause of this overestimation could be the failure to account for impurities. On this basis, an efficiency factor, F, for initiation was fit to the data. It was applied in the following manner.

$$R_I = F\ k_1\ [Fe^{2+}]_w [I]_w$$

The data were fit by trial and error. The best fit corresponded to an F factor of 0.135. The results of the simulation are given in figures 4.10 and 4.11.

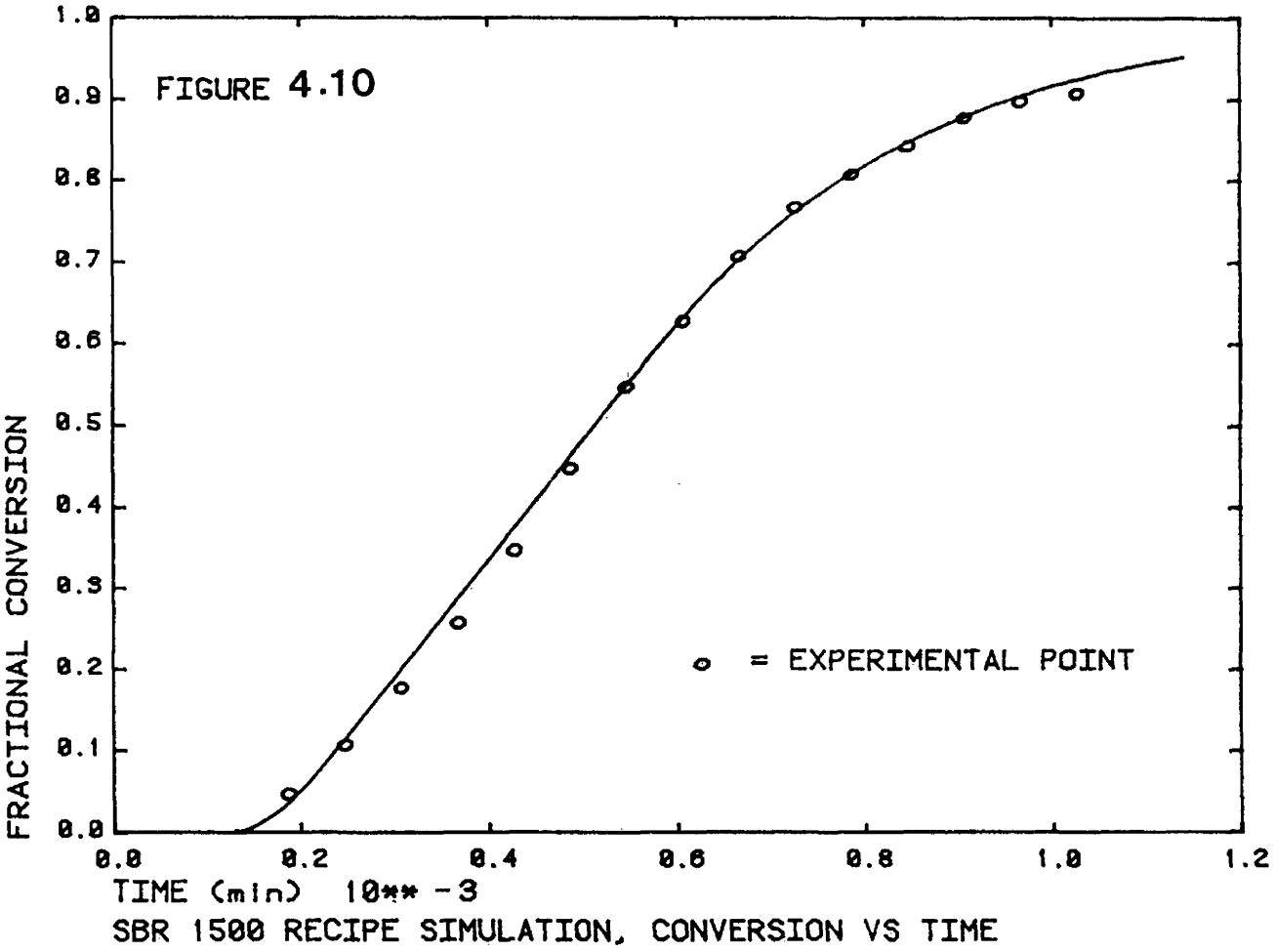
FIGURE 4.10
FRACTIONAL CONVERSION
1.0
0.9
0.8
0.7
0.6
0.5
0.4
0.3
0.2
0.1
0.0
0.0
0.2
0.4
0.6
0.8
1.0
1.2
o = EXPERIMENTAL POINT
TIME (min) 10** -3
SBR 1500 RECIPE SIMULATION, CONVERSION VS TIME

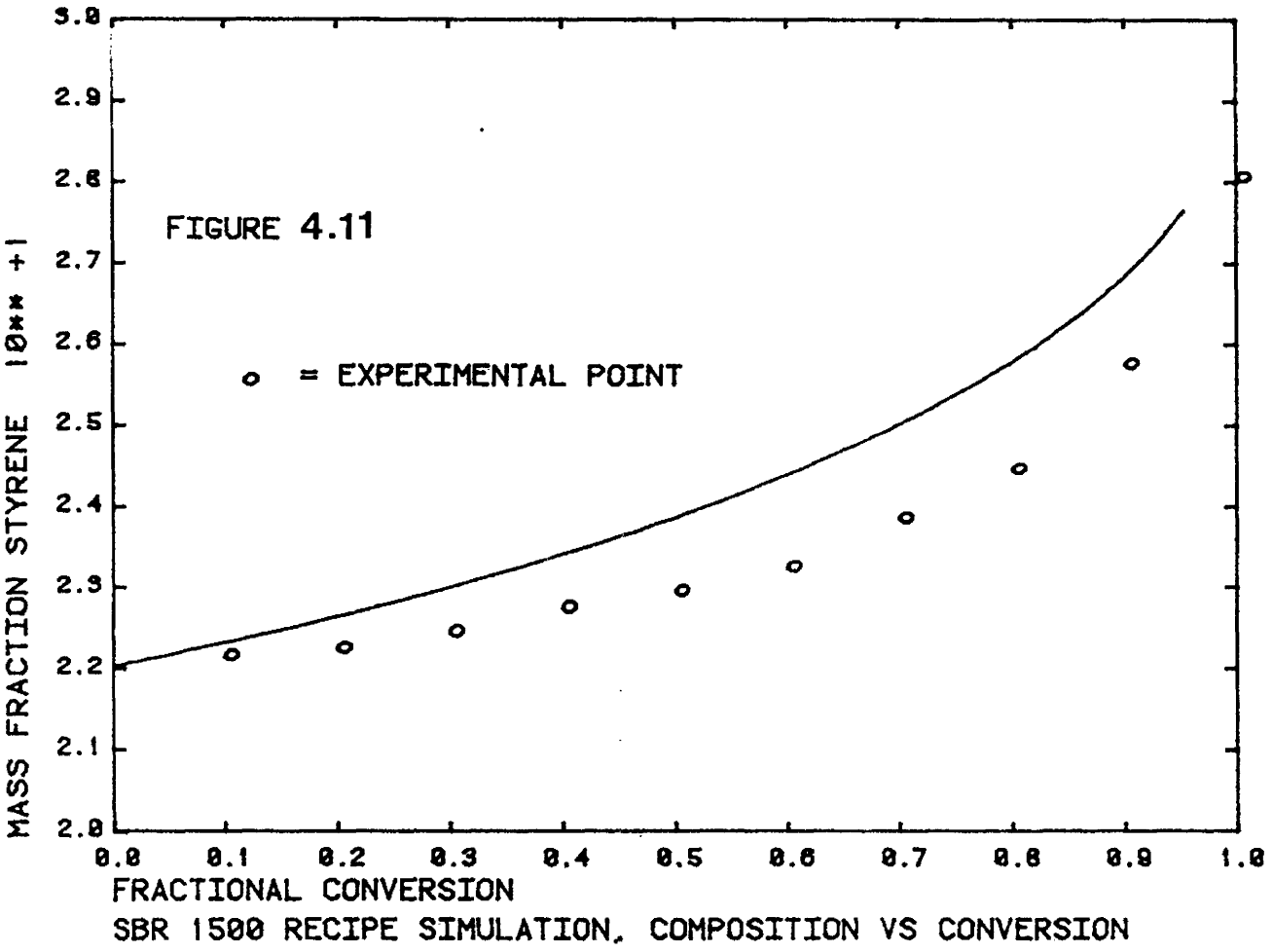

SBR 1500 RECIPE SIMULATION, COMPOSITION VS CONVERSION

The conversion-time data are fit very well. This implies that the chemical kinetic expressions and constants used are reasonable. It may also imply that the partition coefficients are reasonable. However, the composition-conversion data are poorly fit. This suggests that either the partition coefficients or the reactivity ratios are inappropriate. The previously noted inconsistency in the composition data limits the interpretation of the observed fit and precludes an attempt to fit reactivity ratios to the data.

The efficiency factor fit to the data is surprisingly small. It is expected that the true efficiency of initiation is very low ($F \approx 0$) during the inhibition period but then increases and approaches 1 (or perhaps $F = 0.8$ or 0.9) after the inhibition period ends and the impurities have been largely consumed. The efficiency factor actually fit to the data would, therefore, represent the fraction of the initiator not consumed during the inhibition period as well as the effects of subsequent reaction with impurity. It is expected that inadequacies in the initiation kinetic constant k_1 or in the initiator partition coefficients are accounted for in the efficiency factor as well.

Unfortunately, by fitting the efficiency factor, the nucleation and initiation mechanisms have not been tested. A true test of these mechanisms must come from independent experiments. Conditions in plant tests or industrial scale

experiments are probably inappropriate for model testing because of high and undetermined levels of impurities.

4.4.1 Data of Brooks, et al. [1978]

Brooks, et al. [1978] studied the emulsion polymerization of styrene in a continuous stirred reactor (CSTR). The reactor was started full of all ingredients in emulsion form except the initiator. The contents of the reactor were stirred and heated to the reaction temperature. The initiator was fed to the reactor in a separate stream. Brooks, et al. [1978] followed conversion from inception and observed large overshoots and in many cases, damped and even sustained oscillations in conversion. The experimental conditions and results of Brooks, et al. [1978] are summarized in Tables 4.3 through 4.5.

There are apparent inconsistencies in the data of Brooks, et al. [1978] which should be noted. For example, run #6 represents the results of a recipe of equal emulsifier concentration and intermediate initiator concentration compared to runs #1, and #'s 2 and 3. However, the steady state conversion observed in run #6 is 2% lower than the observed steady state conversions of runs 1 and 3. Other inconsistencies are observed between runs 1, 2, 3, 4 and 5.

To simulate these data, reactor conditions and recipes were followed as closely as possible. Concentrations of initiator and emulsifier were assumed to be quoted as moles

Table 4.3

Emulsifier and Initiator Concentrations Corresponding to Experimental Runs of Brooks, et al. (1978)

Run No.	Emulsifier Conc^{n}. $(\frac{mol}{dm^3} * 10^2)$	Initiator Conc^{n}. $(\frac{mol}{dm^3} * 10^2)$
1	3.07	7.87
2	3.07	2.55
3	3.07	2.55
4	2.30	5.11
5	2.30	5.11
6	3.07	4.20
7	3.07	0.93
8	0.75	5.0
9	5.0	4.0
10	6.0	10.0
11	6.0	5.0
12	2.3	2.50
13	2.3	7.5
14	2.85	7.59
15	2.70	7.20

Table 4.4

Comparison of the Experimental Results of Brooks, et al. (1978) and the Simulations of Pollock (1983) and the Present Model: Conversions

Run No.	Peak Conversion (%)			Peak Times (min)		Steady-State Conversion (%)		
	Brooks	Model	Pollock	Brooks	Model	Brooks	Model	Pollock
1	27	27	35	45	35	14	14	15.8
2	23	21.3	28	60	35	13.5	13.9	15.9
3	23	21.3	28	60	35	14.0	13.9	15.9
4	29	18.1	26	45	35	12	9.5	11.5
5	29.5	18.1	26	45	35	12	9.5	11.5
6	23	23.8	31	45	35	12	13.9	15.9
7	9.5	17	23	90	40	7	13.8	15.7
8	11	2.0	8	60	30	6	0.6	2.5
9	38	34.7	43	45	35	29	27	27
10	50	45.6	53	45	30	45.5	43.3	40.5
11	—	——	49	—	—	42	42.8	40.5
12	17.5	15.7	22	60	35	11	9.5	11.4
13	29	20.2	28	45	35	13	9.5	11.4
14	74	38.2	33	120	60	35	16.1	14.6
15	72	36.3	31	120	60	31	15.0	13.7

Table 4.5

Comparison of the Experimental Results of Brooks, et al. (1978) and the Simulations of Pollock (1983) and the Present Model: Particle Radii and $\bar{n}$ at Steady State

Run No	Average Particle Radii at Steady-State (Å)		$\bar{n}$ at Steady-State	
	Brooks	Model	Brooks	Model
1	313	311	0.61	0.505
3	287	310	0.64	0.502
8	251	327	0.26	0.59
9	339	318	0.77	0.501
10	256	336	0.44	0.504
13	350	311	1.08	0.507
14	500	395	4.0	0.517

per dm^3 of latex. The reactor was assumed isothermal. The constants used in the model were consistent with the literature as well as the simulation of the data of Brooks, et al. [1978] by Pollock [1983]. The only exception was that the value of the soap covering potential, A_s used in this simulation was 3.8×10^7 dm^2/mol. The more widely accepted value is 3.67×10^7 dm^2/mol. A table of the constants used in the simulations is given in Appendix B2.

The results of the simulation are presented along with the experimental results of Brooks, et al. [1978] and the simulation results of Pollock [1983] in Tables 4.4 and 4.5. A sample of the simulated dynamic response of run #1 is given in figure 4.12.

For a little more than a half of the experimental runs published, the simulation predicted peak and steady-state conversions to within 2% of the experimental values. The simulation predicted peak conversions for all runs except run #11 for which Brooks, et al. [1978] do not report a peak. If this omission signifies that no peak was observed, it is significant that the model correctly predicted this trend. The model also predicted the steady-state conversion very closely in this case.

The most significant, apparent inadequacy of the model is that it did not predict the observed oscillations, sustained or damped, in any case. In their simulations of the data of Brooks, et al. [1978], neither Pollock [1983] nor Pramojaney

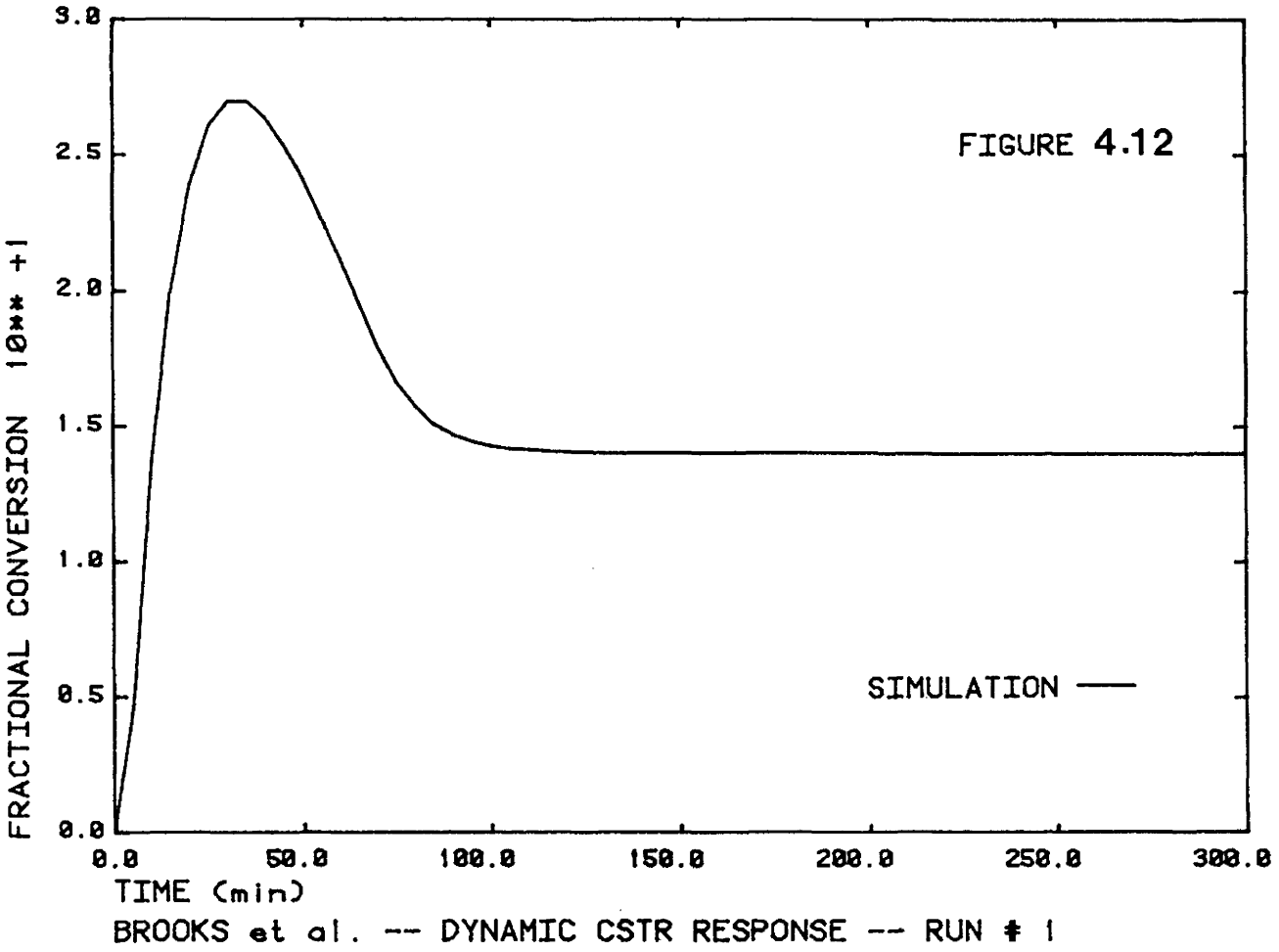
FIGURE 4.12
FRACTIONAL CONVERSION 10** +1
3.0
2.5
2.0
1.5
1.0
0.5
0.0
0.0
50.0
100.0
150.0
200.0
250.0
300.0
TIME (min)
SIMULATION
BROOKS et al. -- DYNAMIC CSTR RESPONSE -- RUN # 1

[1982] could predict the observed oscillations. Brooks et al. [1978] suggest that the observed oscillations are due to the periodic nucleation of particles. This mechanism is explained in more detail in section 5.3. It is of interest to note that the oscillations published by Grene and modelled by Kiparissides, et al. [1979] and the oscillations modelled by Kirrilov, et al. [1978] were believed to be due to the same mechanism but were of a very different nature. The oscillations predicted by these workers are large in magnitude and unsymmetrical. The oscillations observed by Brooks et al. [1978] are small (1 to 4% conversion) and are fairly symmetrical. In fact, given the inconsistencies of the model, the amplitudes of many of the observed oscillations may not be considered significant. The question of oscillations in case II emulsion system is addressed in section 5.3.

The model also predicts the peak conversion times poorly. This is attributed to imperfect mixing or more likely a small induction period due to trace amounts of impurity which were not accounted for by the model. In his simulation, Pramojaney [1982] also showed a transient conversion prediction which predicted an "early" peak time.

Conversions for runs 4, 7, 8, 13, 14 and 15 of the data of Brooks, et al. [1978] were poorly simulated by the model. There is some reason to believe that the significant underestimation of conversion for run #8 may stem from a poor choice of the critical micelle concentration or perhaps from

the lack of accounting for homogeneous nucleation. (Homogeneous nucleation is, however, generally accepted as not important in styrene emulsion homopolymerization). The suspected cause of the poor prediction of runs 14 and 15 is the underestimation of $\bar{n}$ by the model. Brooks et al. [1978] report an experimentally determined $\bar{n}$ of 4.05. This indicates that termination is probably diffusion controlled. The model clearly does not account for this properly; it predicts $\bar{n} = 0.517$. The present model also underestimates particle size significantly in this case. It is of interest that the model of Pollock [1983] does not fit runs 14 and 15 well (Table 4.4) and, in fact, matches the present model in this case. The value of $\bar{n}$ was fixed at $\frac{1}{2}$ in this model. This fact supports the idea that the improper estimation of $\bar{n}$ limits the model predictions in this case.

In conclusion, the model performed relatively well in simulating the data of Brooks et al. [1978]. It did not simulate the observed oscillations. Unfortunately, not enough data were provided to test the nucleation mechanism.

4.4.2 Data of Grancio, et al. [1970]

In a series of emulsion polymerization experiments with styrene, Grancio, et al. [1970] observed a constant reaction rate long after the end of stage 2. To explain their observations, they proposed a heterogeneous morphology for a latex particle which consisted of a polymer rich core and a

monomer rich shell. The concentration of monomer in the monomer rich shell region was assumed to remain at a constant level over a prolonged period. Friis and Hamielec [1973] suggested an alternate interpretation of the data of Grancio, et al. [1970]. Using an empirical correlation obtained from bulk polymerization experiments for the decrease of the termination constant, k_{tp}, with conversion, Friis, et al. [1973] simulated the data successfully by adjusting $\bar{n}$ as a function of k_{tp}, implying that the observed behaviour of the reaction rate was due to diffusion controlled termination (or the "gel effect"). For the purpose of testing the form of the diffusion controlled kinetic constant algorithms, the interpretation of Friis, et al. [1973] was adopted and the data of Grancio, et al. [1970] were simulated.

Five sets of conversion vs. time and monomer mass fraction (in the particles) vs. time data were collected by Grancio, et al. [1970] which corresponded to experiments at two different emulsifier levels. Due to difficulties in recreating initial conditions, perhaps due to impurities, repeat experiments at each emulsifier level were only reproduced to 2% accuracy. Grancio, et al. [1970] measured final particle numbers for experiments for experiments at each level. They used a special combination of emulsifier and stabilizing agent to ensure rapid particle nucleation and preclude any complication of data interpretation because of an extended nucleation period.

One data set from each emulsifier level was simulated. Because Grancio, et al. [1970] used the specialized emulsifier recipe for rapid nucleation, nucleation was not simulated. A constant number of particles was assumed for each run. The number of particles were estimated from the knowledge of the total monomer charged and the final particle sizes measured by Grancio, et al. [1970]. Monomer concentrations were estimated assuming constant monomer volume fractions and the evidence of Grancio, et al. [1970] that the monomer droplets disappeared at 27% conversion. Chemical and physical constants used in the simulation were taken from Friis, et al. [1973]. A list of these constants and recipes for the experiments are given in Appendix B2. The parameters required in the diffusion controlled termination and propagation algorithms are presented, along with their sources in Table 4.6.

It was found by trial and error fitting that A = 0.55 was slightly better than A = 0.6 as given by Sundberg, et al. [1981]. The termination constant at the saturation condition was estimated using the empirical correlation of Hui, et al. (Friis, et al. [1973]) for the conversion X_c = 0.27. This correlation is presented in Appendix B1.

As mentioned in sections 2.2.8 and 3.2.10 the termination constant falls with conversion and levels off at the point where termination is governed by the rate of propagation. This behaviour is shown in figure 4.13 which is a plot of the

Table 4.6

Diffusion Controlled Kinetic Constant Parameters

Parameter	Value	Source
A	0.55	Sundberg, et al. (1981) (A=0.6)
B	0.1275	Harris, et al. (1981)
α_p	0.48×10^{-3}(1/K)	Sundberg, et al. (1981) Harris, et al. (1981)
α_m	1×10^{-3}(1/K)	Sundberg, et al. (1981) Harris, et al. (1981)
Tg_s	167(K)	Sundberg, et al. (1981) Harris, et al. (1981)
Tg_p	365.5(K)	Harris, et al. (1981)
V_{Fcrs}	0.047	Sundberg, et al. (1981)
V_{FIMIN}	0.066	estimated
k_{tp}^{SAT}	7.932 E 8($\frac{dm^3}{mol\ min}$)	estimated

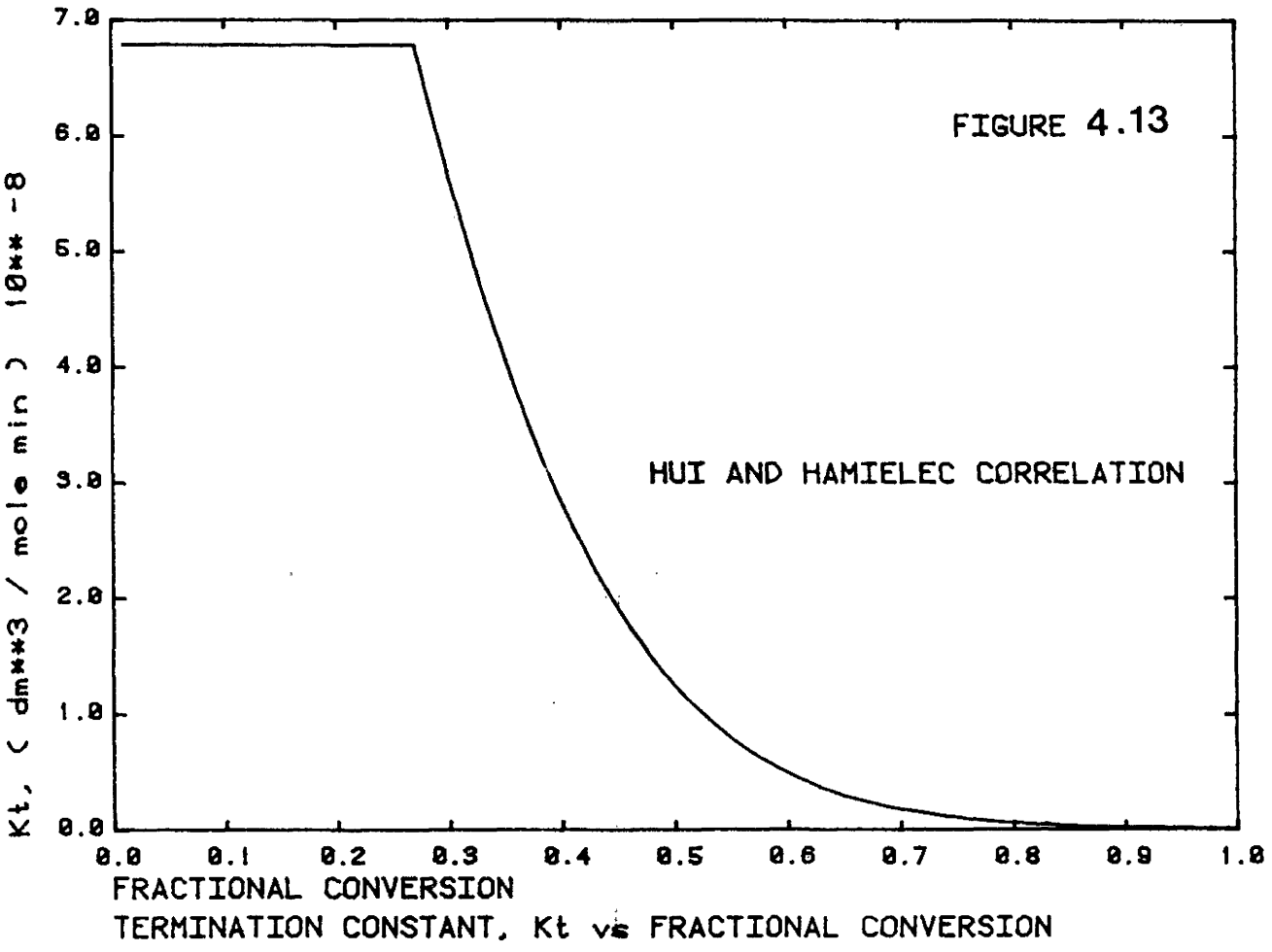

TERMINATION CONSTANT, Kt vs FRACTIONAL CONVERSION

termination constant (Hui correlation) vs. fractional conversion. The initial period of constant termination rate constant occurs while the particles are saturated. To estimate the point at which termination occurs by propagation, V_{FTMIN}, it was convenient to plot $-\ln(k_{tp}/k_{tp}^{SAT})$ vs. $1/V_F$. This plot is shown in figure 4.14. The solid curve represents the correlation. The dashed lines represent the free volume model. The slope of the inclined line is 0.55. The horizontal line represents the constant minimum value of k_{tp}. The point of intersection of these lines represents the point at which termination begins to occur by propagation, V_{FTMIN}.

The results of the simulations are given in figures 4.15 to 4.18. Conversion time histories are predicted well. Both termination and propagation constants are evidently correctly adjusted. Evidence of diffusion controlled propagation is seen in the levelling off of the conversion curve in figure 4.17. Observed discrepancies may be due to the assumption of instantaneous nucleation or unmodelled impurities. The monomer mass fractions are predicted adequately.

This exercise indicated that the diffusion controlled termination algorithm is correctly implemented and at least equivalent to the empirical method of Friis, et al. [1973]. It should be stressed, however, that the free volume parameters used were found in independent literature sources. Unfortunately, once again, the experimental data did not lend themselves to a verification of the nucleation mechanism.

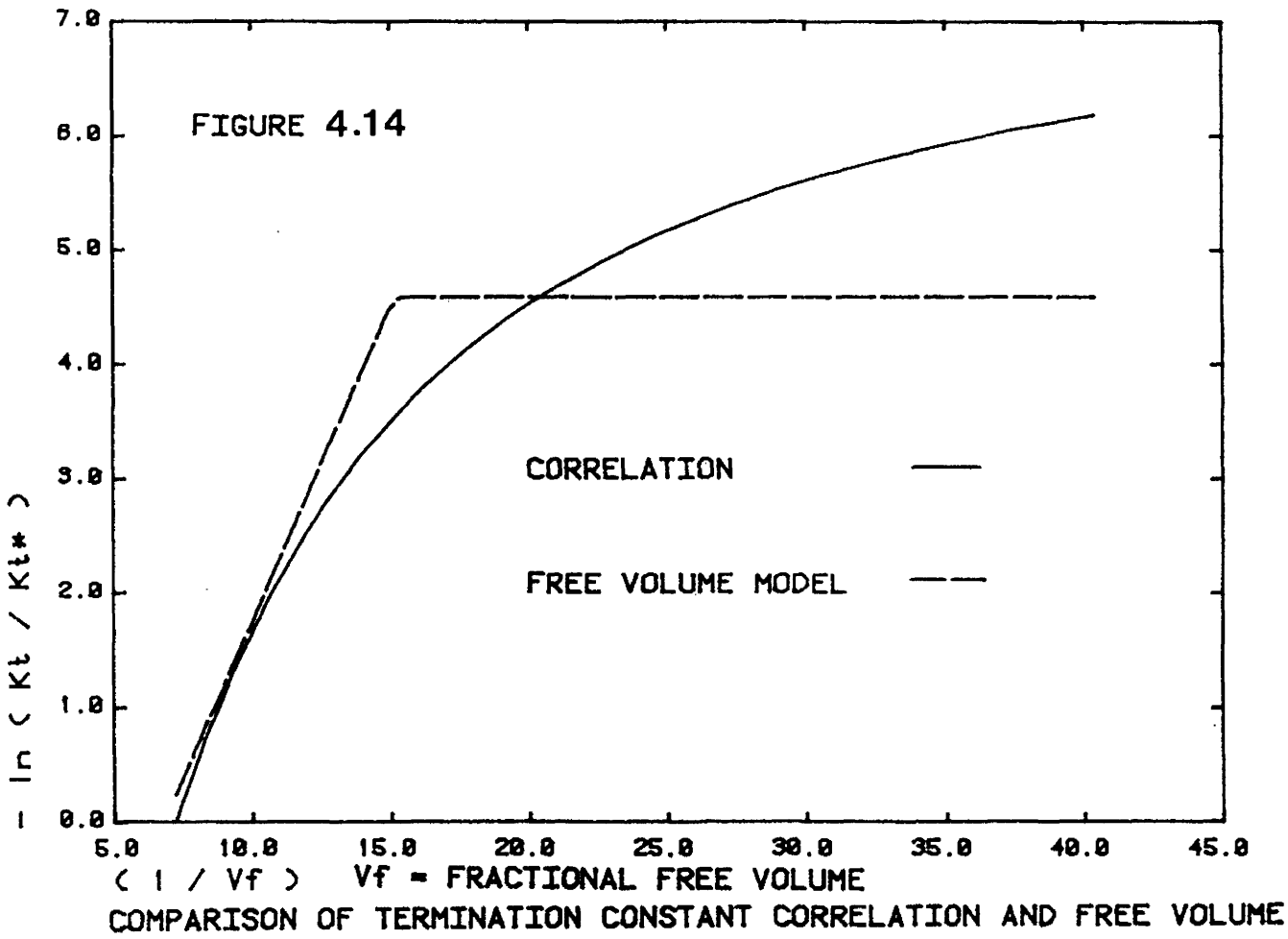

COMPARISON OF TERMINATION CONSTANT CORRELATION AND FREE VOLUME

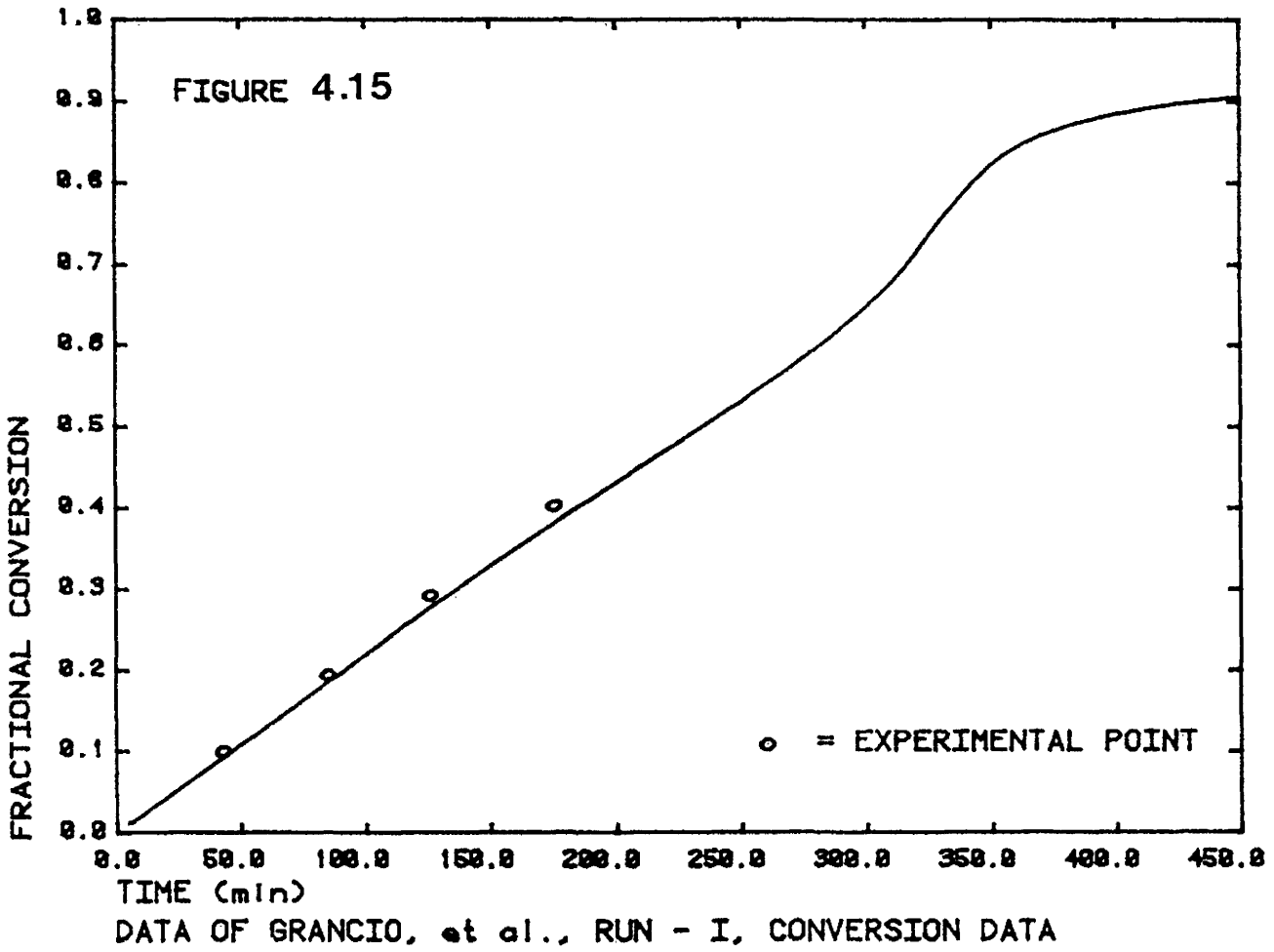
FIGURE 4.15
FRACTIONAL CONVERSION
1.0
0.9
0.8
0.7
0.6
0.5
0.4
0.3
0.2
0.1
0.0
o = EXPERIMENTAL POINT
0.0
50.0
100.0
150.0
200.0
250.0
300.0
350.0
400.0
450.0
TIME (min)
DATA OF GRANCIO, et al., RUN - I, CONVERSION DATA

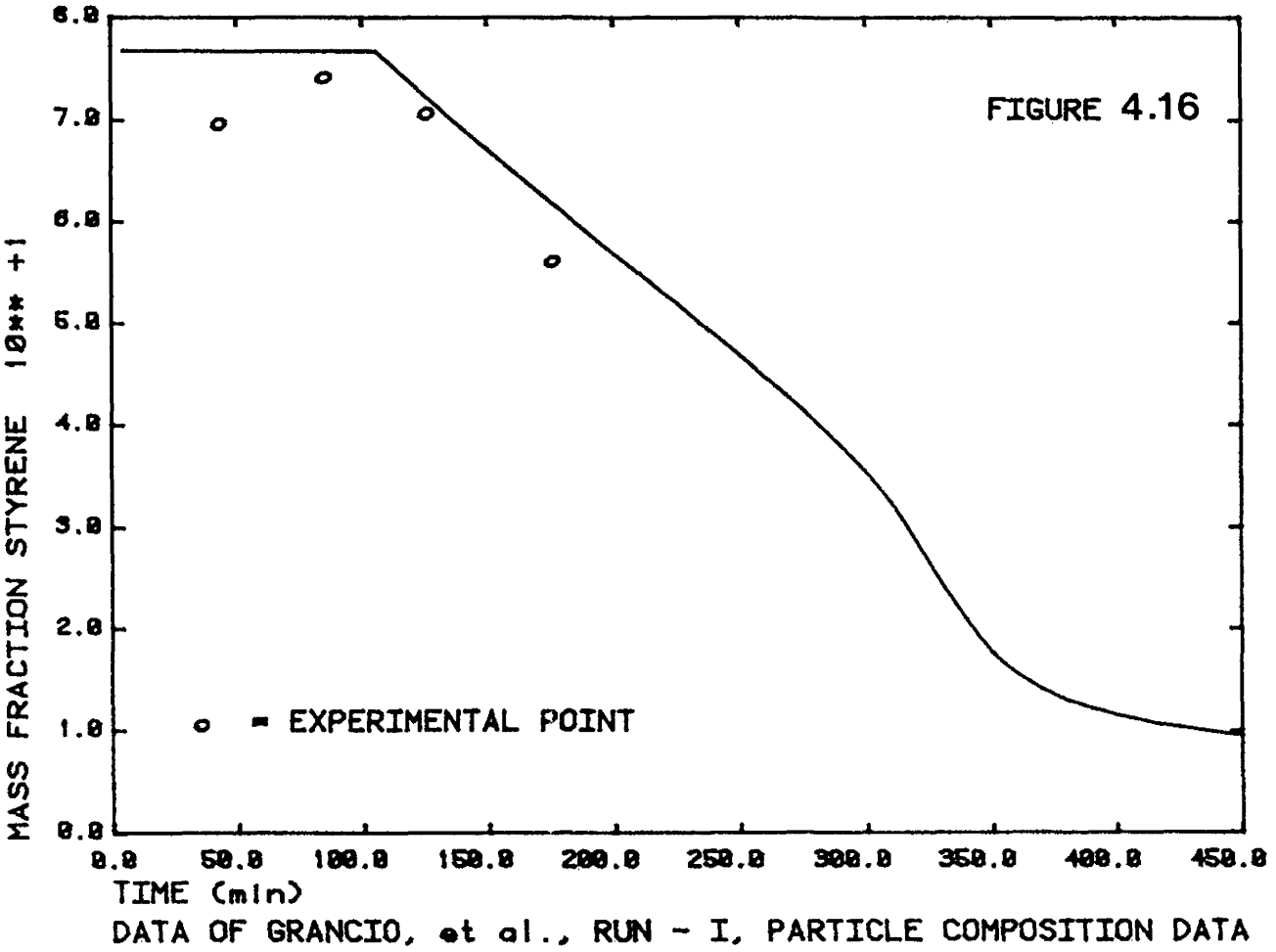
FIGURE 4.16
MASS FRACTION STYRENE 10** +1
6.0
7.0
6.0
5.0
4.0
3.0
2.0
1.0
0.0
o = EXPERIMENTAL POINT
0.0
50.0
100.0
150.0
200.0
250.0
300.0
350.0
400.0
450.0
TIME (min)
DATA OF GRANCIO, et al., RUN - I, PARTICLE COMPOSITION DATA

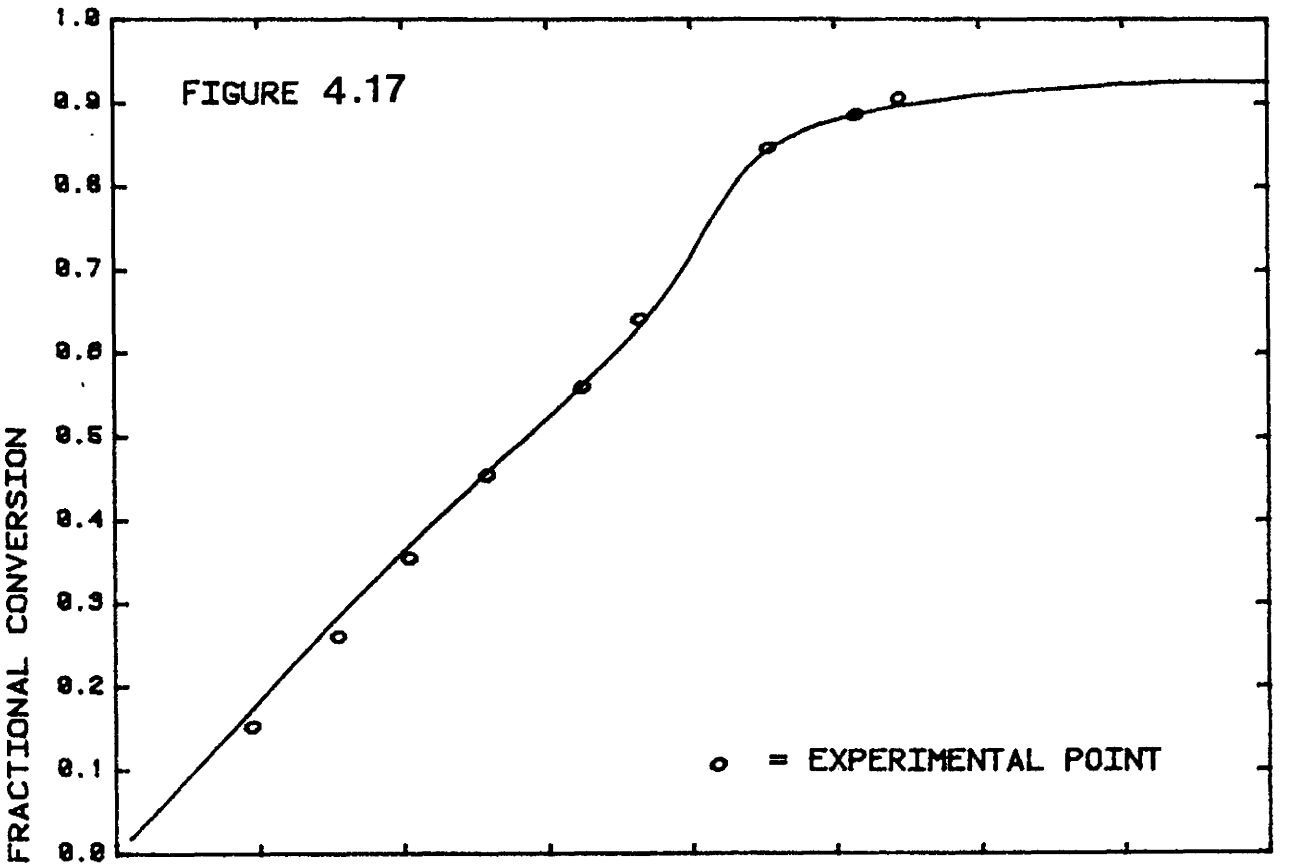

DATA OF GRANCIO, et al., RUN - IV, CONVERSION DATA

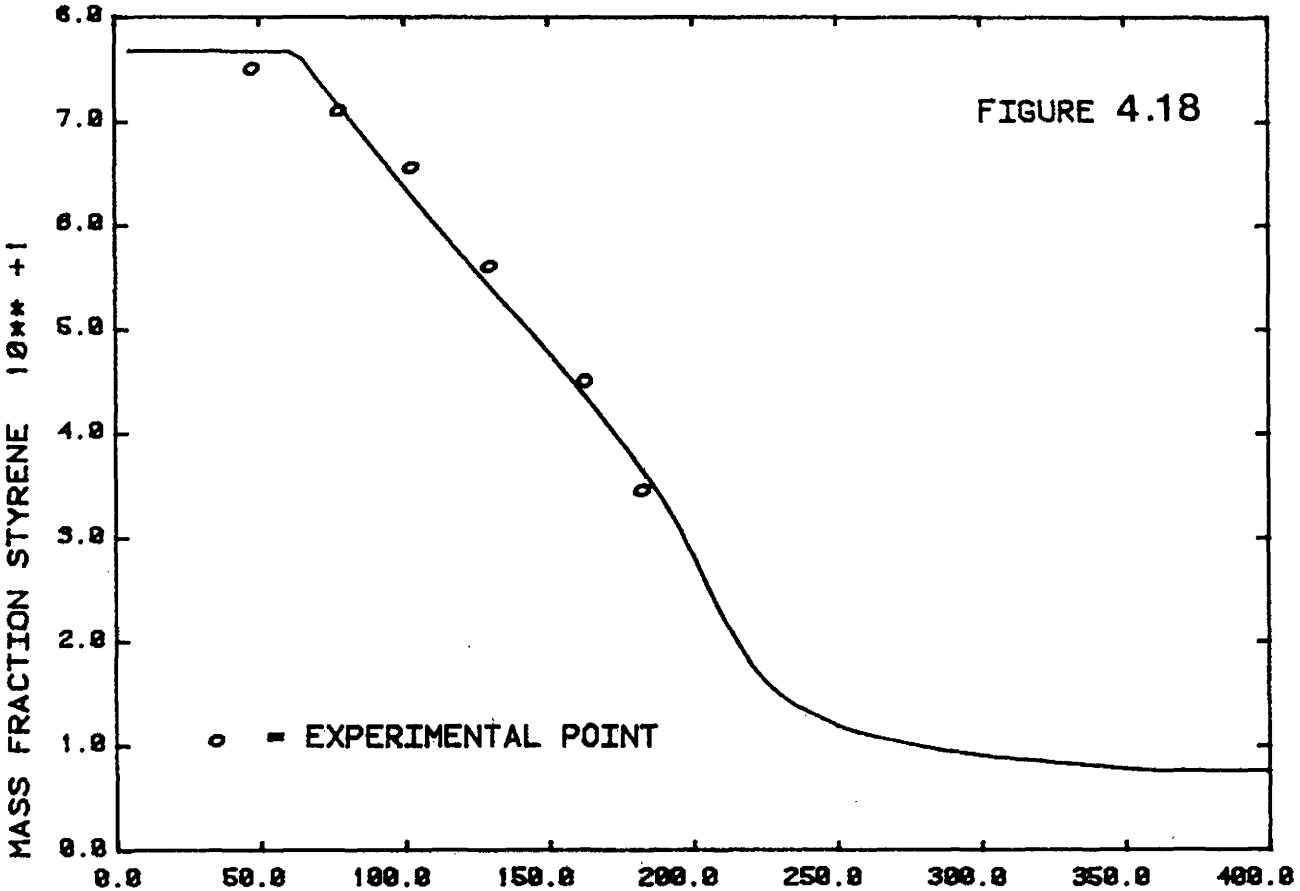

DATA OF GRANCIO, et al., RUN - IV, PARTICLE COMPOSITION

CHAPTER 5

SIMULATION STUDIES

5.1 Introduction

Simulations of batch, continuous and semi-batch (or semi-continuous) reactors are presented in this chapter. Because the model has not been verified fully, its ability to predict trends correctly will be evaluated. The molecular mass and branch frequency average and particle size distribution predictions are highlighted. The purpose of showing the use of the model in various operational modes is to emphasize the enormous amount of information which is potentially available in a predictive model.

5.2 Batch Reactor Simulations

Conversion and composition predictions for batch reactors have been presented in section 4.3. Periods of particle nucleation, constant growth and polymer phase monomer depletion are clearly shown in the accompanying figures to section 4.3. Conversion-time histories are generally well predicted.

The conversion-time history of a cold SBR batch run is presented in figure 5.1. The corresponding molecular mass and branch frequency predictions are shown in figures 5.2 and 5.3 respectively. The cold batch recipe used is given in

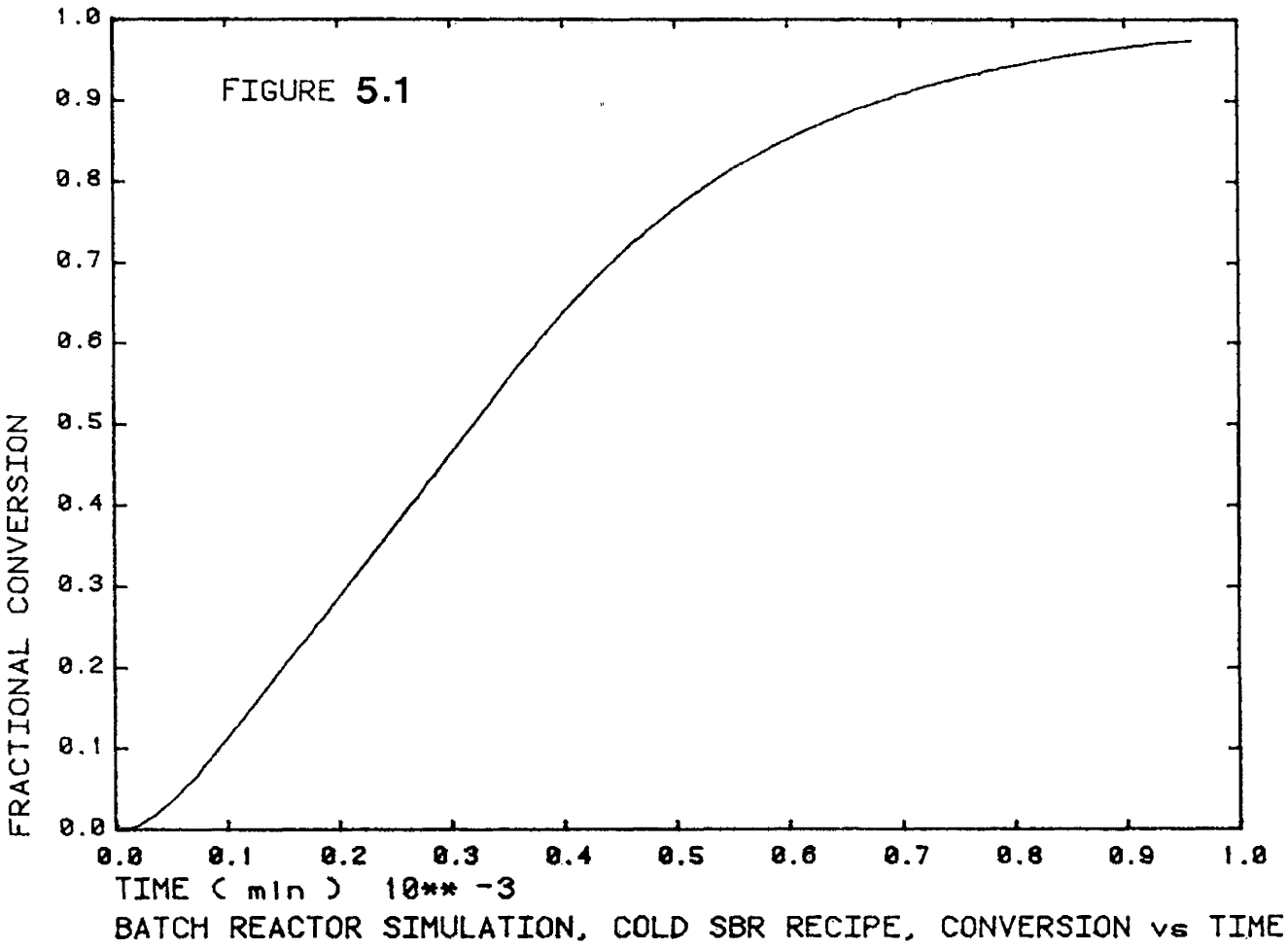
FIGURE 5.1
FRACTIONAL CONVERSION
1.0
0.9
0.8
0.7
0.6
0.5
0.4
0.3
0.2
0.1
0.0
0.0 0.1 0.2 0.3 0.4 0.5 0.6 0.7 0.8 0.9 1.0
TIME (min) 10** -3
BATCH REACTOR SIMULATION, COLD SBR RECIPE, CONVERSION vs TIME

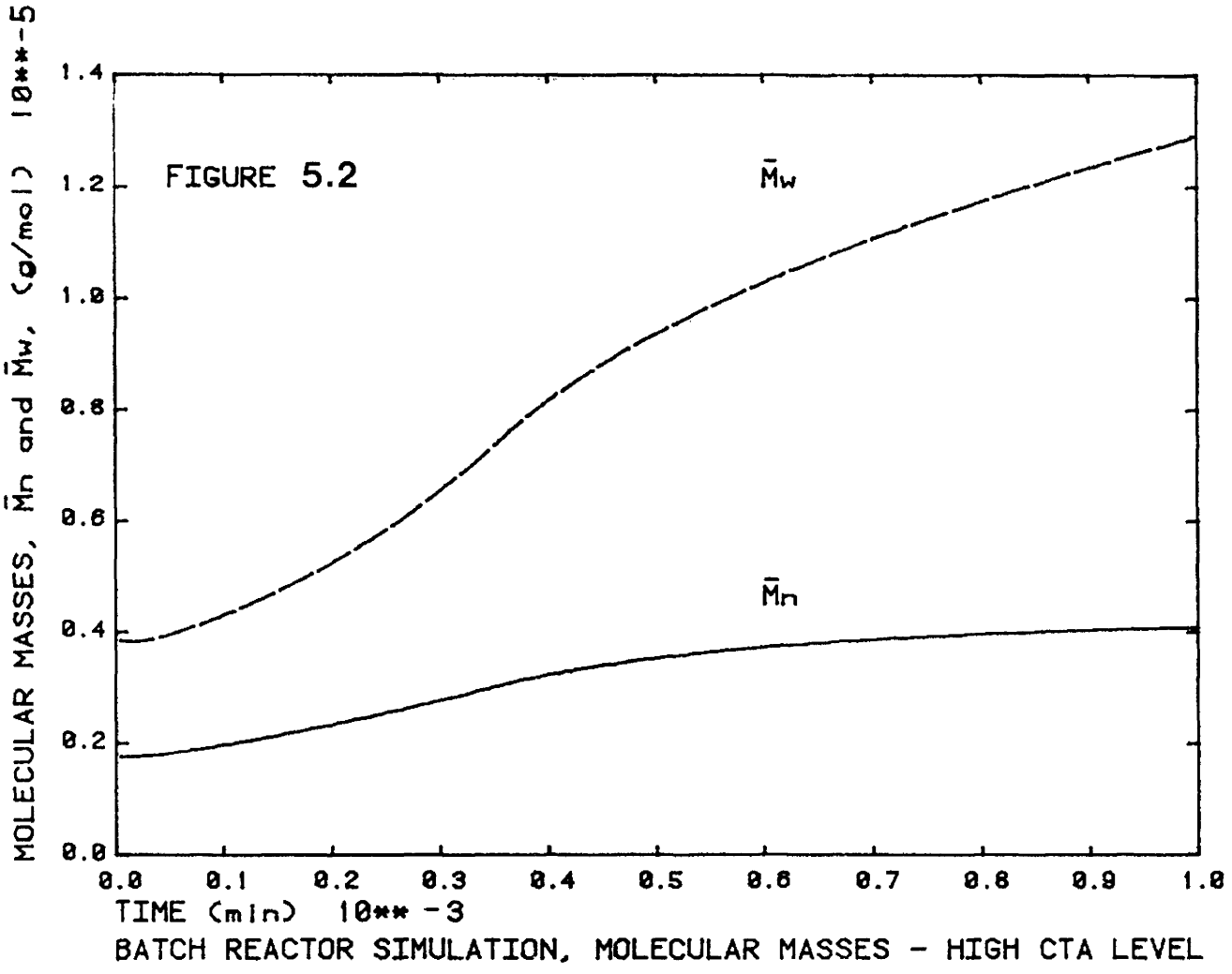

FIGURE 5.2

BATCH REACTOR SIMULATION, MOLECULAR MASSES - HIGH CTA LEVEL

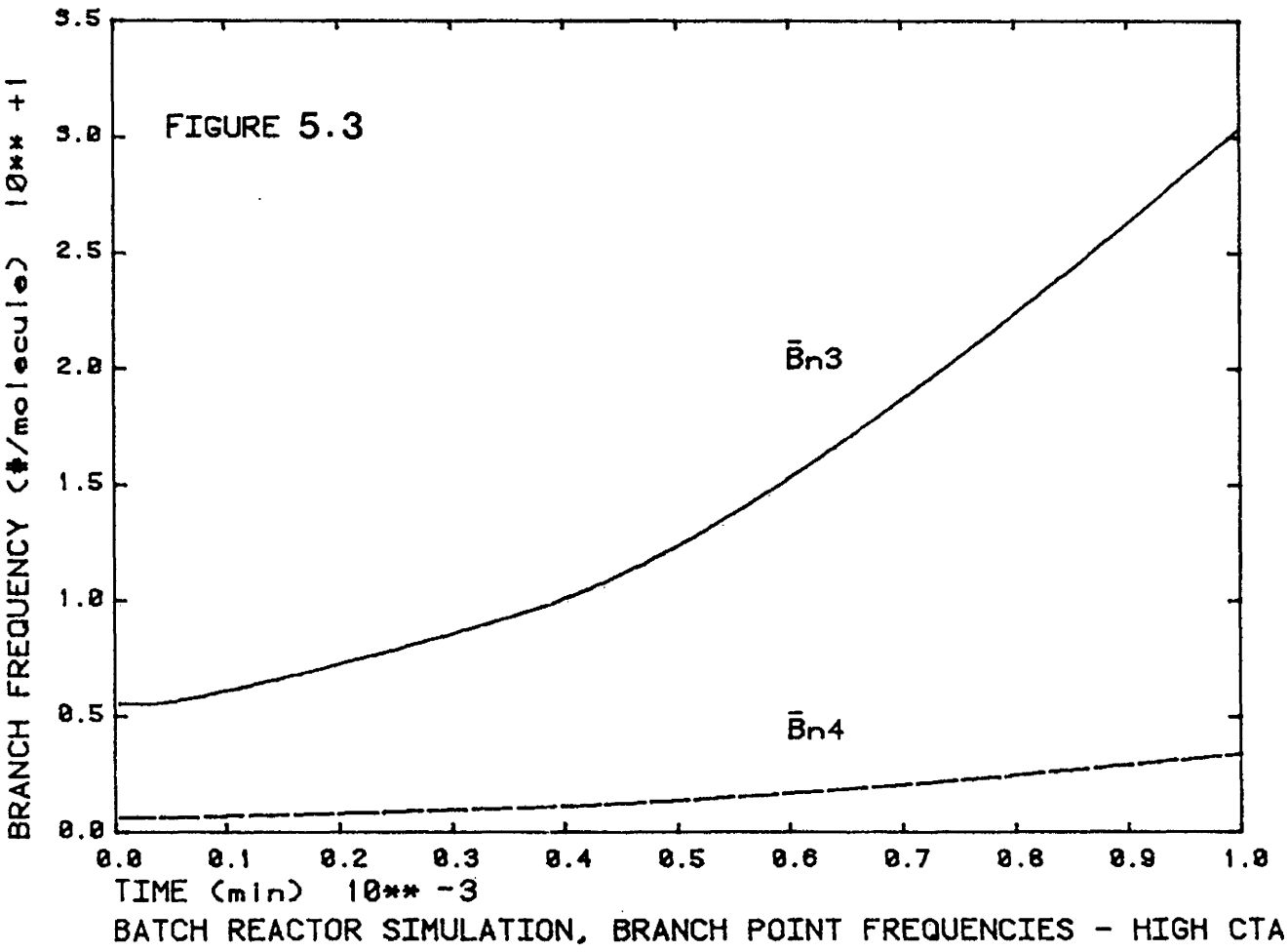

BATCH REACTOR SIMULATION, BRANCH POINT FREQUENCIES - HIGH CTA

Appendix B2. Number and mass average molecular masses are observed to increase rapidly to approximately 60% conversion (or 400 min.) after which the rate of increase is diminished. The branch frequencies increase slowly at first and then more rapidly after 60% conversion. (The reader is referred to figure 5.1 to help interpolate times and corresponding conversions). This latter prediction is in qualitative agreement with experimental observations (Burnett, et al. [1973]). However, since a rise in molecular mass is generally associated with an increase in branch frequency, the molecular mass predictions of figure 5.2 seem to contradict the branch frequency predictions of figure 5.3. This is rationalized on the basis that the transfer to chain transfer agent (CTA) reaction controls molecular mass development. The initial rise in molecular mass corresponds to the observed increase in branching, moderated by CTA. However, after the monomer droplets disappear and the polymer phase monomer concentrations begin to decrease, the transfer to CTA reaction becomes relatively more important compared to propagation. In figure 5.2, the increased significance of transfer to CTA dominates the increased frequency of branching reactions.

Transfer to chain transfer agent does not have a direct effect on branch formation. It has been observed in simulations with the model that the total number of branches remains the same, independent of CTA level. However, as the total number of molecules increases with an increase in CTA level,

the number of branches per molecule decreases.

Figures 5.4, 5.5 and 5.6 show the molecular mass average predictions for cases in which the CTA charge is $\frac{1}{2}$, $\frac{1}{4}$ and $\frac{1}{8}$ respectively of the original charge. Corresponding branch frequency predictions are not shown since the shapes of these predictions do not change with CTA level; only the absolute numbers of branches per molecule change. In figure 5.4, the CTA charge is $\frac{1}{2}$ of its value in figure 5.2. The shapes of the molecular mass curves are basically the same as before, however the increase in mass average ($\overline{M}_w$) molecular mass after 60% conversion (or 400 min.) is more dramatic, reflecting the decreased importance of transfer to CTA. In absolute magnitude, the number average ($\overline{M}_n$) molecular mass and the branch frequencies are approximately increased by a factor of 2 as a result of the CTA decrease. The $\overline{M}_w$ is increased approximately by a factor of three.

Figure 5.5 shows the molecular mass predictions when the charge of CTA is $\frac{1}{4}$ of the original charge. (This is referred to as the "low CTA" simulation in figure 5.5). A dramatic change in $\overline{M}_w$ behaviour is observed. The $\overline{M}_w$ increases exponentially. There is no obvious sign of the effect of CTA on molecular mass. The branch frequencies were observed to double, once again, in magnitude.

Figure 5.6 shows the molecular mass predictions when the charge of CTA is $\frac{1}{8}$ of the original charge. In this case, the $\overline{M}_w$ prediction tends to infinity at approximately 5.5%

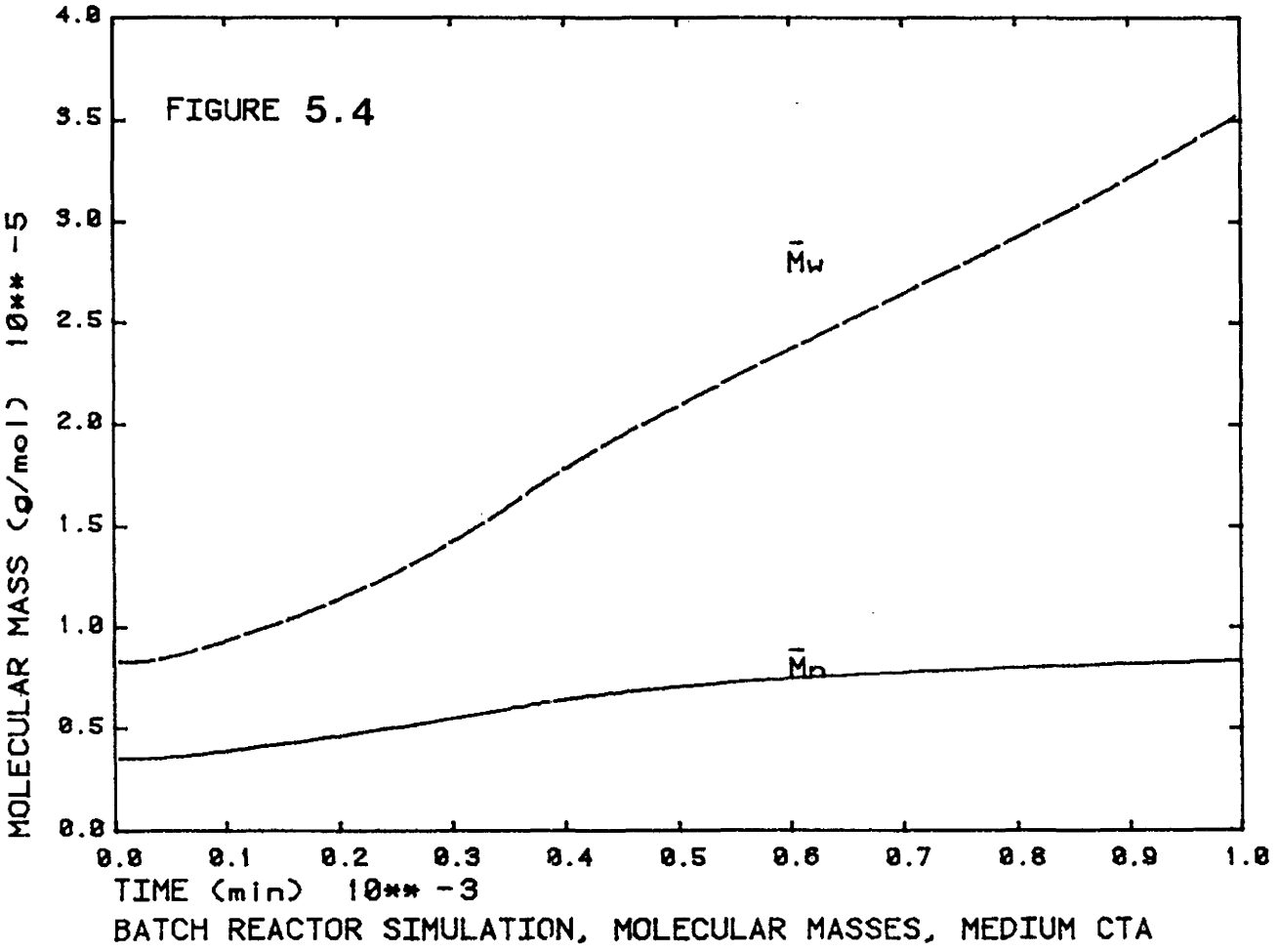
FIGURE 5.4
MOLECULAR MASS (g/mol) 10** -5
4.0
3.5
3.0
2.5
2.0
1.5
1.0
0.5
0.0
$\bar{M}_w$
$\bar{M}_n$
0.0 0.1 0.2 0.3 0.4 0.5 0.6 0.7 0.8 0.9 1.0
TIME (min) 10** -3
BATCH REACTOR SIMULATION, MOLECULAR MASSES, MEDIUM CTA

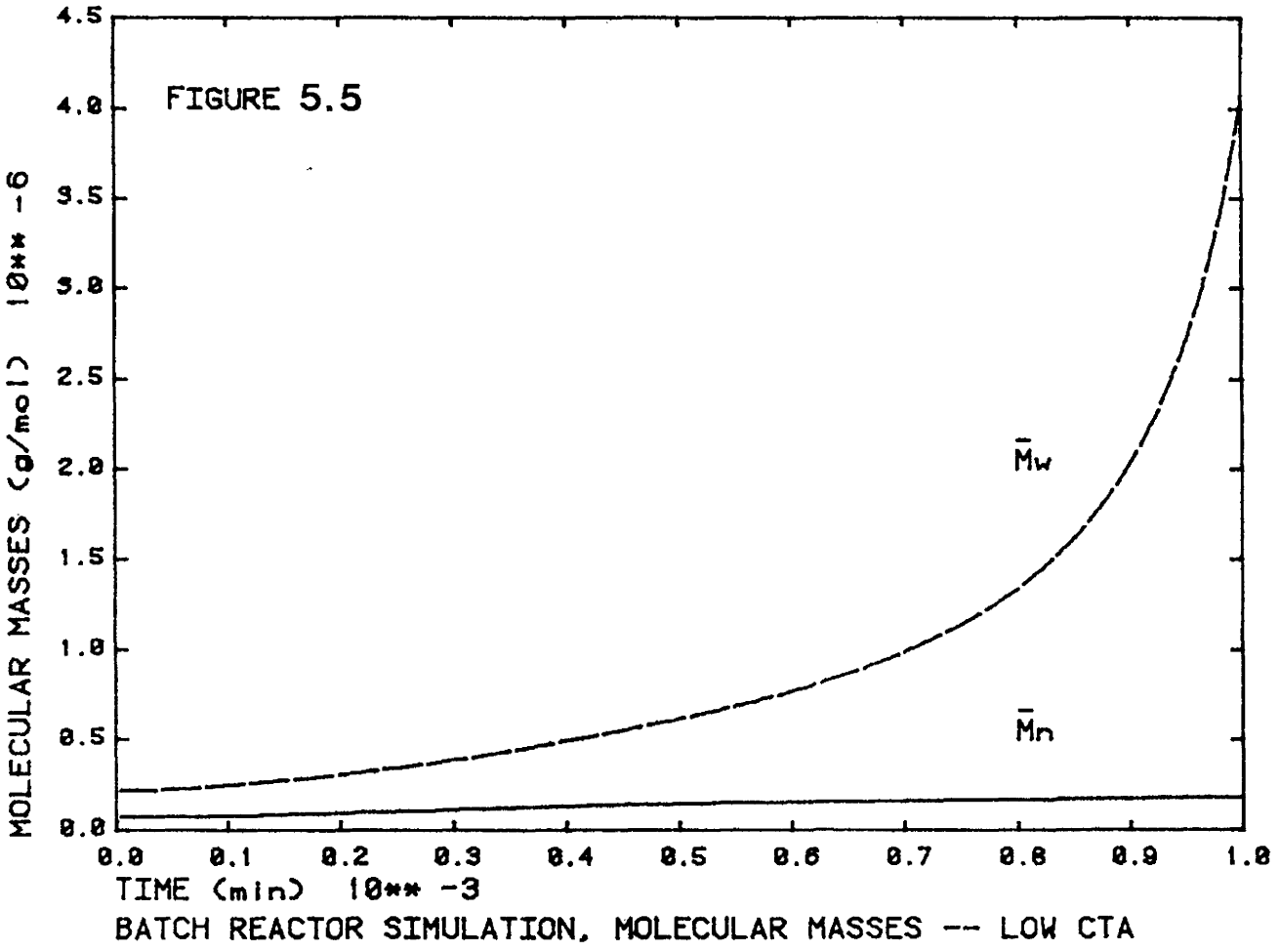
FIGURE 5.5
MOLECULAR MASSES (g/mol) 10** -6
4.5
4.0
3.5
3.0
2.5
2.0
1.5
1.0
0.5
0.0
$\bar{M}w$
$\bar{M}n$
0.0 0.1 0.2 0.3 0.4 0.5 0.6 0.7 0.8 0.9 1.0
TIME (min) 10** -3
BATCH REACTOR SIMULATION, MOLECULAR MASSES -- LOW CTA

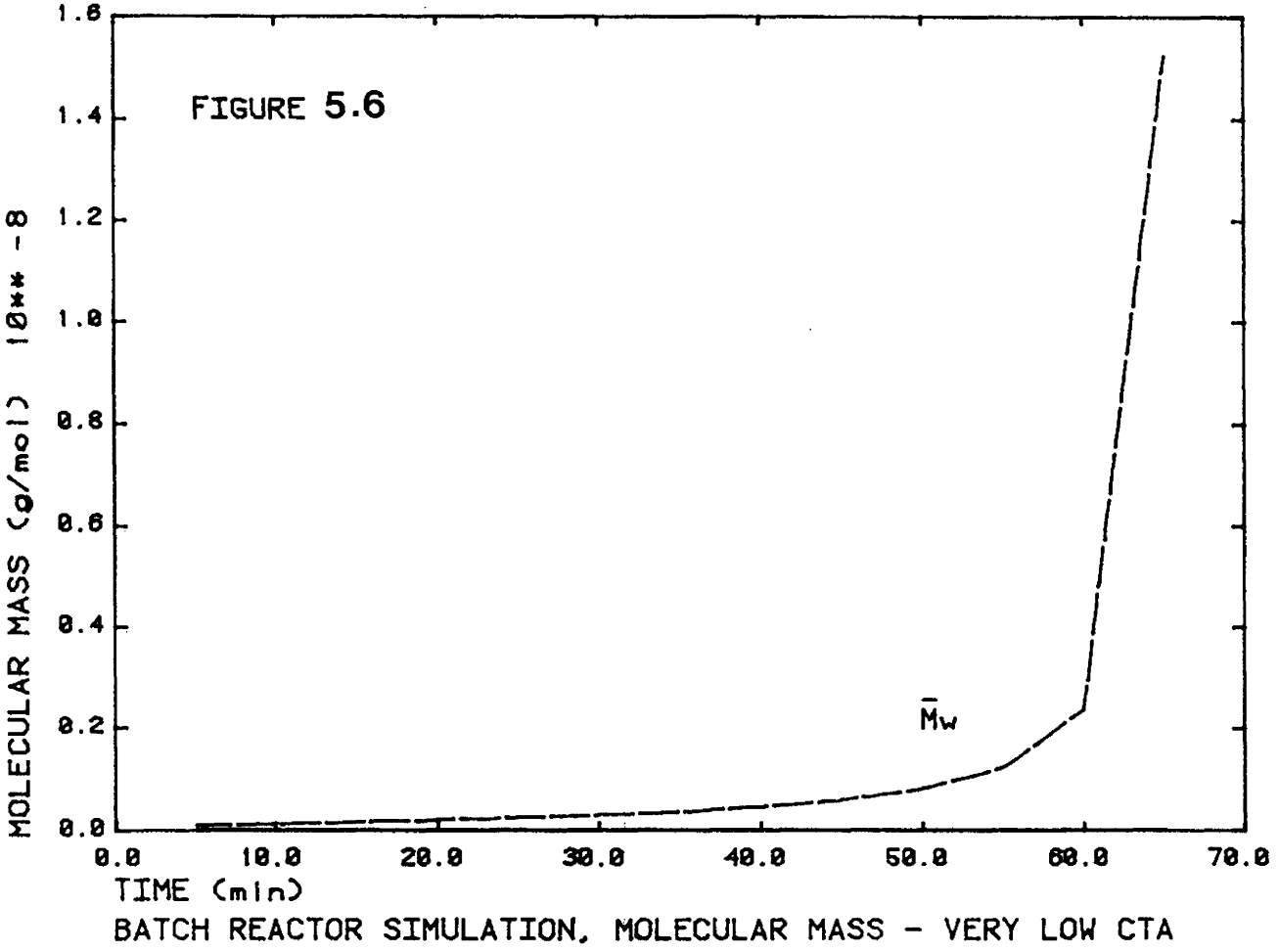

BATCH REACTOR SIMULATION, MOLECULAR MASS - VERY LOW CTA

conversion. An analytical solution for a simplified system showed that the mass average molecular mass or more correctly, the second molecular mass moment differential equation does tend to infinity under certain conditions, inferring that the observed behaviour is not a numeric instability. The infinite molecular masses were therefore interpreted as indicating huge, crosslinked molecules, observed experimentally as gel. In the absence of CTA, gel formation has been observed at very low conversions in SBR polymerization (section 2.2.6). The predicted branch frequencies corresponding to the very low CTA charge are very high from inception. Their initial values are of the size observed during stage 3 of the $\frac{1}{4}$ CTA charge simulation.

It would be of interest to determine the absolute branch frequencies associated with gel formation. One could then ignore the second moment differential equation to ensure the successful solution of the model and subsequently infer the mass average molecular mass from the calculated branch frequencies and number average molecular mass. The transfer to polymer and propagation with polymer constants need to be determined accurately before the aforementioned absolute branch frequencies could be calculated.

There are two additional points which should be mentioned concerning the molecular mass development. First, since not all of the kinetic constants affecting the molecular mass development are known as functions of temperature, the

model predictions of molecular mass are restricted to isothermal conditions. Second, since termination reactions are not considered in the molecular mass development, diffusion controlled termination will have no effect on the molecular mass development. There has been no indication that diffusion controlled termination affects the molecular mass development of SBR from the literature surveyed for this work. However, this matter should be investigated when data becomes available.

Particle size distributions (PSD s) predicted by the model for the cold batch reactor are shown in figure 5.7. They appear as right angle triangles. The sloping sides reflect the essentially linear nucleation rate. They do not appear as conventional distributions because, as mentioned in section 3.2.9, broadening of the distribution due to the stochastic variation of radical residence times in particles is not accounted for. (This form of broadening has been termed statistical broadening for the purposes of discussion).

The distributions appear to become narrower as time progresses. This behaviour is expected if the volume growth rates of all particles are similar. For a given volume growth rate, radii of small particles increase more quickly than radii of large particles. (The conversions corresponding to each distribution may be interpolated from figure 5.1).

The distributions calculated are expected to roughly predict mean particle sizes, distribution breadth and the

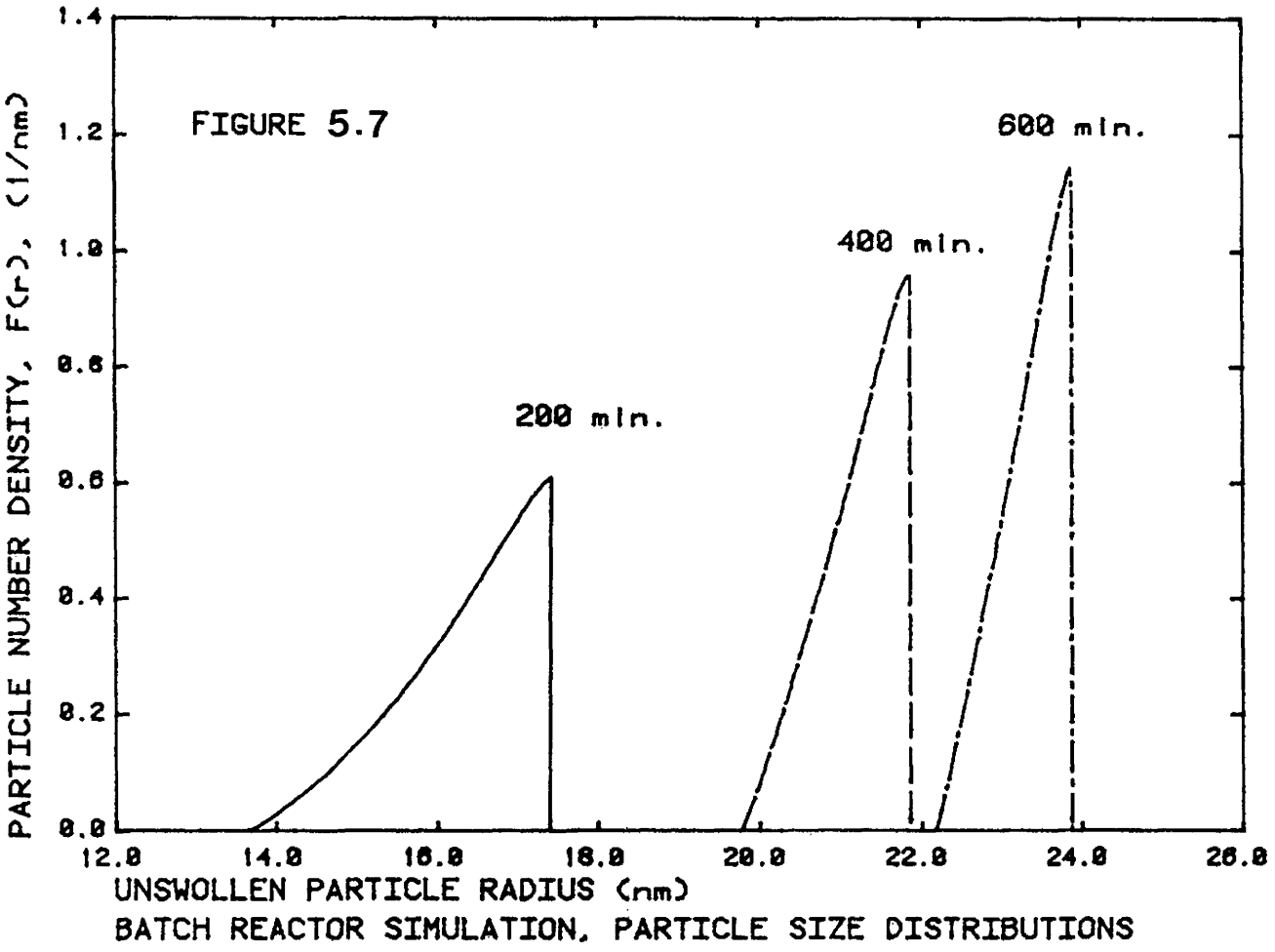
FIGURE 5.7
600 min.
400 min.
200 min.
PARTICLE NUMBER DENSITY, F(r), (1/nm)
1.4
1.2
1.0
0.8
0.6
0.4
0.2
0.0
12.0
14.0
16.0
18.0
20.0
22.0
24.0
26.0
UNSWOLLEN PARTICLE RADIUS (nm)
BATCH REACTOR SIMULATION, PARTICLE SIZE DISTRIBUTIONS

direction of the skewness of the PSD. The breadth of the distribution will be underestimated for narrow PSD s because statistical broadening has been ignored.

Unfortunately, the PSD predictions were not verified experimentally. It is anticipated that if coagulation is important in the development of the distribution, the present model predictions may be inadequate.

Figure 5.8 shows the history of the reactor temperature and cooling jacket feed temperature for a cold batch simulation. With the proportional-integral controller constants K_c (gain) = 20 and τ_I (integral time) = 10 minutes, the temperature in the reactor is maintained constant with only a very slight initial transient. The cooling jacket feed temperature, which is the variable manipulated by the controller, reflects the three stages of emulsion polymerization. During stage 1, the number of particles increases, increasing the heat load which results in a decrease in the cooling jacket feed temperature. During stage 2, the number of particles and the monomer and radical concentrations in the particles are constant resulting in a constant heat load. During stage 3, the reaction slows down due to the depletion of monomer in the particles and therefore, the heat load decreases and the cooling jacket feed temperature increases.

It should be recognized that the design and modelling of the cooling system is oversimplified. For example, this model considers only the area of the cylindrical reactor

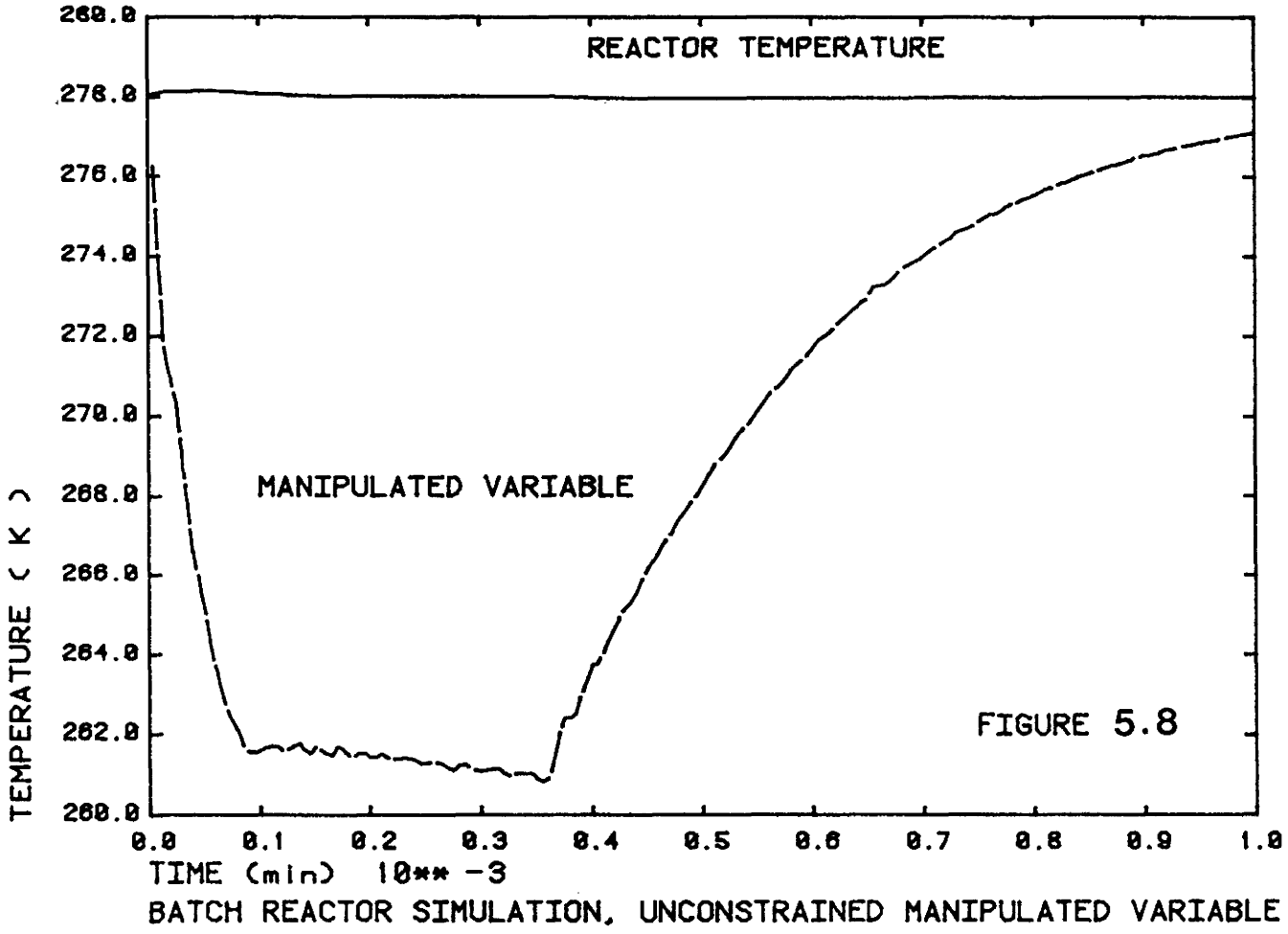

FIGURE 5.8

BATCH REACTOR SIMULATION, UNCONSTRAINED MANIPULATED VARIABLE

walls for heat transfer. In real systems, cooling coils or reflux condensers may be used to greatly increase the heat removal capacity. The evaporation of butadiene has also been disregarded. Furthermore, in this particular simulation, no constraint has been imposed on the manipulated variable. The effect of constraining the manipulated variable has been incorporated in the model and is illustrated in section 5.3.

With the heat balance and temperature controller, a variety of batch operational policies could be investigated. For example, the batch reactor may be run adiabatically, with constant heat removal, or perhaps with a temperature program.

5.3 CSTR Simulations

For continuous reactors, the dynamic reactor model is useful in studying transient behaviour. The model can be used to evaluate reactor start up policies, to design reactor cooling systems for peak loads or to design reactor control schemes. The fitting of the experimental data of Brooks, et al. [1978] (in section 4.4.1) illustrated that unless initial conditions and reactor non-idealitties are well specified, transients will not be predicted perfectly. With this in mind, the discussion of this section should be regarded as indicative of the case where all pertinent information is known.

To illustrate both the model's predictive power and its versatile application, two different start-up policies

were simulated. Conversion, particle number, copolymer composition, $\overline{M}_n$, $\overline{M}_w$, $\overline{B}_{n3}$ and $\overline{B}_{n4}$ are presented in figures 5.9 through 5.13 respectively. In the first start-up policy, the reactor is empty initially. All components are then fed at their steady-state feed rates. Curves representative of this policy are denoted "1" in the aforementioned figures. In the second policy, the reactor was filled initially with water and enough emulsifier and chain transfer agent (CTA) to saturate the water phase. All components were then fed at their steady-state feed rates. It was important to charge CTA initially to prevent the first polymer formed from crosslinking extensively (i.e. the second polymer moment equation from becoming unstable).

The conversion and particle number plots indicate that the first start-up plicy results in an overshoot of these properties (figures 5.9 and 5.10). This overshoot may be attributed to the large number of particles generated and accumulated during the semi-batch filling period. Such an overshoot may present problems in the temperature control of a real system. On the other hand, the first start-up policy approaches the approximate steady-state condition in less time, which may be desirable in some cases.

The composition time curve of figure 5.11 once the scale of the ordinate is considered, predicts that the two start-up policies do not create copolymers of vastly different

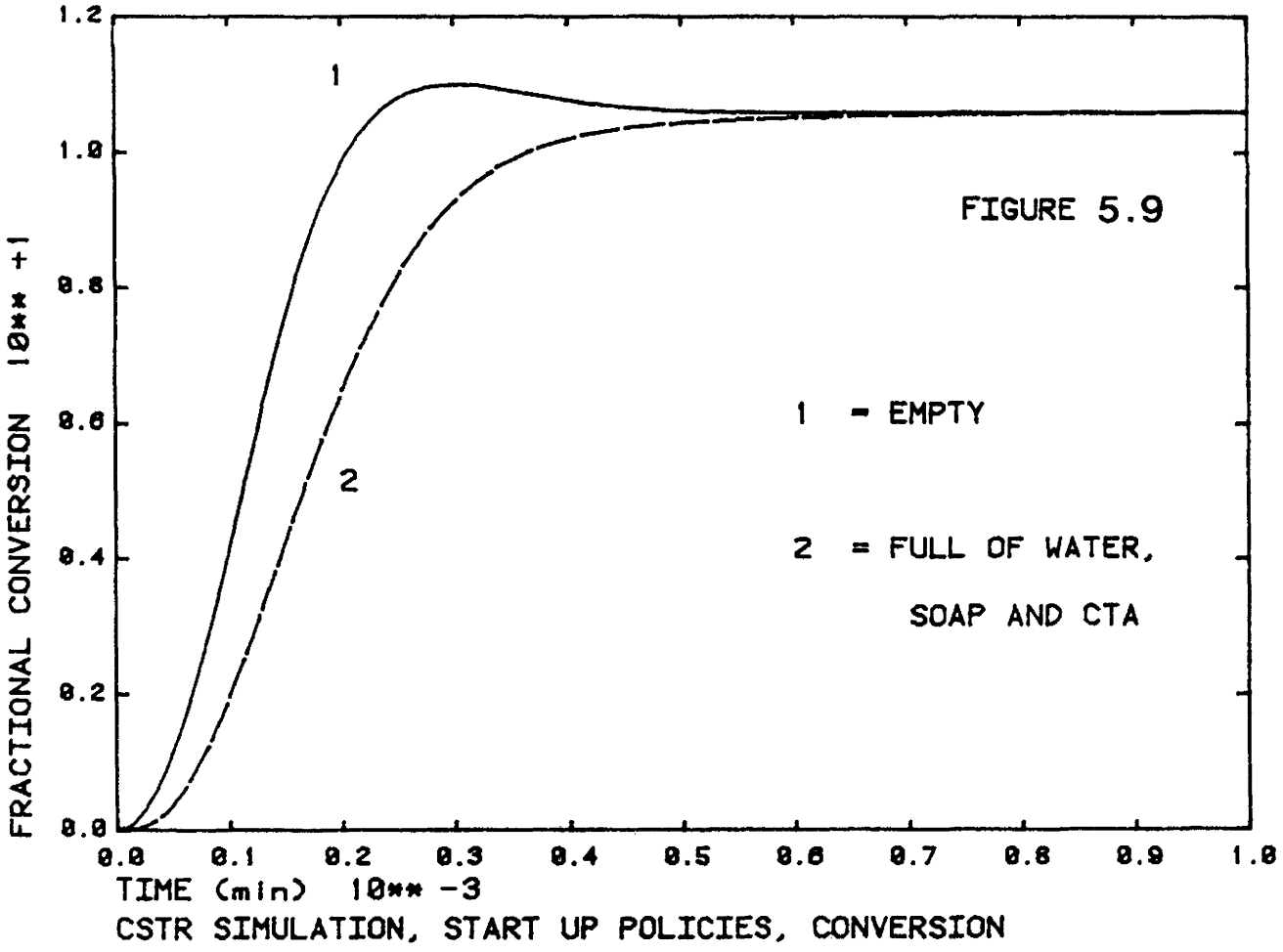
1.2
1.0
0.8
0.6
0.4
0.2
0.0
FRACTIONAL CONVERSION 10** +1
1
2
1 = EMPTY
2 = FULL OF WATER,
SOAP AND CTA
0.0
0.1
0.2
0.3
0.4
0.5
0.6
0.7
0.8
0.9
1.0
TIME (min) 10** -3
CSTR SIMULATION, START UP POLICIES, CONVERSION

FIGURE 5.9

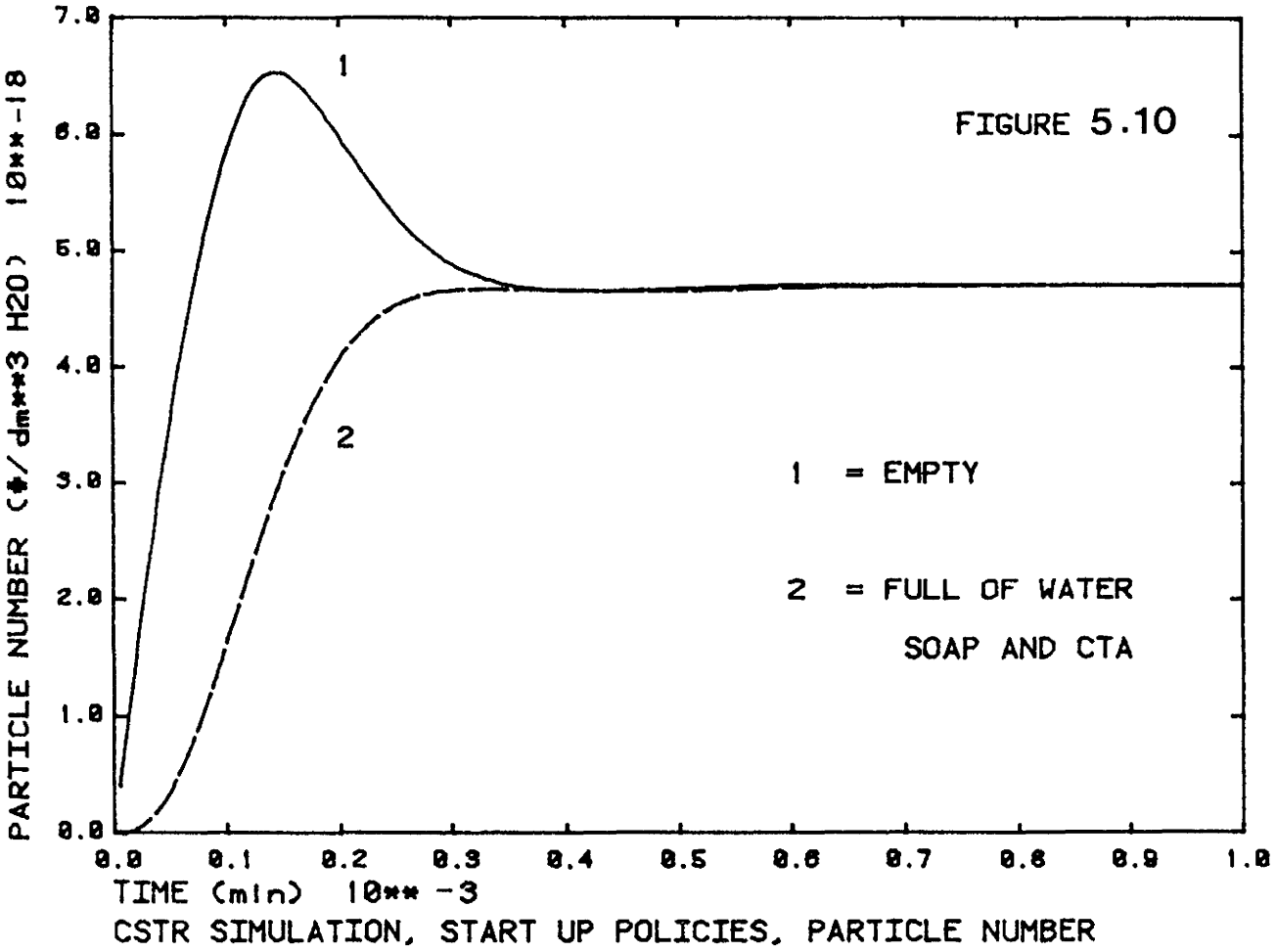
7.0
6.0
5.0
4.0
3.0
2.0
1.0
0.0
PARTICLE NUMBER (#/ dm**3 H2O) 10** -18
1
2
1 = EMPTY
2 = FULL OF WATER
SOAP AND CTA
0.0
0.1
0.2
0.3
0.4
0.5
0.6
0.7
0.8
0.9
1.0
TIME (min) 10** -3
CSTR SIMULATION, START UP POLICIES, PARTICLE NUMBER

FIGURE 5.10

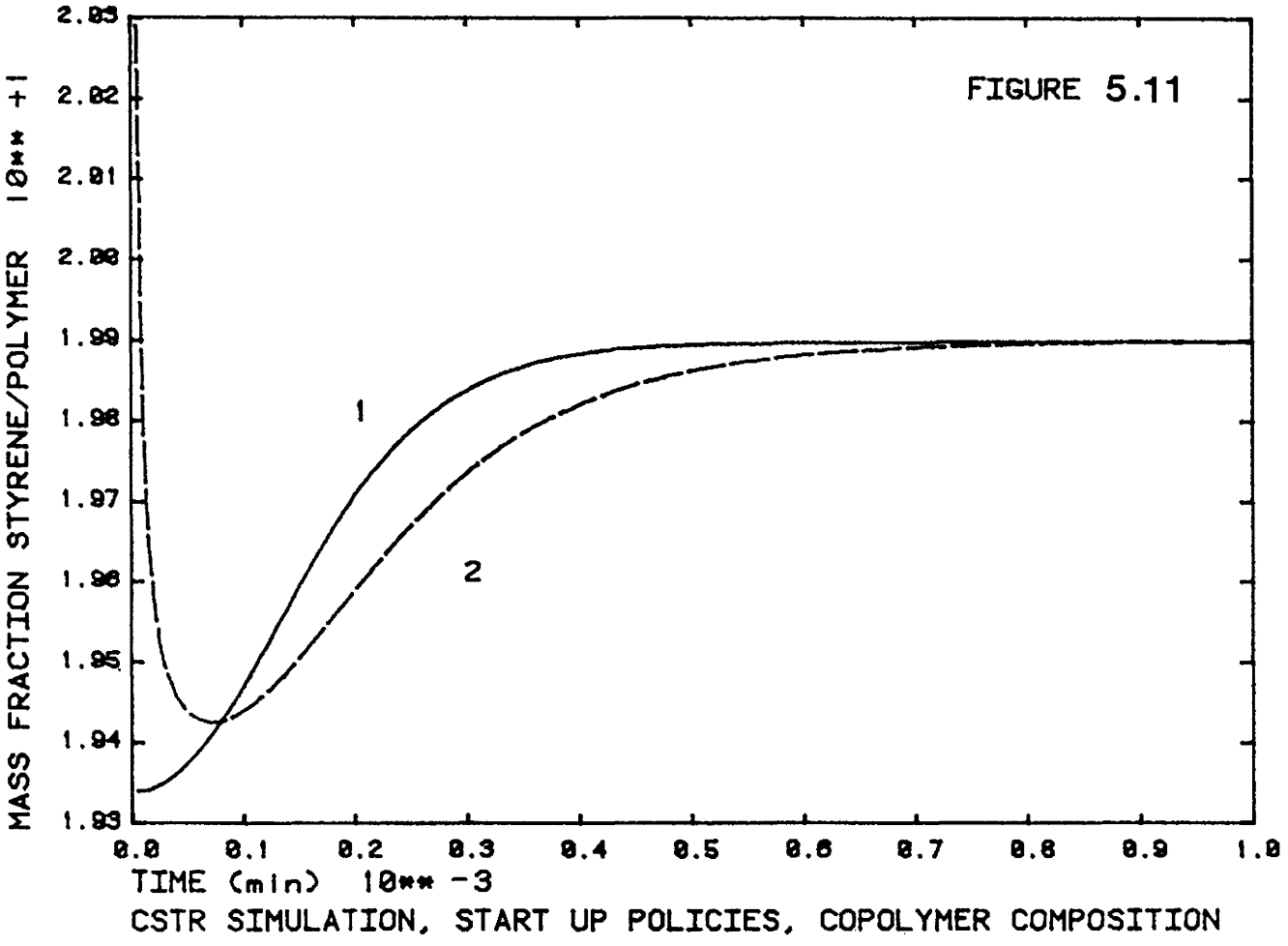
FIGURE 5.11
MASS FRACTION STYRENE/POLYMER 10** +1
2.03
2.02
2.01
2.00
1.99
1.98
1.97
1.96
1.95
1.94
1.93
1
2
0.0
0.1
0.2
0.3
0.4
0.5
0.6
0.7
0.8
0.9
1.0
TIME (min) 10** -3
CSTR SIMULATION, START UP POLICIES, COPOLYMER COMPOSITION

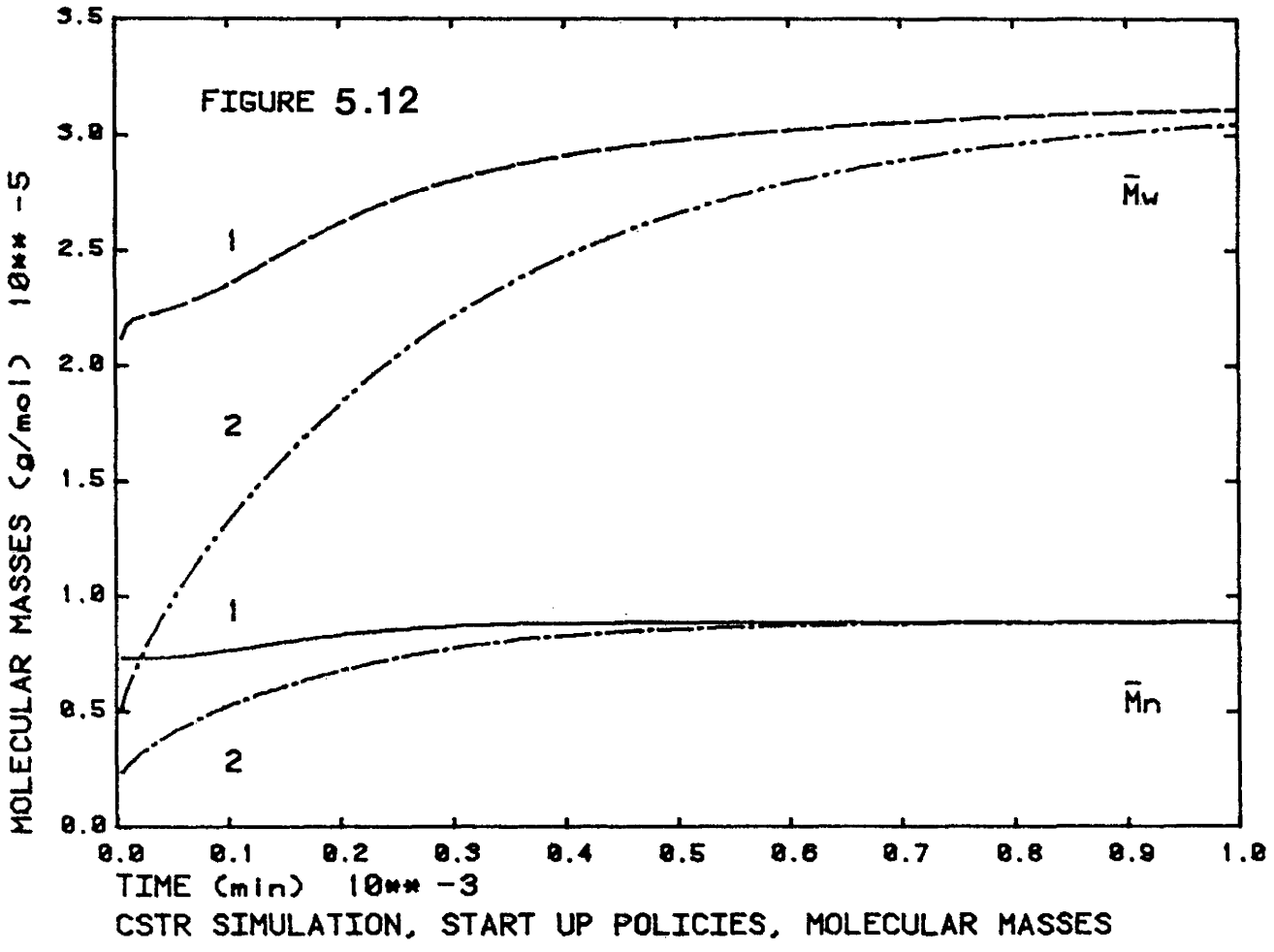
FIGURE 5.12
MOLECULAR MASSES (g/mol) 10** -5
3.5
3.0
2.5
2.0
1.5
1.0
0.5
0.0
1
2
1
2
M̄w
M̄n
0.0
0.1
0.2
0.3
0.4
0.5
0.6
0.7
0.8
0.9
1.0
TIME (min) 10** -3
CSTR SIMULATION, START UP POLICIES, MOLECULAR MASSES

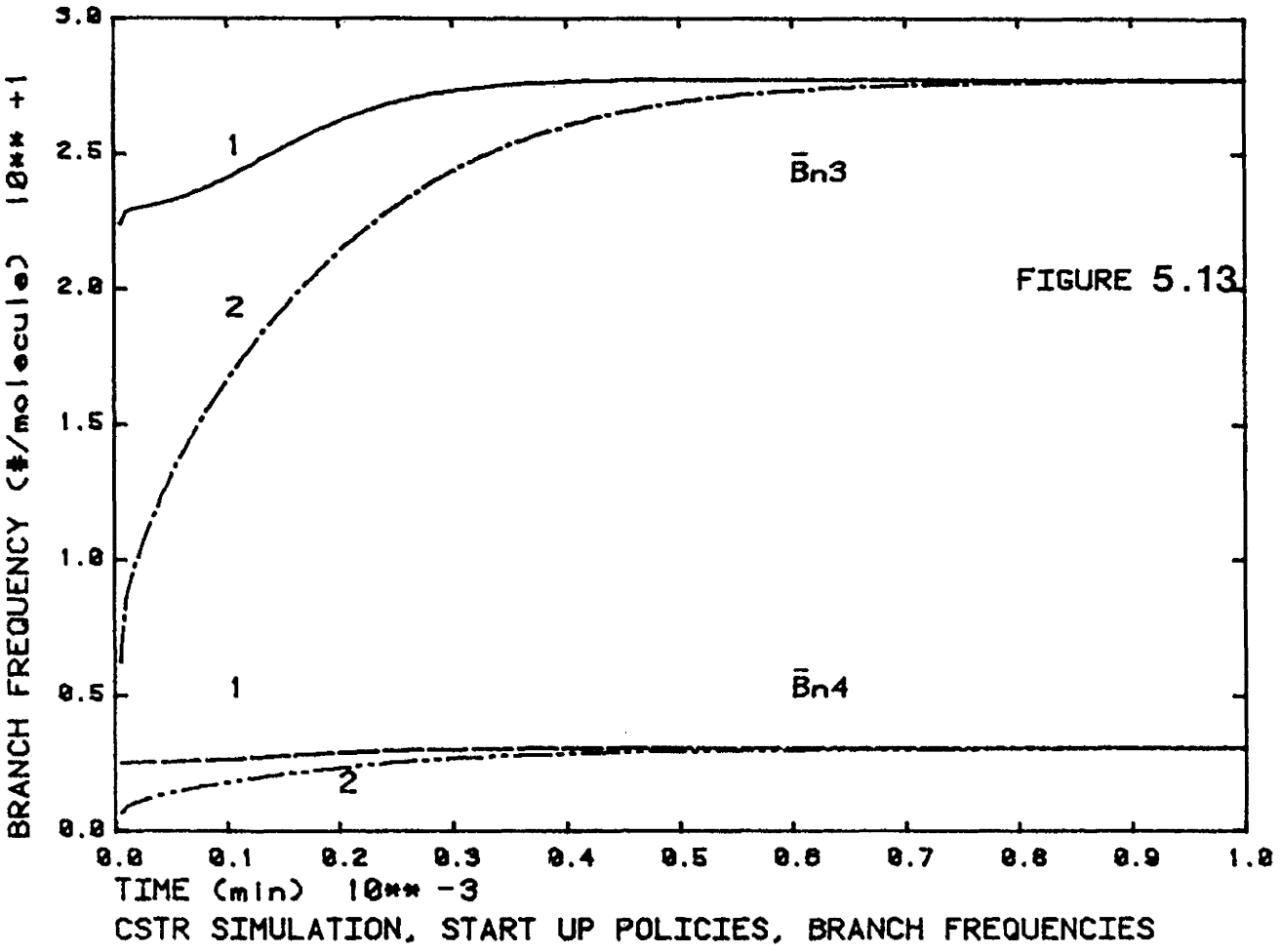
BRANCH FREQUENCY (#/molecule) 10** +1
3.0
2.5
2.0
1.5
1.0
0.5
0.0
1
2
$\bar{B}n3$
1
2
$\bar{B}n4$
0.0
0.1
0.2
0.3
0.4
0.5
0.6
0.7
0.8
0.9
1.0
TIME (min) 10** -3
CSTR SIMULATION, START UP POLICIES, BRANCH FREQUENCIES

FIGURE 5.13

compositions. The second policy is predicted to form a copolymer of slightly higher styrene content initially. This is undoubtedly due to the fact that butadiene is more soluble in water and it consequently takes longer to saturate the water phase and enter the particles.

The molecular mass predictions indicate that perhaps too much CTA was charged initially in the second policy. Initial molecular masses are very low. Though it is not shown in figure 5.12, the mass average molecular masses ($\bar{M}_w$ s) for the two policies do attain the same steady state eventually. Unfortunately, no experimental data is available to verify whether this behaviour is reasonable. It is significant, however, that all other properties attain the same steady state values for both policies.

It is of interest to point out that the conversion peak of policy 1 has little effect on molecular mass properties. Furthermore, once the effects of the excessive charge of CTA in policy 2 are considered, it appears that the two start-up policies are equivalent from the point of view of the molecular mass properties.

The evolution of particle size distributions for the two start-up policies is shown in figures 5.14 and 5.15. The large number of particles formed in the semi-batch filling period of policy 1 is seen to skew the distribution initially and result in a shoulder at large particle sizes for subsequent distributions. The PSD s formed during the second start-up

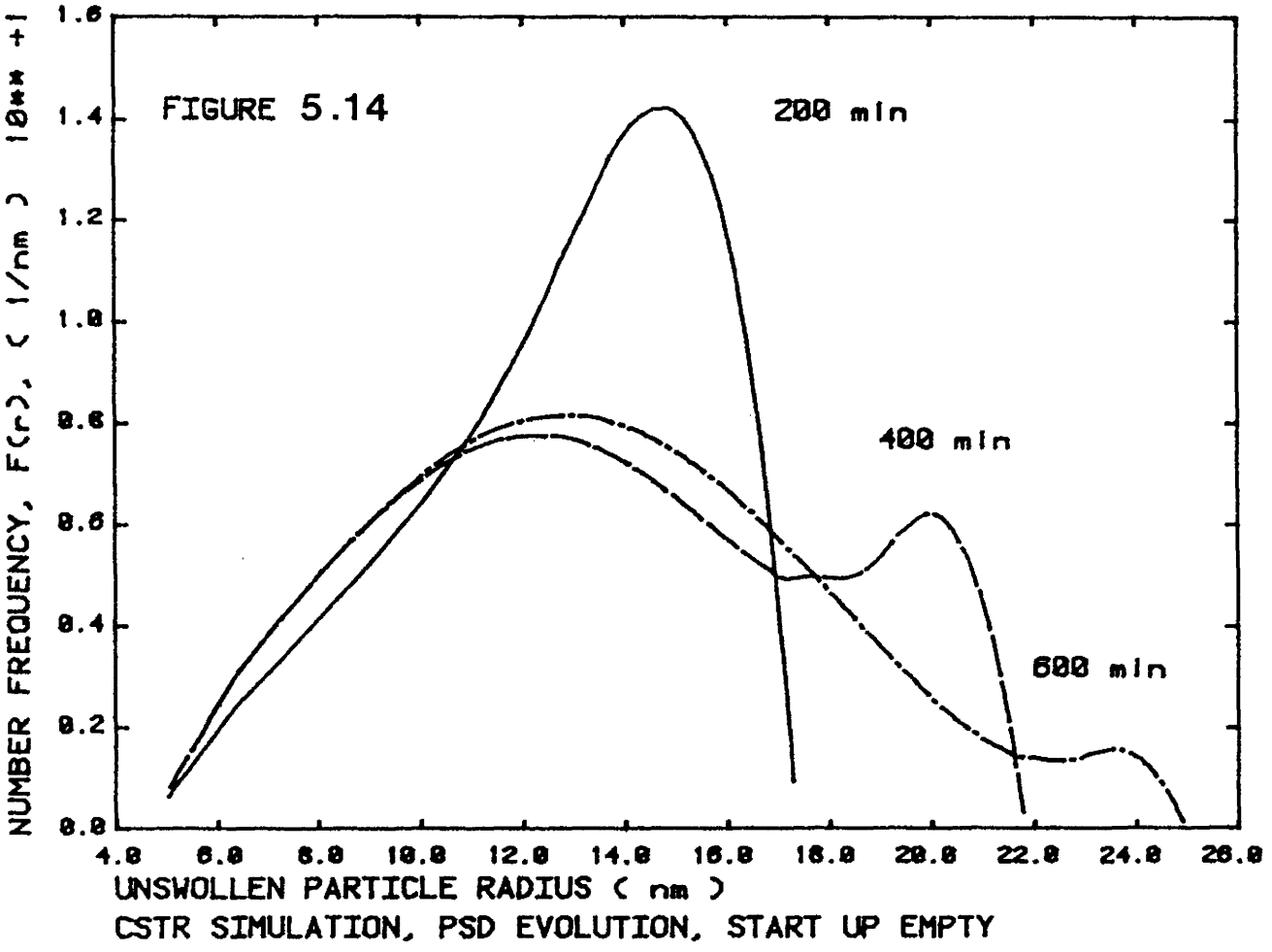
FIGURE 5.14
200 min
400 min
600 min
NUMBER FREQUENCY, F(r), (1/nm) 10** +1
1.6
1.4
1.2
1.0
0.8
0.6
0.4
0.2
0.0
4.0
6.0
8.0
10.0
12.0
14.0
16.0
18.0
20.0
22.0
24.0
26.0
UNSWOLLEN PARTICLE RADIUS (nm)
CSTR SIMULATION, PSD EVOLUTION, START UP EMPTY

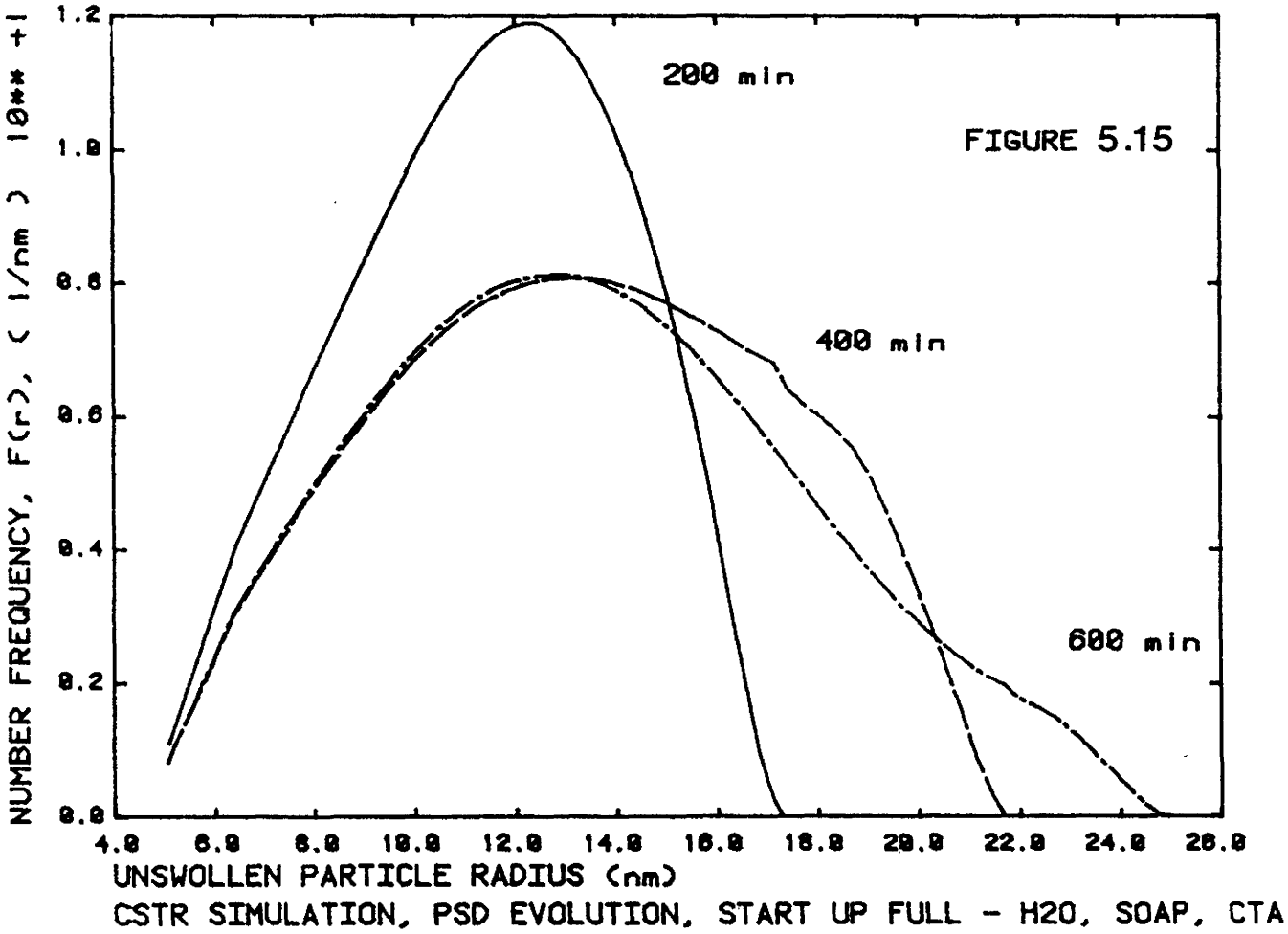
NUMBER FREQUENCY, F(r), (1/nm) 10** +1
1.2
1.0
0.8
0.6
0.4
0.2
0.0
200 min
400 min
600 min
4.0
6.0
8.0
10.0
12.0
14.0
16.0
18.0
20.0
22.0
24.0
26.0
UNSWOLLEN PARTICLE RADIUS (nm)
CSTR SIMULATION, PSD EVOLUTION, START UP FULL - H2O, SOAP, CTA

FIGURE 5.15

policy are much more symmetric. In both cases, the distributions become broader with time, as expected. The differences between the largest and smallest particles in distributions predicted at the same time in both start-up policies are equal. This is the result of constant volume growth rates and the lack of statistical broadening. Steady-state PSD s for both start-up policies are identical and are shown in figure 5.16. The PSD statistics for the steady state distribution are given in Table 5.1 under the 116 minute residence time column. This steady-state distribution agrees closely with the PSD predicted by the model of Wong [1984] which was verified with plant data. The PSD model was also checked by comparing predictions for CSTR s of different residence times. The model predicted the correct trend in that particle sizes were smaller and the distribution was narrower for the reactor with the shorter residence time. The unswollen particle statistics of the distributions at two residence times are given in Table 5.1.

Table 5.1

PSD Statistics at Two Residence Times
(Unswollen Particles)

Statistic	θ (min) 58	116
$\bar{D}_n$(nm)	20.8	26.2
$\bar{D}_w$ (nm)	27.3	34.4
$\bar{D}_w/\bar{D}_n$	1.31	1.31
σ^2/D_n^2 (nm^2)	$2.87*10^{-2}$	$2.93*10^{-2}$

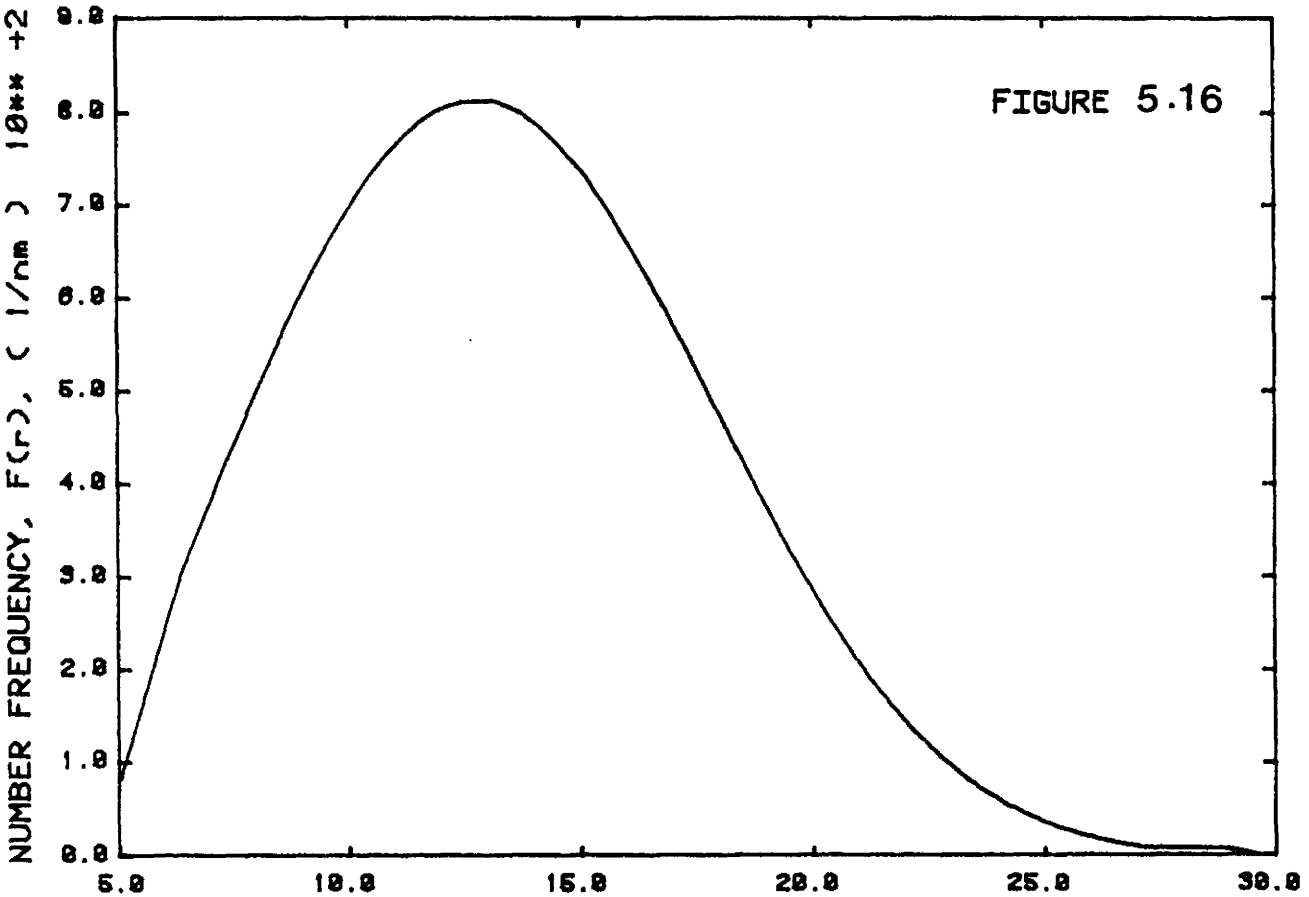
FIGURE 5.16
NUMBER FREQUENCY, F(r), (1/nm) 10** +2
9.0
8.0
7.0
6.0
5.0
4.0
3.0
2.0
1.0
0.0
5.0
10.0
15.0
20.0
25.0
30.0
UNSWOLLEN PARTICLE RADIUS (nm)
CSTR SIMULATION, STEADY STATE PARTICLE SIZE DISTRIBUTION

A qualitative test of the molecular mass predictions was made by comparing the molecular mass variables, $\overline{M}_n$, $\overline{M}_w$, $\overline{B}_{n3}$ and $\overline{B}_{n4}$ at equal concentrations in a batch and a single CSTR. One would expect $\overline{M}_n$, $\overline{M}_w$, $\overline{B}_{n3}$ and $\overline{B}_{n4}$ to be less in the batch than in the CSTR. In a CSTR, polymer radicals always see high polymer concentrations and thus reactions which occur between radicals and polymer molecules occur at a greater rate. The expected trend is observed as shown in Table 5.2. The recipes used ensured equal initial compositions of components.

Table 5.2

Comparison of Batch and CSTR Predictions at Equal Conversions (X = 0.62)

Variable	Batch	CSTR
$\overline{B}_{n3}$ (#/molecule)	0.412	0.588
$\overline{B}_{n4}$ (#/molecule)	0.046	0.065
$\overline{M}_n$ (8/mol)	132500	162800
$\overline{M}_w$ (8/mol)	484000	00*

* It should be noted that infinite mass average molecular masses were predicted for single CSTR s operating in the region where the monomer droplets had disappeared.

Oscillations in particle properties such as conversion and particle number during continuous reactor operation have been reported by Greene and modelled by Kiparissides, et al.

[1979] for vinyl acetate (VA_c). Kirrilov, et al. [1978] have modelled oscillations in continuous methyl methacrylate polymerization. Oscillations have been observed experimentally in the continuous polymerization of styrene by Brooks, et al. [1978]. Schork [1981] has interpreted the variations in SBR end use properties observed by Owen, et al. [1947] as being due to property oscillations.

The generally accepted mechanism for property oscillations in VA_c polymerization involves a cycle of rapid particle nucleation followed by a period of particle growth during which incoming emulsifier is required to stabilize the growing particles rather than for the nucleation of new ones. As particles gradually wash out of the reactor, the free emulsifier builds up to the point where micelles appear and a new, discrete burst of nucleation occurs. (This mechanism will be referred to as the "on/off nucleation mechanism" for further discussion).

It is rationalized that the key to "on/off" property oscillations is a very rapid nucleation period. For case 1 systems such as VA_c, radical desorption from particles is important and consequently radical entry rates are very high. Surface area growth rates, on the other hand, are very low (since $\bar{n} << \frac{1}{2}$). As a result, micelles are consumed almost completely by nucleation rather than by growth and very many particles are created. In case II systems, desorption is not important generally. Radical entry rates are lower, but

in addition particle surface area growth rates are high (since $\bar{n} = \frac{1}{2}$). A significant amount of emulsifier is therefore consumed by particle growth and proportionately fewer particles are generated. Particle nucleation rates are much slower.

Attempts to force a situation in which oscillations could occur for case II systems were largely unsuccessful. (Oscillations of the expected "on/off" form were simulated on one occasion but were found to be a product of a numerical integration problem. This exercise is outlined in Appendix A4). It is believed, as a result, that case II systems are not capable of the rapid generation rates required to initiate oscillations by the "on/off" mechanism.

It is proposed that the oscillations observed experimentally in case II systems are due to mechanisms other than "on/off" nucleation. As an example, the effects of an oscillatory temperature controller were simulated. The controller parameters used were $K_c = 0.5$ and $\tau_I = 10$ min. The resulting oscillations in conversion and in the reactor and cooling jacket feed temperatures are shown in figures 5.17 and 5.18.

The oscillations shown here could be accentuated if the cooling jacket feed temperature reached a minimum value during one of its cycles. To illustrate this, the cooling jacket feed temperature was constrained to a minimum of 259 K for a policy 1 start up (reactor initially empty). The results are shown in figures 5.19 and 5.20. The conversion-time

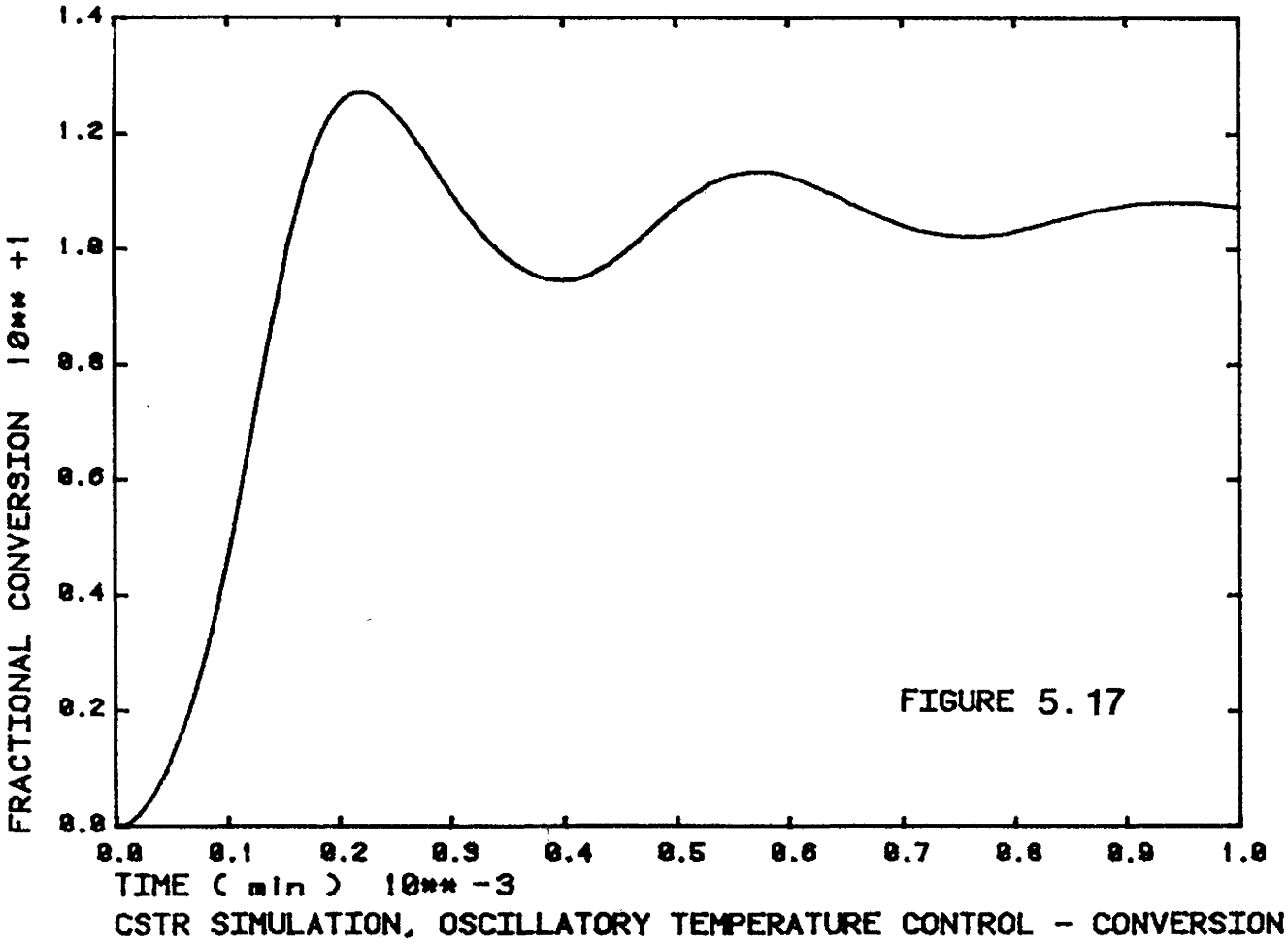
1.4
1.2
1.0
0.8
0.6
0.4
0.2
0.0
FRACTIONAL CONVERSION 10** +1
0.0
0.1
0.2
0.3
0.4
0.5
0.6
0.7
0.8
0.9
1.0
TIME (min) 10** -3
CSTR SIMULATION, OSCILLATORY TEMPERATURE CONTROL - CONVERSION

FIGURE 5.17

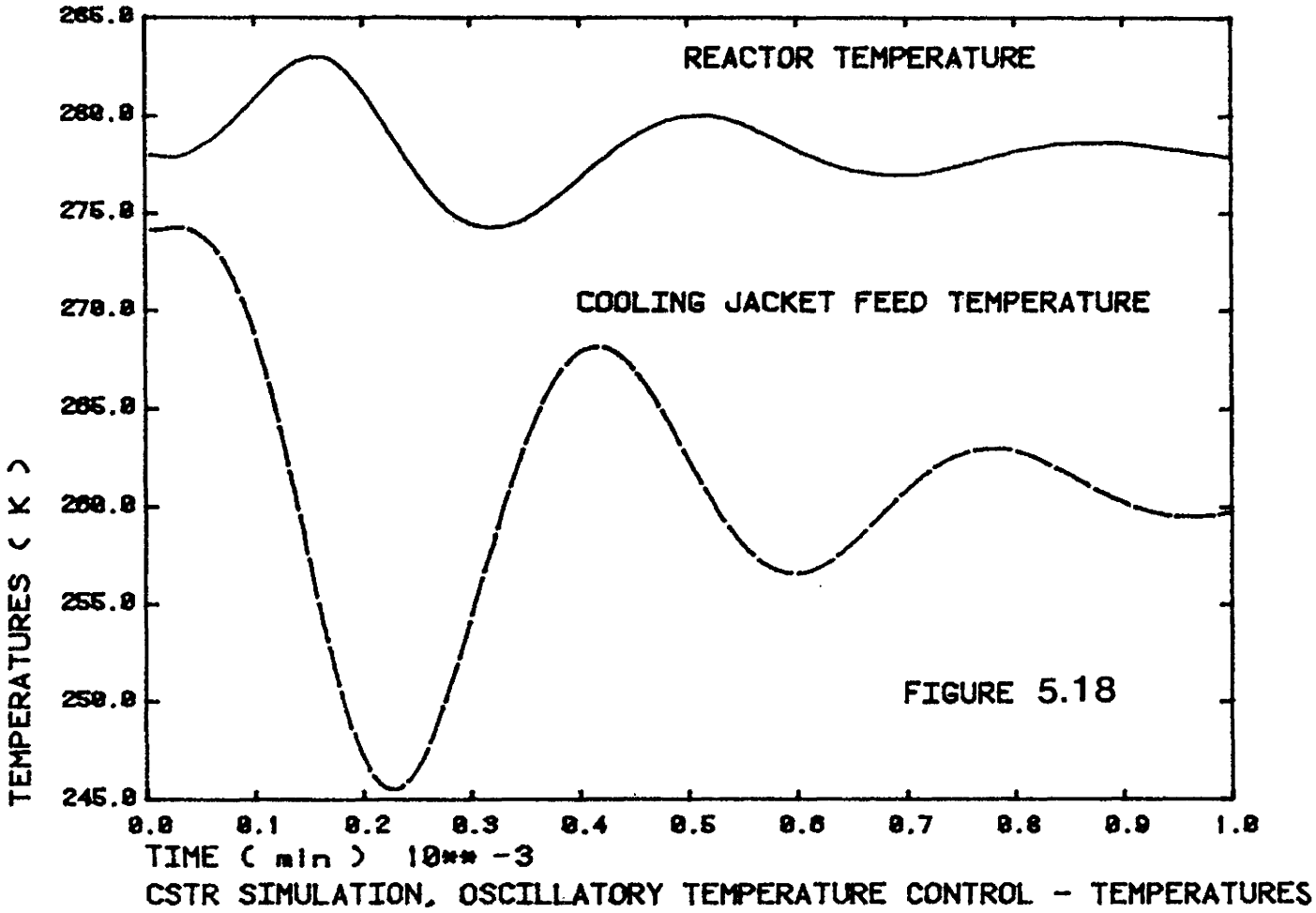

FIGURE 5.18

CSTR SIMULATION, OSCILLATORY TEMPERATURE CONTROL - TEMPERATURES

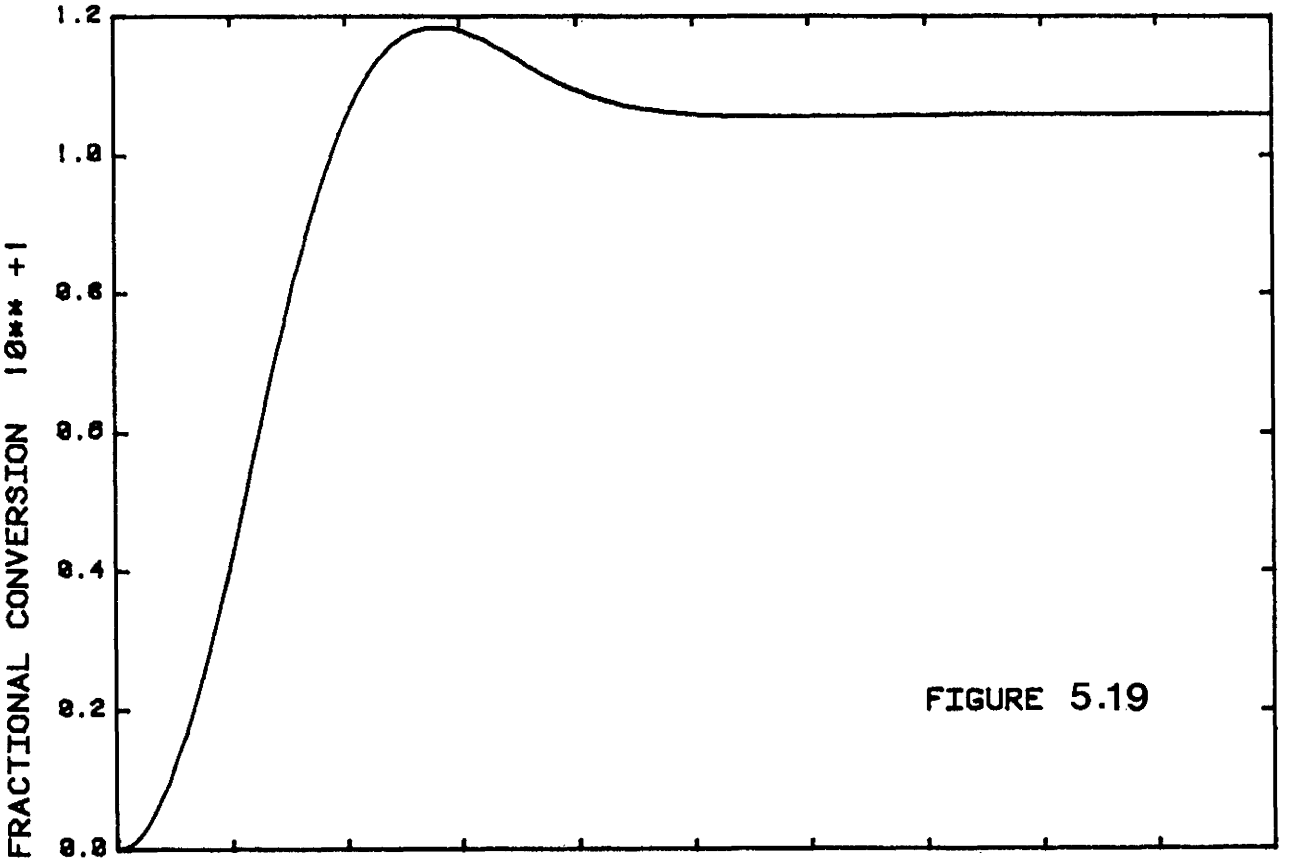
1.2
1.0
0.8
0.6
0.4
0.2
0.0
FRACTIONAL CONVERSION 10** +1
0.0
0.1
0.2
0.3
0.4
0.5
0.6
0.7
0.8
0.9
1.0
TIME (min) 10** -3
CSTR SIMULATION, SATURATED CONTROL VARIABLE - CONVERSION

FIGURE 5.19

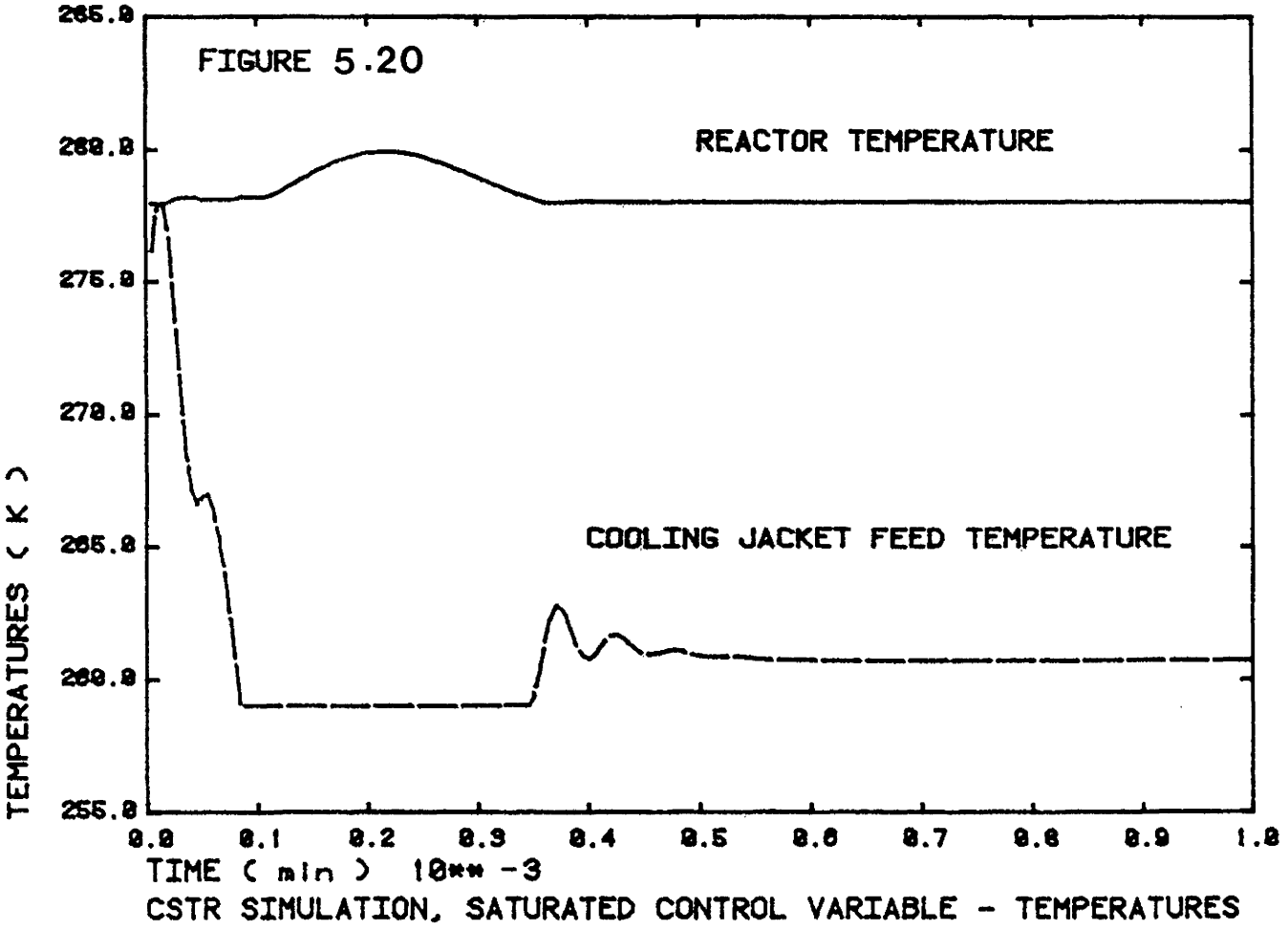
FIGURE 5.20
REACTOR TEMPERATURE
COOLING JACKET FEED TEMPERATURE
TEMPERATURES (K)
285.0
280.0
275.0
270.0
265.0
260.0
255.0
0.0
0.1
0.2
0.3
0.4
0.5
0.6
0.7
0.8
0.9
1.0
TIME (min) 10** -3
CSTR SIMULATION, SATURATED CONTROL VARIABLE - TEMPERATURES

curve may be compared with curve 1 of figure 5.9. Constraining the manipulated variable to 259 K resulted in approximately a three Kelvin temperature excursion and an accentuated conversion peak.

The model was also used to study the adiabatic operation of a CSTR. It was found that the reactor operated stabily though the initial transient peak was large and the steady-state reactor temperature was found to be 10 K higher than the original operating temperature.

5.4 Semi-Batch Reactor Simulations

5.4.1 Introduction

The merits of semi-batch, or semi-continuous, reactor operation in emulsion polymerization have been briefly mentioned in section 1.2. A good introduction to semi-batch emulsion polymerization (of homopolymers) is given by Gerrens [1969]. Of specific interest to copolymer systems is the use of semi-batch reactors to control copolymer composition. Hamielec and MacGregor [1983] address this problem and outline two policies of maintaining copolymer composition. These two policies are studied in the present work.

The goal of the subsequent simulations is to produce a 50:50 mole ratio styrene: butadiene copolymer. It is assumed that persulphate decomposes ideally to initiate polymerization. Appropriate recipes are given in Appendix B2, tables B2.8, B2.9 and B2.10. It is stressed that the

simulations presented herein are qualitative and are intended to illustrate trends only.

5.4.2 Semi-Batch Policy 1

For copolymer systems it is useful to recognize the relative reactivities of the two monomer species. A "fast" monomer is defined as the species which preferentially adds to radicals. Monomers may be categorized as "fast" or "slow" strictly on the knowledge of the homopolymerization rates and the reactivity ratios. For SBR polymerization, butadiene is the fast monomer.

Semi-batch composition control policy 1 consists of charging all of the slower reacting monomer (styrene) into the reactor initially. Enough of the faster reacting monomer is charged to instantaneously produce a copolymer of the desired composition. The fast monomer is then post-fed to maintain a constant ratio of moles of the monomers, which will lead to the desired copolymer composition.

The development of an expression to calculate the required monomer ratio for the desired copolymer composition is simplfied by the assumption that the composition of the monomer droplets equals the monomer composition in the polymer particles. This was stated earlier as equation (3.26). The consequences of this assumption were discussed in section 3.2.1. Ignoring the monomers in the water phase and applying the aforementioned assumption, the ratio of monomers in the

polymer phase may be approximated by the total ratio of monomers in the reactor.

$$\frac{[S]_p}{[B]_p} \simeq \frac{N_s}{N_B} \tag{5.1}$$

After stage 2, this would be a reasonable assumption regardless of the partition coefficients. In semi-batch policy 1, the above ratio must be kept constant.

$$\frac{N_s}{N_B} = \alpha \equiv \text{constant} \tag{5.2}$$

An expression for the monomer mole ratio required for a copolymer of specified composition is based on the definition of the instantaneous copolymer composition, ICC.

$$ICC = \frac{R_{ps}}{R_{ps} + R_{pB}} \tag{3.63}$$

Substituting for R_{ps} and R_{pB} with equations (3.49) and (3.50) and simplifying gives:

$$ICC = \frac{r_s[s]_p^2 + [S]_p[B]_p}{r_s[S]_p^2 + 2[S]_p[B]_p + r_B[B]_p^2} \tag{5.3}$$

Dividing both numerator and denominator of (5.3) by $[B]_p^2$ and substituting with (5.1) and (5.2) gives, upon rearranging:

$$r_S(1-ICC)\ \alpha^2 + (1-2ICC)\ \alpha + r_B ICC = 0 \qquad (5.4)$$

Solving the above quadratic gives:

$$\alpha = \frac{(2ICC-1) + \sqrt{(1-2ICC)^2 + 4r_s r_B ICC(1-ICC)}}{2\ r_s(1-ICC)} \qquad (5.5)$$

The positive root is taken to satisfy the condition ICC = 0; $\alpha = \frac{N_S}{N_B} = 0$.

Equation (5.5) specifies the mole ratio of monomers needed to attain the desired copolymer composition, ICC.

The feedrate of butadiene required to maintain constant copolymer composition is derived from equation (5.2) and equations (3.51) and (3.52).

Differentiating (5.2) gives

$$\frac{dN_S}{dt} = \alpha \frac{dN_B}{dt} \qquad (5.6)$$

Since all styrene is charged initially, equation (3.51) simplifies to:

$$\frac{dN_S}{dt} = - R_{ps}\ V_p \qquad (5.7)$$

Equation (3.52) becomes

$$\frac{dN_B}{dt} = F_{B,in} - R_{pB}\ V_p \qquad (5.8)$$

Substituting (5.7) and (5.8) into (5.6) gives:

$$-R_{ps} V_p = \alpha(F_{B,in} - \frac{R_{ps} V_p}{\alpha}) \quad (5.9)$$

Rearranging (5.9) gives:

$$F_{Bin} = (R_{pB}V_p - R_{ps}V_p/\alpha) \quad (5.10)$$

A more general expression of (5.10) assuming that perhaps styrene could be post fed as well, is:

$$F_{B,in} = (R_{pB}V_p - \frac{(R_{ps}V_p - F_{s,in})}{\alpha} \quad (5.11)$$

The policy 1 simulations studied in this work were based on equations (5.5) and (5.10). Molar (or mass) flows of other components such as water, initiator or chain transfer agent were post fed at rates which were multiples of the monomer feed rates in the proportions called for in the GR-S recipe (Table 1.1). For example, the mass post feed rate of water was calculated:

$$\tilde{F}_{w,in} = 1.8 \quad (\tilde{F}_{s,in} + \tilde{F}_{B,in}) \quad (5.12)$$

A number of policy 1 implementations were attempted. In this report two policy 1 implementations are compared with an equivalent batch run. In the first policy 1 implementation (denoted P1 I1 in all figures) only butadiene was post fed. In the second policy 1 implementation (P1 I4), monomer, water and emulsifier were post fed. In figures 5.21 through 5.28, policies P1 I1 and P1 I4 are compared with batch runs.

Conversion histories are compared in figure 5.21. The rates of conversion of both semi-batch policies are faster than the batch rate initially, but by the end, the batch conversion rate overtakes the semi-batch rates. This observation reflects the difference in compositions of the batch and semi-batch copolymers being formed. The compositions are shown in figure 5.23. It should be explained that though butadiene is the fast monomer, the overall reaction rate increases with an increase in the proportion of styrene. The copolymer formed initially in the batch has a higher butadiene content and therefore a slower rate. Near the end of the reaction in the batch, most of the butadiene is consumed. The greater proportion of styrene in the reaction mixture increases the overall rate. The semi-batch policies, on the other hand, always incorporate the same proportions of each monomer by design.

The conversion profiles of the two semi-batch policies differ by virtue of their two different particle number histories (figure 5.22). In P1 I4 water is post fed with the net effect of diluting the particle concentration in stages 2 and 3 and consequently decreasing the reaction rate.

Figure 5.23 indicates that the composition control of the semi-batch policies is very good. It also illustrates the drift in composition in the batch copolymer.

Figure 5.24 shows the required butadiene feed

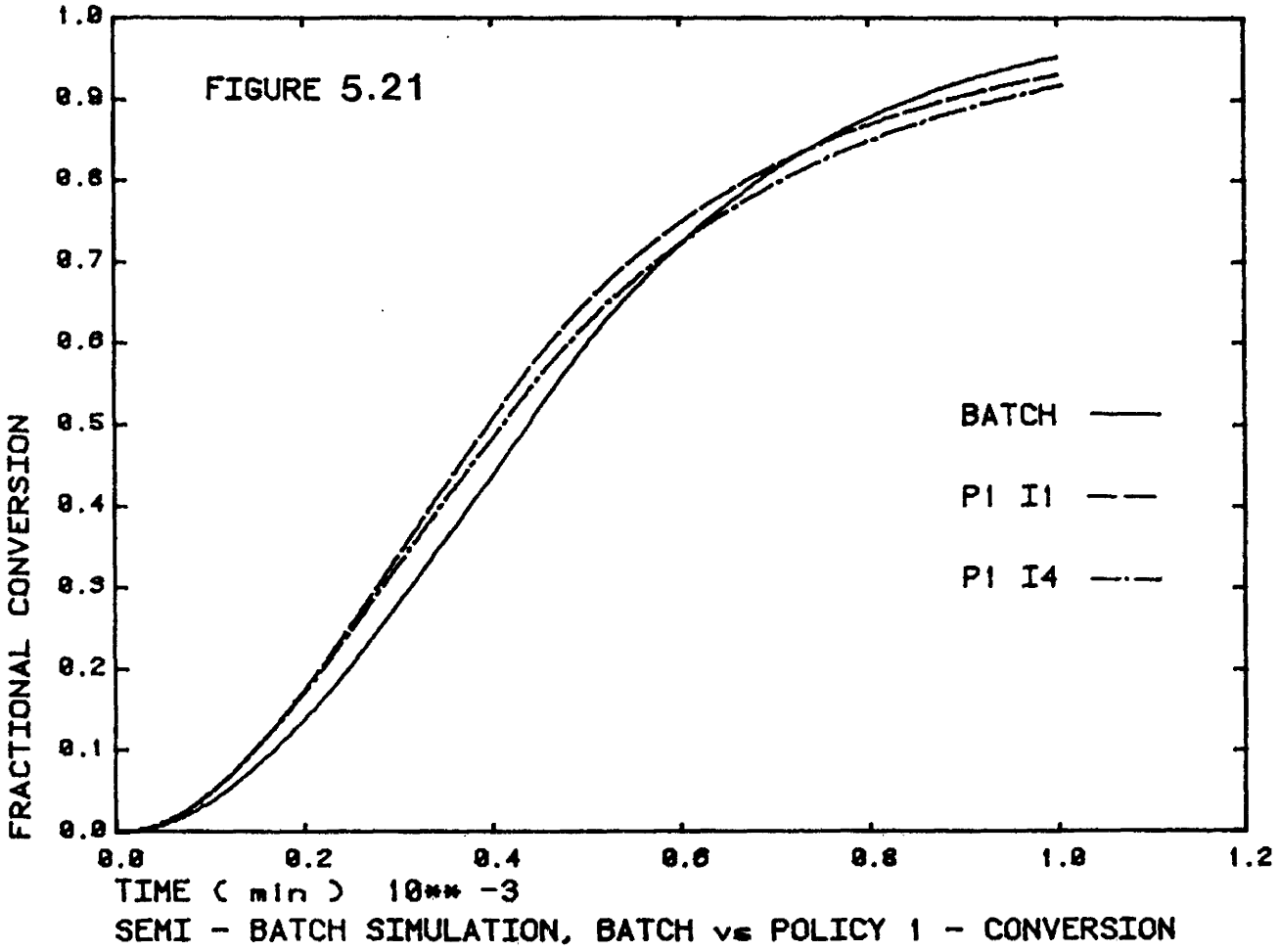
FIGURE 5.21
FRACTIONAL CONVERSION
1.0
0.9
0.8
0.7
0.6
0.5
0.4
0.3
0.2
0.1
0.0
0.0
0.2
0.4
0.6
0.8
1.0
1.2
BATCH
P1 I1
P1 I4
TIME (min) 10** -3
SEMI - BATCH SIMULATION, BATCH vs POLICY 1 - CONVERSION

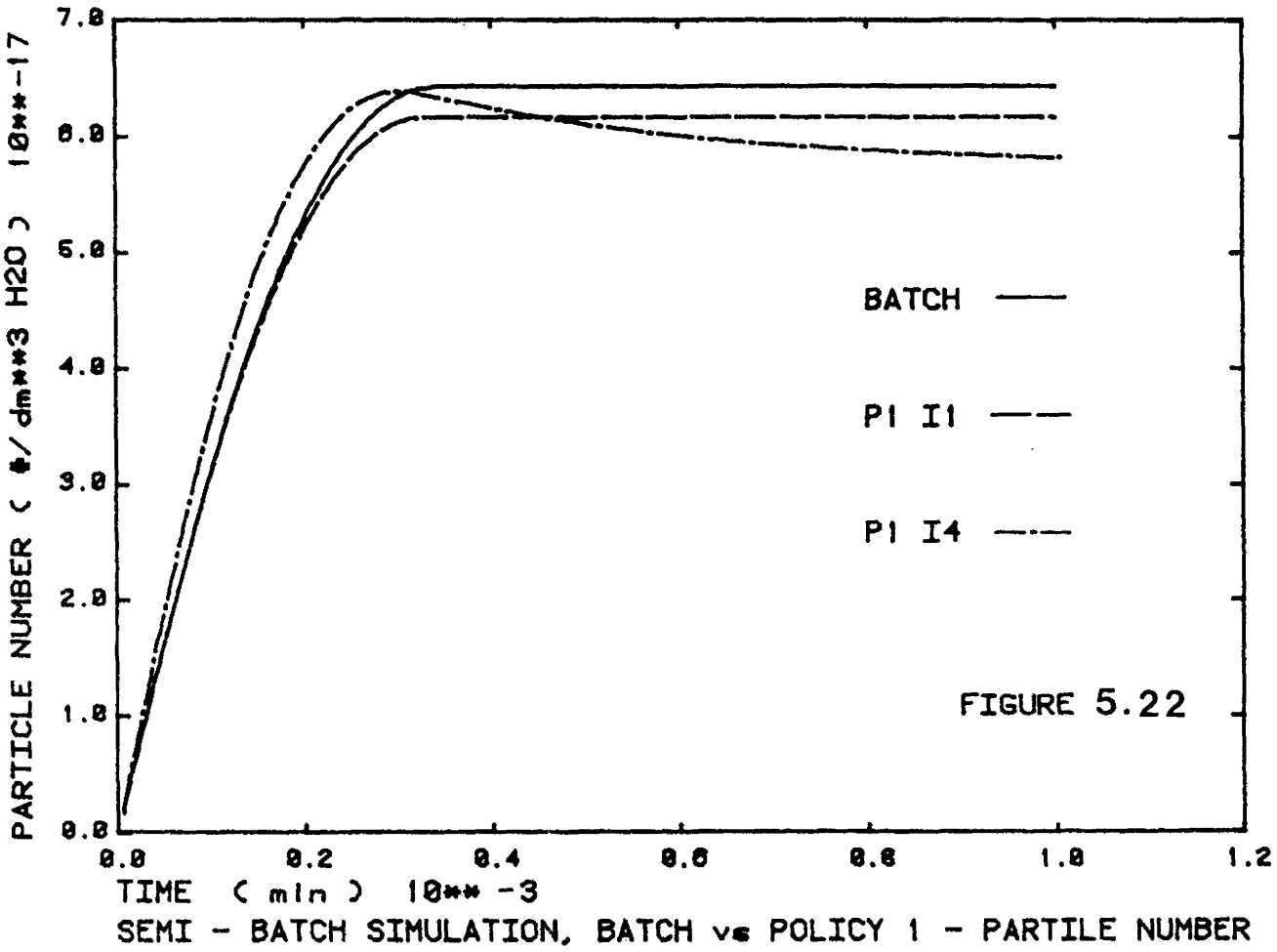
PARTICLE NUMBER (#/ dm**3 H2O) 10**-17
7.0
6.0
5.0
4.0
3.0
2.0
1.0
0.0
0.0
0.2
0.4
0.6
0.8
1.0
1.2
TIME (min) 10** -3
BATCH
P1 I1
P1 I4
FIGURE 5.22
SEMI - BATCH SIMULATION, BATCH vs POLICY 1 - PARTILE NUMBER

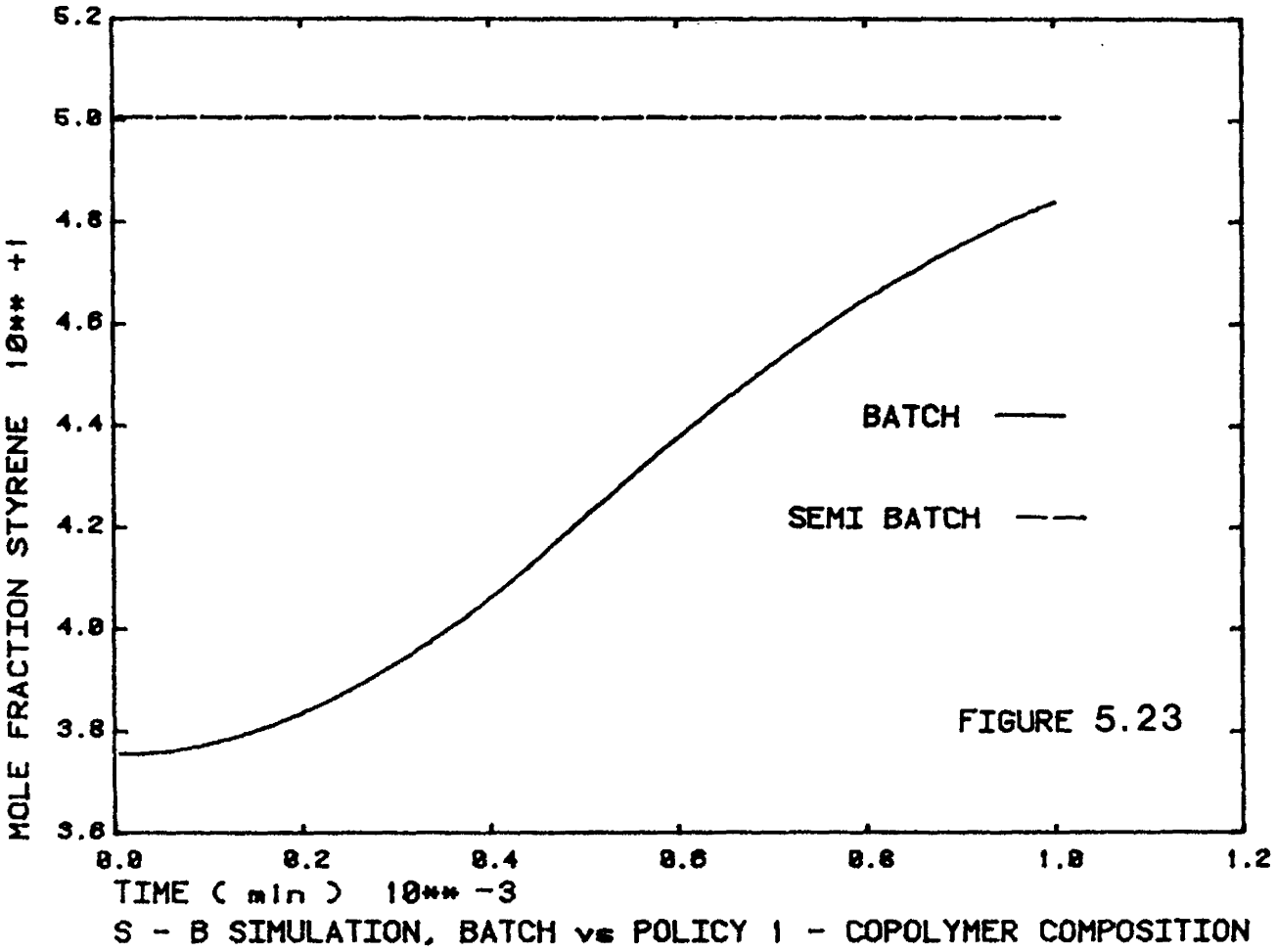

FIGURE 5.23

S - B SIMULATION, BATCH vs POLICY 1 - COPOLYMER COMPOSITION

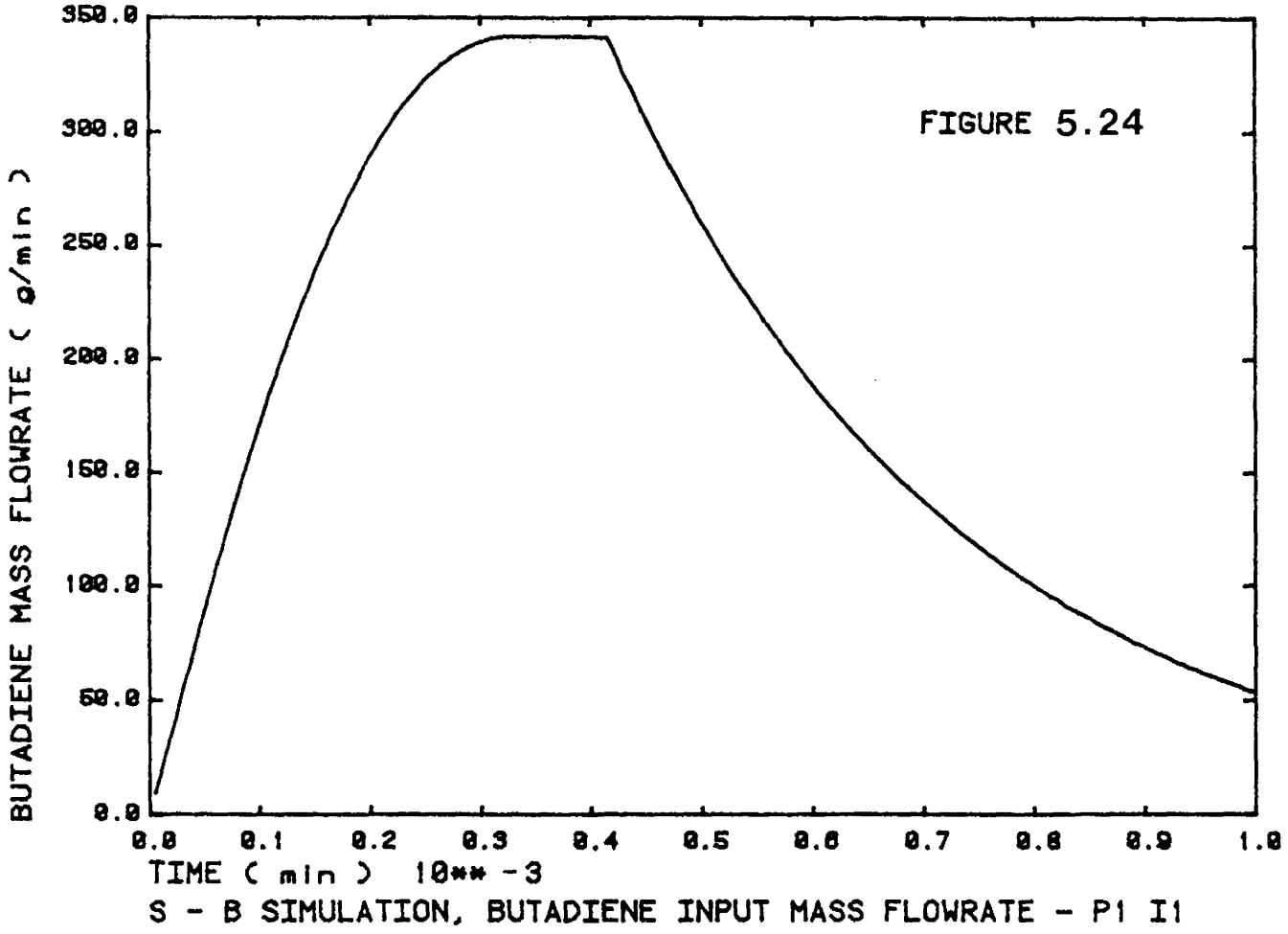
350.0
300.0
250.0
200.0
150.0
100.0
50.0
0.0
BUTADIENE MASS FLOWRATE (g/min)
0.0
0.1
0.2
0.3
0.4
0.5
0.6
0.7
0.8
0.9
1.0
TIME (min) 10** -3
S - B SIMULATION, BUTADIENE INPUT MASS FLOWRATE - P1 I1

FIGURE 5.24

rate for P1 I1. Using the model to correlate butadiene feed rate with instantaneous heat generation rate, one could develop an open loop control strategy for policy 1.

Number and mass average molecular masses are presented in figures 5.25 and 5.26 respectively. The general shapes of the two molecular mass curves are the same for all three policies, and in fact, the shapes reflect the change in the proportion of CTA to monomer in the particles with time. This is explained in section 5.2.

Figures 5.27 and 5.28 show the history of the branch frequencies. The increase in branch frequency near the end of stage 2 is clearly shown.

It is of interest to note that the number average molecular mass for the batch run and for P1 I1 are very similar. This is due to the fact that in both cases all of the water and all of the CTA are charged initially. There is only a small difference in the total organic phase charged initially. In P1 I4, all of the CTA is charged but less water is charged initially. In this case the proportion of CTA in the organic phase is higher and subsequently molecular masses are lower.

A different trend is observed in the branch frequency plots. The semi-batch policies have very similar branch frequency histories which are lower than in the batch case. This reflects the fact that the copolymers made in the semi-

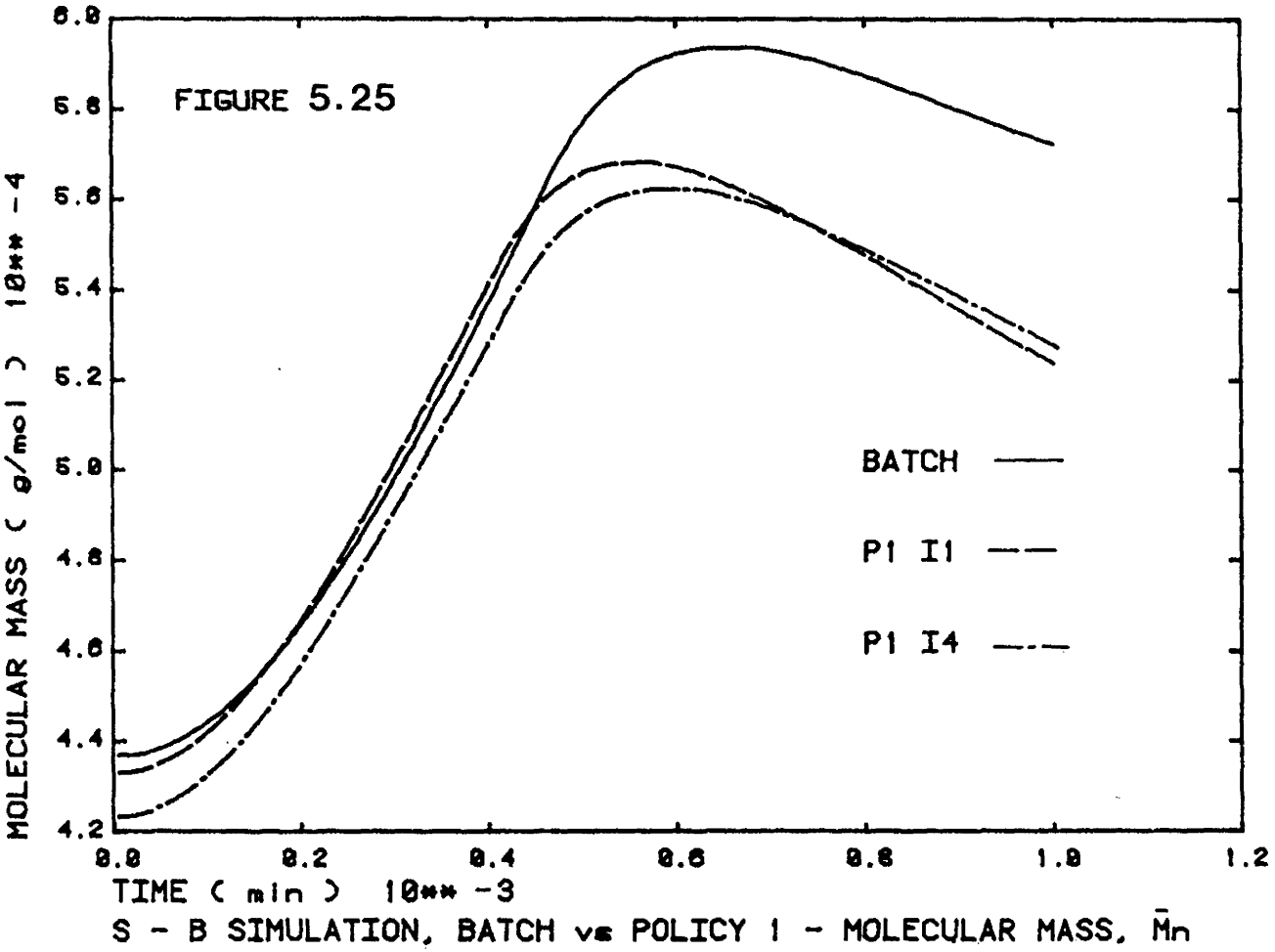
FIGURE 5.25
MOLECULAR MASS (g/mol) 10** -4
6.0
5.8
5.6
5.4
5.2
5.0
4.8
4.6
4.4
4.2
0.0
0.2
0.4
0.6
0.8
1.0
1.2
TIME (min) 10** -3
BATCH
P1 I1
P1 I4
S - B SIMULATION, BATCH vs POLICY 1 - MOLECULAR MASS, $\bar{M}n$

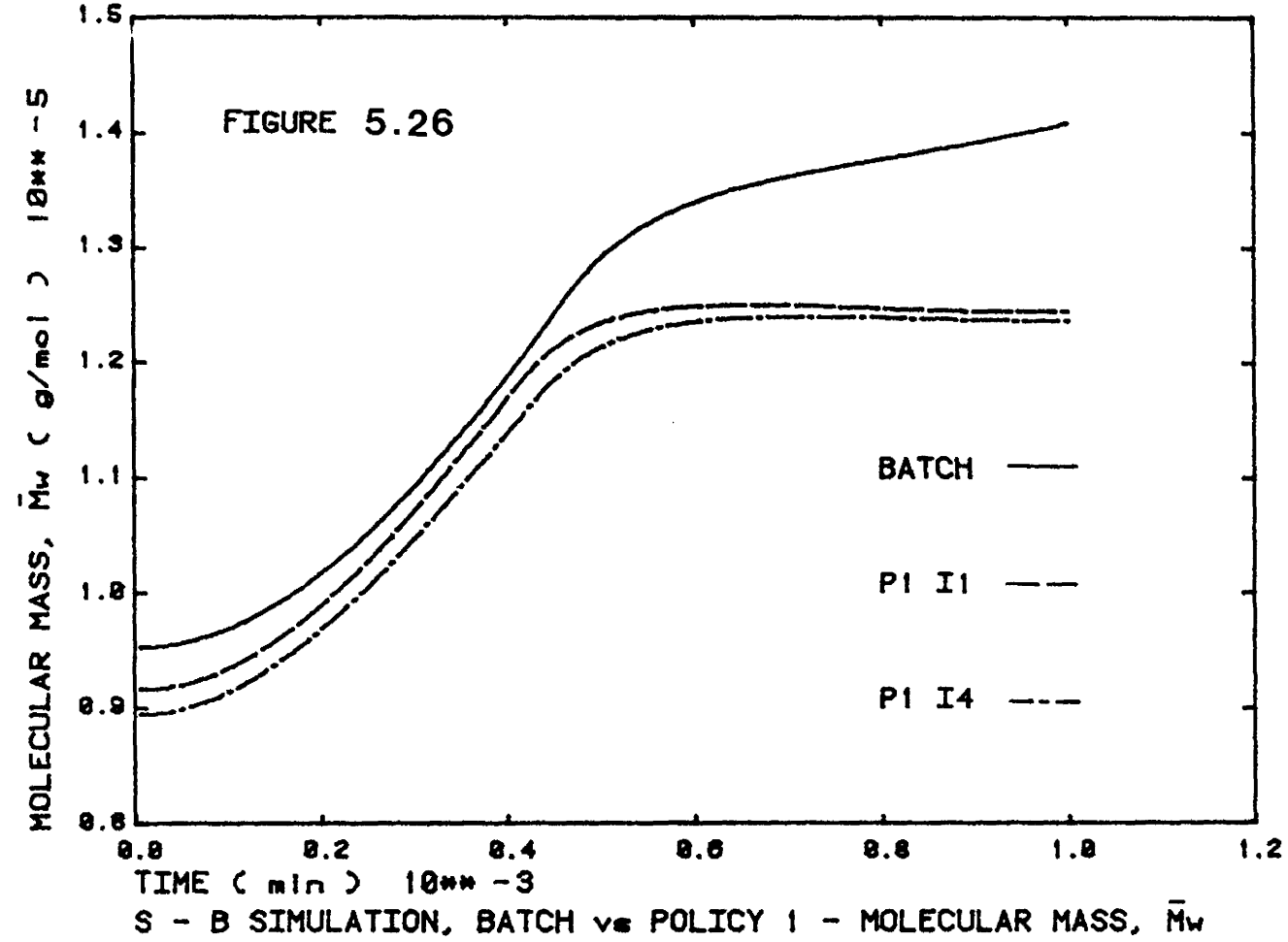

S - B SIMULATION, BATCH vs POLICY 1 - MOLECULAR MASS, $\bar{M}w$

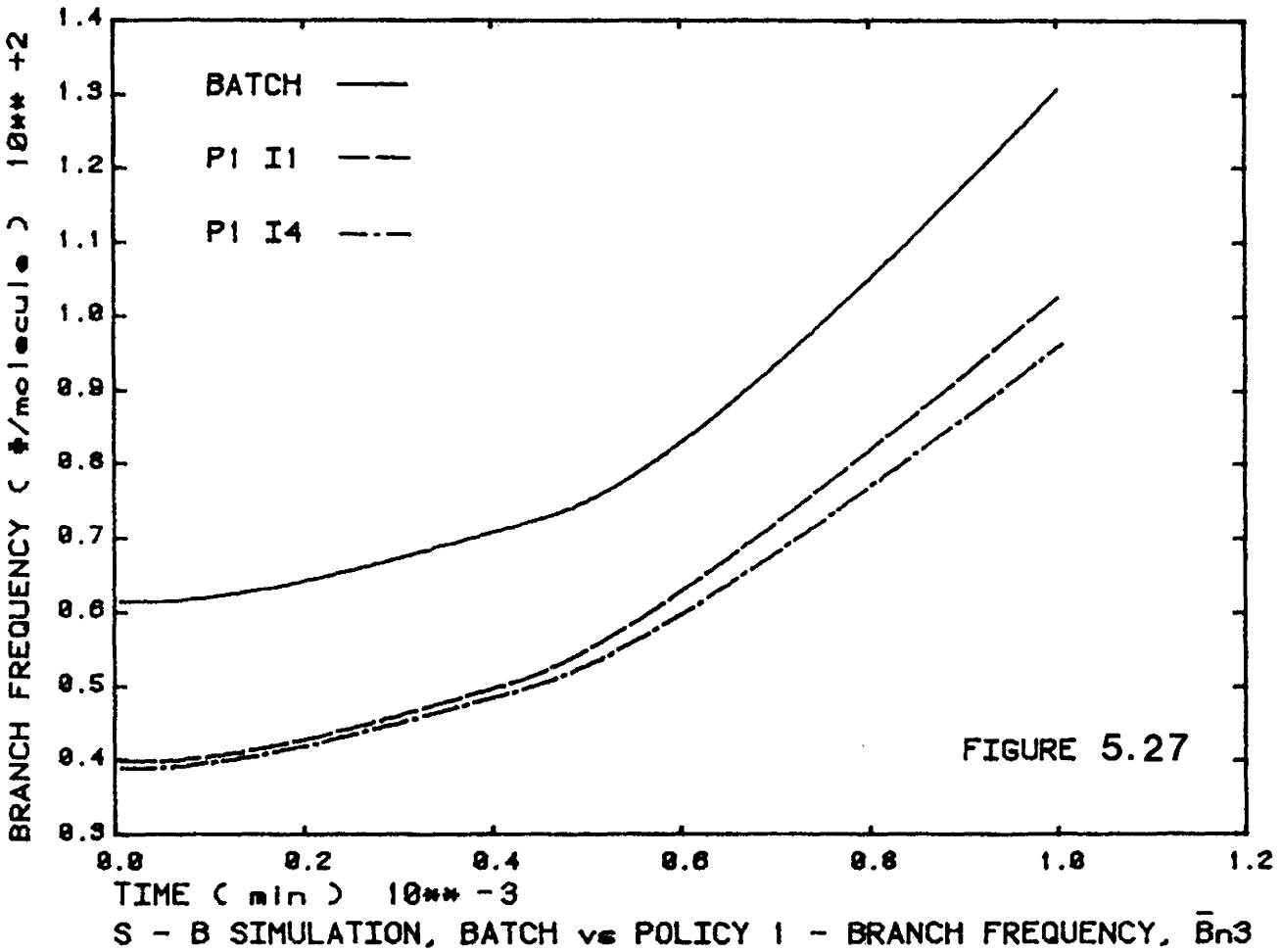

FIGURE 5.27

S - B SIMULATION, BATCH vs POLICY 1 - BRANCH FREQUENCY, $\bar{B}n3$

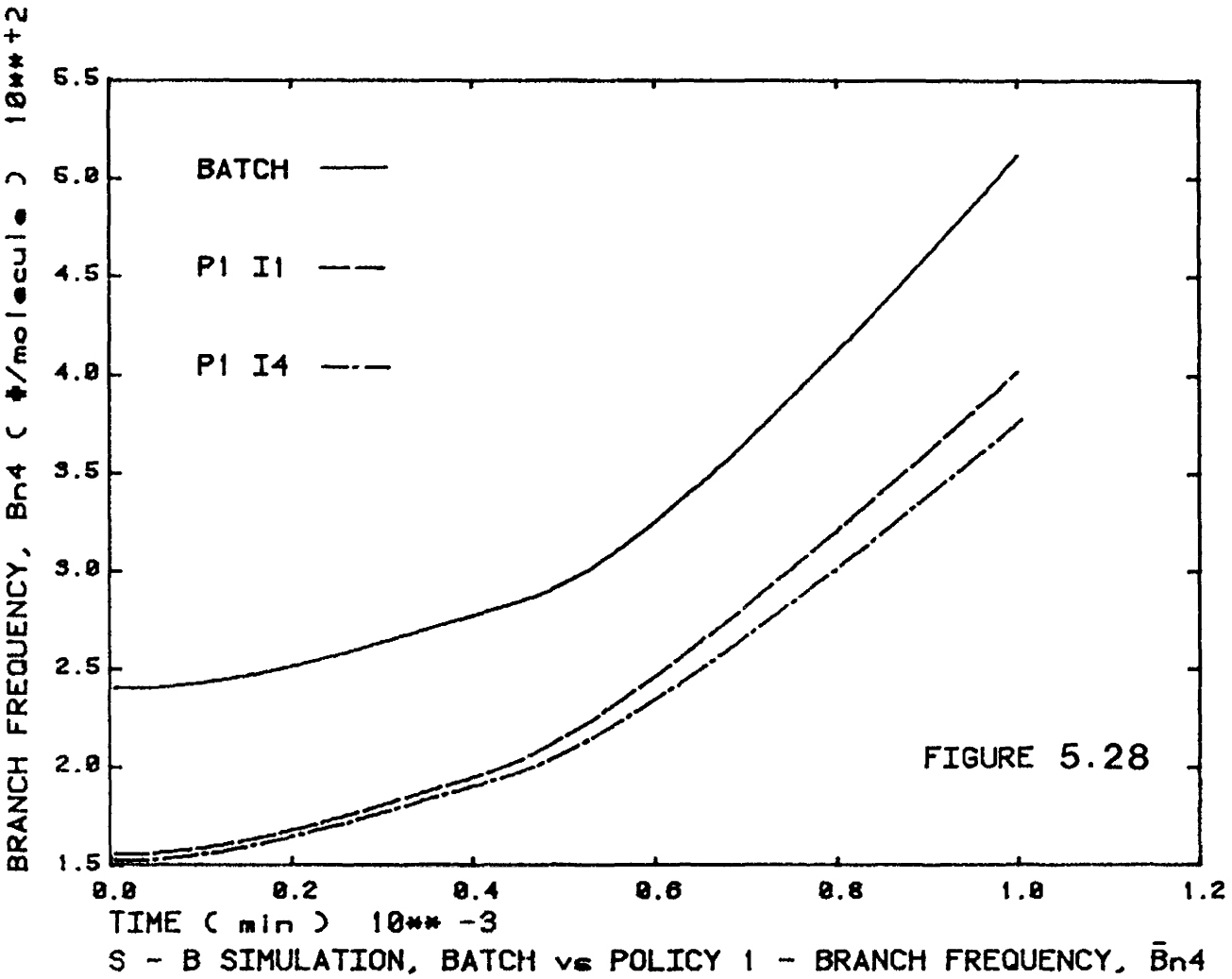

FIGURE 5.28

S - B SIMULATION, BATCH vs POLICY 1 - BRANCH FREQUENCY, $\bar{B}n4$

batch reactors have the same compositions and lower proportions of incorporated butadiene in comparison with the batch copolymer. The degree of branching is related to the transfer to polymer and the propagation with polymer reactions which occur only with incorporated butadiene units. It should also be noted that the higher molecular mass averages of the batch copolymer may be attributed to the higher degree of branching.

For more information on policy 1 semi-batch emulsion polymerization, the works of Hamielec and MacGregor [1983] and Guyot, et al. [1981] are recommended.

5.4.3 Semi-Batch Policy 2

As defined by Hamielec and MacGregor [1983] semi-batch policy 2 involves operating the reactor at a condition in which the particles have a very low but constant monomer concentration, or in other words, a constant conversion. Comonomers are fed in the proportion that they are desired in the copolymer and it is assumed that if the conversion in the reactor is high enough, all monomers fed will be incorporated instantly. An alternative to this is to try to maintain constant monomer concentrations in the ratio given by equation (5.5) for the desired composition. The rates at which monomers must be fed are developed after Hamielec [1984b] as follows:

The rate of change of moles of styrene in the region where particles are monomer starved is given by:

$$\frac{dN_s}{dt} = \frac{d(V_p[S]_p)}{dt} = V_p \frac{d[s]_p}{dt} + [S]_p \frac{dV_p}{dt} \qquad (5.12)$$

similarly for butadiene

$$\frac{dN_B}{dt} = \frac{d(V_p[B]_p}{dt} = V_p \frac{d[B]_p}{dt} + [B]_p \frac{dV_p}{dt} \qquad (5.13)$$

Policy 2 requires that the monomer concentrations in the particles remain constant, or

$$\frac{d[B]_p}{dt} = \frac{d[S]_p}{dt} = 0 \qquad (5.14)$$

Equations (5.12) and (5.13) may be simplified with (5.14) to give:

$$\frac{dN_s}{dt} = [S]_p \frac{dV_p}{dt} \qquad (5.15)$$

and

$$\frac{dN_B}{dt} = [B]_p \frac{dV_p}{dt} \qquad (5.16)$$

Expressions for $\frac{dN_s}{dt}$, $\frac{dN_B}{dt}$ and for $\frac{dV_p}{dt}$ during stage 3 have already been presented in section 3.2.
Simplified for the purposes of this development, these equations are:

$$\frac{dN_s}{dt} = F_{s,in} - R_{ps} V_p \qquad (5.17)$$

$$\frac{dN_B}{dt} = F_{B,in} - R_{pB} V_p \tag{5.18}$$

and

$$\frac{dV_p}{dt} = \frac{\tilde{M}_s F_{s,in}}{\rho} + \frac{\tilde{M}_B F_{B,in}}{\rho_B} - (\tilde{M}_s R_{ps} V_p (\frac{1}{\rho_s} - \frac{1}{\rho_p}) + \tilde{M}_B R_{pB} V_p (\frac{1}{\rho_s} - \frac{1}{\rho_p})) \tag{5.19}$$

Combining equations (5.15) through (5.19) results in two simultaneous algebraic equations in the two unknowns $F_{s,in}$ and $F_{B,in}$. Rather than reduce the following expressions fully into functions of fundamental variables, the simultaneous equations were solved as they appear below.

$$\alpha F_{s,in} + \beta F_{B,in} = \gamma \tag{5.20}$$

$$\delta F_{s,in} + \theta F_{B,in} = \omega \tag{5.21}$$

where

$$\alpha = (\frac{\tilde{M}_s [S]_p}{\rho_s} - 1) \tag{5.22}$$

$$\beta = (\frac{\tilde{M}_B [S]_p}{\rho_B}) \tag{5.23}$$

$$\gamma = SHRINK - R_{ps} V_p \tag{5.24}$$

$$\delta = (\frac{\tilde{M}_s [B]_p}{\rho_s}) \tag{5.25}$$

$$\theta = SHRINK - R_{pB} V_p \tag{5.27}$$

$$\omega = \text{SHRINK} - R_{pB}\, V_p \tag{5.27}$$

$$\text{SHRINK} = \tilde{M}_s R_{ps} V_p \left(\frac{1}{\rho_s} - \frac{1}{\rho_p}\right) + \tilde{M}_B R_{pB} V_p \left(\frac{1}{\rho_B} - \frac{1}{\rho_p}\right) \tag{5.28}$$

To investigate policy 2, simulations at two operating points were investigated. The first run maintained a low monomer concentration corresponding to approximately 95% conversion. The second run maintained a conversion of approximately 60%. Each run was initialized with 100 kg of a seed latex. Initiator, emulsifier and water were post fed in the GR-S recipe (Table 1.1) proportions. A plot of monomer concentrations in the polymer particles vs. time is shown in figure 5.29. The evident drift in styrene concentration is small when the scale of the ordinate axis is considered and may be due to an inaccurately calculated initial condition.

Figure 5.30 compares the production rates of polymer for the two operating points. At low monomer concentration (X = 95%) the production rates are low. This is expected in context with the rate of expressions, equations (3.49) and (3.50). The average number of radicals per particle, $\bar{n}$ is generally constant at a value of $\frac{1}{2}$. The rate constants are functions of temperature only. Clearly, low rates should be expected. Polymers produced commercially in semi-batch reactors at high conversion operating points, (poly(methyl-methacrylate) for example) typically exhibit the effects of

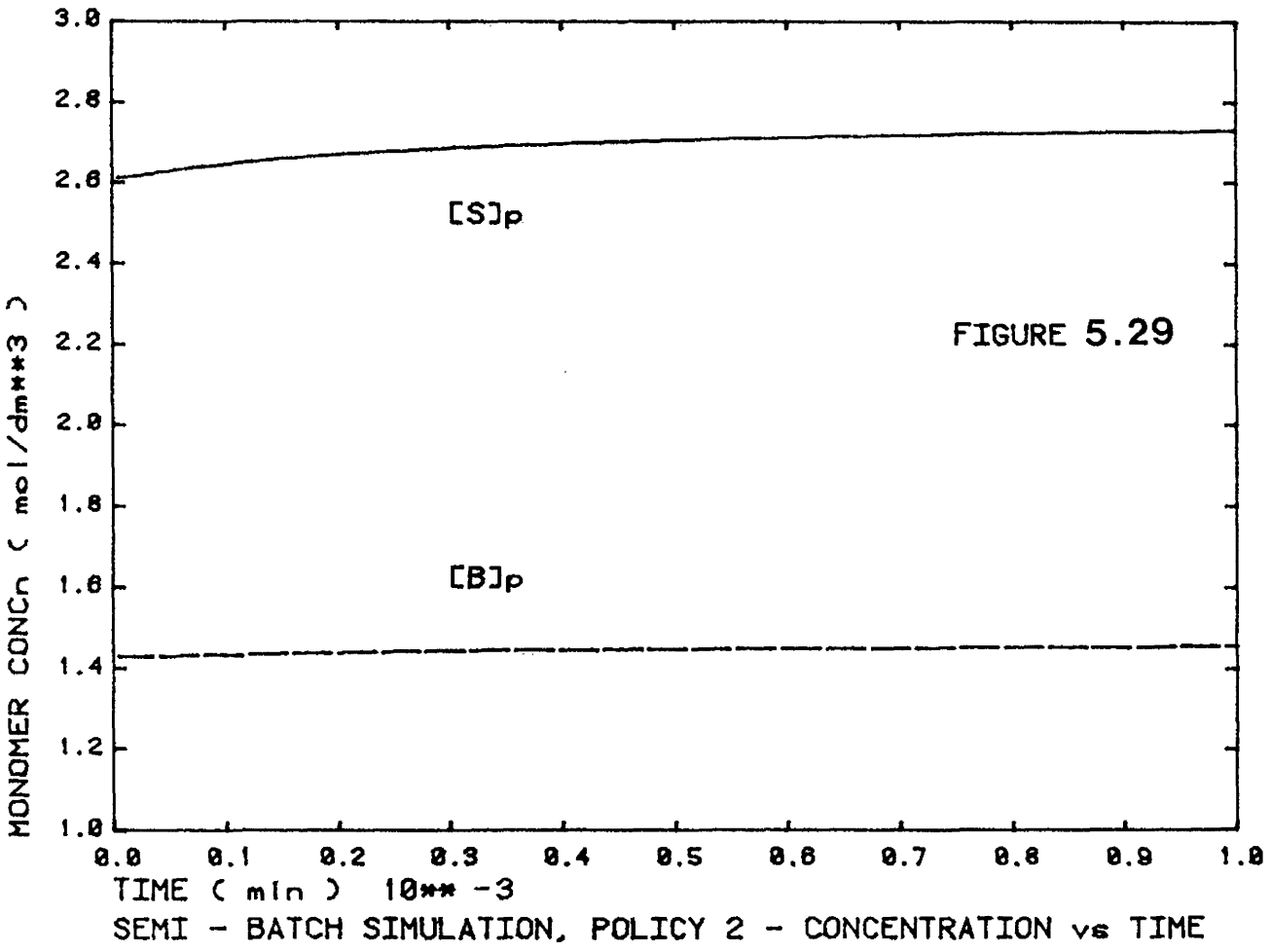
3.0
2.8
2.6
2.4
2.2
2.0
1.8
1.6
1.4
1.2
1.0
[S]p
[B]p
MONOMER CONCn (mol/dm**3)
0.0
0.1
0.2
0.3
0.4
0.5
0.6
0.7
0.8
0.9
1.0
TIME (min) 10** -3
SEMI - BATCH SIMULATION, POLICY 2 - CONCENTRATION vs TIME

FIGURE 5.29

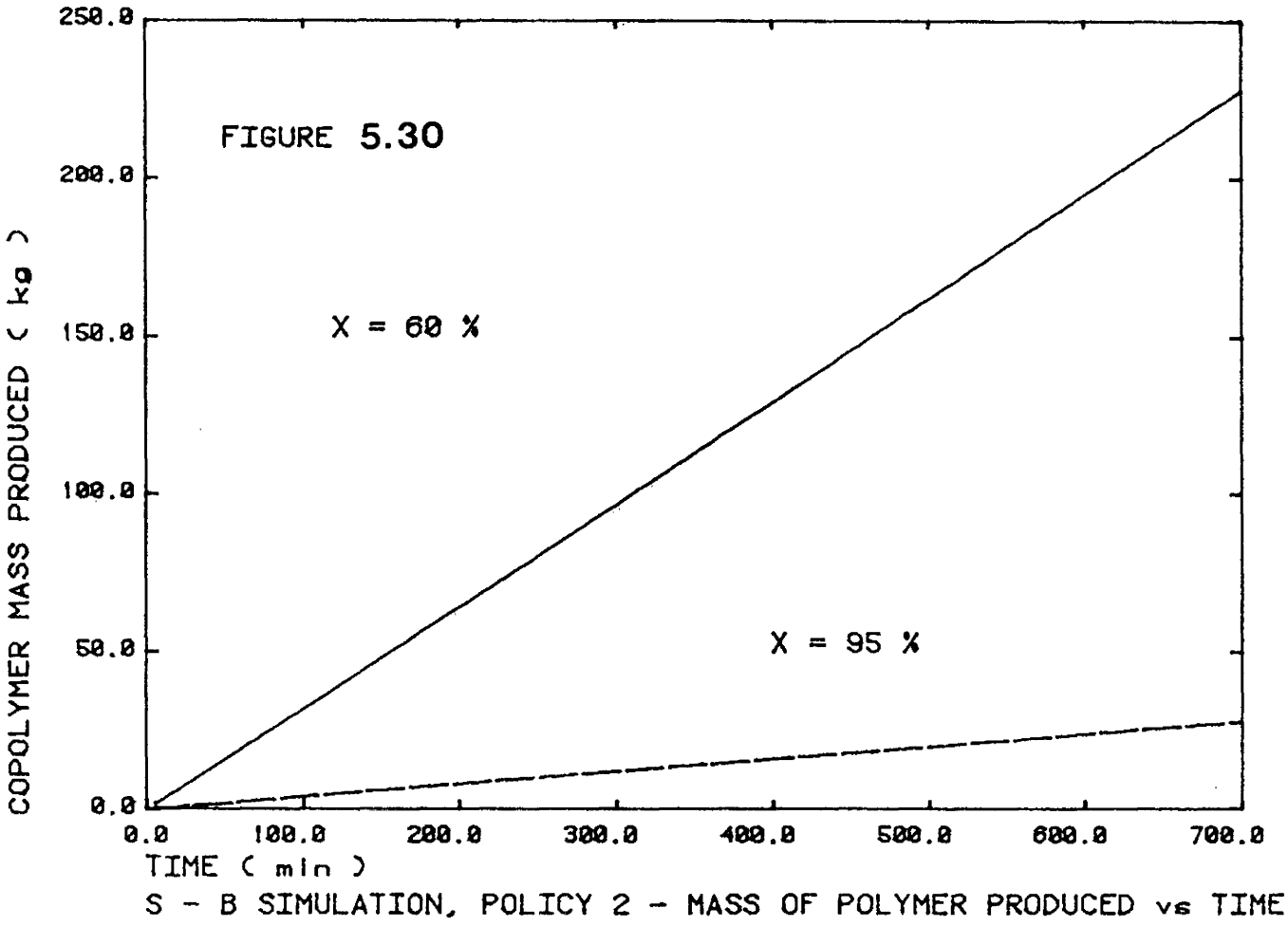
FIGURE 5.30
250.0
200.0
150.0
100.0
50.0
0.0
COPOLYMER MASS PRODUCED (kg)
X = 60 %
X = 95 %
0.0
100.0
200.0
300.0
400.0
500.0
600.0
700.0
TIME (min)
S - B SIMULATION, POLICY 2 - MASS OF POLYMER PRODUCED vs TIME

diffusion controlled termination (or the "gel effect"). The high radical concentrations which result from diffusion controlled termination greatly increase reaction rates at high conversion. The lack of diffusion controlled termination in SBR, with the possible exception of very high styrene content SBR, probably precludes policy 2 operation at high conversions.

Another equally important factor discouraging the production of SBR at high conversion is the possibility of gel formation. This is illustrated in figure 5.31. The mass average molecular mass of the copolymer produced at 95% conversion is seen to approach infinity indicating gel formation. This phenomenon is observed at high concentrations in commercial systems. The higher production rates and relative absence of gel formation favours the operation of policy 2 at lower conversion. In fact, semi-batch SBR is produced commercially in this manner. It should be pointed out that there is an advantage for reactor control in operating at conversions at which particles are not saturated with monomer. At such operating conditions, the reaction rate equals the feed rate. An increase or decrease in feed rate immediately increases or decreases the reaction rate or more appropriately the heat generation rate. If particles are saturated, a decrease in feed rate will not affect the reaction rate until the monomer droplets are consumed which may result in a significant dead time.

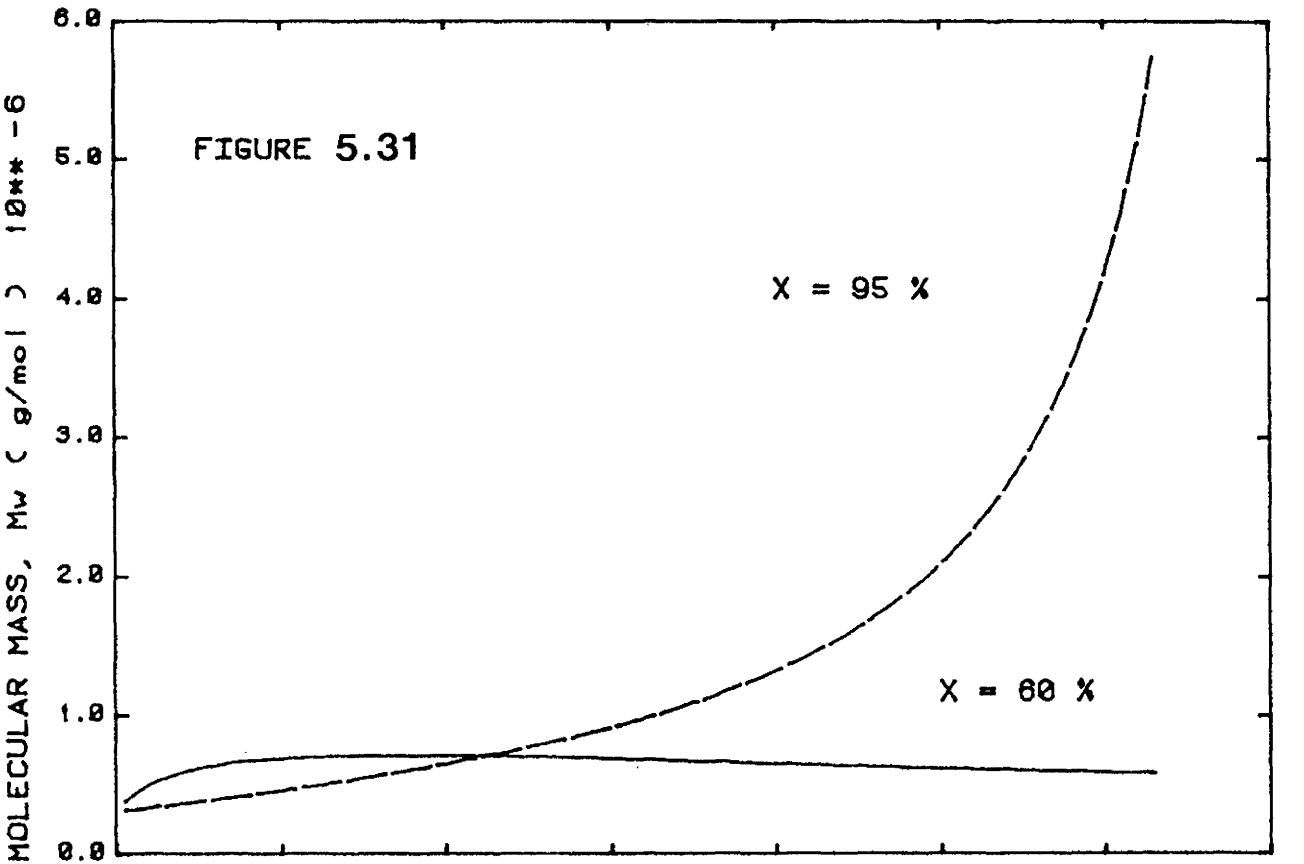

S - B SIMULATION, POLICY 2 - WEIGHT AVERAGE MOLECULAR MASSES

5.4.4 Semi-Batch Policy 3

To implement policy 2 industrially, a polymer seed must be nucleated and, after the policy 2 period of polymerization, the residual monomers in the particles must be polymerized. A combination policy, policy 3, was conceived in which a copolymer seed was nucleated at constant composition with a policy 1 period, the bulk of the monomers were polymerized using a policy 2 feed strategy and the residual monomers were polymerized (or "finished") with a policy 1 period. The recipe used in this simulation is presented in Table B2.10 of Appendix B2.

The monomer feed rates used in this composite policy are shown in figure 5.32. The policy 1 and policy 2 periods are clearly discernable. The concentrations of monomers in the particles are shown in figure 5.33. Once again a small drift in monomer concentrations is observed during the policy 2 period. No explanation for this small drift was determined. However, it did not affect the copolymer composition at all. The copolymer composition never deviated from the desired value.

The production of polymer is illustrated in figure 5.34. It is clear that the final policy 1 period is undesirably long. It is suggested that during this "finishing" period the temperature be allowed to increase adiabatically. This would accelerate the reaction rate and shorten the "finishing" period. The molecular mass averages, $\bar{M}_n$ and $\bar{M}_w$,

are shown in figure 5.35. The observed curves reflect the dominance of CTA over the molecular mass development. The fall of $\bar{M}_n$ and $\bar{M}_w$ at high conversions is the result of post feeding CTA up to high conversions. The branch frequencies, shown in figure 5.36, display a small plateau which reflects the duration at constant conversion during the policy 2 period. Figure 5.37 shows the reactor and cooling jacket feed (manipulated variable) temperatures with time. The fact that a constant cooling jacket feed temperature during the policy 2 period is not observed is due to the dilution of particles by inflowing water.

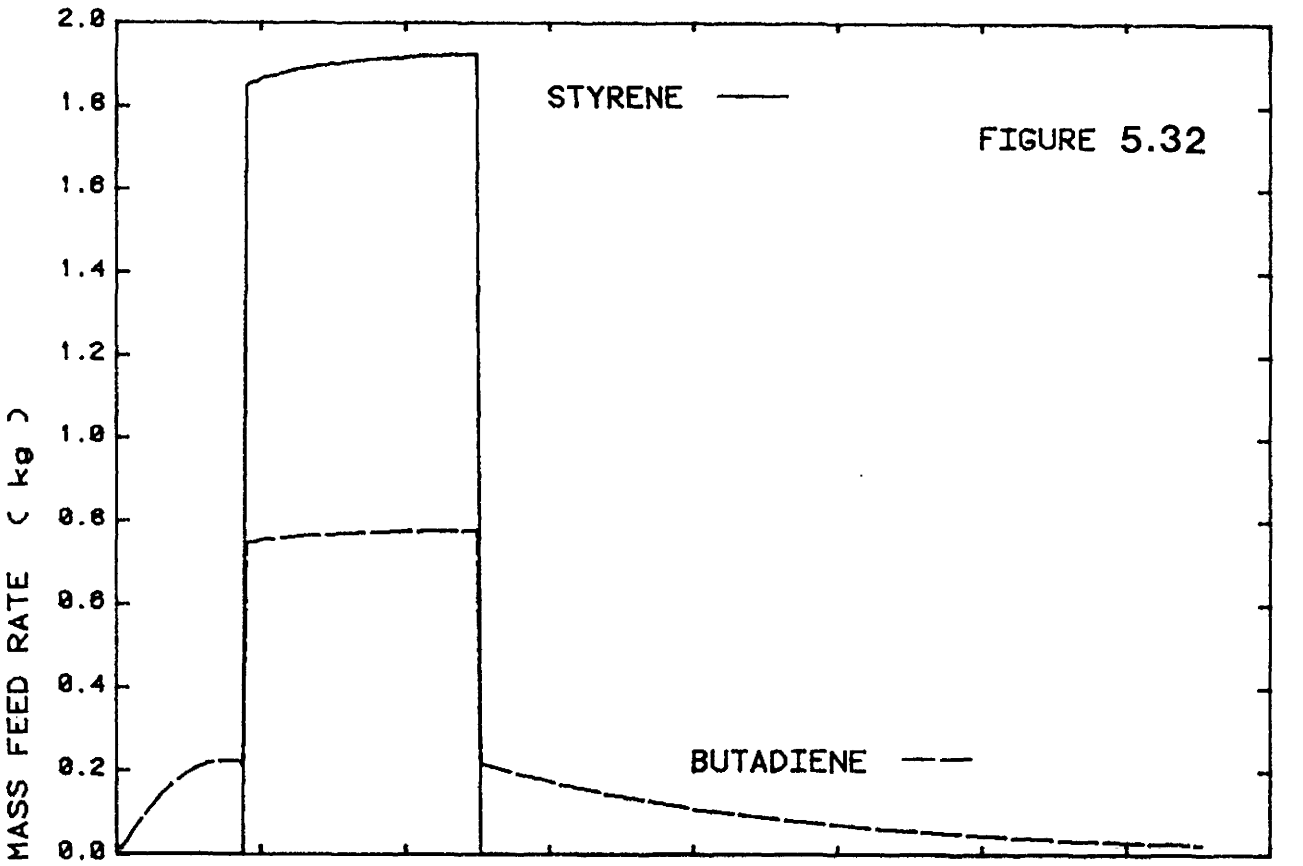

FIGURE 5.32

S - B SIMULATION, POLICY 3 - MONOMER MASS FEED RATES

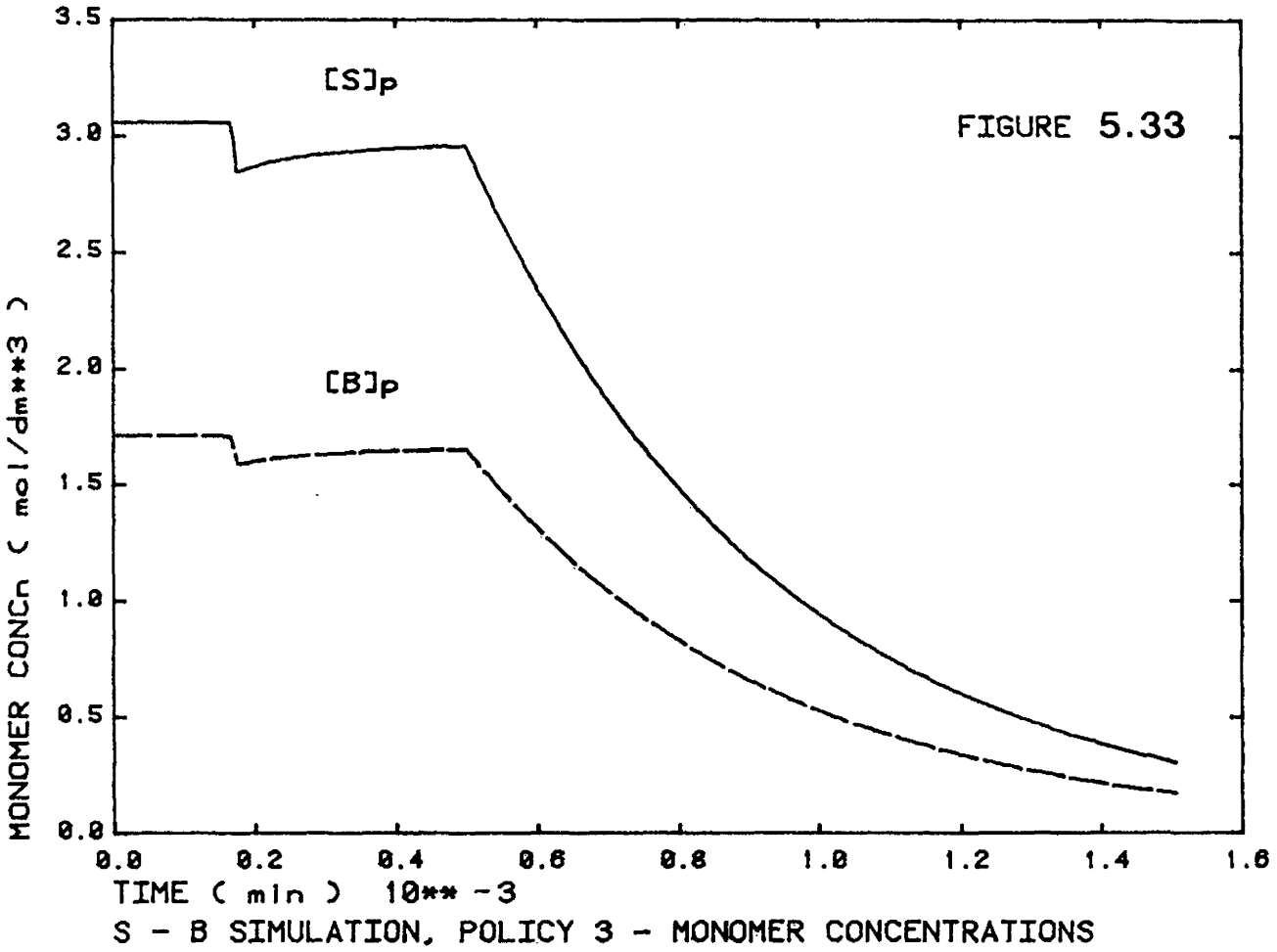

FIGURE 5.33

S - B SIMULATION, POLICY 3 - MONOMER CONCENTRATIONS

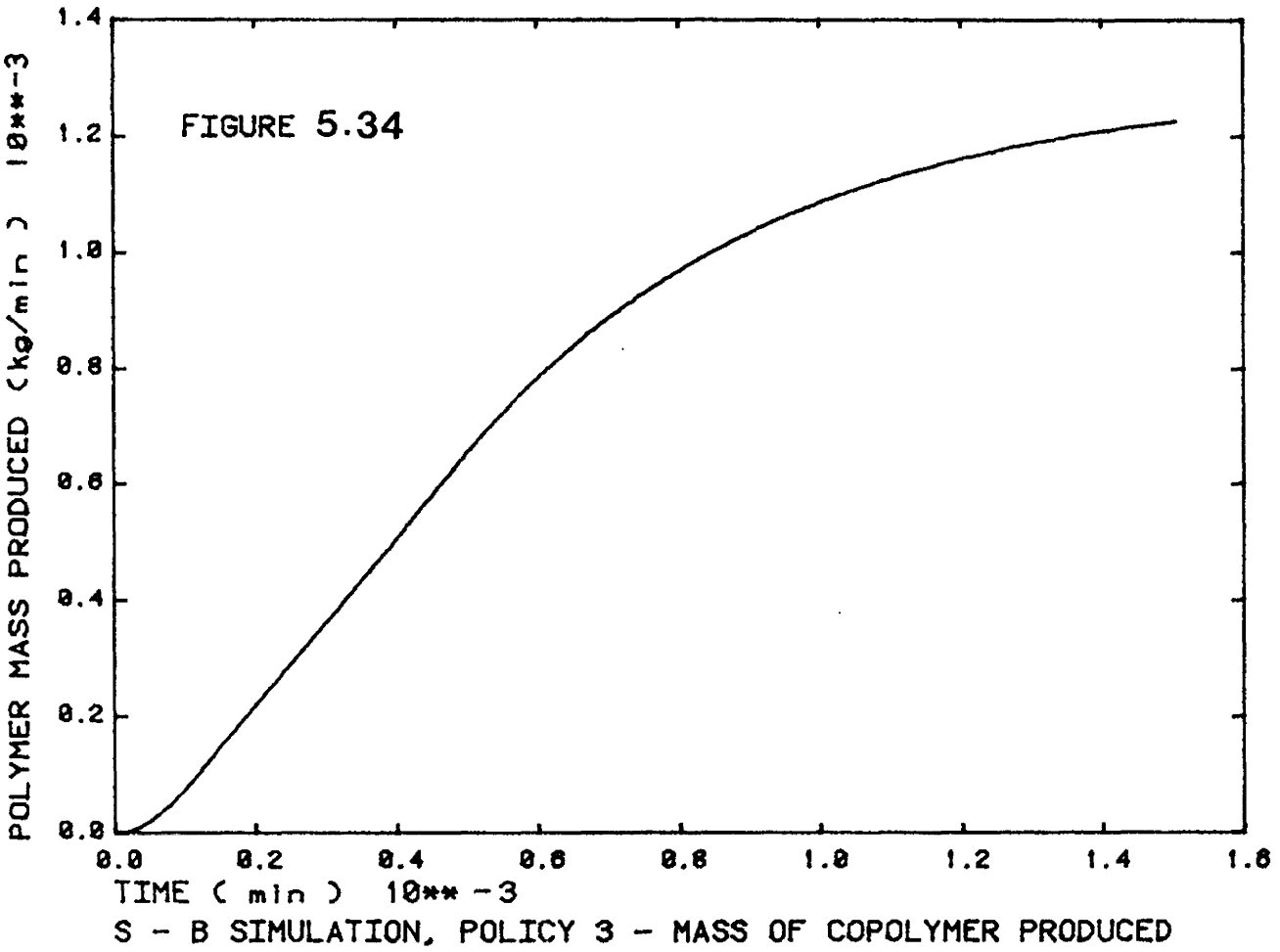
FIGURE 5.34
POLYMER MASS PRODUCED (kg/min) 10**-3
1.4
1.2
1.0
0.8
0.6
0.4
0.2
0.0
0.0
0.2
0.4
0.6
0.8
1.0
1.2
1.4
1.6
TIME (min) 10** -3
S - B SIMULATION, POLICY 3 - MASS OF COPOLYMER PRODUCED

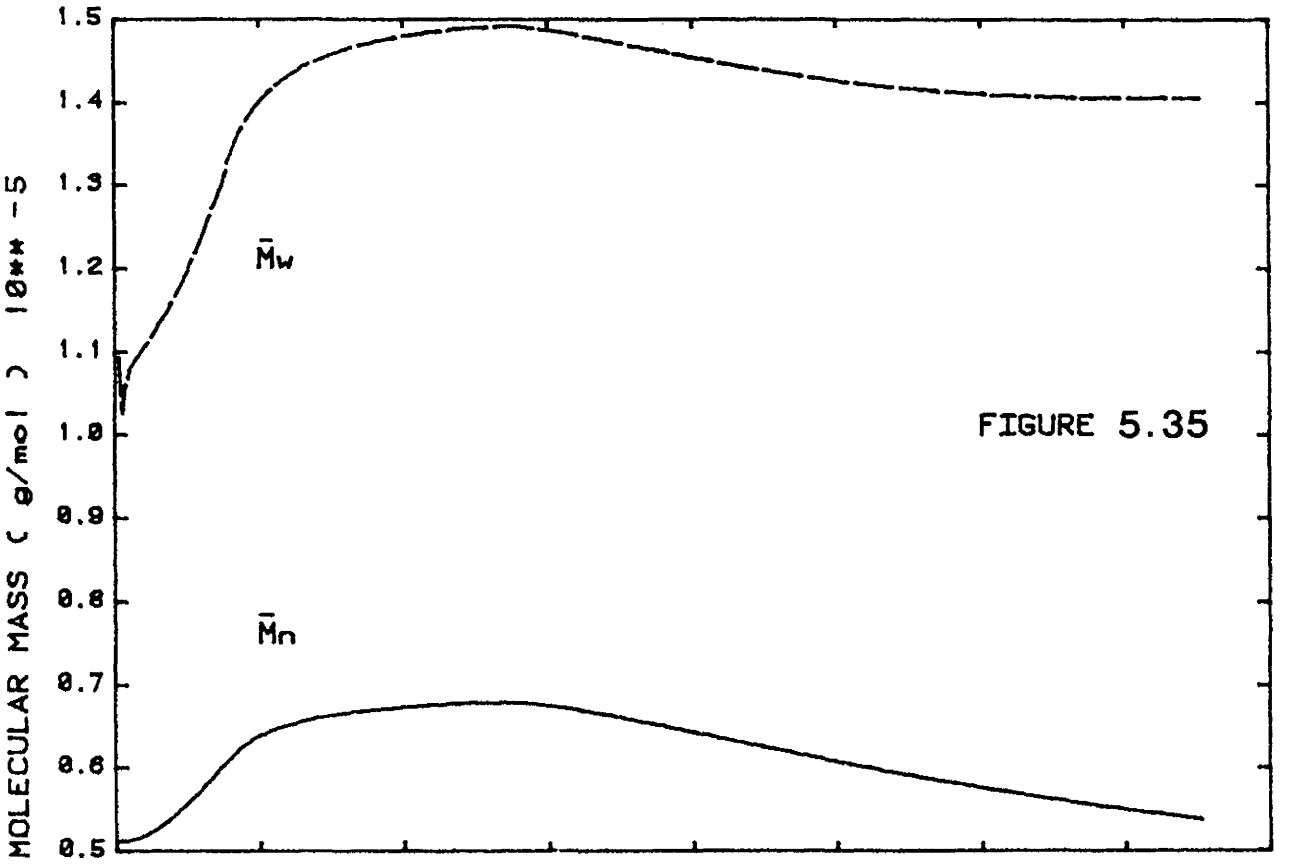

FIGURE 5.35

S - B SIMULATION, POLICY 3 - MOLECULAR MASSES, $\bar{M}n$ and $\bar{M}w$

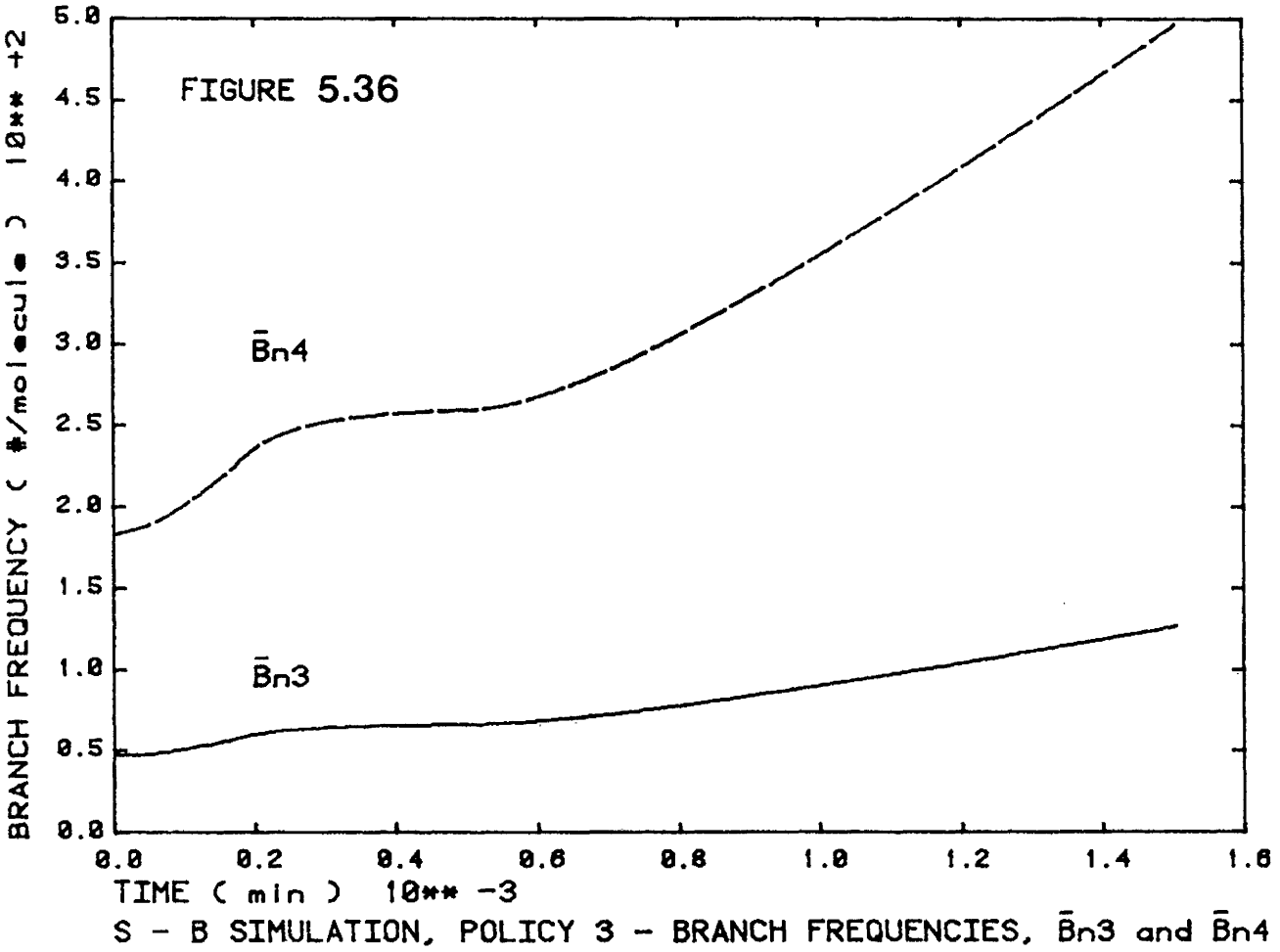
FIGURE 5.36
BRANCH FREQUENCY (#/molecule) 10** +2
5.0
4.5
4.0
3.5
3.0
2.5
2.0
1.5
1.0
0.5
0.0
B̄n4
B̄n3
0.0
0.2
0.4
0.6
0.8
1.0
1.2
1.4
1.6
TIME (min) 10** -3
S - B SIMULATION, POLICY 3 - BRANCH FREQUENCIES, B̄n3 and B̄n4

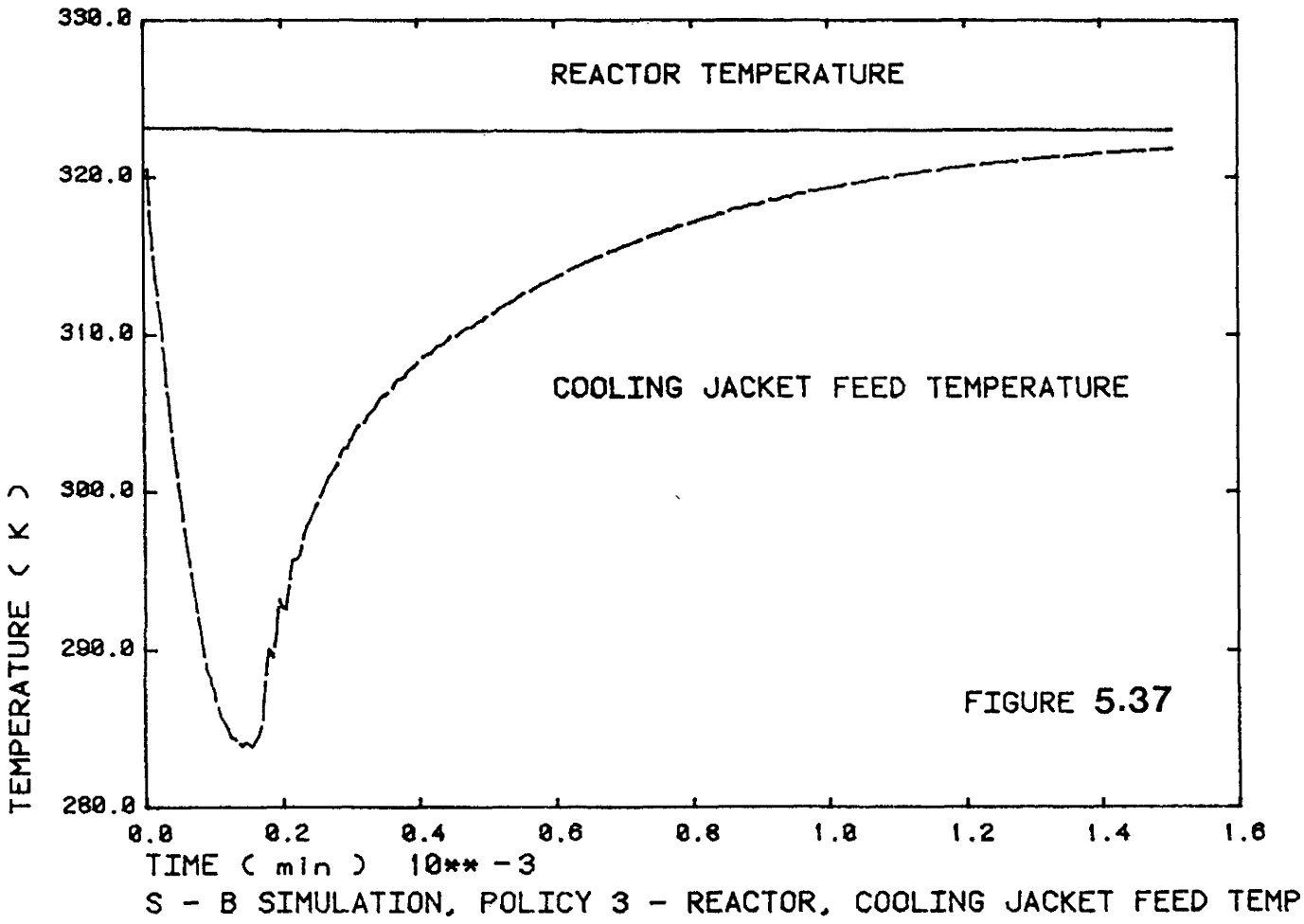

FIGURE 5.37

S - B SIMULATION, POLICY 3 - REACTOR, COOLING JACKET FEED TEMP

CHAPTER 6

SUMMARY, CONCLUSIONS AND RECOMMENDATIONS

6.1 Summary

A dynamic model was developed for the emulsion copolymerization of styrene/butadiene in a perfectly stirred reactor. The model considered the phenomena of particle nucleation, redox initiation, radical concentration dependence on particle size, radical entry rate and radical termination rate and diffusion controlled termination and propagation.

The model mass balances gave the amounts of each species in the reactor, the conversion and the accumulated copolymer composition. The model also calculated number and mass average molecular masses (assuming chain transfer to be the controlling mechanism), tri- and tetra- functional branch frequencies and the distribution of particle sizes. A simple heat balance over the reactor and cooling jacket was included. A proportional-integral controller was simulated to control reactor temperatures.

Batch styrene/butadiene and batch and continuous styrene polymerization data from the literature were modelled. Molecular mass and particle size distribution predictions were examined qualitatively for batch, semi-batch and continuous SBR polymerization. A qualitative analysis of semi-batch

policies designed to produce constant composition copolymer was presented as an example of the potential use of the model.

6.2 Conclusions

A simple parameter sensitivity study revealed that the parameters which affected the model predictions most were: A_s, k_{pss}, k_{pBB}, k_l, r_s, r_B, k_{fsx}, k_{fBx}, ρ_p and the partition coefficients K_{smw}, K_{swp}, K_{bmw}, K_{bwp}^{ρ}, K_{imw}, K_{imp}^{m}, K_{xmw} and K_{xwp}. Of these parameters, the partition coefficients, k_l, k_{fsx} and k_{fBx} were the least well known. It was found that the parameters of the molecular mass development did not affect conversion or particle number predictions and it was concluded that they could be fit independently of the other model parameters. The rate constants k_{fsx} and k_{fBx} were found to affect the molecular mass properties most strongly.

Fitting the model to literature data illustrated two important points. First, literature data are generally inappropriate for comprehensive model testing since they are invariably undesigned for this purpose. Second, the effect of impurities in experimental and especially plant data makes the determination of fundamental constants very difficult. Both points highlight the necessity of undertaking independent experiments to determine fundamental and semi-empirical constants. Furthermore, to successfully apply a model to commercial processes, the reactions of impurities need to

be identified and quantified.

The results of the data fitting generally indicated that the basic kinetic expressions of the model as well as the propagation constants and the reactivity ratios used were reasonably good. The use of partition coefficients to account for the distribution of monomers appeared to be adequate. It was recognized that these coefficients should be determined experimentally for the temperature and monomer and polymer compositions of the simulations.

The lack of a fundamental mechanism for diene-persulphate-mercaptan initiation hindered the use of the model in hot SBR simulation. A constant rate of initiation was fit to the literature data in this case.

Modelling the dynamic CSTR, styrene data of Brooks, et al. [1978] was fairly successful. However, observed oscillations in conversion could not be simulated. Investigations designed to force the conditions suspected to cause oscillations did not succeed. The results of simulations with the present model suggested that styrene, styrene/butadiene and perhaps all case II systems do not exhibit oscillations of the type exhibited by case I systems due to their slow nucleation and rapid growth rates.

The diffusion controlled termination and propagation algorithms were tested successfully for the homopolymerization of styrene using the data of Grancio, et al. [1970].

Molecular mass and branch frequency predictions were

examined qualitatively for batch and continuous reactors and were found adequate. However, some of the molecular mass controlling kinetic constants were not known as functions of temperature restricting the model predictions to isothermal conditions. The differential equation for the second moment of the molecular mass distribution was found to be unstable under conditions of low chain transfer agent concentration in the particles. This behaviour was interpreted as an indication of the formation of highly cross-linked polymer (gel).

The particle size distributions predicted by the model lacked the dispersion resulting from the statistical variation of radical residence in particles of the same size. Both batch and CSTR model predictions were deemed qualitatively adequate, however data was not available for quantitative verfication of the PSD model. The CSTR PSD prediction did, however, agree closely with the model prediction of Wong [1984]. It was anticipated that, in general, number and mass average particle diameters would be estimated satisfactorily, but that the distribution variance would be underestimated.

The heat balance model was found useful in the simulation of the SBR process. It provided an approximate picture of the heat load on the reactor cooling system and successfully simulated the effects of an unstable temperature controller.

The semi-batch operating policies studied controlled copolymer composition well. The second policy studied (Policy 2) was found to be inappropriate for SBR polymerization if operated at high latex particle conversion. It was recognized that for SBR or other monomers which are not affected by diffusion controlled termination rates, production rates at high conversions are not commercially feasible. Furthermore, the model indicated that a high degree of cross-linking in the produced polymer should be anticipated. Policy 2 implemented at lower latex particle conversions, such as 60%, was found acceptable.

6.3 Recommendations

Experimental

The need for independently determined fundamental model parameters has been explained in the previous section. Those parameters which most desparately need evaluation are: the rate constants for redox initiation or for persulphate-diene-mercaptan initiation, all partition coefficients and the rate constants for the reactions governing the molecular mass development, notably the transfer to chain transfer agent rate constants. If the availability of chain transfer agent to the particles is found to be diffusion controlled perhaps appropriate correlations could be developed. It is recommended that as a basis of investigation, the tentative persulphate-diene-mercaptan initiation mechanism presented

in Appendix A1 be adopted. The density of copolymer should be determined at compositions of interest or perhaps correlated with composition.

After the parameters have been investigated, batch SBR simulations should be performed to verify the model. Conversion, particle number, copolymer and particle compositions, molecular mass distributions or averages and, if possible, particle size distributions need be measured to test the model fully. Depending on the adequacy of the model fit to such data, other fundamental parameters such as propagation constants or soap parameters (A_s, $[E]_{cmc}$) may need to be re-evaluated independently.

Independent experiments may also be attempted to estimate parameters for the diffusion controlled termination and propagation algorithms. This is only expected to be necessary for high temperature, high styrene SBR.

Modelling

As experimental data becomes available, model inadequacies may become identified. Potential model improvements have been suggested throughout the literature review and model development chapters and will not be repeated here. It is suggested that a study be undertaken, once satisfactory kinetic parameters become available, to correlate the degrees of tri- and tetra-functional branching with the point at which the second molecular mass moment equation becomes unstable.

In cases where a gel product is anticipated, the unstable equation could be deleted and the program solved to the desired endpoint. Mass average molecular mass and the proportion of crosslinked product (gel) could be then inferred from the number average molecular mass and the branch frequencies.

A comparison of the particle size distribution predictions of the present model with a more precise method, such as one of those presented in section 2.2.7, would be of interest.

To improve the heat balance part of the model, it is recommended that the evaporation of butadiene be considered. A more realistic cooling system design should be investigated. It may be of interest to also consider the dynamics of the control actuator. With a better heat balance and with a complete set of temperature dependent rate constants, it may be of interest to examine adiabatic, constant cooling or temperature programmed modes of reactor operation.

Aside from simulations regarding SBR production, several theoretical studies may be tried. For example, simulating a hypothetical monomer which is strongly affected by diffusion controlled termination and propagation, the possibilities of multiple reactor steady-states or oscillations may be investigated.

REFERENCES

Anderson, H. M., Proctor, S. I., J. Polym. Sci., Part A, 3, 2343-2366 (1965).

Ballard, M. J., Napper, D. H., Gilbert, R. G., J. Polym. Sci. P. C. ed., 19, 939-954 (1981).

Blackley, D. C., Emulsion Polymerization Theory and Practice, Wiley and Sons, New York, (1975).

Bobrow, S., Johnson, A. I., Ponton, J. W., "Dynsys Manual and Application Studies", Dept. of Chem. Eng., McMaster U., Hamilton (1970).

Brandrup, J., Immergut, E. H., (ed.), Polymer Handbook, Wiley-Interscience, New York (1975).

Brooks, B. W., Kropholler, H. W., Purt, S. N., Polymer, 19, 193-196 (1978).

Brooks, B. W., J. C. S. Faraday, I., 76, 1599-1605 (1980).

Brysdon, J. A., "Styrene-Butadiene Rubber", Chapter 2 in Developments in Rubber Technology-2, Whelan, A., Lee, S. K. Ed., Applied Science Pub., London, (1981).

Bueche, F., Physical Properties of Polymers, Interscience Pub., New York (1962).

Burnett, G. M., Cameron, G. G., Thorat, P. L., J. Polym. Sci, A1, 8, 3435-3442 (1970a).

Burnett, G. M. Cameron, G. F., Thorat, P. L., J. Poly. Sci., A1, 8, 3443 (1970b).

Burnett, G. M., Cameron, G. G., Chapter 6 in ACS Advances in Chemistry series 128 (1973).

Campbell, J. D., Daniel, R. W., Lis, J., "Dynamic Simulation of Cold SBR Production", Senior Design Project, McMaster U. (1983).

Carr, C. W., et al., J. Polym. Sci., 5(2), 201-206 (1950).

Cauley, D. A., Thompson, R. W., J. Appl. Polym. Sci., 27, 363-379 (1982).

Chiang, A. S. T., Thompson, R. W., AIChE J., 25(3), 552-554 (1979).

Chiu, W. Y., Carratt, G. M. Soong, D. S., AIChE National Meeting, Los Angeles (1982).

Encyclopedia of Polymer Science and Technology, Vol. 5, Wiley and Sons, New York (1966).

Encyclopedia of Chemical Technology (Kirk-Othmer), Vol. 8, John Wiley and Sons Pub., New York, pp. 608-625 (1979).

Friis, N., Hamielec, A. E., J. Polym. Sci., P. C. ed., 11, 3321-3325 (1973).

Friis, N. et al. J. Appl. Polym. Sci., 18, 1247-1259 (1974).

Friis, N., Hamielec, A. E., "Gel-Effect in Emulsion Polymerization of Vinyl Monomers", ACS Symposium Series 24, (1976).

Friis, N., Hamielec, A. E., "Heterophase Polymerization", Polym. Reaction Engng. Short Course, McMaster U., Hamilton (1982).

Gardon, J. L., J. Polym. Sci., A-1, 6, 2859-2879 (1968).

Gardon, J. L., Rubb. Chem. Technol., 43, 74-94 (1970).

Gerrens, H., J. Polym. Sci., Part C, (27), 77-93 (1969).

Grancio, M. R., Williams, D. J., J. Polym. Sci., A-1, 8, 2617-2629 (1970).

Guyot, A., Guillot, J., Pichot, C., Rios-Gererrero, L., Emulsion Polymers and Emulsion Polymerization, Basset, D. R. Hamielec, A. E. (ed.) ACS Symposium Series, 165, Washington, D.C., 415-436 (1981).

Hamielec, A. E., "Synthesis Kinetics and Characterization of Poly (Vinyl Acetate) - Molecular Weight and Long Chain Branching Development", Chapter 4 in Emulsion Polymerization of Vinyl Acetate, El-Aaser, M., Vanderhoff, J. W. (ed.), Applied Science Pub., New Jersey (1981).

Hamielec, A. E., "Introduction to Polymerization Kinetics", Chapter I of Polymer Reaction Engineering Course Notes, McMaster University, Hamilton, Ont. (1982a).

Hamielec, A. E., Chemical Engineering 771 Course Notes, Department of Chemical Engineering (1982b).

Hamielec, A. E., MacGregor, J. F., Proc. Int. Berlin Workshop on Polymer Reaction Engineering, Berlin, Germany, (Oct. 1983).

Hamielec, A. E., personal communications (1984a).

Hamielec, A. E., Chemical Engineering 771 Course Notes, Department of Chemical Engineering (1984b).

Hansen, F. K., Ugelstad, J., J. Polym. Sci., A-1, 17, 3047-3067 (1979).

Harada, M., et al., J. App. Polym. Sci., 16, 811-833 (1972).

Harris, B., Hamielec, A. E., Marten, F. L., Emulsion Polymers and Emulsion Polymerization, Basset, D. R., Hamielec, A. E. (ed.), ACS Symposium Series, 165, Washington, D.C., 315-326 (1981).

Hoffman, E. J., Master's Thesis, McMaster U., Hamilton (1984).

Hoffman, T. W., "The Modeling of Emulsion Copolymerization Reactors", Polym. Reaction Engng. Short Course, McMaster U., Hamilton (1982).

Kalfus, M., Grzywa, E., Polym. J., 10 (6), 583-590 (1978).

Kao, C. I., Gundlach, D. P., Nelsen, R. I., "Kinetics of Emulsion Polymerization of Styrene-Simulation Model with Varying Free Radical Capture Efficiency", submitted to the J. of App. Polym. Sci., (1983).

Kiparissides, C., MacGregor, J. F., Hamielec, A. E., J. Appl. Polym. Sci., 23, 401-418 (1979).

Kiparissides, C., Ponnuswamy, S. R., Chem. Eng. Commun., 10, 283-291 (1981).

Kirillov, V. A., Ray, W. H., Chem. Eng. Sci., 33, 1499-1506 (1978).

Kolthoff, I. M., Harris, W. E., J. Polym. Sci., 2, 41-48 (1947).

Kolthoff, I. M. Meehan, E. J., Carr, C. W., J. Polym. Sci., 6(1), 73-81 (1951a).

Kolthoff, I. M., Meehan, E. J., Carr, C. W., J. Polym. Sci., 7(6), 577-586 (1957b).

Kolthoff, I. M., Miller, I. K., J. Am. Chem. Soc., 73, 3055-3059 (1951c).

Kolthoff, I. M., Miller, I. K., J. Am. Chem. Soc., 73, 5118-5122 (1951d).

Kolthoff, I. M., O'Connor, P. R., Hansen, J. L., J. Poly. Sci., 15, 459-473 (1955).

Krigbaum, W. R., Carpenter, D. K., J. Polym. Sci., 14, 241-259 (1954).

Leffew, K. W., Ph.D. Thesis, U of Louisville (1981).

Lichti, G., Gilbert, R. G., Napper, D. H., J. Polym. Sci., 15, 1957-1971 (1977).

Lichti, G., et al., J. Polym. Sci., P.C. Ed., 19, 925-938 (1981).

Lichti, G., Gilbert, R. G., Napper, D. H., J. Polym. Sci., 21, 269-291 (1983).

Lin, C. C., Ku, H. C., Chiu, W. Y., J. Appl. Polym. Sci., 26, 1327-1342 (1981).

Lord, M. G., Master's Thesis, McMaster U. (1984).

Manickam, S. P., Venkatarao, K., Subbaratnam, N. R., European Polym. J., 15, 483-487 (1979).

Marten, F. L., Hamielec, A. E., ACS Symposium Series, 104, 43-70 (1979).

Marten, F. L., Hamielec, A. E., J. Appl. Polym. Sci., 27, 489-505 (1982).

Matheson, M. S., et al., J. Am. Chem. Soc., 73, 1700-1706 (1951).

Meehan, E. J., J. Am. Chem. Soc., 71, 628-633 (1949).

Min, K. W., Ray, W. H., J. Macro Sci. Revs. Marco. Chem, C11, 177-255 (1974).

Min., K. W., Ray, W. H., J. Appl. Poly. Sci., 22, 89-112 (1978).

Min, K. W., Gostin, H. I., Ind. Eng. Chem. Prod. Res. Dev., 18, 272-278 (1979).

Minhas, B. S., Ph.D. Thesis, U. of Ottawa (1983).

Mitchell, J. M., Williams, H. L., Can. J. Res., 27 (F), 35-46 (1948).

Morton, M. Salatiello, P. P., Landield, H., J. Polym. Sci., 8(2), 215-224 (1952a).

Morton, M., Salatiello, P. P., Landfield, H., J. Polym. Sci., 8(3), 279-287 (1952b).

Morton, M., Kaizerman, S., Altier, M. W., J. Coll. Sci., 9, 300-312 (1954).

Morton, M., Rubber Technology, 2nd ed., Van Nostrand Reinhold Co. (1973).

Nomura, M., et al., J. App. Polym. Sci., 15, 675-691 (1971).

Nomura, M., et al., J. App. Polym. Sci., 27, 2483-2501 (1982).

Nomura, M., Fujita, K., AIChE Spring National Meeting Paper No. 38b, (1983a).

Nomura, M., et al., AIChE Spring National Meeting Paper No. 38e, (1983b).

O'Toole, J. T., J. App. Polym. Sci., 9, 1291-1297 (1965).

Penlidis, A., Technical Progress Report for the Department of Chemical Engineering, McMaster U, Hamilton (1982).

Pollock, M. J., Ph.D. Thesis, McMaster U. (1983).

Pramojaney, N., Ph.D. Thesis, Lehigh U. (1982).

Rudin, A., The Elements of Polymer Science and Engineering, Academic Press, New York (1982).

Schork, F. J., Ph.D. Thesis, U. Wisconsin at Madison (1981).

Soh, S. K., Sundberg, D. C., J. Polym. Sci., 20, 1299-1313 (1982a).

Soh, S. K., Sundberg, D. C., J. Polym. Sci., 20, 1315-1329 (1982b).

Starkweather, H. W., et al., Ind. Engng. Chem., 39, 210-222 (1947).

Stickler, M., Die Makromol Chemie, 184, 2563 (1983).

Stickler, M., Panke, D., Hamielec, A. E., "Polymerization of Methyl Methacrylate upto High Degrees of Conversion: Experimental Investigation of the Diffusion Controlled Polymerization", accepted for publication in Die Makromol. Chemie (1984).

Stockmayer, W. H., J. Polym. Sci., 24, 314-317 (1957).

Sundberg, D. C., J. App. Polym. Sci., 23, 2197-2214 (1979).

Sundberg, D. C. Hsieh, J. Y., Soh, S. K., ACS Symposium Series 165, 327-343 (1981).

Ugelstad, J., Mork, P. C., Aasen, J. O., J. Polym. Sci., A-1, 5, 2281-2288 (1967).

Ugelstad, J., Hansen, F. K., Rubber Chem. Technol., 49, 536-609 (1976).

Uraneck, C. A., "Butadiene-Styrene Rubbers...", Ch. 4, in Polymer Chemistry of Synthetic Elastomers, Kennedy, J. P., Tornqvist, E. G. M., ed., Interscience Pub., New York (1968).

Uraneck, C. A., Rubber Chem. Technol., 49, 610-649 (1976).

Wong, F. Y. C., Master's Thesis, McMaster U. (1984).

APPENDIX A1

HYPOTHETICAL PERSULPHATE/DIENE/ MERCAPTAN INITIATION MECHANISM

The mechanism of initiation in the emulsion polymerization of dienes is unknown. The rate of the promoting effect of aliphatic mercaptans in this system is also unknown. On the basis of the information presented in Section 2.2.3 of this thesis, a hypothetical mechanism was proposed for the purposes of the mathematical modelling of persulphate initiated styrene/butadiene systems. It should be stressed that this mechanism is not intended as a fundamental interpretation of the facts but rather a starting point for modelling and future experimental investigation.

The mechanism is based on the assumption that ionic persulphate-ended oligomeric radicals must grow to a certain length before the active radical cite can penetrate the negatively charged micelles. This water phase polymerization is relatively slow due to the low water solubility of both monomers, but when considering the number of units added to a complete chain, the time of water phase polymerization is short. The persulphate decomposition and water phase polymerization reactions are summarized in equations A1.1 to A1.7.

$$I_2 \xrightarrow{k_d} 2I^{\cdot} \qquad \text{(A1.1)}$$

$$I^{\cdot} + S \xrightarrow{k_{pIs}} {}^{-}S_1^{\cdot} \qquad (A1.2)$$

$$I^{\cdot} + B \xrightarrow{k_{IB}} {}^{-}B_1^{\cdot} \qquad (A1.3)$$

$${}^{-}Sn^{\cdot} + S \xrightarrow{k_{pss}} {}^{-}S_{n+1}^{\cdot} \qquad (A1.4$$

$${}^{-}S_n^{\cdot} + B \xrightarrow{k_{psB}} {}^{-}B_{n+1}^{\cdot} \qquad (A1.5)$$

$${}^{-}B_n^{\cdot} + S \xrightarrow{k_{pBs}} {}^{-}S_{n+1}^{\cdot} \qquad (A1.6)$$

$${}^{-}B_n^{\cdot} + B \xrightarrow{k_{pBB}} {}^{-}B_{n+1}^{\cdot} \qquad (A1.7)$$

It is proposed that the reaction of unit or oligormeric radicals with butadiene molecules results in an inactive product.

$$B_n^{\cdot} \xrightarrow{k_1} X \text{ (inactive)} \qquad (A1.8)$$

This infers that reactions (A1.6) and (A1.7) are improbable. Furthermore, the reactivity ratios of SBR polymerization dictate that the reaction of a unit or styrene-ended radical with butadiene is very likely. (i.e. $r_s = k_{pss}/k_{psB} = 0.44$) Also, butadiene is slightly more soluble in water than styrene and will therefore be in greater proportion.

On this basis it is assumed that during the short water phase polymerization period most radicals are de-activated through reaction with butadiene before they grow long enough to penetrate micelles or particles.

When mercaptans are added to the reaction mixture it is assumed that they react with active water phase radicals (via transfer to CTA) to form a non-ionic oligomeric radical which readily penetrates micelles. This is expressed:

$$I^{\cdot} + RSH \xrightarrow{k_{fIX}} RS^{\cdot} + IH^{-} \qquad (A1.9)$$

$$^{-}S_n^{\cdot} + RSH \xrightarrow{k_{fsx}} RS^{\cdot} + {}^{-}S_nH \qquad (A1.10)$$

From this mechanism, the rate of initiation, or the rate at which radicals which can penetrate micelles are produced is equal to the rates of equations (A1.9) or (A1.10).

The experimentally observed independence of the reaction rate from mercaptan level is assumed due to the fact that mercaptans are very insoluble and quickly saturate the water. The proposed mechanism does not, unfortunately, conform to the experimentally observed independence of initiation rate on persulphate concentration. It is proposed that non-ionic initiators are not affected by dienes because they, like the mercatyl radicals, can penetrate micelles unimpeded.

Two methods of testing this hypothesized mechanism immediately would be to examine the formed polymer for sulphate groups or to analyze the aqueous phase in search of a candidate for the unspecified inactive product of reaction (A1.8).

For modelling purposes, the mechanism may be summarized in three steps:

$$I_2 \xrightarrow{k_d} 2I^{\cdot}$$

$$I^{\cdot} + B \xrightarrow{k_{PIB}} X \text{ (inactive)} \qquad (A1.11)$$

$$I^{\cdot} + RSH \xrightarrow{k_{fIX}} RS^{\cdot} + IH \qquad (A1.12)$$

Only reactions of unit radicals are considered; oligomeric radicals are ignored. The rate of initiation is then based on equation (A1.12):

$$R_I = k_{fIX}\,[I^{\cdot}][RSH] \qquad (A1.13)$$

The concentration of unit radicals in the water phase is obtained from a radical balance.

$$\frac{d[I^{\cdot}]_w}{dt} = 2\,k_a[I]_w - k_{pIB}[I^{\cdot}]_w[B]_w - k_{fIX}[I^{\cdot}]_w[RSH]_w \qquad (A1.14)$$

Applying the steady-state hypothesis for radicals gives:

$$2\,k_d[I]_w = k_{pIB}[I^{\cdot}]_w[B]_w + k_{fIX}[I^{\cdot}]_w[RSM]_w >> \frac{d[I^{\cdot}]_w}{dt} \qquad (A1.15)$$

upon rearranging:

$$[I^{\cdot}]_w = \frac{2\,k_d[I]_w}{k_{pIB}[B]_w + k_{fIX}[RSH]_w} \qquad (A1.16)$$

Substituting (A1.16) into (A1.13) gives:

$$R_I = \frac{2\,k_d\,k_{fIX}[RSH]_w[I]_w}{k_{pIB}[B]_w + k_{fIX}[RSH]_w} \qquad (A1.17)$$

or

$$R_I = (2\,k_d[I]_w)\,.\,\left(\frac{k_{fIX}[RSH]_w}{k_{fIX}[RSH]_w + k_1[B]_w}\right) \qquad (A1.18)$$

In the form of (A1.18) the initiation rate may be viewed as

the decomposition rate of initiator multiplied by a factor reflecting the diene/mercaptan effect. It should be noted that when butadiene is not present, equation (A1.18) reduces to the initiation rate typically associated with styrene polymerization. It is recommended that for future hot SBR modelling efforts, equation (A1.17) be used.

Estimates of the unknown rate constants for reactions (A1.11) and (A1.12) may be obtained as follows. From fitting the data of Mitchell, et al. [1948] in Section 4.3.1, R_I for the persulphate-diene system was found to be $5 \times 10^{-9} \frac{\text{mol}}{\text{min.dm}^3\text{H}_2\text{O}}$. For persulphate initiated polystyrene:

$$R_I \simeq 2\, k_d [I]_w \simeq 2(6\times10^{-5}\tfrac{1}{\text{min}})(10^{-3}\tfrac{\text{mol}}{\text{dm}^3\text{H}_2\text{O}}) = 12\times10^{-7}\ \frac{\text{mol}}{\text{min.dm}^3\text{H}_2\text{O}}$$

The ratio of R_I's for the diene to styrene systems is equal to the right hand most quantity in equation (A1.18) (i.e. $5\times10^{-9}/12\times10^{-7} \simeq 0.04$), or

$$\frac{k_{fIX}[RSH]_w}{k_{pIB}[B]_w + k_{fIX}[PSH]_w} \simeq 0.04 \qquad \text{(A1.19)}$$

Simplifying (A1.19) gives:

$$k_{pIB} \doteq 25\ \frac{k_{fIX}[X]_w}{[B]_w}$$

As a first approximation, the value of k_{fIX} may be assumed equal to the equivalent polymer phase reaction rate, k_{fsx}, in equation (3.18).

APPENDIX A2

TEMPERATURE CONTROLLER PARAMETER TUNING

To implement the heat balance and temperature controller portion of the model, an estimate of the controller parameters was required. Linearized transfer functions were developed in order to apply the classical design techniques. A stability analysis was performed on the basis of the transfer functions to estimate the controller parameters.

The reactor and cooling jacket dynamics are coupled. They had to be considered simulataneously when deriving a transfer function for the process. The reactor temperature equation, (3.84) was simplified by ignoring the temperature dependence of the heat of polymerization, ΔH_p and by applying a first order Taylor series approximation for the non-linear Arrhenius temperature dependence of the reaction rate. To facilitate the differentiation of the reaction rate term, an average of the styrene and butadiene activation energies, $\bar{E}_a$, was used. Assuming that there were no disturbances in the feed temperatures (T_{in}) or the heat loss ($Q_{R\ LOSS}$), re-writing the equation in perturbation variables and applying Laplace transforms gave:

$$\tau_R\ s\ T - T = g_1\ T_J \qquad (A2.1)$$

where

$$\tau_R = \frac{\sum_i M_i \tilde{C}_{pi}}{\frac{\bar{E}_a}{RT_s^2} \Delta H_p R_p V_p - UA_J - \sum_i \tilde{F}_{i,in}} \qquad (A2.2)$$

and

$$g_1 = \frac{UA_J}{\frac{\bar{E}_a}{RT_s^2} \Delta H_p R_p V_p - UA_J - \sum_i \tilde{F}_{i,in}}$$

The temperature T_s represents the point at which the linearization was performed.

Ignoring disturbances in the heat loss term ($Q_{J\ LOSS}$) of equation (3.85) and applying perturbation variables and Laplace transforms, the following expression for jacket temperature was developed.

$$\tau_J\ s\ T_J + T_J = g_2\ T + g_3\ T_{J,in} \qquad (A2.4)$$

where

$$\tau_J = \frac{\rho_w\ V_J\ \tilde{C}_{pw}}{\tilde{F}_{Jw}\ \tilde{C}_{pw} + UA_J} \qquad (A2.5)$$

$$g_2 = \frac{UA_J}{\tilde{F}_{Jw}\ \tilde{C}_{pw} + UA_J} \qquad (A2.6)$$

$$g_3 = \frac{\tilde{F}_{Jw}\ \tilde{C}_{pw}}{\tilde{F}_{Jw}\ \tilde{C}_{pw} + UA_J} \qquad (A2.7)$$

Solving equations (A2.1) and (A2.4) simultaneously

gives the following process transfer function.

$$\frac{T(s)}{T_{J,in(s)}} = \frac{g_1 g_3}{\{(\tau_J s+1)(\tau_R s+1) - g_1 g_2\}} \qquad (A2.8)$$

The transfer function of a P.I. controller is:

$$\frac{T_{J,in}(s)}{\ell(s)} = K_c \left(1 + \frac{1}{\tau_J s}\right) \qquad (A2.9)$$

A stability analysis was performed on the loop transfer function of the process, which is the product of equations (A2.8) (A2.9). Clearly, the time constants and gains defined in equations (A2.2), (A2.3), (A2.5), (A2.6) and (A2.7) are time varying. This makes the control problem very difficult. Some form of adaptive control would clearly be of advantage for this system. However, for the present case, controller parameters were evaluated at different conditions (i.e., different τ_R, τ_J, g_1, g_2 and g_3 combinations) and the least demanding controller parameters were applied. These initial estimates were not, in general, adequate, and some on line tuning of the parameters was required.

APPENDIX A3

SECOND MOLECULAR MASS DISTRIBUTION MOMENT EQUATION ANALYSIS

The mass average molecular mass prediction, or more specifically, the second molecular mass distribution moment (Q_2) equation was found to be unstable at low chain transfer agent (CTA) levels. The Q_2 equation tended to infinite values at very low conversions. If the level of CTA was increased, the model predicted to higher conversions before becoming unstable. Eventually if enough CTA was added, the moment equation did not become unstable.

The purpose of the work presented in this appendix was to determine if the observed instability were a real effect or a fault in the modelling, implementation or numerical solution of the moment equation.

It was suspected initially that the source of instability was the term representing the propagation with polymer, or crosslinking reaction. To test this hypothesis, the model was solved with the crosslinking term, C_k, and the transfer to polymer term, C_p, set to zero and the chain transfer agent charge set very small. Under these conditions the model predictions were stable. In fact, the predicted polydispersity ($\bar{M}_w / \bar{M}_n$) was equal to 2, as expected. Setting C_p to its original value did not affect the model adversly. However, as C_k was increased, the mass average molecular mass predictions increased and eventually, at a level close to the typical value

of C_k, the molecular mass prediction became infinite at high conversions. Increasing C_k further, decreased the conversion at which the instability occurred. This evidence clearly indicated that the instability involved the crosslinking term.

To further study the solution of the Q_2 differential equation, a simplified version of the equation was solved analytically. The equation was adapted to represent the homopolymerization of butadiene in a batch reactor. Only propagation, transfer to monomer and crosslinking reactions were considered. During stages 1 and 2, the concentration of butadiene (or monomer) $[M]_p$, was assumed constant, and the particle volume was considered a function of conversion only. During stage 3 the particle volume was assumed constant and $[M]_p$ fell with increasing conversion. The Q_2 equation (3.99) was modified by setting inflow and outflow terms, C_p and C_x, the chain transfer to CTA term, equal to zero. By dividing (3.99) by:

$$\frac{dX}{dt} = \frac{1}{N_{mo}} k_p [M]_p Y_o Y_p \qquad \text{(A3.1)}$$

where N_{mo} is the moles of monomers initially charged, a differential equation with respect to conversion is obtained.

For stages 1 and 2 the resulting differential equation is:

$$\frac{dX}{X} = \frac{dQ_2}{\alpha+\beta Q_2+\gamma Q_2^2} \qquad \text{(A3.2)}$$

where $\alpha = \frac{2}{C_m \eta}$

$$\eta = \frac{\tilde{M}_B}{\rho_p \phi_p} \tag{A3.4}$$

$$\beta = \left(\frac{4C_k}{C_m} \frac{1}{[M]_p^{\eta}} - 1\right) \tag{A3.5}$$

$$\gamma = \frac{2C_k^2}{[M]_p^2} \cdot \frac{1}{C_m^{\eta}} \tag{A3.6}$$

The appropriate solution for the particular constants used was:

$$Q_2 = \frac{\sqrt{q} \tan\{\frac{\sqrt{q}}{2} (\ell n|X| + IC)\} - B}{2\gamma} \tag{A3.7}$$

$$\text{where} \quad q = 4\alpha\gamma - \beta^2 \tag{A3.8}$$

Clearly, this solution is not defined at zero conversion so that a reasonable, non-zero X and Q_2 were needed to solve equation (A3.7).

The resulting differential equation for stage 3 was:

$$\frac{dX}{(1-X)} = \frac{dU}{a+bU+cU^2} \tag{A3.9}$$

$$U = \frac{Q_2}{(1-X)}$$

$$\text{where} \quad a = \frac{2N_{mo}}{C_m V_p} \tag{A3.10}$$

$$b = \frac{4}{C_m} + 1 \tag{A3.11}$$

$$c = \frac{2C_k^2}{C_m N_{mo}} \tag{A3.12}$$

The solution of the Q_2 equation for stage 3 was:

$$Q_2 = \frac{(1-X)\{(\sqrt{-q}-b)+(b+\sqrt{-q})[\frac{d}{1-X}]^{\sqrt{-q}}\}}{2\,c(1-[\frac{d}{1-X}]^{\sqrt{-q}}} \tag{A3.13}$$

where

$$\sqrt{-q} = b^2 - 4ac \tag{A3.14}$$

and

$$d = (1-X_c)\left(\frac{2c\,\frac{Q_2^c}{(1-X_c)} + b - \sqrt{-q}}{2c\,\frac{Q_2^c}{(1-X_c)} + b + \sqrt{-q}}\right)^{\sqrt{-q}} \tag{A3.15}$$

Q_2^c is evaluated at X_c.

When tested, the analytical solutions, (A3.7) and (A3.13) agreed with the numeric solution of the model. Infinite Q_2 values were observed to occur in exactly the same places. The analytical and numeric solutions agreed over a range of C_k values. It was of interest to note that the analytical solution (A3.13) was always a rapidly increasing function.

It may be concluded from these observations that the

observed infinite values were not due to numerical instabilities or an error in implementing the numerical solution. Of course, quantitative verification that equation (3.97) models the system accurately can only be determined through experiments. Qualitatively the observed infinite values may be interpreted as signifying the formation of molecules of infinite molecular mass (so-called micro-gel). As mentioned in the text of this thesis, micro-gel formation is often observed at low conversions in the polymerization of butadiene.

It is perceived that physically chain transfer agent reduces the effect of branching by acting to form a large number of chains. The total number of branches per unit mass of polymer is not affected but since more chains are formed, there are fewer chains per molecule. In terms of the differential equation (3.99), the chain transfer agent term dominates the equation making the crosslinking term less important.

By rearranging equation (3.99), this point may be illustrated more clearly:

$$\frac{d(V_p Q_2)}{dt} = \frac{2\, k_p [M]_p\, Y_o V_p}{C_m + C_x \frac{[X]_p}{[M]_p} + C_p \frac{Q_1}{[M]_p}} \left(1 + C_x \frac{[X]_p}{[M]_p}\right.$$

$$\left. + \left(C_p + 2C_k + C_x C_k \frac{[X]_p}{[M]_p}\right) \frac{Q_2}{[M]_p} \right.$$

$$\left. + C_k \left(C_p + C_k\right) \frac{Q_2^2}{[M]_p^2} \right. \qquad \text{(A3.16)}$$

By increasing the importance of transfer to chain transfer agent, the constant and linear terms of the quadratic in Q_2 become more important. When C_k is zero, clearly the quadratic term disapperas and, as observed, the equation is stable.

Another curious feature of the molecular mass predictions were that they failed to reach a steady state (in the CSTR mode) until long after all other properties, including branching, had reached their steady state values. This observation is illustrated in figure 5.12. A satisfactory explanation of this behaviour was not obtained.

APPENDIX A4

PROBLEMS WITH THE NUMERIC SOLUTION OF THE MODEL

The model equations, reflecting the vast difference between the rate of particle formation and the rates of the other important processes in emulsion polymerization, are stiff. The fact that particle nucleation may reoccur further complicates the equations' solution.

Several integration methods and subroutines were tried. The IMSL, variable order Adams (predictor-corrector) integrating subroutine was unsuccessful in solving the model. A fourth order Runge-Kutta (IMSL) routine worked satisfactorily as long as the nucleation period started at the beginning of the integration. When nucleation occurred for the first time after the start of integration, the Runge-Kutta routine was unable to solve the equations.

The model was successfully solved under all conditions using an IMSL routine employing Gear's method for stiff equations. However, a very small initial step size (10^{-12}) was required to start integration. Also, the Gear's routine displayed a few idiosyncratic problems. For example, when semi-batch reactors were being simulated, the introduction of a new input flow caused the integrating routine to stop. Increasing the desired tolerance for a successful integration step typically resolved such problems. On a few occasions, the integration would stop as a result of an apparent undefined exponentiation

or division by zero. Examination of the vectors of integrated variables revealled unreasonable solutions to the equations, such as negative amounts of species in the reactor. Decreasing the tolerance in this case corrected the problem. A cursory examination of the conditions and data sets which caused these problems did not lead to an answer. It was found that a tolerance of 10^{-5} was adequate in most cases.

The model was also solved successfully using the Adams-Moulton-Shell routine in the DYNSYS executive (Bobrow, et al. [1970]) program. Campbell, et al. [1983] applied the DYNSYS executive with the present model to simulate a train of CSTR's. Their simulations were successful, however, they did uncover a potential problem in the numeric solution of the model. Constrained by long computing times and data storage limits, they fixed the minimum integration step size to 1 minute. In the course of their research, they tried to simulate the oscillations in particle number and conversion due to the on-off nucleation mechanism discussed in section 5.3. By increasing the rate of initiation by 450% and decreasing the amount of emulsifier by 75% compared to their respective typical steady state levels, Campbell, et al. [1983] observed the oscillations shown in figure A4.1. Each line shown in figure A4.1 represents the number of particles in each reactor of a train of 4 CSTR's. The nature of the observed oscillations was exactly as one would expect if on-off nucleation were occurring; huge bursts of nucleation followed by periods of no nucleation

and particle wash out. However, the number and size of the oscillations were found later to be a function of integration step size. As the step size was decreased, the oscillations decreased in magnitude, occurred less regularly and eventually disappeared. The oscillations were determined to have occurred because the extremely high instantaneous nucleation rates were maintained artifically over a relatively long integration period. In the real case, the rapid growth of particles consumes emulsifier quickly and and nucleation rate decreases sharply within the period of 1 minute.

The point of presenting this material has been to illustrate the types of problems which may occur due to improperly chosen integration parameters. It is of interest, however, to note that the model would have predicted continuous oscillations, had the conditions for their existence been met. This exercise also emphasizes that the relatively slow nucleation rates and the rapid growth rate, preclude oscillations due to on-off nucleation in SBR, styrene and perhaps all case II systems.

There is a numerical problem in the model which has not been corrected to date. It stems from a difficulty in specifying the point at which the reactor overflows. No problem is encountered when simulating polymer production in large, commercial sized vessels. However, when small reactors (less than 1 dm^3) are simulated, the volume of the reaction mixture has been observed to fall below the reactor volume leading to

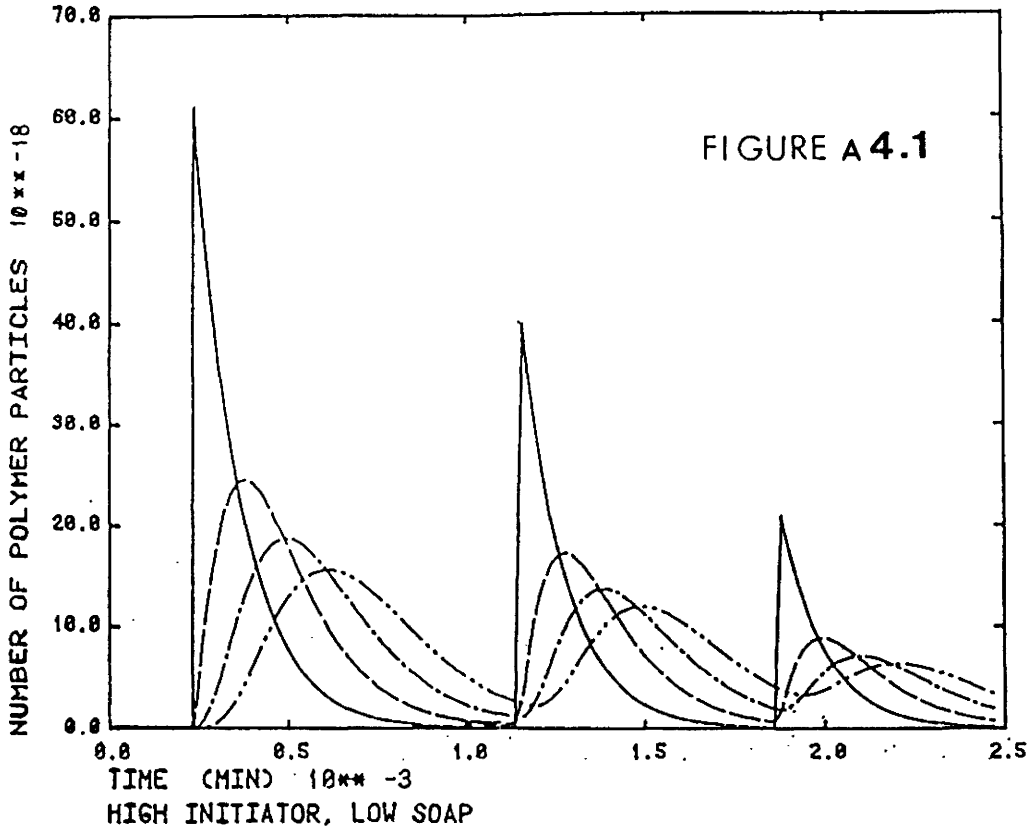

FIGURE A 4.1

OSCILLATIONS OBSERVED BY CAMPBELL, et al. (1983)

cessation of outflow. In a real system a reactor can stop overflowing when inflows are shut off or when inflows are less than the volume contraction rate of the reaction mixture. In the model's case, the reactor can stop overflowing when the integration routine steps backward in time or due to numerical error. The integration routine used to solve the model often took backward steps in time when it approached an apparent discontinuity. The abrupt change to the model equations as outflows became important represented one such discontinuity. The fact that the integrating routine required backward steps in time precluded the simplest solution to the problem; simply fixing the reactor volume after the point of initial overflow. A satisfactory solution to this problem was not found, but as pointed out initially, the problem was not encountered for large reactors.

APPENDIX B1

FUNDAMENTAL MODEL PARAMETERS

The following table lists all constants and their sources, required in the solution of the model.

Improvements in the model have been suggested throughout this work. The following table includes a number of physical constants which may be of use in implementing of the aforementioned improvements.

The reader is referred to Encyclopedia (1966) for constants pertaining to SBR (23.5 mass % styrene) mechanical properties.

Table B1.1

Fundamental Model Parameters

Parameter	Value/Expression	Source
A	see Table 4.6	
A_s	$3.67 \times 10^7 \frac{dm^2}{molecule}$ (Sodium Dodecyl Sulphate)	Brandrup, et al. (1975)
B	see Table	
C_{ps}	186.2 J/mol.K	
C_{pB}	123.4 J/mol.K	
C_{pw}	75.4 J/mol.K	
C_{pp}	1.89 J/g.K	"
$[E]_{CMC}$	9×10^{-3} mol dm^3	"
ΔH_p	-70000 J/mol	
K_{SMW}	3400	Wong (1984)
K_{SWP}	5.88×10^{-4}	"
K_{BMW}	800	"
K_{BWP}	2.5×10^{-3}	"

Table B1.1 Cont'd.

Fundamental Model Parameters

Parameter	Value/Expression	Source
k_{fsx}	$1.7\times10^{7}\exp(-6400/(RxT))$ $(\frac{dm^3}{mol\ min})$	Wong (1984)
k_{fBx}	$5.1\times10^{7}\exp(-6400/(RxT)$ $(\frac{dm^3}{mol\ min})$	Wong (1984)
	$3.1\times10^{8}\exp(-6400/(RxT)$ $(\frac{dm^3}{mol\ min})$	Morton, et al. (1952a)
k_p^*	$8.1\times10^{8}\exp(-14150/(RxT))$ $(\frac{dm^3}{mol\ min})$	Burnett, et al. (1970b), Wong (1984)
k_{pBl}^*	$8.1\times10^{8}\exp(-14150/(RxT))$ $(\frac{dm^3}{mol\ min})$	Burnett, et al. (1970b), Wong (1984)
	$1.1\times10^{11}\exp(-16800/(RxT))$ $(\frac{dm^3}{mol\ min})$	Morton, et al. (1952a)
k_{tp}	$7.77\times10^{10}\exp(-2370/(RxT))$ $(\frac{dm^3}{mol\ min})$	Matheson, et al. (1951)
$\tilde{M}_s$	104.15 (g/mol)	
$\tilde{M}_B$	54.09 (g/mol)	
$\tilde{M}_w$	18.0 (g/mol)	
$\tilde{M}_E$	288.38 (Sodium Dodecyl Sulphate)	
$\tilde{M}_{RA}$	154.0 (g/mol)	
$\tilde{M}_I$	172.0 (p-menthane hydroperoxide)	
	271.3 ($K_2S_2O_8$) (g/mol)	
$\tilde{M}_{Fe}$	278.0 (g/mol)	

Table B1.1 Cont'd.

Fundamental Model Parameters

Parameter	Value/Expression		Source
$\tilde{M}_x$	202.4	(g/mol)	
N_A	6.022045×10^{23}	#/mol	
R	1.987	$\frac{cal}{mol\ K}$	
r_s	0.44	(278 K)	Brandrup, et al. (1975)
r_B	1.4	(278 K)	Brandrup, et al. (1975)
T_{ref}	298 K		by definition
T_{gp}	211 (209-214) K (23.5 mass % Styrene)		Encyclopedia (1966)
T_{gs}	167 K		Sundberg, et al. (1981)
T_{gB}	108 K		
V_F^*	see Table 4.6		
V_{FIMIN}	see Table 4.6		
V_{FCRS}	see Table 4.6		
V_{FCRB}	0.035		estimate
U	170.6 J/m^2K		
α_p	?		
Coefficient of Volume Expansion	660×10^{-6} (1/K) (23.5 mass % Styrene)		Encyclopedia (1966)
α_s	1×10^{-3} (1/K)		Bueche (1962)
α_B	1×10^{-3} (1/K)		Bueche (1962)

Table B1.1 Cont'd.

Fundamental Model Parameters

Parameter	Value/Expression	Source
π	3.141592653	
ρ_s	906 kg/m^3 (29 K)	
ρ_B	645.2 kg/m^3 273 K	
	633.3 kg/m^3 283 K	
	621.1 kg/m^3 293 K	
	581.8 kg/m^3 323 K	
ρ_w	1000 kg/m^3	
ρ_p	933 (932.5 - 933.5) kg/m^3 (23.5 mass % Styrene)	Encyclopedia (1966)

Table B1.2

Potentially Useful Fundamental Constants

Parameter	Value/Expression	Source
Tg_p	323 K $\frac{(-85 + 135S)}{(1 - 0.5S)}$ (^oC)	
	278 K $\frac{(-78 + 128\ S)}{(1 - 0.5\ S)}$ (^oC)	Morton (1973)
	where S mass fraction styrene in the copolymer	
Enthalpy of Vapourization of Butadiene	(298.16 K) 384.36 $\frac{kJ}{kg}$	Minhag (1983)
	(268.75 K and 101.325 kPa) 406.45 $\frac{kJ}{kg}$	
Gaseous Heat Capacity of Butadiene	(273.16 K) 1.36 $\frac{kJ}{kg}$. K	Minhag (1983)
	(298.16 K) 1.47 $\frac{kJ}{kg}$. K	
	(373.16 K) 1.78 $\frac{kJ}{kg}$. K	
Antoine Vapour Pressure Equation	$\ln(P) = A - \frac{B}{T+C}$	
	where P ≡ mm Hg; T ≡ K	
	Styrene / Butadiene	
A	16.0193 / 15.7727	
B	3328.57 / 2142.66	
C	-63.72 / -34.30	
Solubility of Styrene (298 K)	0.0271%	Min, et al. (1974)

Table B1.2 Cont'd.

Potentially Useful Fundamental Constants

Parameter Description	Value/Expression	Source
Solubility of Butadiene (298 K, 101.3 kPa)	0.081%	Min, et al. (1974)
Correlation for the Diffusion Controlled Termination Constant of Styrene in Bulk Polymerization	$k_{tp}=(k_{tp})_o \exp -2(Bx+Cx^2+Dx^3)$ $B = 2.57 - 5.05 \times 10^{-3} T$ $C = 9.56 - 1.76 \times 10^{-2} T$ $D = -3.03 + 7.85 \times 10^{-3} T$ $T \equiv$ absolute temperature (K) $(k_{tp})_o \equiv$ chemically controlled termination constant	Friis, et al. (1973)
Kuhn-Mark Relation	$[\eta] = K M^a$ $[\eta] \equiv$ intrinsic viscosity (aL/g) at 323 K $M \equiv$ molecular mass	Morton (1973)
a	0.66 (23.5 mass % styrene)	
K	5.3×10^{-4} (23.5 mass % styrene)	

APPENDIX B2

MODELLED RECIPES

The following appendix presents recipes and additional constants used in the simulations presented in Chapters 4 and 5. The recipes are presented in terms of variables, defined in the Nomenclature section and used consistently throughout the model development and in the format used in the computer model. These recipes represent initial charges or steady-state flow rates for batch and semi-batch or continuous reactors respectively.

The parameters used to simulate the Mitchell and Williams [1948] data were generally the same as those given in Appendix B1. The exceptions are as follows:

$$r_s = 0.5$$

$$r_I = 5 \times 10^{-9} \text{ mol/min.dm}^3\text{H}_2\text{O}$$

The parameters used in fitting the data of Carr, et al. [1950] were effectively identical to those used in the fitting of the Mitchell and Williams [1948] data. Specific emulsifier constants and fitted R_I values are given in Table 4.2 of Chapter 4. The recipe used is presented in Table 1.1 of Chapter 1. The only necessary additional pieces of information are:

$$T = 323 \text{ K}$$

$$V_R = 1 \text{ dm}^3$$

Table B2.1

CSTR Data Set Representing the

Recipe of Wong [1984]

Input Variable	Numerical Value	
V_R	21387	dm^3
T	278.15	K
$\tilde{F}_{s,in}$	14.2	kg/min
$\tilde{F}_{B,in}$	40.5	kg/min
$\tilde{F}_{w,in}$	104.6	kg/min
$\tilde{F}_{I,in}$	0.0345	kg/min
$\tilde{F}_{Fe,in}$	0.00766	kg/min
$\tilde{F}_{RA,in}$	0.0276	
$\tilde{Fe}_{,in}$	2.44	kg/min
$\tilde{F}_{x,in}$	0.0656	kg/min

Table B2.2

Batch Reactor Data Set Representing Recipe of Mitchell and Williams [1948]

Input Variable	Numerical Value	
V_R	0.23	dm^3
T	318	K
V_s	} 50 g total: in Styrene: Butadiene mass ratios of 50:50, 60:40, 70:30, 80:20, 90:10.	
	- inputed to the model as volumes	
V_w	0.1125	dm^3 (112.5 g)
M_I	0.15 g	
M_E	2.25 g	
M_x	0.075 g	

Table B2.3

Batch Reactor Data Set Representing SBR 1500 Recipe

Input Variable	Numerical Value	
V_R	4000	dm^3
T	278.15	K
V_s	320.09	dm^3
V_B	1143.13	dm^3
V_w	2000	dm^3
M_I	1.2	kg
M_{Fe}	0.4	kg
M_{RA}	1.0	kg
M_E	45	kg
M_x	0.656	kg

It should be stressed that an efficiency factor, pre multiplying the rate of initiation, R_I, was used. The fitted value of this factor was:

$F = 0.135$

Table B2.4

CSTR Data Set Representing the Recipe of Brooks, et al. [1978]

Input Variable	Numerical Value
V_R	1.5 dm^3 2.6 dm^3
T	323 K
V_s V_w	} in a water:styrene mass ratio of 2.87
M_E	to specification in Table 4.3
$\tilde{F}_{s,in}$ $\tilde{F}_{w,in}$	} water: styrene mass ratio of 2.87
$\tilde{F}_{I,in}$	to specification in Table 4.3
$\tilde{F}_{E,in}$	

Table B2.5

Parameters Specifically Required for the Simulation of the Data of Brooks, et al. [1978]

Parameter	Value	Source
K_{smw}	3328	estimated
K_{swp}	3.8×10^{-4}	
ρ_s	900 kg/m^3	Pollock [1983]
ρ_p	1040 kg/m^3	
$\tilde{M}_I$	224.16 g/mol	
A_s	3.8×10^7 dm^2/mol (3.67×10^7 - literature)	

Grancio, et al. [1970] belived that all particles were nucleated almost instantaneously. For this reason, the number of particles are initialized, using the estimates of Friis, et al. [1973] and the charges of emulsifier are ignored. Appropriate constants for potassium persulphate as well as the propagation constant of Friis, et al., [1973] k_{pss} = 23100 $dm^3/mol.min.$, were employed in this simulation.

Table B2.6

Batch Reactor Data Set Representing Simulated Recipes of Grancio, et al. [1970]

Input Variable	Numerical Value	
V_R	1	dm^3
T	333	K
V_s	0.111	dm^3
V_w	0.18	dm^3
	13%/hr	21%/hr
N_p	5.4×10^{16} #/dm^3	9.1×10^{16} #/dm^3
M_I	0.15 g	0.30g

Table B2.7

Cold Batch Data Set (Used in Section 5.2)

Input Variable	Value	
V_R	5000	dm^3
T	278	K
V_s	156.73	dm^3
V_B	652.07	dm^3
V_w	1046.	dm^3
M_I	345.	g
M_{Fe}	76.6	g
M_{RA}	276.0	g
M_E	24.4	kg
M_x	2735.	g
	1368	g
	656	g
	328	g

Table B2.8

Data Sets Representing Semi-Batch Policy 1 Recipes

(Simulated in Section 5.4.2)

Input Variables		Batch	P1 I1	P1 I4
V_R	(dm^3)	5000	5000	5000
T	(K)	323	323	323
V_s	(dm^3)	1026.5	1026.5	1026.5
V_B	(dm^3)	777.6	435.9	435.9
V_w	(dm^3)	2543.3	2543.3	2161.3
M_I	(g)	4.234	4.234	4.234
M_E	(kg)	52.93	52.93	45.03
M_x	(kg)	7.06	7.06	7.06
$\tilde{F}_{JN}$	(kg/min)	200	200	200
V_J	(dm^3)	791.7	791.7	791.7
K_c		30	30	30
τ_I	(min)	10	10	10
Desired Copolymer Composition		0.5	0.5	0.5

Table B2.9

Data Sets Representing Semi-Batch Policy 2 Recipes (Simulated in Section 5.4.3)

Input Variable		Operating Points X = 60%	X = 95%
V_R	(dm^3)	5000	5000
T	(K)	323	323
V_s	(dm^3)	56.99	4.50
V_B	(dm^3)	24.204	1.91
V_w	(dm^3)	2543.3	2543.3
W_p	(kg)	100	100
N_p	(#/$dm^3 H_2 0$)	1×10^{17}	1×10^{17}
ACCM		0.658	0.658
$\overline{M}_n$	(g/mol)	88500	88500
$\overline{M}_w$	(g/mol)	3050000	305000
$\overline{B}_{n3}$	(#/molecule)	0.2772	0.2772
$\overline{B}_{n3}$	(#/molecule)	0.0306	0.0306
M_I	(kg)	4.234	4.234
M_x	(kg)	0.025	0.025
		Cooling Jacket/Temperature Control parameters as in Table B2.8	

Table B2.10

Data Set Representing the Semi-Batch Policy 3 Recipe (Simulated in Section 5.4.4)

Input Variable		Policy 3
V_R	(dm^3)	7000
T	(K)	323
V_s	(dm^3)	256.6
V_B	(dm^3)	109.0
V_w	(dm^3)	635.83
M_I	(kg)	6.0
M_E	(kg)	20.0
M_x	(kg)	1.5
$\tilde{F}_{Jw}$	(kg/min)	200
V_J	(dm^3)	791.7
K_c		40.0
τ_I	(min)	10.0
Desired Copolymer Composition		6.5
End of first Policy 1 period (min)		175
End of Policy 2 period (min)		500